2019

Dopamine and the Temporal Dependence of Learning and Memory

Annie Handler

DOPAMINE AND THE TEMPORAL DEPENDENCE OF LEARNING AND MEMORY

A Thesis Presented to the Faculty of

The Rockefeller University

in Partial Fulfillment of the Requirements for

the degree of Doctor of Philosophy

by

Annie Handler

June 2019

DOPAMINE AND THE TEMPORAL DEPENDENCE OF LEARNING AND MEMORY

Annie Handler, Ph.D.

The Rockefeller University 2019

Animal behavior is largely influenced by the seeking out of rewards and avoidance of punishments. Positive or negative reinforcements, like a food reward or painful shock, impart meaningful valence onto sensory cues in the animal's environment. The ability of animals to form associations between a sensory cue and a rewarding or punishing reinforcement permits them to adapt their future behavior to maximize reward and minimize punishments. Animals rely on the timing of events to infer the causal relationships between cues and outcomes — sensory cues that precede a painful shock in time become associated with its onset and are imparted with negative valence, whereas cues that follow the shock in time are instead associated with its cessation and imparted with positive valence. While the temporal requirements for associative learning have been well characterized at the behavioral level, the molecular and circuit mechanisms for this temporal sensitivity remain incompletely understood.

Using the simple architecture of the mushroom body, an olfactory associative learning center in *Drosophila*, I examined how the relative timing of olfactory inputs and dopaminergic reinforcement signals is encoded at the molecular, synaptic, and circuit level to give rise to learned odor associations. I show that in *Drosophila,* opposing olfactory associations can be formed and updated on a trial-by-trial basis depending on the temporal relationship between an odor cue and dopaminergic reinforcement during conditioning. Additionally, both negative and

positive reinforcements equivalently instruct appetitive and aversive olfactory associations — odors preceding a negative reinforcement or following a rewarding reinforcement acquire an aversive valence, while odors instead following a negative reinforcement or preceding a rewarding reinforcement become attractive. Furthermore, functional imaging revealed that synapses within the mushroom body are bidirectionally modulated depending on the temporal ordering of odor and dopaminergic reinforcement, leading to synaptic depression when an odor precedes dopaminergic activity or synaptic facilitation when dopaminergic activity instead precedes an odor. Through the synchronous recording of neural activity and behavior, I found that the bidirectional regulation of synaptic transmission within the mushroom body directly correlates with the emergence of learned olfactory behaviors. This temporal sensitivity arises from two dopamine receptors, DopR1 and DopR2, that couple to distinct second-messengers and direct either synaptic depression or potentiation. Loss of either receptor renders the synapses of the mushroom body capable of only unidirectional plasticity and prevents the behavioral flexibility of writing opposing associations depending on the temporal structure of conditioning.

Together, these results reveal how the distinct intracellular signaling pathways of two dopamine receptors can detect the order of events within an associative learning circuit to instruct opposing forms of synaptic and behavioral plasticity, providing a mechanism for animals to use both the onset and offset of a reinforcement signal to instruct distinct associations. Additionally, this bidirectional modulation allows animals to flexibly update olfactory associations on a trial-by-trial basis when temporal relationships are altered, permitting them to contend with a complex and changing sensory world.

To my parents, Ann and Henry,

for nourishing my curiosity and intellectual growth

To Josh, my partner in life,

for unwavering support and love

Acknowledgements

I would first like to thank the people who contributed throughout the evolution of the work presented in this thesis. Raffi Cohn laid the foundation for describing the bidirectional plasticity in the mushroom body circuitry, and in my early years as a PhD student, we worked together closely in characterizing the temporal dependence for neural modulation. He taught me how to perform two-photon imaging and designed the closed-loop olfactory paradigm that was central to linking neural and behavioral plasticity. Ianessa Morantte, who in addition to providing steadfast support as I learned basic molecular biology, offered her immense intellectual and technical skills throughout this work. She created the first DopR1 mutant animal compatible with two-photon imaging, a resource the field has already shown great appreciation for. I am lucky to have worked with and learned from Thomas Graham, a former post-doc in the lab, who designed the behavioral chambers and provided immense support in experimental design and analysis throughout this project. I would also like to thank Andy Siliciano, a talented MD/PhD student in the lab, who carried out beautiful experiments characterizing the signaling properties of *Drosophila* dopamine receptors and who spent many afternoons thinking deeply with me about this project and Josie Clowney, a former post-doc in the lab, who was instrumental in the sorting and sequencing of the different Kenyon Cell populations. Nathan Hu, a very talented SSRP high school student, and Tom Hindmarsh Sten, a graduate student in the lab, provided great insight into how *Drosophila* learn new memories through their behavioral experiments. In addition, I'd like to thank Jim Petrillo and the Rockefeller Precision Fabrication Facility, and Patrick Stock, an engineer in the lab, for their technical support and design of novel behavioral equipment used in this study. Jaime de Juan-Sanz, a post-doc in the Ryan lab, provided the ER calcium sensor

and helped with preliminary experiments. I am also grateful to Yulong Li and his graduate student, Jianzhi Zeng, for providing the dopamine and acetylcholine sensor. Many people also contributed their thoughts and provided feedback on our manuscript, including Sandeep Datta, Larry Abbott, Barbara Noro, and other members of the Ruta lab. I also feel very fortunate to have overlapped with the members of the Ruta lab, past and present, with whom I have shared countless conversations that both aided me in my science and kept my grounded throughout my PhD. Ari Zolin, my long-term baymate, Rory Coleman, Joel Butterwick, and Josefina del Mármol were always gracious in providing technical help and helpful feedback through informal scientific discussions and through their thoughtful questions during lab meetings.

I would like to thank the Rockefeller community for providing such a fervent environment for pushing the boundaries of science. Especially, I would like to thank Dr. Paul Greengard, who welcomed me into his lab in the summer of 2011 and taught me how to think like a scientist. I feel indebted to the Dean's office—Cris Rosario, Emily Harms, Stephanie Fernandez, Sid Strickland, Marta Delgado, and Kristen Cullen—for inviting me to be a SURF student at Rockefeller in 2011 and for their continued support throughout my time at Rockefeller and for the assistance they provided to the Summer Neuroscience Program. Also, I would like to acknowledge all the help and support provided by the members of RockEDU that helped the growth of the Summer Neuroscience Program over the years. I would like to thank all the invertebrate neuroscience labs at Rockefeller, BSVMRKYZ, for the engaging scientific discourse and helpful feedback on this project throughout my PhD. I am also incredibly grateful to all the friends and colleagues I've met throughout my time here at Rockefeller, including all my classmates; especially, I'd like to thank Elisabeth Murphy and Ryan Farrell for all the dog walks and morning swims.

I am fortunate to have learned from the members of my faculty advisory committee: Tim Ryan, Cori Bargmann, and Gaby Maimon. Their scientific advice throughout my PhD forced me to think critically and rigorously about my research and helped shape the work presented in this document. I must also thank Nic Tritsch for serving as my external examiner of my thesis committee.

Most of all, I consider myself incredibly fortunate to have had Vanessa Ruta as my advisor and mentor at Rockefeller. On a warm summer afternoon in 2014, I sat side-by-side with Vanessa as she taught me her tricks for whole-cell patching a *Drosophila* neuron that I would end up studying for the next five years of my PhD. At the time, I didn't realize my studies would focus on the properties of this one particular neuron; however, in that moment it was obvious that I was under the guidance of an incredible scientist who carried infectious enthusiasm for science and discovery and a strong dedication to mentorship and teaching. As such, the work I present in this document would not have been possible without the unwavering support and intellectual guidance from Vanessa.

Finally, I must thank my family, by blood and by marriage, for their dedicated support throughout my studies—for always asking how my flies were doing and what I've taught them lately. None of this work would have been possible without their persistent love, support, and guidance. My parents, Ann and Henry, fostered my interest and curiosity in science and supported my educational pursuits every step along the way. My brothers, Patrick and Skye, kept me grounded and light-hearted throughout my studies. Lastly, my husband, Josh, was a constant throughout graduate school—always encouraging me and supporting me through the peaks and valleys. He calmed my nerves and always made sure my life was so full of happiness. I couldn't have done it without him.

Table of Contents

Chapter 3

Chapter 4

Chapter 5

Chapter 6

Chapter 7

List of Figures

List of Abbreviations

AMPA-R	α-amino-3-hydroxy-5-methyl-4-isoxazolepropionic acid receptor
CS+	Paired conditioned stimulus
CS-	Unpaired conditioned stimulus
CAMKII	Calcium/calmodulin-dependent protein kinase II
cAMP	Cyclic adenosine monophosphate
CREB	cAMP response element-binding protein
DAN	Dopamine neurons
FACS	Fluorescence activated cell sorting
GPCR	G-protein coupled receptor
IP3	Inositol trisphosphate
KC	Kenyon Cell
LTP	Long-term potentiation
LTD	Long-term depression
MB	Mushroom body
MBON	Mushroom body output neuron
NMDA-R	N-methyl-D-aspartate receptor
PAM	protocerebral anterior medial
PDE	Phosphodiesterase
PIP2	Phosphatidylinositol 4,5-biphosphate
PKA	Protein kinase A
PKC	Protein kinase C
PPL	Protocerebral posterior lateral
RPE	Reward prediction error
SNc	Substantia nigra pars compacta
STDP	Spike-timing dependent plasticity
VTA	Ventral tegmental area

Chapter 1

Introduction

1.1 The Timing of Learning and Memory

Our ability to learn from our past experiences is a central feature shaping who we are as individuals and the fabric of our civilizations. The remarkable capacity to acquire new knowledge and skills in the form of memories molds our personality over a lifetime and enables us to learn societal values and adapt appropriate behaviors within a given cultural framework. However, this ability to learn and form meaningful memories is not a unique skill observed only in humans; it is conserved across a wide variety of animals, ranging from those with simple nervous systems containing only hundreds of neurons to highly intricate nervous systems possessing billions of neurons and even more recently apparent in computers through the advent of machine learning. In fact, it has recently been suggested that single-celled organisms have the capacity to habituate behavioral responses, raising the question of the key biological element involved in learning and memory and the role of a centralized nervous system in these processes (Boisseau et al., 2016). This shared capacity for learning and memory permits adaptive strategies for contending with changes in the environment over time.

The complexity of learning ranges from simple non-associative learning in the form of habituation, in which a reflexive response dwindles with repeated stimulation, to more complex forms such as observational learning, where animals learn new behaviors simply through

observing the behavior of peers. Underlying all forms of learning and memory in both biological and artificial systems is an experience-dependent change, or plasticity, between the connections within a network that persists for some period of time. While some of these changes are fleeting, lasting on the order of milliseconds only long enough for turnover of cellular machinery and de-phosphorylation of proteins, other memories persist for a lifetime. In fact, our memory systems are fine-tuned to learn and retain memories on different timescales depending on their emotional saliency. While this calibration of learning and memory is ideal for forgetting irrelevant information while retaining important events in one's life, it also lends itself to emotional anguish in the diseased state. Emotional distress from memory loss can be appreciated in the agony suffered by those in the early stages of dementia, whereas distress from a forgetting-deficit constitutes the intrusive symptoms of post-traumatic stress disorder. Therefore, understanding the biological and neural basis for how animals extract meaningful information from their past to inform future behaviors is a central question in modern neuroscience research.

One of the simplest and most conserved forms of learning within the animal kingdom is associative learning, in which animals use the relative timing and order of events in their environment to extract the causal relationship between a sensory stimulus and a rewarding or punishing outcome. Across both invertebrates and vertebrates, the neural circuits involved in associative learning integrate sensory signals with rewarding or punishing reinforcement cues (Aso et al., 2014b; Bromberg-Martin et al., 2010; Lerner et al., 2015; Schultz et al., 1997a; Waddell, 2016). This convergence of sensory and reinforcement pathways is thought to induce the circuit plasticity that underlies adaptive changes in behavior (Cohn et al., 2015; Hige et al., 2015; Owald et al., 2015; Reynolds and Wickens, 2002; Shen et al., 2008).

A strict temporal relationship between a sensory signal, such as an auditory tone or an odor, and a reinforcement is required to drive learning: in order for the tone to predict an ensuing positive or negative outcome, it must consistently precede the reinforcement in time. This tight temporal contiguity represents a basic tenant of classical conditioning (Brunelli et al., 1976; Carey and Lisberger, 2002; Kandel et al., 1983; Mauk and Donegan, 1997; Pavlov, 1927; Rescorla, 1967; 1988; Tully and Quinn, 1985), as it permits animals to understand the causal structure of the world around them.

It is generally accepted that a sensory cue, such as sound that precedes, and therefore predicts, a shock in time will be imparted with the same negative valence as the painful shock. This kind of associative conditioning, or classical conditioning, was first described experimentally through, Russian psychologist, Ivan Pavlov's research into the reflexive behavior of salivation in dogs (Pavlov, 1927). Pavlov theorized that learning entailed the acquisition of new behaviors to a previously ineffective stimulus and that this kind of learning could be achieved through the temporal association of stimuli in an animal's environment. His work on classical conditioning demonstrated that a previously ineffective stimulus (the conditioned stimulus, CS+), which elicited no overt behavioral response, could elicit a new behavioral response after it was paired with a reinforcement, such as food or a painful shock (the unconditioned stimulus, US) (Kandel et al., 2000; Pavlov, 1927). The reinforcement by food or shock provokes an innate, unconditioned behavioral response, such as salivation or freezing behavior. The repeated pairing of the conditioned stimulus with the reinforcement stimulus imparts the CS+ with predictive value: if the reinforcement is a food reward, the CS+ becomes an appetitive cue, whereas, a

painful shock, would reinforce the CS+ as being noxious or aversive. The central feature of Pavlov's work of associative conditioning rests on the temporal contiguity of the conditioned and unconditioned stimulus.

The role of timing in shaping the formation of associative memories during classical conditioning was expanded through the research of American psychologist, Robert Rescorla who showed that these memories were heavily influenced by the contingency or likelihood of the two stimuli occurring repeatedly together (Rescorla, 1967). This dependence on contingency is adaptive in ensuring animals distinguish truly predictive and causal relationships in their environments from those that are only randomly associated at any single time. Classical conditioning, therefore, likely evolved to enable animals to use the temporal relationships between events in their environment to predict causal relationships.

In addition to learning what sensory cues are predictive of the onset of a reinforcement, it is equally important for animals to learn which sensory cues can be associated with the offset of the reinforcement. Research in the 1950s demonstrated that cues contiguous with the end of shock would acquire a rewarding reinforcement value, and elicit future approach behavior (Smith and Buchanan, 1954). Additional work in sea slugs, flies, rodents, monkeys, and humans supported this theory that relief from pain served as a rewarding reinforcement (Andreatta et al., 2012; 2015; Baxter and Byrne, 2006; Bergado Acosta et al., 2017; Davis et al., 2008; Davis, 2011; Dubnau and Tully, 2001; Gerber et al., 2004; 2019; Heisenberg, 2003; Lechner and Byrne, 1998; Mayer et al., 2018; Tanimoto et al., 2004). Furthermore, conditioning using an appetitive, unconditioned stimulus leads to the opposite effect, whereby animals avoid odors associated with

the offset of reward (Felsenberg et al., 2013). Together these data suggest that animals can form opposing associations with a sensory stimulus depending on whether it precedes or lags a reinforcement in time. Despite these observations at the behavioral level, the underlying molecular or circuit basis for how this temporal sensitivity is achieved in associative learning circuits to give rise to these bidirectional behavioral responses remains incompletely understood.

1.2 The Synapse: A Site for Learning and Memory

Understanding how neural circuits are transformed through associative learning to form and maintain memories remains a central question in neuroscience research. The complexities of nervous systems observed across animals that are capable of learning associative memories span an immense spectrum: ranging from a nervous system of 302 neurons in the adult *C. elegans* to 86 billion neurons in the human brain (Azevedo et al., 2009; Herculano-Houzel, 2009)—a number on par with a rough estimate for the number of stars in the Milky Way galaxy. This diversity in nervous system complexity contrasts with the shared capacity for learning and memory, raising the interesting question of where learning occurs in the brain and where memories are stored.

For example, the cell body or soma has been suggested to serve as the hub of memory formation and storage in associative learning circuits (Technau and Heisenberg, 1982; Tully et al., 1994). Alternatively, epigenetic markers have been proposed to act as a regulator in memory storage in post-mitotic neurons across a diversity of animals, allowing for stable, experience-dependent changes in gene expression that shape neural and behavioral responses to stimuli (Zovkic et al.,

2013). Furthermore, experimental evidence suggests the synapses between neurons is the relevant site for memory formation and storage (Bolshakov and Siegelbaum, 1994; Kandel et al., 1976; Zucker et al., 1971). Indeed, the idea of the synapse as the site of learning and memory dates back to the prescient Spanish neuroscientist, Ramón y Cajal who, in his Croonian Lecture to the Royal Society in 1894, posited that the strength of synaptic connections between neurons was not immutable and that such flexibility in synaptic weights could underlie learning and the storage of memories (Cajal, 1894). Although there likely exist numerous redundant sites for memory formation and regulation in the nervous system, my thesis focuses on the role of the synapse in learning and memory.

Despite Cajal's proposal of synaptic re-weighting as the basis of learning and memory, the question of how the close temporal pairing of an unconditioned and conditioned stimulus could alter the weight between synapses within a neural circuit remained unresolved for decades. In 1949, a mechanistic basis for Cajal's theory was proposed by Canadian psychologist, Donald Hebb, in his book *The Organization of Behavior* (Hebb, 1949). Hebb postulated that neurons that are synchronously activated undergo a gain in their synaptic connections. This form of plasticity, coined Hebbian plasticity, provided a basis for how the connections between cell assemblies could be strengthened as a result of experiencing a tight temporal pairing between two input signals, such as a tone and painful shock. Hebb's theory gave rise to research into the biological process of spike-timing dependent plasticity (STDP). In 1983, Levy and Steward found that the temporal contiguity between inputs within the dentate gyrus of the mouse brain determines the direction of synaptic plasticity—with bidirectional plasticity observed in the post-synaptic neuron depending on the ordering of input neuron activity (Levy and Steward, 1983). The

biphasic curves for STDP reveal that synapses within learning circuits undergo bidirectional plasticity depending on the relative timing of spikes in pre- and post-synaptic neurons—an observation that mirrors the behavioral modulation dependent on the ordering of the conditioned and unconditioned stimulus during training (Bell et al., 1997; Bi and Rubin, 2005; Cassenaer and Laurent, 2012; Dan and Poo, 2004). However, STDP requires nearly coincident firing patterns on a millisecond timescale, far more rapid than the temporal relationships between stimuli typically required for associative learning, which has made the timescales of STDP-dependent neural plasticity and learned, associative behaviors difficult to reconcile. Furthermore, electrophysiological recordings in associative circuits have demonstrated that neural responses to the conditioned stimulus during learning generally end before the delivery of reward, suggesting that STDP cannot explain the re-weighting of synaptic connections that occurs during associative conditioning (Meeks and Holy, 2008). Instead, experiments suggest that neuromodulators, such as dopamine and serotonin, play a central role in sculpting the synaptic plasticity of associative learning (Cassenaer and Laurent, 2012; Kandel et al., 1976).

1.3 Neuromodulation in Learning Circuits

Associative learning circuits are heavily innervated by neuromodulatory neurons. This innervation permits a fixed set of neurons to undergo rapid and reversible modulation, creating a potential for wide diversity of neural activity states (Bargmann, 2012). The rapid and reversible nature of neuromodulation within a circuit is an ideal driving force for learning and memory, as it allows for a flexible reconfiguration of anatomically static neuronal circuits.

Across a diversity of animals dopaminergic neurons represent the presence of a reward or punishment and serve as a crucial regulator in the learning instructed by appetitive and aversive experiences. In the mammalian brain, the dopamine-releasing neurons in the subcortical regions of the substantia nigra pars compacta (SNc) and the ventral tegmental area (VTA) serve as the major source of dopamine input to cortical and subcortical regions (Björklund and Dunnett, 2007). Behavioral experiments by Olds and Milner suggested a key role for dopamine in driving motivated behaviors by demonstrating that animals continuously press a lever that leads to the stimulation of brain areas heavily innervated by rewarding dopamine neurons (Corbett and Wise, 1980; Olds and Milner, 1954). Over the following decades, electrophysiological recordings of dopamine neurons further refined our understanding for the role of dopamine in neural plasticity and associative learning.

Within the striatum, a brain center that receives convergent input from SNc projecting dopamine neurons and thalamic and cortical projecting sensory neurons, dopamine release induces synaptic plasticity thought to play a central role in driving reward-seeking behaviors (Reynolds et al., 2001; Roseberry et al., 2016). Recalling Pavlov's dogs, the conditioned stimulus of the tone is imbued with positive salience after repeatedly pairing the tone with food reward, prompting salivation upon the tone's presentation in the future. Seminal work by Wolfram Schultz demonstrated that reward-responsive dopamine neurons within the mammalian brain acquire responses to the conditioned stimulus (Schultz et al., 1997) during associative conditioning. After repeatedly pairing the CS+ and US, dopamine neurons shift their response profile from responding strongly to the unconditioned reward to instead responding to the now predictive CS+, suggesting a mechanism for the acquisition of the learned, salivation response (Schultz et

al., 1997; Waelti et al., 2001; Watabe-Uchida et al., 2017). Furthermore, the omission of the reward induces depression in dopamine neurons, whereas a reward greater than predicted by the CS+ elicits a stronger dopamine response (Hollerman et al., 1998; Watabe-Uchida et al., 2017). Based on these key observations, Schultz proposed that dopamine neurons represent the difference between expected and experienced outcomes and serve as a reward-prediction error (RPE) signal. The activation or depression of dopamine neurons in situations where the reward is better or worse than expected is thought to interact with two distinct signaling pathways in the striatum to modify synaptic strength related to reward-seeking behaviors (Bromberg-Martin et al., 2010; Montague et al., 1996). In this way, dopamine neurons are able to make predictions about the likelihood of a conditioned stimulus to give rise to reward and enable the animal to continuously track the correlation between events in the environment and update incorrect associations. RPE signals encoded by dopamine neurons have been observed in monkeys, rodents, humans, and suggested to exist in flies (Bayer and Glimcher, 2005; Cohen et al., 2012; D'Ardenne et al., 2008; Eshel et al., 2015; Felsenberg et al., 2017; Flagel et al., 2011; Hollerman et al., 1998; Roesch et al., 2007; Waelti et al., 2001), highlighting a conserved strategy for dopamine neurons in representing the statistics of reward and driving reward-related changes in behavior.

Research over the past two decades, however, has revealed a more complex and heterogeneous picture for the role of dopaminergic neurons within the mammalian brain, suggesting that encoding RPE is not the single function of dopamine neurons in associative learning. While indeed there is strong evidence supporting the role of dopamine in reward-related behaviors, recent technological advances allowing for cell-type specific functional imaging with higher

spatial resolution revealed two populations of striatal-projecting SNc dopamine neurons that respond differentially to aversive electrical shock (Lerner et al., 2015). In addition, electrophysiological recordings in the VTA dopamine neurons reveal strong excitation to a painful tail pinch and attenuation of this response minimizes the behavioral response to aversive conditioning (Zweifel et al., 2011). Furthermore, the heterogeneity of dopamine neurons is complicated by the observation that populations of midbrain dopamine neurons show bidirectional responses to reward and punishment (Matsumoto et al., 2016). Together, these results suggest that some populations of dopamine neurons are able to represent reward and punishment along a single axis, whereas other populations of dopamine neurons exhibit phasic activation to either unexpected reward or punishment.

1.4 Dopamine-Dependent Modulation in Neural Activity

In addition to the multiplexed encoding of signals by heterogeneous dopaminergic populations, the release of dopamine on downstream neural circuits regulates their activity in diverse ways. This includes altering the pre-synaptic release probability by adjusting the size of the reserved vesicle pool, the localization of proteins to the active zone, and the influx of presynaptic calcium in axon terminals (Higley and Sabatini, 2010; Logsdon et al., 2006; McKay et al., 2007; Nadim and Bucher, 2014; Regehr et al., 2009; Tritsch and Sabatini, 2012). Furthermore, dopamine can tune post-synaptic activity via the modulation of expression and properties of neurotransmitter receptors (Sun et al., 2005). In addition to the effects on protein function and localization, dopamine can influence synaptic tone over a multitude of timescales and distances (Arbuthnott and Wickens, 2007; Matsuda et al., 2009). The activity level of mesolimbic dopamine neurons is

thought to be consistently low, supplying a near constant tonic level of dopamine release. This tonic activity is briefly interrupted by strong, phasic bursts or pauses in dopamine activity thought to convey the surprising presence or absence of reward (Schultz, 2002). Therefore, neural circuits innervated by dopamine neurons are constantly influenced by activity patterns of dopaminergic neurons. However, how this ongoing tonic and infrequent phasic input of dopamine influences information flow within neural circuits to influence goal-directed behavior is an ongoing question of much interest.

The release of dopamine is translated into neural modulation by way of a diversity of G-protein coupled receptors (GPCRs). The mammalian brain expresses five dopamine receptors (D1-D5), which can be subdivided into two groups of receptors, D1-like and D2-like. The D1-like class of receptors include D1 and D5 and have been shown to preferentially couple to the stimulatory G-protein, Gαs, while the D2-like receptors, which include D2-D4, instead preferentially couple to the inhibitory G-protein, Gαi. The stimulatory and inhibitory nomenclature refers to the G-proteins regulation of downstream enzymes involved in the production of the second messenger, cyclic adenosine monophasphate (cAMP) (Beaulieu and Gainetdinov, 2011; Neve et al., 2004). In the mammalian brain, D1- and D2-like receptors act antagonistically on downstream signaling pathways by way of opposing effects on PKA activity levels. D1-like receptor activation of PKA promotes phosphorylation of the neuronal phosphoprotein, DARPP-32, while D2-like receptors act to dephosphorylate DARPP-32 (Flores-Hernandez et al., 2000). DARPP-32, therefore, acts as an integrator of neuromodulation and influences a variety of ligand- and voltage-gated channels to bidirectionally alter synaptic transmission within downstream circuits (Flores-Hernández et al., 2002; Greengard, 2001; Yan et al., 1999).

Expression patterns reveal that D1 and D2 receptors are the most highly expressed dopamine receptors in the mammalian brain with the greatest expression in the dorsal and ventral striatum and the olfactory tubercle. D1 and D2 receptors are both expressed in the GABAergic striatal projection neurons as well as in cholinergic interneurons within the striatum and in subcategories of pyramidal and interneurons within cortical regions (Tritsch and Sabatini, 2012). Despite the observed overlap in expression pattern within brain regions, transcriptional analysis, pharmacological experiments and advances in the use of cell-type reporters revealed a dichotomy in the striatal projection neurons, with the direct striatonigral projection neurons expressing the D1 receptor while the indirect striatopallidal projection neurons express the D2 receptor (Gerfen, 1992; Gerfen et al., 1990; Gerfen and Surmeier, 2011). This segregation of D1 and D2 receptors into these distinct streams is thought to drive differential modulation on downstream circuits through the fine balance of inhibition and excitation on cortical circuits involved in the regulation of animal behavior. However, recent work using cell-type specific markers and *in vivo* imaging has revealed a great diversity of response profiles across these mesolimbic dopamine pathways, with some dopamine neurons encoding reward, punishment, and locomotion, either exclusively or in combination (Coddington and Dudman, 2018; Engelhard et al., 2018; Lammel et al., 2014; Lerner et al., 2015). Together these results raise the question of how the D1 and D2 receptors are selectively engaged during different tasks and how the engagement of the direct and indirect pathway influence downstream circuits to ultimately drive changes in animal behavior. While this question remains a central focus of mammalian neuroscience, addressed through the use of novel and elegant genetic and functional imaging tools, the simple and well-characterized neural architecture of the *Drosophila* brain provides the unique opportunity to link

conserved signaling molecules to the emergence of neural and behavioral plasticity at the same, identifiable synapses across individual animals.

1.5 The Mushroom Body: A Simple Learning Circuit

1.5.1 The Mushroom Body Anatomy

The mushroom body (MB) brain structure, an associative learning center in the insect brain, was first identified in 1850 by French biologist Félix Dujardin, who argued that this brain structure was the seat of free will and intelligence based on correlative comparisons between MB size and behavioral complexity in solitary and social honeybees (Dujardin, 1850). He even went so far as to compare the MB to the vertebrate cerebral cortex in terms of both structure and function. While the MB seems a unique neuropil present in all annelids and anthropods except crustaceans, analogous circuits can be seen in the anatomical structure of the vertebrate cerebellum and cerebellar-like circuits suggesting convergent organization of learning circuits (Strausfeld et al., 1998).

The MB has long been known to be an essential neural locus for olfactory learning. In the MB of *Drosophila*, odor information is carried by the intrinsic Kenyon Cells (KCs) whose parallel axon bundles form output lobes. The KCs receive olfactory information from projection neurons originating from the antennal lobe that synapse onto the dendrites of KCs within a neuropil called the calyx. Each mushroom body contains roughly 2,000 KCs whose axons fasciculate to form 5 output lobes of the MB: the α and α' lobes project dorsally while the γ, β, and β' project

medially. The lobes of the MB are segmented into discrete compartments defined by the innervation patterns of extrinsic neurons including the efferent neurons regulating animal behavior and the afferent, neuromodulatory neurons encoding valence such as reward or punishment.

Functional and behavioral experiments suggest that the three classes of KCs (γ, α/β, and α'/β') have distinct physiological properties and play different roles in short- versus long-term memories (Groschner et al., 2018). An individual KC samples from converging input from, on average, 7-10 second-order projection neurons, and a given odor activates only 5% of KCs (Campbell et al., 2013; Caron et al., 2013; Murthy et al., 2008; Turner et al., 2008), creating a sparse sensory representation of olfactory information. In addition, anatomic tracing of glomerular inputs onto KCs reveals stochastic wiring, implying the activity pattern of KCs for a given odor vary across individual animals (Caron et al., 2013). This kind of sparse and combinatorial code is ideal for ensuring sensitivity to a vast array of olfactory stimuli and offers animals the capacity to contextualize a rich diversity of odors as a result of experience.

The KC axons form en passant synapses onto the spatially compartmentalized dendrites of a small repertoire of mushroom body output neurons (MBONs) that innervate the output lobes of the MB. These MBONs exhibit diverse innervation patterns with spatially restricted dendrites that tile the lobes, distinct axonal projection patterns, use of neurotransmitters, and effects on behavior (Aso et al., 2014a; Aso et al., 2014b). Activation of individual MBONs biases animals towards either attraction or avoidance behavior (Figure 1A). Based on this anatomical lay out, it

Figure 1.1, Cellular Anatomy of Compartmentalized Mushroom Body Architecture.
(A-B) Schematized structure of mushroom body architecture, focusing specifically on the gamma output lobe involved in short-term memory regulation. **(A)** Compartmentalized organization of γ2-γ5 mushroom body output neurons (MBONs). Activation of γ2/γ3 lead to odor attraction while γ4/γ5 lead to odor avoidance (Aso et al., 2014b). **(B)** The logic of valence coding by dopamine neurons (DANs) innervating the γ2-γ5 compartments of the MB. The proximal γ2/γ3 DANs respond to painful shock punishment while the distal γ4/γ5 DANs respond to reward-related experiences like sugar ingestion. **(C)** Mushroom body neuropil in the *Drosophila* brain with KCs labeled in blue. The images on the right highlight the compartmentalized and overlapping architecture of the MBONs and DANs innervating a single compartment of the MB.

Figure 1.1

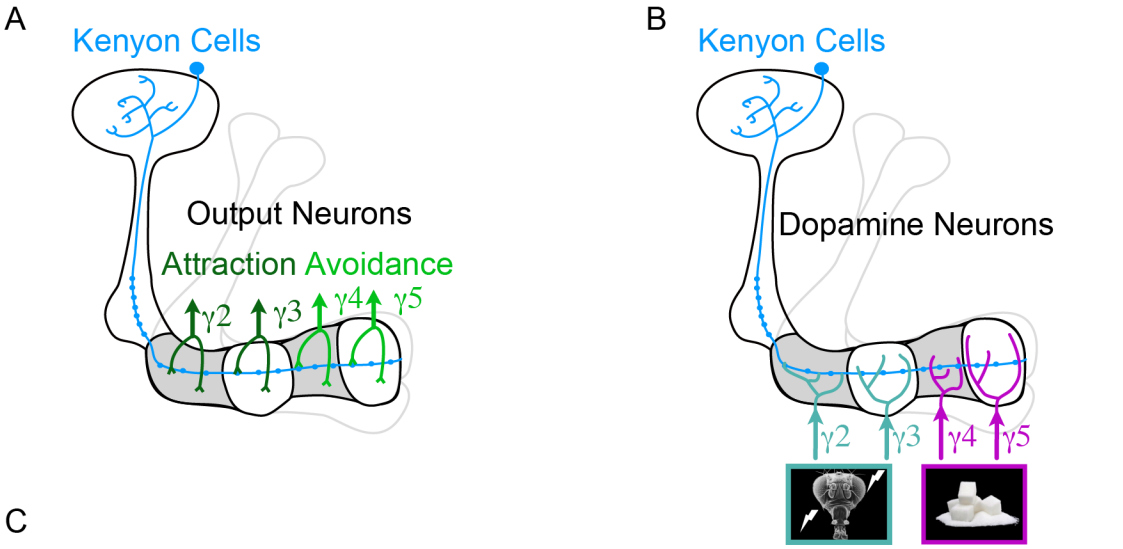
A
Kenyon Cells
Output Neurons
Attraction Avoidance
γ2
γ3
γ4
γ5
B
Kenyon Cells
Dopamine Neurons
γ2
γ3
γ4
γ5

C

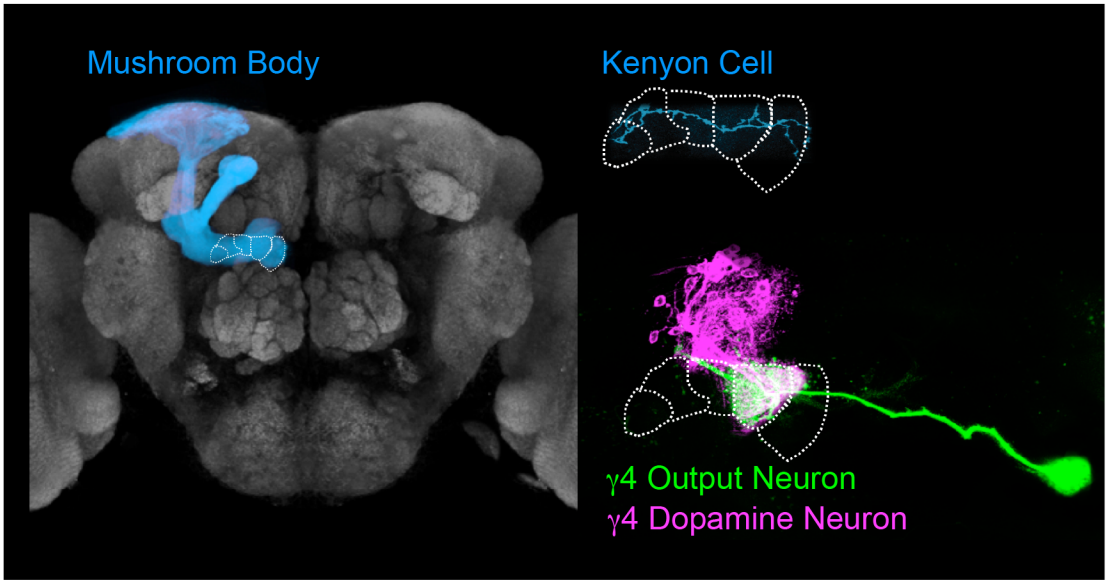
Mushroom Body
Kenyon Cell
γ4 Output Neuron
γ4 Dopamine Neuron

is thought that these MBONs encode the valence of a learned odor and work in concert to guide a fly's behavior towards odor attraction or odor avoidance as a result of learning (Aso et al., 2014b; Owald et al., 2015).

The axon terminals of dopamine neurons (DANs) overlap with the MBON dendrites creating a compartmentalized architecture in which DAN activity can locally modify KC-MBON synapses to drive learned changes in odor attraction (Figures 1.1B-C). The acquisition of olfactory memories depends on DAN activity, and indeed, exogenous stimulation of a subset of DANs is sufficient to induce fictive olfactory memory formation (Aso and Rubin, 2016; Aso et al., 2012; 2010; Burke et al., 2012; Claridge-Chang et al., 2009; König et al., 2018; Liu et al., 2012). Rewarding and punishing experiences are encoded by distinct subsets of these DANs (Figure 1.1B), conveying either positive or negative valence information to different KC-MBON synapses (Burke et al., 2012; Cohn et al., 2015; Qin et al., 2012; Yamagata et al., 2015). Specifically the *protocerebral posterior lateral* (PPL) DANs carry predominantly aversive signals (Aso and Rubin, 2016; Aso et al., 2010; 2012; Claridge-Chang et al., 2009; Mao and Davis, 2009) while the *protocerebral anterior medial* (PAM) DANs convey reward information (Aso and Rubin, 2016; Burke et al., 2012; Liu et al., 2012; Yamagata et al., 2015). Such an anatomical segregation of valence is reminiscent of the mammalian dopaminergic system, highlighting organizational parallels across neuromodulatory systems.

1.5.2 Associative Learning and the Mushroom Body

Drosophila melanogaster have been used as a model for studying learning and memory since the 1970s when scientists in Seymour Benzer's lab showed that pairing a neutral odor with a painful

electric shock instructed a negative association with the paired odor, driving flies to avoid this odor upon future encounter (Quinn et al., 1974). Since then, *Drosophila* have served as a powerful system for studying the molecular and circuit mechanisms underlying learning and memory.

The focus on the MB in *Drosophila* arose from seminal work by German neuroscientist and geneticist Martin Heisenberg, who showed olfactory learning deficits that correlate with structural and biochemical perturbations to the MB circuitry (de Belle and Heisenberg, 1994; Heisenberg et al., 1985). Similar to the dynamics of memories in mammalian circuits, *Drosophila* exhibit both short-term memory that is protein-synthesis independent and long-term memory that depends on the synthesis of novel proteins. These distinct forms of memory are thought to be anatomically segregated within the mushroom body, with short-term memories processing in the medially-projecting γ lobe and long-term memories stored in the dorsal and medially-projection α and β lobes (Cervantes-Sandoval et al., 2013; Krashes et al., 2007; Trannoy et al., 2011).

The current model for associative learning in the mushroom body suggests that the convergence of the conditioned stimulus, coded by the odor-responsive KCs, and the unconditioned stimulus, carried by the reward- or punishment-responsive DANs, within the compartment of the MB alters KC-MBON synaptic transmission, leading to odor-specific changes in behavior (Cohn et al., 2015; Hige et al., 2015; Owald and Waddell, 2015; Owald et al., 2015; Séjourné et al., 2011). Behavioral experiments examining the temporal dependence for associative learning in *Drosophila* show that animals will form opposing olfactory associations depending on whether

the odor precedes a shock reinforcement or lags the shock reinforcement in time (Tanimoto et al., 2004). This form of bidirectional modulation of associative memories depending on timing is conserved in mammals and can be recapitulated using the artificial activation of the shock-responsive DANs innervating the MB by way of optogenetics (Aso and Rubin, 2016; König et al., 2018). This sensitivity to the timing of events suggests that animals are able to form distinct associations depending on the temporal relationships within their environment and suggests a synaptic or circuit based mechanism for determining the order of events lies within the MB circuitry.

1.6 Conservation of Molecular Pathways Involved in Learning

Over the past four decades, *Drosophila* behavioral neurogenetic screens have identified several proteins, conserved across species, that regulate dopamine signaling and are required for proper learning (Berry et al., 2012; Dudai et al., 1976; Kim et al., 2007; Levin et al., 1992; Livingstone et al., 1984; Tomchik and Davis, 2013). These proteins include dopamine receptors, adenylate cyclases, phosphodiesterases, and kinases among others (Tomchik and Davis, 2013). Two dopamine receptors highly expressed in the MB, DopR1 and DopR2, have both been shown to increase production of cAMP through *in vitro assays* (Han et al., 1996; Sugamori et al., 1995). However, mutant studies highlight a dual, opposing role for these receptors in regulating memory, in which DopR1 acts to promote memory formation (Kim et al., 2007; Qin et al., 2012) while DopR2 serves to degrade memory (Berry et al., 2012). The role of DopR2 as a memory suppressor suggests an active mechanism underlying the erosion of irrelevant memories that opposes the role of DopR1 in memory acquisition. However, how these two receptors work in

opposition at the synapse to drive memory acquisition and erosion is unknown and has never been probed using functional imaging or electrophysiological experiments.

Another learning mutant, *rutabaga,* involves a mutation in the calcium/calmodulin-sensitive catalytic domain of the type I-like adenylate cyclase protein, which has been suggested to act as a coincidence detector and underlie synaptic plasticity both in vertebrates and invertebrates (Gervasi et al., 2010; Kandel et al., 1983; Livingstone et al., 1984; Mons et al., 1999; Tomchik and Davis, 2009). These early genetic screens implicated additional genes involved in cAMP regulation or signaling such as *dunce,* a gene that encodes a cAMP phosphodiesterase, and the catalytic and regulatory domain of the cAMP dependent protein kinase-A (PKA) (Dudai et al., 1976; Goodwin et al., 1997; Skoulakis et al., 1993). In addition, a conserved role of NMDA receptors and the transcription factor, CREB, have been proposed to play a role in long-term memory regulation in *Drosophila* (Xia et al., 2005; Yin et al., 1994). Although the behavioral contribution of these genes in learning has been extensively studied in *Drosophila*, their functional role in synaptic plasticity remains elusive.

1.7 Linking Neural Plasticity and Learned Behavior

A central goal in the study of learning and memory has been to link changes in neural activity to the emergence of learned behavior. This has been difficult due to a mismatch in the relevant timing for STDP and modulation observed at the behavioral level. Heterosynaptic plasticity arising from neuromodulation has been suggested as a mechanism to extend the temporal requirements for STDP to a behaviorally relevant timescale (Cassenaer and Laurent, 2012). In

addition, recent work has suggested that non-Hebbian plasticity mechanisms, involving multi-second calcium plateaus, play a role in shaping synaptic plasticity in hippocampal place cells (Bittner et al., 2017).

In the last several years, a number of experiments have examined the temporal requirements for synaptic plasticity in the MB using conditioning paradigms relevant for animal behavior. The compartmentalized organization of the MB means that DANs can independently tune the strength of KC-MBON synapses within each compartment (Berry et al., 2018; Cohn et al., 2015; Hige et al., 2015; Owald et al., 2015), reweighting the net activity of the output population to bias an animal's attraction to odor through learning. Indeed, pairing of an odor with DAN activation has been shown to drive depression of KC-MBON synapses (Berry et al., 2018; Cohn et al., 2015; Hige et al., 2015; Owald et al., 2015; Séjourné et al., 2011), weakening the MBON's response to the conditioned odor. While conditioning with shock-responsive DANs depresses the odor responses of MBONs that drive attraction, pairing an odor with activation of the sugar-responsive DANs depresses the responses of MBONs that mediate avoidance (Aso et al., 2014b). Together, these experiments suggest that the clear delineation in the valence of DANs and MBONs across the MB architecture permits appetitive and aversive experiences to drive either odor approach or odor avoidance through a unified plasticity rule of depression within the compartment innervated by the activated DANs. The ability to use similar conditioning paradigms to induce neural plasticity that also function to drive learned-changes in behavior offers the promising opportunity to directly relate changes in neural activity to the emergence of learned behaviors.

While the coding properties of odors among KCs together with the compartmentalized wiring pattern of MBONs and DANs along the output lobes clearly allows *Drosophila* to contextualize a wide-array of odors as a result of conditioning, two significant questions remain: 1) how is temporally sensitivity achieved in these learning circuits and 2) how do animal's update neural plasticity and alter their behavior when a learned association is re-contextualized. My thesis aims to address these two questions through experiments that combine high-resolution behavioral analysis with functional imaging at identifiable synaptic sites to investigate how the *Drosophila* MB detects the precise temporal ordering of events to extract meaningful relationships from the environment and update associations as the temporal relationship between events is altered. The work presented in subsequent chapters shows that flies can write opposing olfactory associations on a trial-by-trial basis depending on the relative timing of odor cues and a dopaminergic reinforcement, recapitulating the bidirectional behavior described earlier. In addition, use of a novel closed-loop olfactory system to monitor neural activity as an animal navigates in a virtual olfactory environment, reveals that these bidirectional changes in odor tracking correlate with bidirectional changes in KC-MBON signaling within a compartment, linking plasticity at identified synapses to the emergence of learned behavior. Furthermore, I show that the temporal specificity of this circuit relies on two dopamine receptors that couple to distinct intracellular signaling cascades and play opposing roles in regulating KC-MBON synaptic strength. Loss of either receptor renders the synapses of the mushroom body capable of only unidirectional plasticity, preventing this behavioral flexibility. By examining dopamine receptor second messenger signaling, neural plasticity, and behavioral plasticity on the same timescales, these experiments reveal how biochemical pathways confer temporal sensitivity to this circuit, allowing animals to maintain accurate predictions in a changing environment.

Chapter 2

Event Timing Instructs Opposing Olfactory Associations

2.1 Introduction

Despite a half-century of work on associative learning in *Drosophila melanogaster,* few experiments have explored the full range of temporal relationships that give rise to learned behaviors. Most often experiments focus on the behavioral effect of presenting an odor and reinforcement either synchronously or with the odor slightly preceding the reinforcement in time (forward pairing). Forward pairing is used to examine whether an animal is able to learn that the CS+ is predictive and correlated with the reinforcement. However, a number of experiments in animals have demonstrated that animals are able to use a larger variety of temporal relationships to instruct distinct associations (Gerber et al., 2019; 2014). Additionally, most experiments in *Drosophila* measure learning in a preference assay in which the preference for the paired odor (CS+) is compared to the preference for an unpaired odor (CS-) as an aggregate value from a large number of flies. From these experiments it is difficult to appreciate 1) how individual animals change their behavior to the conditioned odor since measurements are only observed at the population level, 2) the dynamics for how animal behavior changes due to conditioning since preferences are assessed only as an end-point measurement, and 3) how the behavior to the conditioned and unconditioned odor is specifically altered in individual animals given these assays only measure relative preference between the odor pair.

In addition, to contend with a complex and dynamic environment, animals must be able to re-contextualize an association as the environmental conditions are altered. Experiments across a variety of animals have suggested that animals are capable of learning an association after a single conditioning trial, a process called single-shot learning (Lee et al., 2015). This type of learning is distinct from gradual learning, in which an animal acquires knowledge slowly over time as a result of trial and error and repeated exposure. While single-shot learning is ideal in allowing animals to rapidly adapt behaviors as a result of a salient or recent experience, it may also be detrimental in a complex and dynamic environment causing animals to associate a sensory stimulus that is only briefly correlated with the salient experience but is not truly causally related. While experiments have explored how the repeated presentation of the CS+ without reinforcement leads to extinction, a process believed to involve the re-evaluation of the odor and formation of a new association in which the odor is now is associated with a lack of reinforcement (Felsenberg et al., 2017; 2018), few experiments have examined how changing the temporal relationship between the conditioned and unconditioned stimulus alters a learned association. In the following chapter, I describe how the use of a novel chamber design has revealed new insights into how the event timing of conditioning instructs bidirectional behavior to the conditioned odor.

2.2 The Development of a Behavior Chamber for Odor Tracking

To explore how *Drosophila* adapt to changes in the temporal structure of their environment, we developed methods to monitor the olfactory preferences of flies over long periods of time while

precisely varying the timing of odor stimuli and dopaminergic reinforcement. To do this, Thomas Graham, a former post-doc in the lab, designed clear chambers, containing a central empty chamber (20 mm x 50 mm) flanked by two manifolds. Narrow channels were etched between the manifolds, permitting airflow between the chamber and the manifolds while confining flies within the central chamber. Two valves were used to control the direction of airflow, and additional valves were used to switch between clean air and different odors (Figure 2.1A). The ability to switch the direction of airflow between odor presentations allowed for repeatedly testing odor-tracking behaviors in the same individual animals over multiple trials. The chambers were imaged from above with a string of LEDs arrayed below a transparent platform, permitting the use of optogenetics in place of using food reward or shock punishment as reinforcements.

A common navigational strategy many animals employ is to reorient and increase their upwind velocity when they encounter an attractive olfactory plume (Cardé and Willis, 2008), as this will lead them to the odor source. Indeed, we see that an individual animal will exhibit robust upwind tracking in response to the appetitive odor, apple cider vinegar (ACV), evident from visualizing the animal's trajectory prior to and after the onset of the odor (Figure 2.1B). A distinct advantage of this chamber design and assay, in contrast to traditional paradigms like the T-maze, is that it allows for repeated training and testing of the same individuals over several hours, permitting longitudinal examination of how odor attraction is altered in response to an animal's ongoing experience. In addition, high-resolution behavioral tracking allows us to specifically explore how animal behavior is altered to the conditioned odor.

Figure 2.1, Novel Behavioral Assay for Tracking Odor Behaviors
(A) Illustration of chamber assay showing how airflow switches across manifolds between odor presentations to come from the top or bottom of chamber on alternating odor presentations. Additional valves were used to switch air flow from glass bottle containing water to an odor-containing bottle. **(B)** Behavior of an individual animal in a chamber. Odor and wind direction is marked by the white arrow. The trajectory of the animal from 3 seconds prior to odor onset to 3 seconds following odor onset was plotted. When the animal is presented with the appetitive odor apple cider vinegar, it re-orients and tracks the odor plume upwind.

Figure 2.1

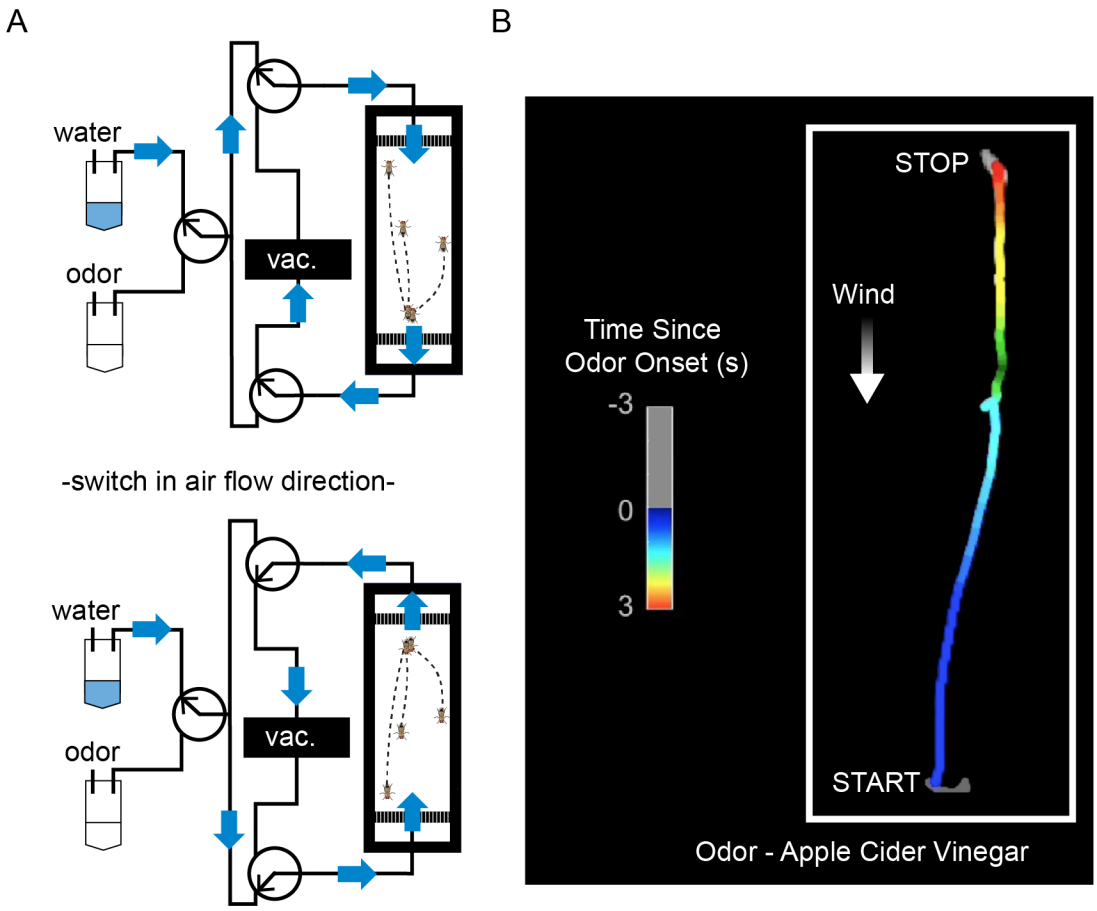
A
water
odor
vac.
-switch in air flow direction-
water
odor
vac.
B
Time Since
Odor Onset (s)
-3
0
3
STOP
Wind
START
Odor - Apple Cider Vinegar

2.3 Timing of Events Tunes Punishment and Reward

We began by asking whether we could suppress the innate attraction to ACV by pairing it with optogenetic activation of the PPL dopaminergic neurons that are responsive to punitive cues, such as electric shock, and are sufficient to drive aversive memory formation (Aso and Rubin, 2016; Aso et al., 2010; 2012; Claridge-Chang et al., 2009; König et al., 2018). To assess how odor tracking behavior was altered as a result of the timing of associative conditioning, we placed a small cohort of 4-7 flies in a chamber in constant laminar air flow and analyzed their walking trajectories in response to a brief (2 sec) pulse of the inherently appetitive odor, apple cider vinegar (ACV). We used an intersectional genetic strategy (Aso and Rubin, 2016) to selectively express the light-activated ion channel, CsChrimson, in a subset of PPL neurons innervating six compartments of the mushroom body (Figure 2.2A), allowing for temporally precise, light-evoked dopaminergic reinforcement. After just a single forward conditioning trial, in which the ACV stimulus preceded the onset of PPL activation, flies showed significantly reduced upwind tracking to the odor in a subsequent test trials (Figure 2.2B). This aversive conditioning resulted in both fewer flies tracking upwind in response to the odor and an overall decrease in their upwind velocity (Figures 2.2B-C). While a majority of olfactory memory experiments use neutral odors as the CS+, the strong decrease in attraction to the 'innately' appetitive food odor, ACV, suggests that associative conditioning in the MB is sufficient to suppress and override innately attractive cues whose valence is thought to be determined by processing in the distinct neural circuitry of the lateral horn in the *Drosophila* brain. This suggests an interesting interplay between hard-wired and learned behaviors in the regulation of odor behaviors (Keene and Waddell, 2007; Masse et al., 2009).

The attenuated attraction to ACV after forward conditioning persisted for at least 20 minutes—a short-term memory in the life of a fly—with little erosion due to passive decay or extinction by repeated presentation of the conditioned odor without reinforcement (Figure 2.2D). The strength of this association further underscores that a single aversive reinforcement can drive lasting behavioral modulation.

However, we found that if the same animals subsequently experienced a single backward conditioning trial, in which ACV instead followed PPL stimulation, the weakened attraction was immediately reversed, rendering flies strongly attracted to the odor again (Figures 2.2B-C and 2.2E). This suggests that the MB is incredibly plastic, instructing rapid changes in animal behavior depending on the current temporal relationships in the environment. This reversible plasticity provides an adaptive mechanism allowing animals to rapidly re-contextualize an olfactory association as temporal relationships are altered. Without this capacity for updating associations animals may be stuck with an association that does not properly reflect meaningful relationships in their environment.

Indeed, interleaving forward and backward pairing reliably modulated the animals' attraction to ACV for 50 conditioning trials. Plotting the upwind displacement of animals over time generated a saw-tooth pattern, as their upwind tracking was alternately suppressed or enhanced with each conditioning trial (Figures 2.3A-B). This systematic behavioral modulation was not evident in control animals, in which light alone had a minimal effect on behavior (Figures 2.3C-D). Flies therefore have the capacity to write and update odor associations on a trial-by-trial basis if the

Figure 2.2, Timing of Punishment Leads to Rapid Reversals in Odor Attraction

(A) Anatomy of PPL (teal; MB504B split-Gal4 line) (left). Innervation within mushroom body neuropil and schematic of compartmentalized innervation in the mushroom body lobes (right). (**B**) Top: behavioral protocol to compare tracking of apple cider vinegar (ACV) odor after forward pairing (FP) and backward pairing (BP) with optogenetic activation of PPL DANs (top). In baseline, post-forward pairing, and post-backward pairing trials, animals experienced two odor presentations—one originating from the top of the chamber and one from below and the upwind velocities and displacements for these two odor presentations were averaged together. Bottom: trajectories of individual flies from one representative experiment, aligned to common origin and wind direction. Flies that did not move in response to the odor were positioned at origin. The upwind displacement of all flies in the odor measured as change in the center of mass is shown at right (teal) (see methods). (**C**) Upwind velocity of flies in baseline trials, post-forward pairing trials, and post-backward pairing trials (odor indicated with gray box) measured by tracking the change in the center of mass of flies over the course of a trial. Representative example from (B) is plotted in teal. N = 8 with 6 animals per experiment; mean in bold and individual experiments in thin lines. (**D**) Left: Average upwind displacement for flies in odor (apple cider vinegar, ACV) during 3 baseline trials and 15 trials following a single forward pairing (FP) of ACV with optogenetic activation of PPL DANs (post-forward pairing trials highlighted with gray background). Right: Raster of average upwind velocity of flies for the corresponding trials. 2-s odor presentation noted above raster. (**E**) Left: Same as in (D) except that after a single post-forward pairing trial animals were trained with a single backward pairing (BP). Right: Raster of average upwind velocity of flies for the corresponding trials. Significance is indicated as follows: *** $p \leq 0.001$, ** ≤ 0.01, NS ≥ 0.05, paired t-test with Bonferroni correction. For (D-E) n = 11 experiments with 6 animals per experiment, mean ± SEM. Black arrowheads mark when forward pairing and backward pairing was performed.

Figure 2.2

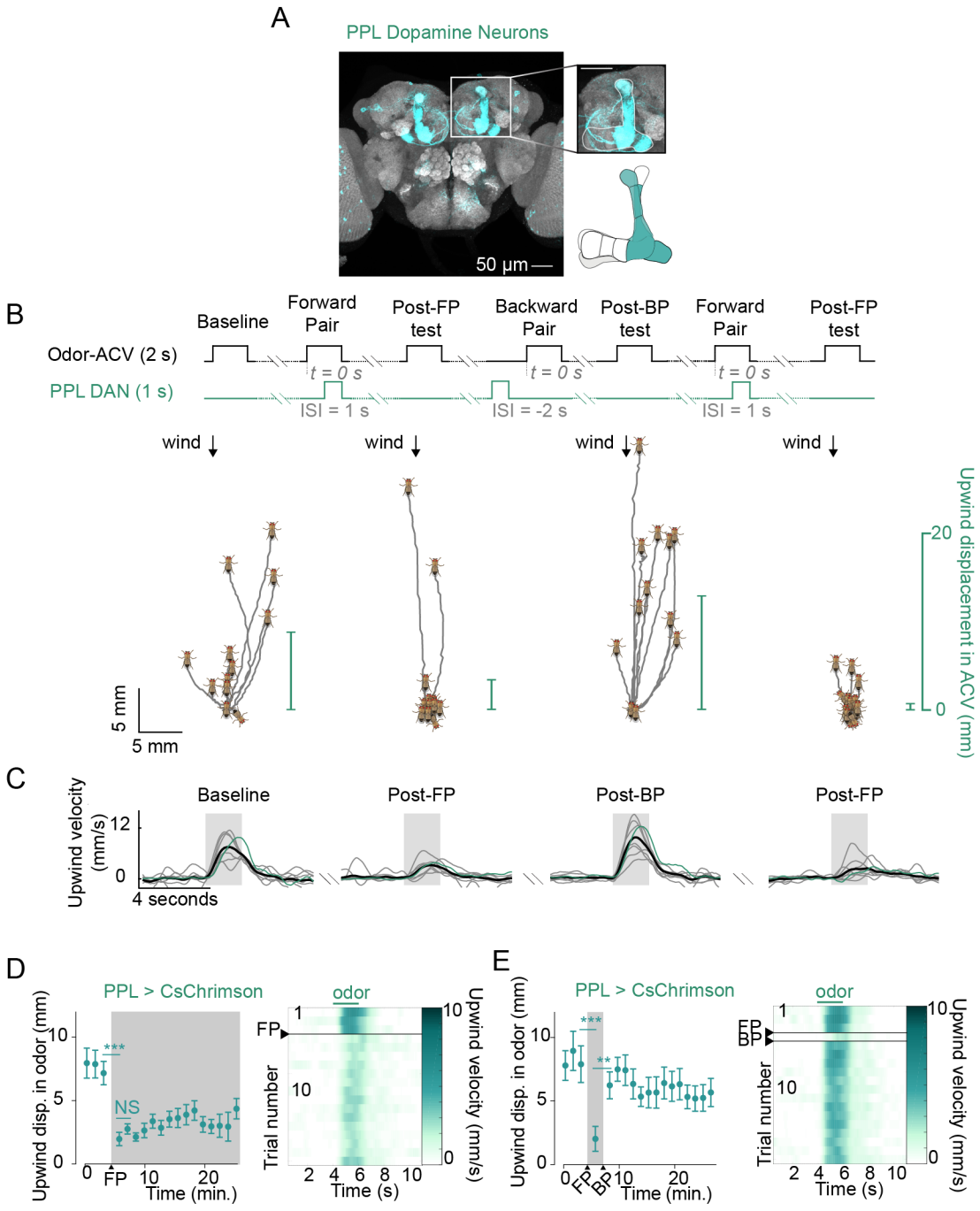
A
PPL Dopamine Neurons
50 µm
B
Baseline
Forward Pair
Post-FP test
Backward Pair
Post-BP test
Forward Pair
Post-FP test
Odor-ACV (2 s)
PPL DAN (1 s)
t = 0 s
ISI = 1 s
ISI = -2 s
ISI = 1 s
wind
5 mm
5 mm
Upwind displacement in ACV (mm)
20
0
C
Upwind velocity (mm/s)
12
0
4 seconds
Baseline
Post-FP
Post-BP
Post-FP
D
PPL > CsChrimson
Upwind disp. in odor (mm)
10
5
0
***
NS
0
FP
10
20
Time (min.)
odor
1
10
FP
10
Trial number
2 4 6 8 10
Time (s)
Upwind velocity (mm/s)
E
PPL > CsChrimson
Upwind disp. in odor (mm)
10
5
0
***
**
0
FP
BP
10
20
Time (min.)
odor
1
10
FP
BP
10
Trial number
2 4 6 8 10
Time (s)
Upwind velocity (mm/s)

Figure 2.3, Forward and Backward Pairing Modulate Behavior on a Trial-By-Trial Basis. (**A**) At left, raster plot of average upwind velocity of flies across trials using the same protocol as in Figure 2.2B. The first row in the raster corresponds to the baseline trial. Subsequent rows correspond to trials after alternating forward or backward pairing trials (total of 25 forward pairing and 25 backward pairing trials across each experiment). At right, upwind displacement during odor presentation for the corresponding row in the raster plot, mean ± SEM. (**B)** Change in upwind displacement in odor after forward and backward pairing for PPL conditioned animals. The change in upwind displacement was measured relative to the preceding odor trial. Each data point represents the mean change in displacement after the 25 forward pairing trials (post-FP) or 25 backward pairing trials (post-BP) in each experiment. (**C**) Raster plot of average upwind velocity of flies (left) and mean ± SEM upwind displacement (right) as in (A) except using UAS-CsChrimson flies lacking a Gal4 driver. (**D**) Change in upwind displacement in odor same as in (B) except using UAS-CsChrimson flies lacking a Gal4 driver. n = 8 experiments with 6 flies per experiment for all genotypes, mean ± SEM. Significance for change in upwind displacement post-FP and post-BP across all genotypes is indicated as follows: *** $p \leq 0.001$, * $p < 0.05$, NS ≥ 0.05; one-sample t-test against zero with Bonferroni correction.

Figure 2.3

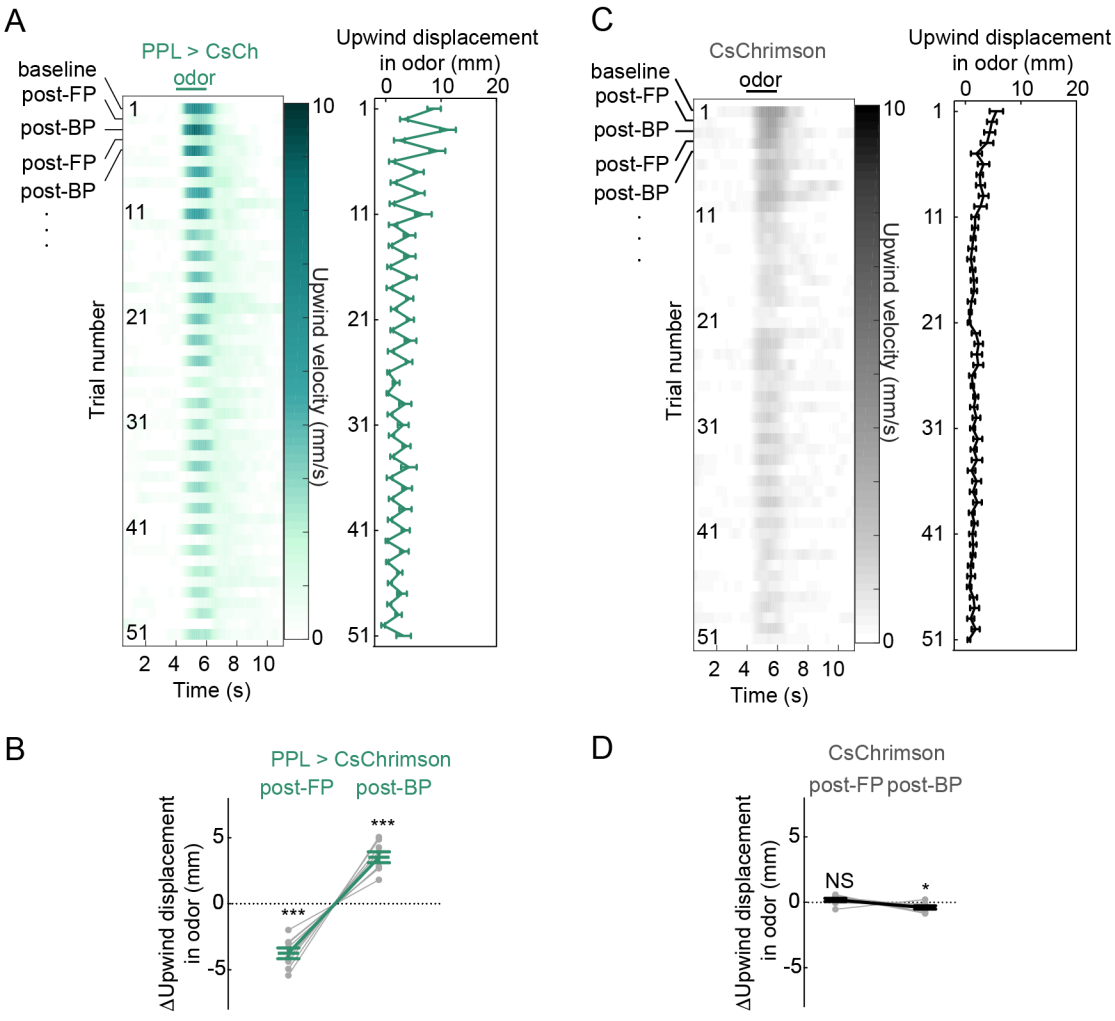
A
PPL > CsCh
odor
baseline
post-FP
post-BP
post-FP
post-BP
Trial number
Time (s)
Upwind velocity (mm/s)
Upwind displacement
in odor (mm)
C
CsChrimson
odor
B
PPL > CsChrimson
post-FP post-BP
ΔUpwind displacement
in odor (mm)
D
CsChrimson
post-FP post-BP
NS

predictive value of an odor changes. Furthermore, the reversal in odor tracking with forward and backward conditioning parallels previous observations that animals will avoid odors that predict punishment but become attracted to odors associated with its termination (Aso and Rubin, 2016; König et al., 2018; Tanimoto et al., 2004).

Similar to reinforcement circuits in the mammalian brain, the DANs of *Drosophila* are heterogeneous in their response profiles to punishing and rewarding experiences. While experiments in *Drosophila* have explored how punishment can instruct both avoidance and attraction behavior depending on the temporal structure of conditioning, the question of whether dopamine neurons that convey reward to the MB are able to similarly instruct opposing associations depending on timing has not yet been explored.

To examine this we asked whether olfactory associations could be similarly reversed via optogenetic activation of the PAM cluster of dopaminergic neurons that encode rewarding stimuli and drive appetitive learning (Aso and Rubin, 2016; Burke et al., 2012; Liu et al., 2012) (Figure 2.3A). Forward pairing of ACV with PAM activation modestly enhanced the upwind tracking of ACV in naïve animals (Figure 2.3B). However, a single backward conditioning trial after forward pairing or even from a naïve state suppresses odor tracking far below the baseline of naïve animals (Figures 2.3B and D). This suggests that backward pairing can overwrite the innate attraction to ACV if the odor becomes associated with the cessation of reward. In addition, this suggests the backward pairing does not simply modulate behavior by eroding a prior association, but instead instructs a new association with a valence opposite to that of the

Figure 2.4, Timing of Events Turns Reward Into Punishment

(**A**) Anatomy of PAM (teal; MB042B split-Gal4 line) (left). Innervation within mushroom body neuropil and schematic of compartmentalized innervation in the mushroom body lobes (right). (**B**) At left, raster plot of average upwind velocity of flies across trials using PAM DANs expressing CsChrimson for training. The first row in the raster corresponds to the baseline trial. Subsequent rows correspond to trials after alternating forward or backward pairing trials (total of 25 forward pairing and 25 backward pairing trials across each experiment). Timing of forward and backward pairing same as indicated in Figure 2.2B. At right, upwind displacement during odor presentation for the corresponding row in the raster plot, mean ± SEM. (**C**) Change in upwind displacement in odor same as in (Figure 2.3B) except using PAM > CsChrimson flies. n = 8 experiments with 6 flies per experiment for all genotypes, mean ± SEM. Significance for change in upwind displacement post-FP and post-BP across all genotypes is indicated as follows: *** $p \leq 0.001$, * $p < 0.05$, NS ≥ 0.05; one-sample t-test against zero with Bonferroni correction. (**D**) Upwind displacement in odor in a single baseline trial and following a single backward pairing (post-BP) trial of ACV paired with optogenetic activation of PAM DANs. n = 8 experiments with 5-7 flies per experiment, mean ± SEM. Statistical significance for difference in upwind displacement between baseline and post-BP is indicated as follow ** $p \leq 0.01$; paired t-test.

Figure 2.4

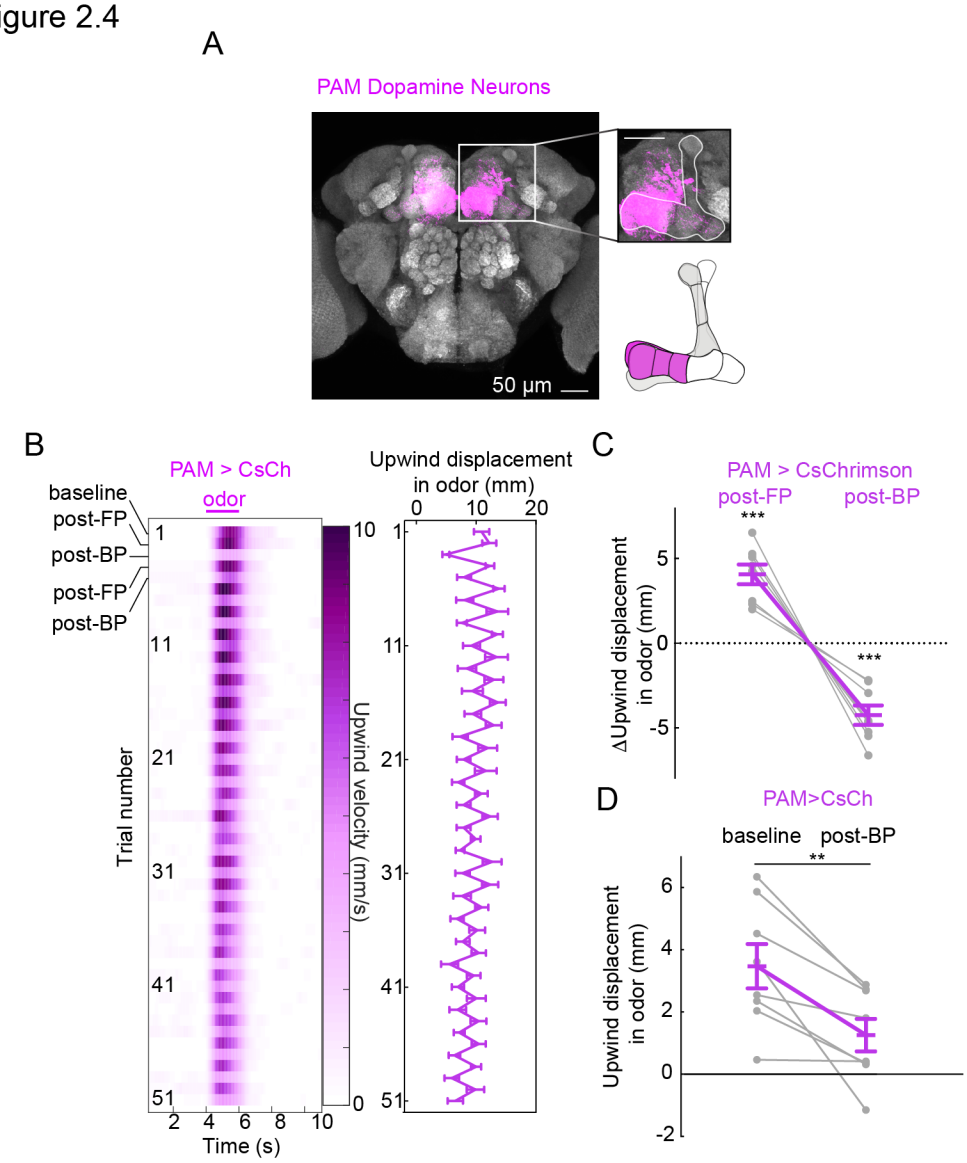
A
PAM Dopamine Neurons
50 µm
B
PAM > CsCh
odor
baseline
post-FP
post-BP
post-FP
post-BP
Trial number
Time (s)
Upwind velocity (mm/s)
Upwind displacement in odor (mm)
C
PAM > CsChrimson
post-FP
post-BP
ΔUpwind displacement in odor (mm)
D
PAM>CsCh
baseline
post-BP
Upwind displacement in odor (mm)

reinforcer. As with PPL conditioning, alternating forward and backward pairing of ACV with PAM activation modulated odor attraction with each trial, enhancing upwind tracking after forward pairing and suppressing tracking after backward pairing (Figures 2.3B-C). Thus both PAM and PPL DANs are sufficient to bidirectionally modify behavior such that activation of either dopaminergic population can produce appetitive or aversive associations depending on the relative timing of the dopaminergic reinforcement to an odor cue.

2.4 High-Resolution Analysis of Learned Behaviors

Associative conditioning allows animals to adapt their behaviors in order to maximize reward and minimize punishment. However, the actions that animals take to achieve this goal are varied. Animals have evolved behavioral responses to contend with inherently fearful or rewarding experiences. For example, when fearful, animals show a startle response and freeze for a period of time before deciding to stay in position or run away if an escape route is available (LeDoux, 1996; Phelps and LeDoux, 2005). Interestingly, it is thought that escape, or active avoidance, is mediated through distinct and opposing neural circuits than drive freezing, highlighting the complex neural circuit interactions governing these adaptive behaviors (Moscarello and LeDoux, 2013). On the other hand, when presented with a food reward, animals exhibit enhanced arousal and increased locomotion in preparation for the imminent intake of food (Mistlberger, 1994). Following associative conditioning, animals express these adaptive behavioral responses to the reinforced conditioned stimulus in the anticipation of reward or punishment. In *Drosophila*, appetitive and aversive memories are most often assessed through end-point preference assays in which flies are able to choose between the CS+ and CS-. While this analysis provides a simple

metric for learning, it obscures insight into the behaviors the animal adopted to the CS+ as a result of associative conditioning.

The analysis used in previous figures 2.2-2.4 assessed animal behavior by measuring the upwind velocity of the center of mass of the entire population of 4-7 flies within an individual chamber. While the use of this single metric offers simplicity and clarity in the analysis of animal behavior, we were interested in determining the specific aspects of animal behavior that are modulated as a result of conditioning. To more thoroughly examine animal behavior in this chamber assay, we analyzed the trajectories of each individual animal within a chamber and tracked their speed along the wind axis and the cross-wind axis, the velocity upwind and crosswind, as well as the fraction of animals within a chamber walking upwind, downwind, or crosswind during the odor and the fraction of animals that remained stationary during the odor (Figures 2.5A-H).

In comparing these behavioral parameters, we observe that a number of metrics are bidirectional modulated by forward and backward pairing with the most strongly affected parameters being speed and velocity along the axis of air and odor (Figures 2.5A and 2.5 C) and the fraction of animals walking upwind (Figure 2.5E) and stationary during the odor (Figure 2.5H). Forward pairing with PPL activation or backward pairing with PAM activation both decrease the fraction of animals walking upwind and increase in the fraction of flies stationary, suggesting that animals exhibit a decreased mobilization in situations where they can not escape an unpleasant

Figure 2.5, Forward and Backward Pairing Modulate Numerous Behavioral Metrics
(**A-J**) Behavioral analysis comparing behavioral metrics affected by forward (post-FP) and backward (post-BP) pairing in PPL > CsChrimson and PAM > CsChrimson animals. Left traces represent average behavior over duration of trial including pre-odor, odor, and post-odor period. Right graphs represent average behavioral response in the odor. (**A**) Directional information of X and Y axis relative to air/odor flow in behavioral chambers. (**B**) Speed in the Y direction (upwind or downwind) for all animals. (**C**) Speed in the Y direction only for animals moving (>1 pixel/s or 0.3mm/s). (**D**) Upwind velocity for all animals. (**E-F**) Speed in the X direction (left or right) (E) and crosswind velocity for all animals (F)**.** (**G**) Fraction of animals walking upwind. (**H**) Fraction of animals stationary. (**I**) Fraction of animals walking downwind. (**J**) Fraction of animals walking crosswind. Mean ± SEM, n = 8 experiments for PPL and PAM with 6 flies per experiment. See methods for details in behavioral analysis. Significance for difference in behavior post-FP and post-BP for both PPL > Chrimson and PAM > Chrimson animals were tested using Wilcoxon match-paired sign rank test: ** ≤ 0.01, NS p ≥ 0.05.

Figure 2.5

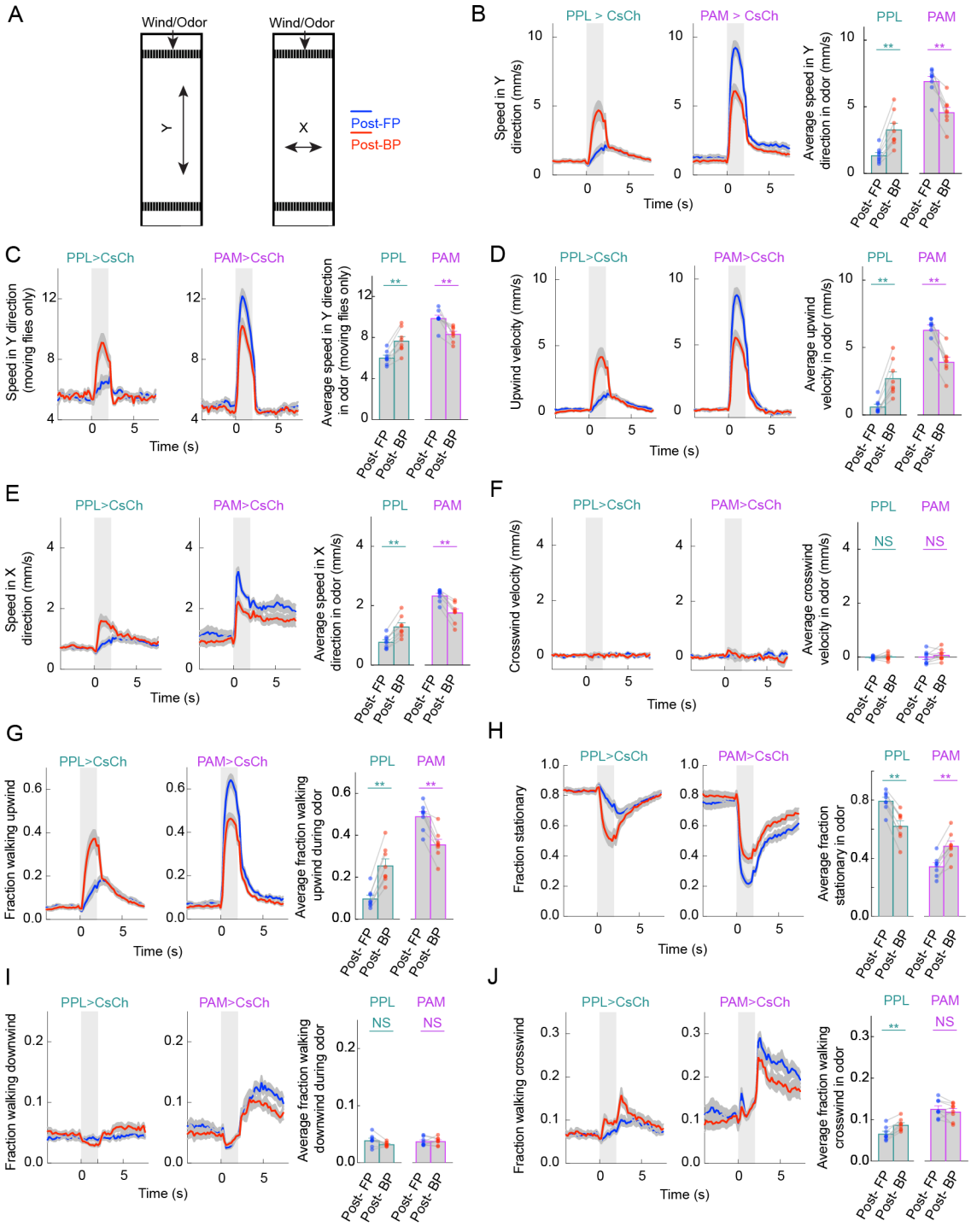
A
Wind/Odor
Wind/Odor
Y
X
Post-FP
Post-BP
B
PPL > CsCh
PAM > CsCh
Speed in Y direction (mm/s)
Time (s)
PPL
PAM
Average speed in Y direction in odor (mm/s)
Post- FP
Post- BP
C
PPL>CsCh
PAM>CsCh
Speed in Y direction (moving flies only)
Average speed in Y direction in odor (moving flies only)
D
Upwind velocity (mm/s)
Average upwind velocity in odor (mm/s)
E
Speed in X direction (mm/s)
Average speed in X direction in odor (mm/s)
F
Crosswind velocity (mm/s)
Average crosswind velocity in odor (mm/s)
NS
G
Fraction walking upwind
Average fraction walking upwind during odor
H
Fraction stationary
Average fraction stationary in odor
I
Fraction walking downwind
Average fraction walking downwind during odor
J
Fraction walking crosswind
Average fraction walking crosswind in odor

experience. While it is possible for animals in these chambers to track downwind in conditioned odor, we do not see an increase in this behavioral response following aversive experiences. This is in contrast to preference assays, in which animals track downwind in the CS+ and approach the CS- upwind after aversive conditioning (Claridge-Chang et al., 2009). This high-resolution analysis of behavior in response to the conditioned odor reveals a conserved behavioral strategy for contending with an aversive odor reinforced either through forward pairing with PPL or backward pairing with PAM DANs.

2.5 Backward Pairing Instructs a Distinct Memory

The Rescorla-Wagner model of associative conditioning expanded on Pavlov's observations to suggest that the strength of an association depends on how predicted the unconditioned stimulus is by the conditioned stimulus and propose that animals attend to changes in contingency to modify prior associations (Rescorla, 1971). This model, proposed by Robert Rescorla and Allan Wagner in 1972, was used to explain the process of memory erosion by way of a change in contingency between the CS and US. A change in contingency can include the decoupling of the CS and US, or by varying the relationship from a positive contingency (CS predicts an increase in the probability of US occurring or forward pairing) to a negative contingency (CS predicts a decrease in the probability of US occurring or backward pairing), or vice versa. However, how these changes in contingency act mechanistically to update or erode an association is unclear.

The discovery of reward prediction errors in the mammalian midbrain dopamine neurons added further weight to the model, providing a neural circuit basis to allow animals to update and

change associations as the contingencies between the CS and US are altered over time. Additional work in *Drosophila* and rodents suggested that the process of memory erosion due to decoupling of the CS and US arises from the formation of a parallel opposing memory and relies on neural circuitry and molecular pathways distinct for those involved in the initial learning (Berman and Dudai, 2001; Bouton, 2004; Felsenberg et al., 2018; Shuai et al., 2010). However, these experiments challenged long-term memories with an extinction protocol in which the memory was re-activated with the CS+ hours to days after the initial memory was formed, a timescale much longer than the rapid reversals in behavior we see on the minute timescale with backward pairing. In addition, most behavioral or functional assays used to assess memory erosion and decay examine the effects only of memory re-activation with an unpaired presentation of the CS+ or US, limiting insight into potentially distinct forms of memory re-evaluation resulting from different changes in contingency (Aso and Rubin, 2016; Berry et al., 2012; Bouton, 2002; Felsenberg et al., 2017; 2018).

We were interested in testing whether backward pairing resulted in behavioral reversals distinct from the effect of decoupling the odor and DAN reinforcement. To explore this, we compared the effects of backward pairing to the re-exposure of the conditioned odor alone or the unpaired activation of the DANs alone. In our assay neither odor re-exposure nor DAN re-activation alone was sufficient to drive the strong bidirectional modulation of behavior observed with backward pairing (Figures 2.6A-B). Activation of PAM DANs weakly dampened odor tracking, consistent with the idea that dopamine release in the absence of an odor can actively erode past associations (Berry et al., 2012; 2015; Cohn et al., 2015), but this effect was significantly weaker than the modulation that ensued from backward pairing (Figure 2.6C).

Figure 2.6, Modulation by Backward Pairing Depends on Convergence of Odor and DAN
(**A**) Top: Behavioral protocol to test for memory erosion by re-exposure to odor alone. Protocol for training was similar to Figure 2.2B except that instead of backward pairing animals experienced 2-s re-exposure to ACV odor (Odor Alone) during the training trial. Animals experienced a total of 25 forward pairing (FP) and 25 Odor Alone trials in alternating succession across each experiment. Bottom: Average raster plot of upwind velocity of flies (left) and mean ± SEM upwind displacement in ACV odor (right). Training with PPL DANs expressing CsChrimson (PPL > CsCh) shown in teal; training with PAM DANs expressing CsChrimson (PAM > CsCh) shown in magenta. (**B**) Same as in Figure 2.2B, except instead of backward pairing animals experienced 1-s LED illumination to re-activate DANs expressing CsChrimson (DAN Alone). (**C**) Mean change in upwind displacement post-forward pairing (FP), post-backward pairing (BP), post-Odor Alone (Odor), and post-DAN Alone (DAN) for PPL > CsCh (teal) and PAM > CsCh (magenta) animals. Experiments where forward pairing and backward pairing alternate (left) are compared to experiments where forward pairing and Odor Alone alternate (middle) and where forward pairing and DAN Alone alternate (right). Odor Alone (Odor) and DAN alone (DAN) lead to weaker modulation of behavior than backward pairing (BP) for both PPL > CsCh (teal) and PAM > CsCh (magenta), mean ± SEM, n = 7-8 experiments with 5-7 flies per experiment for all genotypes. Statistical significance for difference from BP is indicated as follows ** $p \leq 0.01$, *** ≤ 0.001; Mann-Whitney test with Bonferroni correction.

Figure 2.6

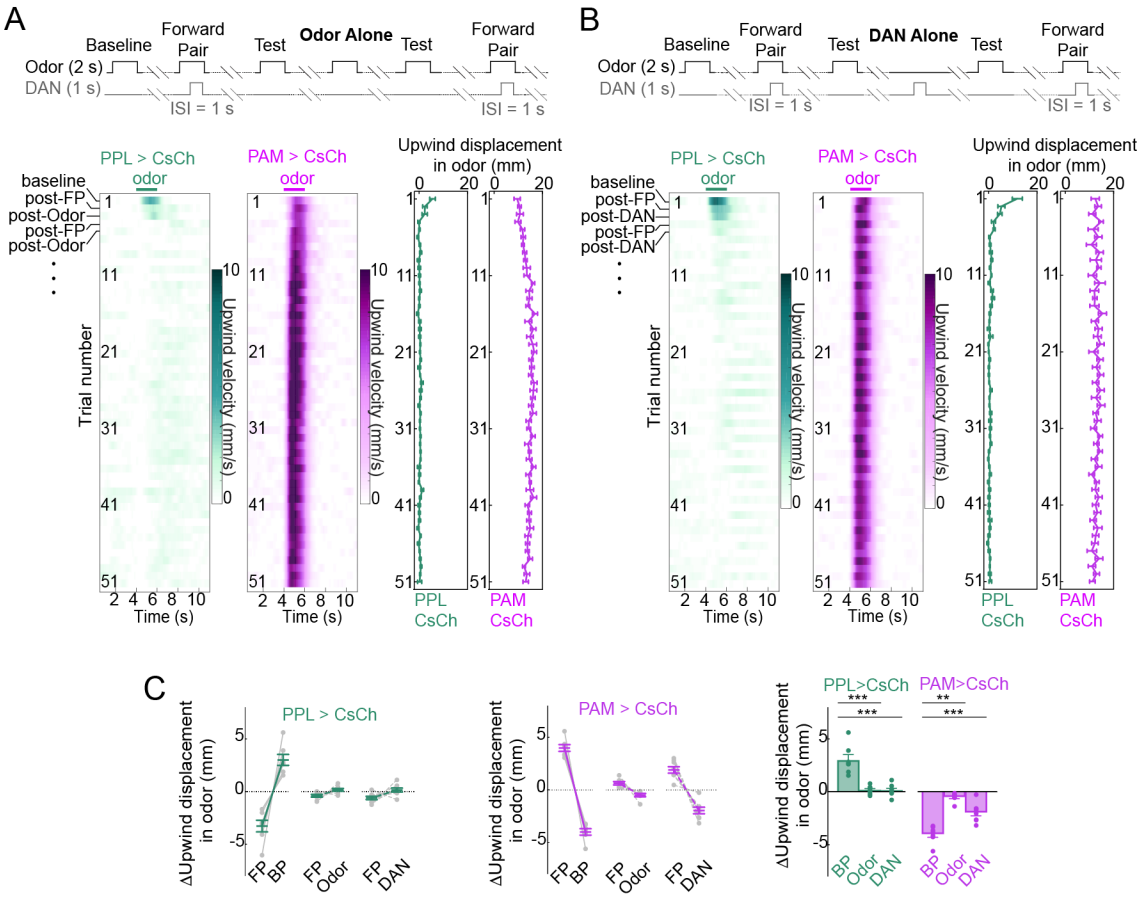
A
Baseline
Forward Pair
Test
Odor Alone
Test
Forward Pair
Odor (2 s)
DAN (1 s)
ISI = 1 s
ISI = 1 s
PPL > CsCh
PAM > CsCh
odor
baseline
post-FP
post-Odor
post-FP
post-Odor
Trial number
Upwind velocity (mm/s)
Time (s)
Upwind displacement in odor (mm)
PPL CsCh
PAM CsCh
B
Baseline
Forward Pair
Test
DAN Alone
Test
Forward Pair
Odor (2 s)
DAN (1 s)
ISI = 1 s
ISI = 1 s
PPL > CsCh
PAM > CsCh
odor
baseline
post-FP
post-DAN
post-FP
post-DAN
Trial number
Upwind velocity (mm/s)
Time (s)
Upwind displacement in odor (mm)
PPL CsCh
PAM CsCh
C
PPL > CsCh
PAM > CsCh
ΔUpwind displacement in odor (mm)
FP BP
FP Odor
FP DAN
PPL>CsCh
PAM>CsCh
***
***
**
***
BP
Odor
DAN

These observations reveal that the reversal of an association by backward pairing requires input from both olfactory and dopaminergic pathways and suggests that the convergence of olfactory and DAN input to the mushroom body conveys information about their causal relationship offering a mechanism to more rapidly update a memory when temporal relationships change. Together, our results suggest that the memory erosion by backward pairing reflects the formation of a new memory in which the odor, once predictive of a reinforcement, is now associated with its termination.

2.6 Discussion

In order to make meaningful predictions about the likelihood of events occurring, animals use the temporal structure of their environment to learn novel associations between events. This sensitivity to timing allows animals the capacity to approach things associated with reward and avoid others instead associated with punishment or pain. Since Pavlov's seminal research on associative conditioning (Pavlov, 1927), scientists have debated the features of the environment that animals use to instruct meaningful associations and the statistics that they rely on to update or re-evaluate the utility of a prior memory (Rescorla, 1967). Specifically, the behavioral effects of backward pairing have been left unspecified due to conflicting results in which some experiments suggest backward pairing results in the opposite behavioral response to forward pairing (Moscovitch and LoLordo, 1968; Siegel and Domjan, 1971) while other results demonstrate the inverse effect (Heth and Rescorla, 1973). However, more recently, experiments have systematically explored the multiple temporal features an animal uses to inform

associations (Andreatta et al., 2012; 2015; Baxter and Byrne, 2006; Bergado Acosta et al., 2017; Davis et al., 2008; Davis, 2011; Dubnau and Tully, 2001; Gerber et al., 2004; 2019; Heisenberg, 2003; Lechner and Byrne, 1998; Mayer et al., 2018; Tanimoto et al., 2004).

Using the simple neural architecture of *Drosophila* and precise optogenetic activation of rewarding or punishment DANs, we explored the temporal dependence of associative learning and found that both rewarding and aversive DANs equivalently instruct the formation of appetitive and aversive associations, simply depending on the relative timing of events during conditioning. This is inline with previous results in *Drosophila,* revealing bidirectional behavior that depends on the timing of odor and shock punishment during conditioning (König et al., 2018; Tanimoto et al., 2004). Interestingly, we show that the 'innately' attractive food odor, ACV, could be rendered unattractive by either forward pairing with shock-responsive PPL DANs or backward pairing with the rewarding PAMs. This suggests the capacity of experience to overwrite the innate valence of an attractive odor cue. In line with this observation, recent anatomic and functional experiments have suggested that lateral horn neurons involved in innate attraction, receive input from mushroom body neurons, emphasizing a likely intimate connection between hard-wire and flexible circuits in dynamically regulating odor attraction behavior as a result of an animal's experience (Dolan et al., 2018).

Furthermore, we found a change from a positive contingency (forward pairing) to a negative contingency (backward pairing) was sufficient to instruct rapid reversals in attraction to the conditioned odor over the brief timescale of minutes. A number of studies have examined the molecular and circuit mechanisms for the re-evaluation of a learned association and have

suggested that the process occurs through a circuit-based mechanism, often involving the formation of a new, parallel association of opposing valence (Auchter et al., 2017; Quirk and Mueller, 2008; Shuai et al., 2015). Indeed, recent work in *Drosophila* has demonstrated that the extinction of a memory by repeated re-exposure to the conditioned odor induces plasticity in neural circuits that work to antagonize the neural correlate of the original memory (Felsenberg et al., 2017; 2018). In addition, research has suggested distinct mechanisms exist for the decay of memory that occurs with the passage of time and ongoing behavioral locomotion of an animal that involves bidirectional modulation within an individual compartment of the mushroom body and the distinct engagement of two dopamine receptors that work in opposition to regulate memories (Berry et al., 2012; Cohn et al., 2015). Together, these results highlight the complexity of mechanisms in how animals update and re-evaluate associations over a short and long timescale.

In contrast to these forms of memory re-evaluation, we show that the converging input of odor and DAN reinforcement is sufficient to rapidly reverse odor associations on the minute timescale. The rapidity with which animals update associations following backward pairing is in stark contrast to the hour-long process for memory re-evaluation that occurs with re-exposure to the CS+; these distinct timescales suggests backward pairing may rely on a distinct mechanism from the circuit mechanism proposed for memory re-evaluation following odor re-exposure. In addition, the observation that forward and backward pairing of an odor with activation of a single class of DANs is able to equivalently drive attraction or avoidance suggests an appealing model in which bidirectional neural plasticity within the individual compartments innervated by the reinforcing DANs reversibly modulates odor signaling through the MBONs. This type of

bidirectional plasticity would be distinct from other circuit models for memory re-evaluation and is a model I focus on in the following chapters.

Chapter 3

Linking Bidirectional Behavior with Neural Plasticity

3.1 Introduction

Linking changes in neural activity to measureable changes in behavioral responses has been a central goal across all fields of neuroscience. While offering sometimes only correlative insight, providing a direct link between neural responses and changes in hormone production, emotional state, and behavior provides a foothold for further untangling the complex relationship between the properties of brain circuits and our internal states, drives, and ultimately behaviors.

In both vertebrate and invertebrate brains, experiments have linked the location of a memory to specific brain centers through chemical and surgical ablation of specific brain regions (de Belle and Heisenberg, 1994; Milner and Penfield, 1955; Moyer et al., 1990; Ryou et al., 1998; Thompson, 2005). The use of electrophysiological recordings coupled with the advent of cell-type specific drivers provided the opportunity to more specifically link the processing of memory to identifiable cell types within a neural circuit. The discovery of long-term potentiation and depression (LTP and LTD) in the cerebellum and hippocampus, brain centers known to be central to learning and memory, sparked excitement among neurobiologist who recognized that this form of activity-dependent plasticity may serve as a readout, or engram, of the early stages of memory formation (Bliss and Lømo, 1973; Ito and Kano, 1982; Ito et al., 1982). However,

despite decades of research, there is little direct evidence to link LTP and LTD to the learning rules relevant for the emergence of acquired behaviors. The recent advance in neural imaging technologies has offered scientist the opportunity to observe and correlate neural signals with changes in learned behavior in unprecedented detail. For example, in the mammalian field of learning and memory, imaging experiments performed in awake and behaving animals have provided clarity into the plasticity and learning rules involved in the emergence of place-fields in the CA1 region of the hippocampus (Bittner et al., 2017; Sheffield and Dombeck, 2019).

Directly linking synaptic and behavioral plasticity requires the identification of synaptic sites that undergo modulation during learning and maintain an altered state of neural activity during the behavioral expression of the learned association. The simple anatomy of the mushroom body and well-characterized function of the neural cell types within the circuitry, provide an appealing system for linking the rules of neural and behavioral plasticity. The combination of optogenetic, imaging, and behavioral experiments in *Drosophila* have provided four important observations that suggest that compartmentalized KC-MBON synapses are the site of memory storage and that changes in the strength of these synapses is sufficient to drive changes in behavior: 1) odor identity is encoded by sparse ensembles of activated KCs and ablation of subsets of KCs impairs memory (Campbell et al., 2013; Pascual and Préat, 2001; Tomchik and Davis, 2013), 2) optogenetic activation of MBONs directly drives changes in animal behavior and silencing subsets of MBONs impairs the behavioral expression of a learned association (Aso et al., 2014b; Owald et al., 2015; Séjourné et al., 2011), 3) aversive and appetitive DANs are sufficient instruct learned associations (Aso and Rubin, 2016; Aso et al., 2010; 2012; Burke et al., 2012; Claridge-Chang et al., 2009; König et al., 2018; Liu et al., 2012) and 4) the distinct innervation pattern of

aversive and appetitive DANs across the lobes of the mushroom body allow for compartmentalized modulation of post-synaptic sites (Boto et al., 2014; Cohn et al., 2015). However, while functional experiments in *Drosophila* have identified changes in neural activity at specific synaptic sites in the MB following associative conditioning (Berry et al., 2018; Cohn et al., 2015; Hige et al., 2015; Owald et al., 2015; Séjourné et al., 2011), minimal work has been done to directly compare the rules of synaptic and behavioral plasticity and to directly correlate the emergence of synaptic plasticity with learned behaviors in the same individual animal.

In the following chapter, I explore the temporal window within which both behavioral and neural plasticity is observed in *Drosophila melanogaster,* and I examine the direct correlation between odor tracking behavior and neural plasticity using a novel closed-loop olfactory system to monitor neural activity as an animal navigates in a virtual olfactory environment. In addition, the following experiments aim to describe a general rule for bidirectional synaptic plasticity within the short-term memory circuit of the gamma lobe of the mushroom body. While it is nearly impossible to probe all synaptic nodes within the mushroom body circuitry, these experiments provide a strong link between the induction of plasticity at KC-MBON synapses and the emergence of learned behaviors.

3.2 Defining the Temporal Window for Behavior Modulation

To first define the temporal window within which pairing an odor with DAN activation modulated animal behavior, we trained animals for 50 trials while varying the timing between odor and dopaminergic reinforcement, randomly selecting from a set of 5 different inter-stimulus

intervals (ISI) for each conditioning trial (-6 s, -2 s, 0 s, 1 s, and 6 s). The ISI is defined as the difference in time between odor onset and the start of DAN activation; therefore, a negative ISI represents a negative contingency between the odor and DAN reinforcement while a positive ISI represents a positive contingency. The random selection from this set of five distinct ISIs served as an important control to test the ability of an ISI to modulate animal behavior regardless of the prior conditioning structure.

Using the behavioral chambers described in the previous chapter, we found that shifting the relative timing between odor presentation and PPL activation by only a few hundred milliseconds was sufficient to induce a switch from conditioned avoidance to attraction (Figures 3.1A-B) mirroring past observations (Aso and Rubin, 2016; König et al., 2018; Tanimoto et al., 2004). However, while these previous experiments generated a biphasic curves of odor attraction using naïve animals following only a single conditioning trial, our experiments examined the capacity of the same individual animals to rapidly update prior associations as the temporal relationship between events are altered over many trials, mimicking a more naturalistic dynamic environment. In addition, we observed a similar effect using PAM DANs for activation where conditioned attraction could be transformed to conditioned avoidance by simply shifting the timing of DAN activation from lagging to preceding the odor stimulus in time by a few hundred milliseconds (Figures 3.1A-B). The biphasic curves that emerge as a result of conditioning with PPL and PAM activation suggest both of these DAN populations can equivalently instruct learned attraction and avoidance depending on the structure of conditioning.

Figure 3.1, PPL and PAM DANs Equivalently Instruct Attraction and Avoidance
(**A**) Analysis examining how changes in upwind displacement depend on the inter-stimulus (ISI) between odor (apple cider vinegar, ACV) and optogenetic dopaminergic reinforcement during conditioning (right). ISI is the time of DAN onset minus the time of odor onset. Each cohort of animals was conditioned for 50 trials. The ISI for each conditioning trial was randomly chosen from the 5 ISIs shown. PPL > CsChrimson (teal), PAM > CsChrimson (magenta), and CsChrimson (black). Mean ± SEM, n = 6-7 experiments with 4-6 flies per experiment. The change in upwind displacement for each ISI was measured relative to the preceding trial. Each data point in (A) represents the mean change in displacement for that particular ISI in an experiment. Statistical significance for behavioral modulation compared to CsChrimson controls indicated as follows: * $p < 0.05$, ** ≤ 0.01, NS ≥ 0.05; Mann-Whitney test with Bonferroni correction. (**B**) Bidirectional behavioral modulation in PPL > CsChrimson and PAM > CsChrimson animals as a function of training with different ISIs.

Figure 3.1

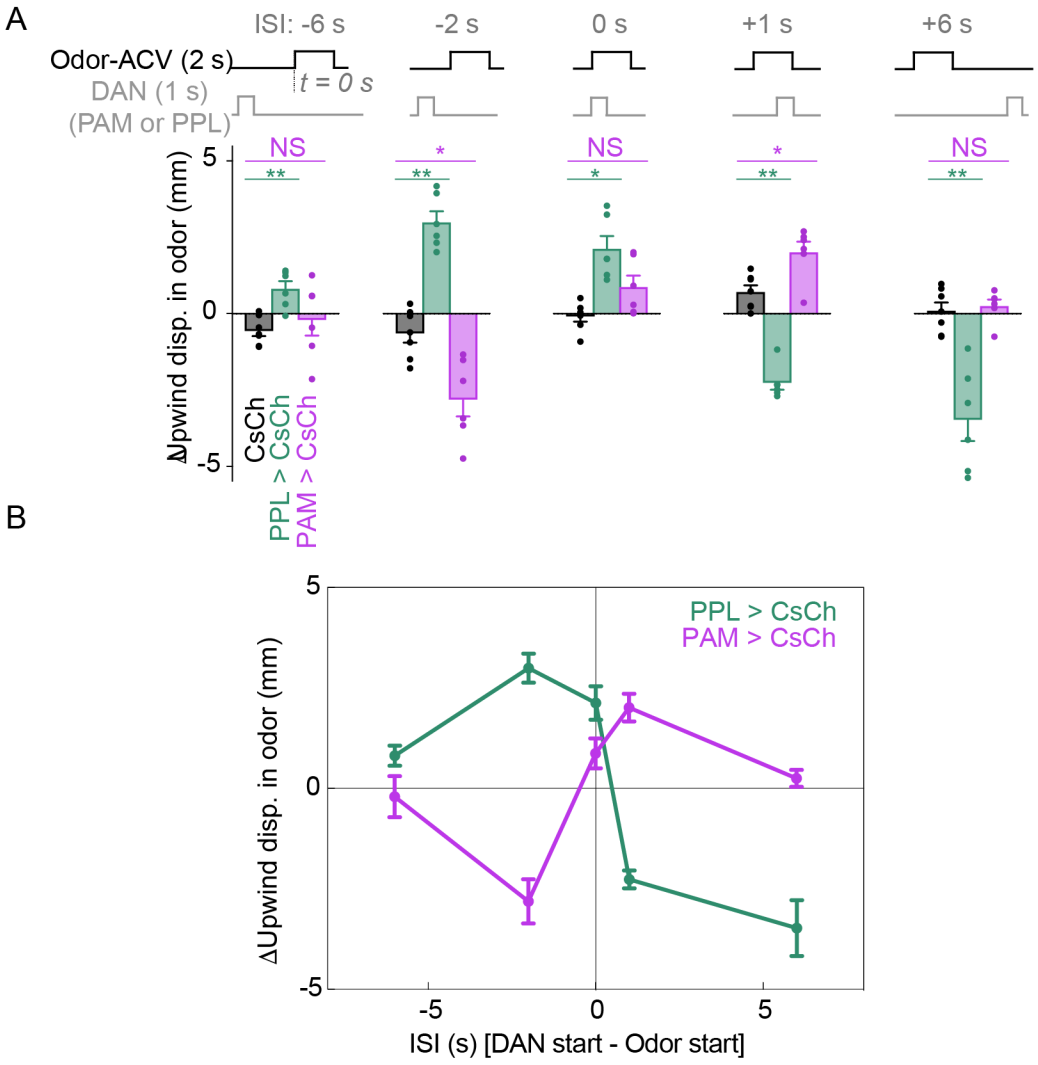
A
ISI: -6 s
-2 s
0 s
+1 s
+6 s
Odor-ACV (2 s)
t = 0 s
DAN (1 s)
(PAM or PPL)
NS
*
**
5
0
-5
ΔUpwind disp. in odor (mm)
CsCh
PPL > CsCh
PAM > CsCh
B
PPL > CsCh
PAM > CsCh
ΔUpwind disp. in odor (mm)
ISI (s) [DAN start - Odor start]

Interestingly, the temporal sensitivity of PPL and PAM conditioning differed, with PPL neurons able to drive aversive behaviors over a longer time window; while this observation may simply be due to differences in expression across the two genotypes, it supports evidence that different mushroom body DANs write and update olfactory associations with distinct rules (Aso and Rubin, 2016).

In addition, the weakened behavioral modulation observed with longer ISIs, most notable with PAM activation, is inline with a wealth of behavioral literature suggesting that as the delay between the CS and US is extended, the behavioral expression of the association grows weaker (Aso and Rubin, 2016; König et al., 2018; Roberts, 1930). This same effect likely occurs with PPL activation but would require an extension of ISIs tested. Together these experiments demonstrate the exquisite temporal sensitivity of the mushroom body to odor and dopaminergic reinforcement. This sensitivity instructs distinct associations of opposing valence and of varying magnitude depending on the ISI tested, and endows animals with the capacity to use current temporal relationships between events in their environment to form and update prior associations on a trial-by-trial basis in a manner that scales with the predictive value of cue for reinforcement. While it remains a difficult task to recapitulate a dynamic sensory environment in the laboratory, these experiments reveal that animals can use rapidly changing relationships in their environment to update and instruct up-to-date associations.

3.3 Defining the Temporal Window for Neural Plasticity

What neural mechanism might account for this bidirectional behavioral modulation? One possibility is that distinct compartments within the mushroom body could be sensitive to forward and backward conditioning such that opposing memories are written in parallel at different sites within the circuit. Such a distributed circuit-based mechanism has been proposed to underlie the re-evaluation of memories in *Drosophila* whereby an aversive association can be extinguished by the formation of a competing appetitive association in an anatomically distinct compartment (Felsenberg et al., 2018). Alternatively, bidirectional behavioral modulation could reflect reversible plasticity of KC-MBON synapses within each compartment. Indeed, dopamine has been shown to bidirectonally tune the strength of KC-MBON signaling with forward conditioning driving depression of KC-MBON synapses (Cohn et al., 2015; Hige et al., 2015; Owald et al., 2015; Séjourné et al., 2011) while strong dopamine release in the absence of odor leads to synaptic potentiation (Cohn et al., 2015; Berry et al. 2018). Furthermore, while forward conditioning with PPL neurons depresses the odor responses of MBONs that drive attraction, forward pairing with PAM neurons depresses the responses of MBONs that mediate avoidance (Aso et al., 2014b). Therefore, potentiating or depressing KC-MBON signaling within a compartment could alter the balance of activity across the MBON population, enabling animals to avoid odors that predict punishments and approach odors that predict reward or learn the opposite associations with odors that follow the positive or negative reinforcements in time. Yet whether neurons of an individual compartment are sensitive to the temporal order of odor and reinforcement remains unclear.

We therefore examined how varying the timing of dopaminergic reinforcement shapes KC-MBON signaling within a single compartment. We used a brain explant preparation, which allows for precise temporal control over both KC and DAN activation and examined plasticity in the γ4 compartment, where KC-MBON signaling undergoes robust dopamine-dependent modulation (Cohn et al., 2015). KCs were directly stimulated by iontophoresing acetylcholine onto their dendrites in the mushroom body calyx, simulating olfactory input (Figure 3.2A). Similarly, γ4 DANs were stimulated by driving expression of the ATP-gated $P2X_2$ channel in the PAM dopaminergic cluster and iontophoresing ATP onto their dendrites (Figure 3.2A). We expressed the genetically encoded indicator GCaMP6s in the γ4 MBON and used KC-evoked dendritic calcium within the γ4 compartment to assess the strength of KC-MBON signaling.

We found that after a single forward conditioning trial, the response of the MBON to the same KC input was strongly attenuated (Figure 3.2B), consistent with previous reports (Cohn et al., 2015; Hige et al., 2015; Owald et al., 2015; Séjourné et al., 2011). The depression of KC-MBON signaling decayed slowly over the course of ten minutes despite repeated stimulation of the KCs, but could be reversed and even driven above baseline through a single backward conditioning trial (Figure 3.2B). Conversely, backward pairing from a baseline state led to lasting potentiation of KC-MBON signaling and could be reversed and driven below baseline by a single forward conditioning trial (Figure 3.2C). Forward and backward pairing therefore bidirectionally regulate KC-MBON signaling on a trial-by-trial basis, mirroring the observed behavioral flexibility.

We found that varying the timing between KC and DAN stimulation during conditioning revealed a narrow temporal window over which the strength of KC-MBON signaling was

Figure 3.2, Forward and Backward Pairing Instruct Bidirectional Neural Plasticity
(**A**) Schematic of mushroom body preparation used to measure KC-MBON plasticity. GCaMP6s was expressed in γ4 MBON using VT026001-Gal4 driver. KCs were directly stimulated by iontophoresis of acetylcholine into the calyx. The $P2X_2$ channel was expressed in PAM DANs (including γ4-γ5 DANs) using the 58E02-LexA driver and activated by application of ATP onto their dendrites. (**B**) Average KC-evoked GCaMP response in γ4 MBON prior to and after forward pairing and backward pairing using the experimental set up shown in Figure 3.2A. KCs were activated by iontophoresis of acetylcholine onto their dendrites in the calyx. Two baseline trials are shown prior to forward pairing KC activation with activation of the g4 DANs expressing the ATP-gated $P2X_2$ channel under 58E02-LexA driver. Following forward pairing (noted by first dashed line), 10 responses to KC stimulation are shown to assess decay in plasticity prior to backward pairing (denoted by second dashed line). Two KC-evoked calcium responses in g4 MBON are shown after backward pairing, n = 6, mean ± SEM. Representative example below of the heat map of fluorescence changes in g4 MBON dendrites evoked by KC stimulation for each time point. (**C**) Same as in (B) except backward pairing was performed first, marked by first dashed line, and forward pairing was performed second, marked by second dashed line, n = 6, mean ± SEM. Black arrowheads mark times of KC stimulation.

Figure 3.2

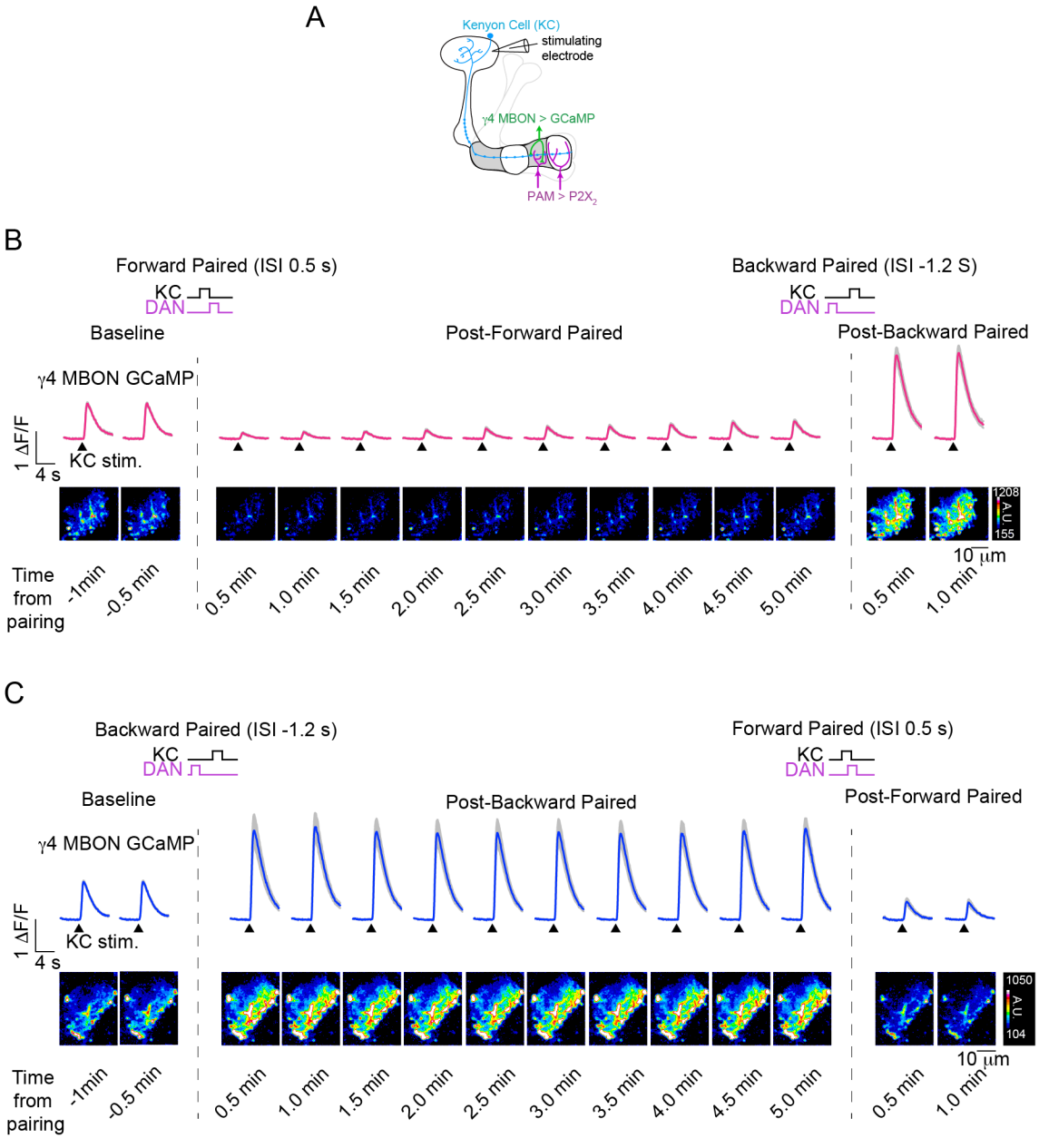
A
Kenyon Cell (KC)
stimulating electrode
γ4 MBON > GCaMP
PAM > P2X2
B
Forward Paired (ISI 0.5 s)
KC
DAN
Backward Paired (ISI -1.2 S)
KC
DAN
Baseline
Post-Forward Paired
Post-Backward Paired
γ4 MBON GCaMP
1 ΔF/F
4 s
KC stim.
1208
AU
155
10 μm
Time from pairing
-1min
-0.5 min
0.5 min
1.0 min
1.5 min
2.0 min
2.5 min
3.0 min
3.5 min
4.0 min
4.5 min
5.0 min
0.5 min
1.0 min
C
Backward Paired (ISI -1.2 s)
KC
DAN
Forward Paired (ISI 0.5 s)
KC
DAN
Baseline
Post-Backward Paired
Post-Forward Paired
γ4 MBON GCaMP
1 ΔF/F
4 s
KC stim.
1050
AU
104
10 μm
Time from pairing
-1min
-0.5 min
0.5 min
1.0 min
1.5 min
2.0 min
2.5 min
3.0 min
3.5 min
4.0 min
4.5 min
5.0 min
0.5 min
1.0 min

Figure 3.3, Relating Neural Plasticity with Behavioral Modulation

(**A**) Average KC-evoked GCaMP responses in the γ4 MBON prior to (pre) and after (post) pairing KC and DAN activation (arrow head denotes time of KC stimulation) across different inter-stimulus intervals (ISI = time of DAN onset minus time of KC onset), mean ± SEM. (**B**) Black: Change in peak γ4 MBON response plotted as a function of ISI, mean ± SEM. n = 5-6. Magenta: Behavioral data for PAM > CsChrimson animals re-plotted from (B). Significant change in γ4 MBON response after pairing was observed for ISI = -1.2 s ($p \leq 0.001$), 0 s ($p < 0.05$), and 0.5 s ($p \leq 0.01$); one-sample t-test against zero with Bonferroni correction. (**C**) Normalized GCaMP signal in γ4 MBON to odor stimulus pre (black) and post (red) forward pairing, backward pairing, or no pairing (unpaired odor) shows odor-specific depression and potentiation with unpaired odor responses unaffected. N = 3 in tact tethered animals with odor presented to antenna of animal, mean ± SEM.

Figure 3.3

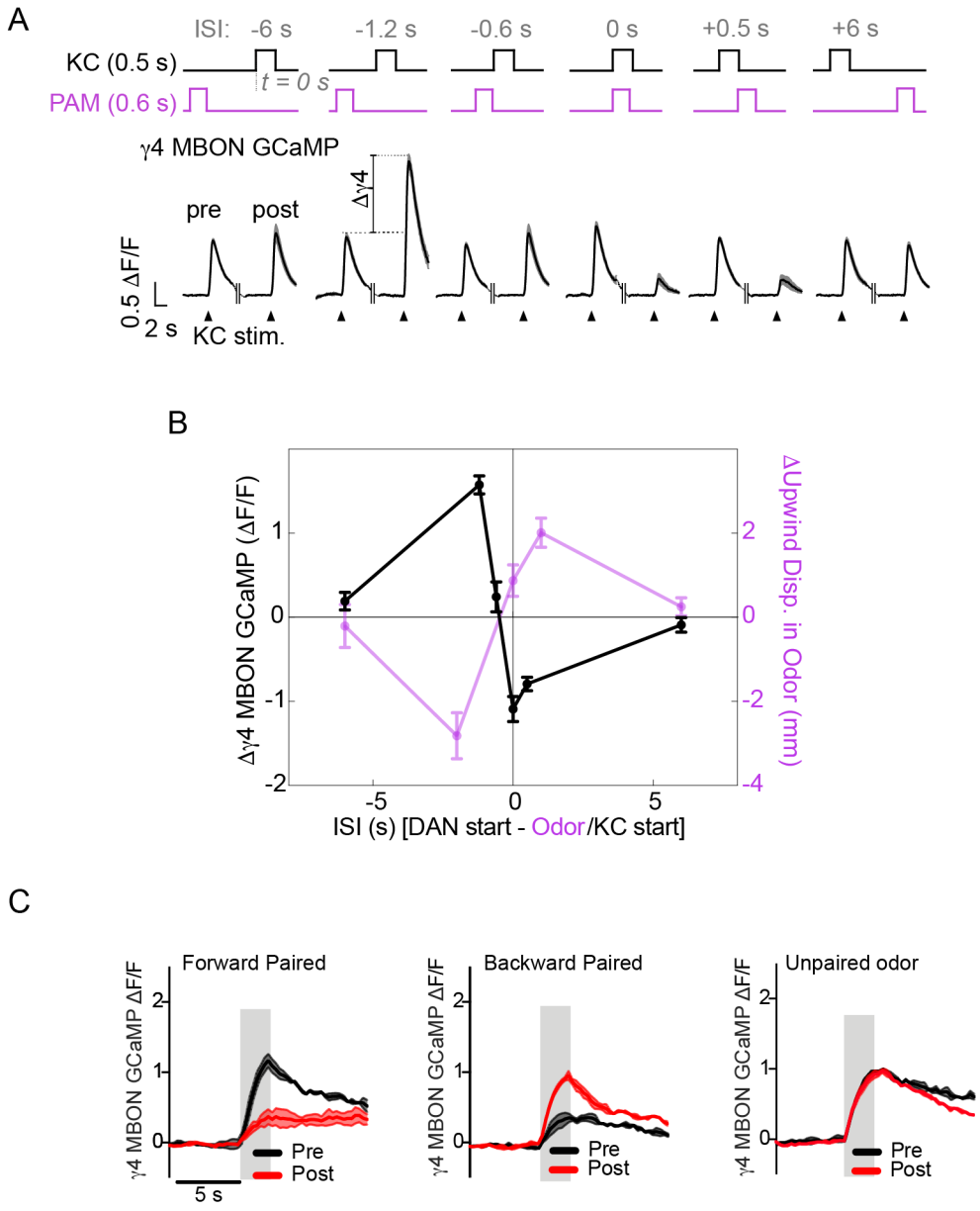
A
ISI: -6 s
-1.2 s
-0.6 s
0 s
+0.5 s
+6 s
KC (0.5 s)
t = 0 s
PAM (0.6 s)
γ4 MBON GCaMP
pre
post
Δγ4
0.5 ΔF/F
2 s
KC stim.
B
Δγ4 MBON GCaMP (ΔF/F)
ΔUpwind Disp. in Odor (mm)
ISI (s) [DAN start - Odor/KC start]
C
Forward Paired
Backward Paired
Unpaired odor
γ4 MBON GCaMP ΔF/F
Pre
Post
5 s

bidirectionally modulated, shifting from potentiation when DAN stimulation preceded KC activation to depression when DAN stimulation was coincident or followed KC activation (Figure 3.3A). While stronger or more prolonged dopamine release in the absence of an odor has been shown to potentiate KC-MBON signaling (Berry et al., 2018; Cohn et al., 2015), we found that extending the KC-DAN inter-stimulus interval to 6 seconds resulted in minimal plasticity (Figure 3.3A) consistent with behavioral evidence that nearly synchronous dopaminergic and olfactory input is required for robust modulation. Importantly, the temporal dependence of KC-MBON plasticity within a single compartment innervated by the PAM DANs matched the timescale of behavioral plasticity evoked using the same PAM dopaminergic reinforcement (Figure 3.3B), suggesting that bidirectional regulation of KC-MBON signaling may underlie the temporal sensitivity at the behavioral level.

A basic tenant of associative learning is that the acquired knowledge and behavioral response is specific to the paired conditioned stimulus (CS+) and is not observed in response to an unpaired conditioned stimulus (CS-) that is temporally unrelated to reinforcement. In order to test this, we presented flies with an odor that was either forward or backward paired (CS+) and an odor that was unpaired (CS-). We found the bidirectional neural plasticity was only observable in the odor paired with reinforcement with the γ4 MBON showing no modulation in its response to the unpaired odor (Figure 3.3C).

These odor-specific changes, in addition to supporting that the neural modulation we observe is a relevant form of synaptic plasticity to instruct odor-specific behavioral associations, also highlights an important coding property of the MB architecture: the capacity of dopamine to

bidirectionally modulate specific KC-MBON synapses depends on the current activity state of the synapses.

Dopamine neurons in both the vertebrate and invertebrate brain are know to influence synaptic transmission through volume release of dopamine (Floresco et al., 2003; Gonon, 1997; Takemura et al., 2017). Modulation by dopamine, therefore, depends on the geometric parameters of diffusion and the uptake characteristics of post-synaptic sites. Indeed, a recent connectome of the adult MB revealed that only 6% of KC-MBON synapses receive direct synaptic input from DANs (Takemura et al., 2017). One interesting implication from this high-resolution structural information is that while the percentage of direct DAN input is low within the MB lobes, the density of KC-MBON synapses is very high suggesting that dopamine need only diffuse 2 μm to reach all KC-MBON synapses and ensure minimal "spill over" into neighboring compartments. While this interpretation of the connectome would indeed allow for compartment-specific modulation by innervating DANs, it raises the interesting question for how odor-specificity is achieved in the DAN-dependent modulation that occurs during learning. The narrow temporal window in which bidirectional plasticity shapes γ4 MBON output (Figure 3.3A) suggests that dopamine modulation depends on the activity state of the KC-MBON synapses—dopamine depresses synapses only if it follows a high-activity state and potentiates synapses selectively if it precedes a high-activity state. This suggests two distinct mechanisms likely exist to account for these different plasticity rules. On the one hand, the requirement for convergence of KC and DAN input suggests a coincidence detection mechanism exists within the MB circuitry. In addition, the sign of plasticity (potentiation or depression) depends on the ordering

of KC and DAN input, emphasizing the need for order detection in the KC-MBON synapses, a topic further discussed in Chapter 5.

3.4 Bidirectional Plasticity Across Gamma Lobe Compartments

When assessed at the level of animal behavior, different KC and DAN populations have distinct capacities for writing and updating associative memories and for the storage of multiple memories (Aso and Rubin, 2016; Blum et al., 2009; Qin et al., 2012; Trannoy et al., 2011). The mechanistic basis for these discrepancies across cell types remains unclear and raises the question of whether the rules for synaptic plasticity differ across the compartments of the MB. We were, therefore, interested in assessing the capacity for bidirectional plasticity across different compartments within the γ lobe of the MB.

Across the γ lobe, the KC axons are thought to be homogenous and are tiled by the input of cell-type specific MBONs and DANs. We first asked whether the γ5 compartment, a compartment innervated by the PAM DANs, shows similar bidirectional plasticity to its neighboring γ4 compartment. Indeed, a single conditioning trial in which direct KC stimulation was forward paired with chemogenetic activation of γ5 DANs was sufficient to induce depression in the γ5 MBON response to KC input while backward pairing drove strong potentiation of the MBON's response (Figure 3.4A).

By contrast the γ2 compartment of the MB is innervated by the shock-responsive PPL DANs. Despite this difference in DAN valence, we again found that the timing of inputs directed

bidirectional plasticity: synchronous activation of KC and the γ2 DAN led to depression of the γ2 MBON while backward pairing drove potentiation (Figure 3.4B). Interestingly, coincident activation of KC and the γ2 DAN led to much more consistent depression than if KC activation preceded γ2 DAN activation (data not shown) unlike the γ4 MBON, which exhibited strong depression under both pairing conditions; while this may simply be do to driver differences, it raises the possibility that the temporal window for neural plasticity differs across the different compartments of the MB. Furthermore, similar bidirectional and reversible modulation in the γ2 MBON's response to odor could be elicited by conditioning with a naturalistic aversive reinforcement in which an electric shock was applied to the abdomen of a fly in place of optogenetic activation of PPL DANs (3.5A-C). Together, these experiments suggest that direct activation of MB DANs is sufficient to drive bidirectional plasticity in the KC-MBON synapses across a variety of compartments in the γ lobe.

These experiments support a model in which PAM and PPL DANs can direct either conditioned avoidance or attraction by driving bidirectional KC-MBON plasticity in each of the multiple compartments they innervate. This coordinated plasticity could reweight the net output of the MBONs, allowing animals to learn to avoid odors that predict punishment by depressing the responses of MBONs that mediate approach, including the γ2 MBON (Aso et al., 2014b), or become attracted to odors that predict reward by weakening the responses of MBONs that drive avoidance, like the γ4 or γ5 MBONs (Aso et al., 2014b), or learn opposite associations with odors that follow these reinforcements in time by potentiating the activity of the same population of MBONs.

Figure 3.4, Bidirectional Plasticity Across the Gamma Lobe

(**A**) γ5 MBON calcium responses to direct KC stimulation (black arrowhead) by iontophoresis of acetylcholine in the calyx pre and post forward (ISI = 0.5 s, n = 8) and backward (ISI = -1.2 s, n = 6) pairing of KC stimulation with activation of γ5 DANs using the 58E02-LexA driver. Right: Change in KC-evoked calcium response in γ5 MBON post-forward pairing (post-FP) and post-backward pairing (post-BP). Mean ± SEM (**B**) Same as in (A) except for γ2 MBON responses pre and post forward pairing (ISI = 0 s, n = 6) and backward pairing (ISI = -1.2 s, n = 7) pairing with γ2 DANs using the 73F07-LexA driver. Significant change in γ5 and γ2 MBON responses after pairing was tested with a one-sample t-test against zero with Bonferroni correction: *** $p \leq 0.001$, ** ≤ 0.01.

Figure 3.4

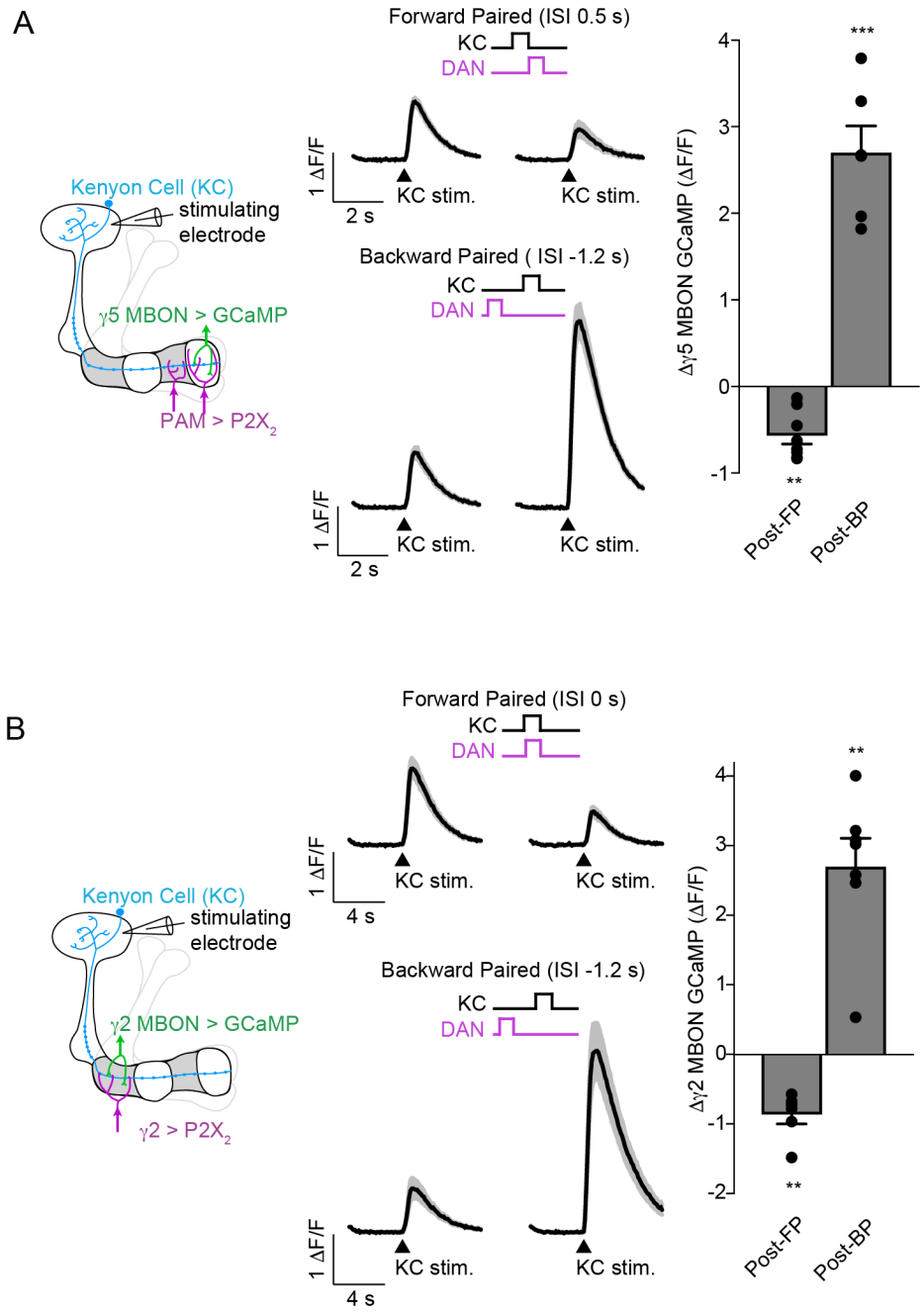
A
Forward Paired (ISI 0.5 s)
KC
DAN
1 ΔF/F
2 s
KC stim.
KC stim.
Backward Paired (ISI -1.2 s)
KC
DAN
1 ΔF/F
2 s
KC stim.
KC stim.
Kenyon Cell (KC)
stimulating
electrode
γ5 MBON > GCaMP
PAM > P2X2
Δγ5 MBON GCaMP (ΔF/F)
***
**
Post-FP
Post-BP
B
Forward Paired (ISI 0 s)
KC
DAN
1 ΔF/F
4 s
KC stim.
KC stim.
Backward Paired (ISI -1.2 s)
KC
DAN
1 ΔF/F
4 s
KC stim.
KC stim.
Kenyon Cell (KC)
stimulating
electrode
γ2 MBON > GCaMP
γ2 > P2X2
Δγ2 MBON GCaMP (ΔF/F)
**
**
Post-FP
Post-BP

Figure 3.5, Naturalistic Reinforcement Replicates Bidirectional Plasticity

(**A**) Schematic for conditioning fly with odor (apple cider vinegar, ACV) and electric shock applied to the abdomen of the fly. (**B**) Odor-evoked responses in the γ2 MBON during baseline, post-forward pairing, and post-backward pairing. Odor presentation is 2 seconds in duration. Two 1-s, 70V shocks separated by 0.2 s were applied to the abdomen of the fly. In forward conditioning, the odor preceded the shock by 0.5 s; in backward pairing, the shock preceded the odor by 3 s. (**C**) Change in odor-evoked calcium response in γ2 MBON post-FP and post-BP, mean ± SEM, n = 7. Significant change in γ2 MBON responses after shock conditioning was tested with Wilcoxon Signed Rank Test against zero with Bonferroni correction: * < 0.05.

Figure 3.5

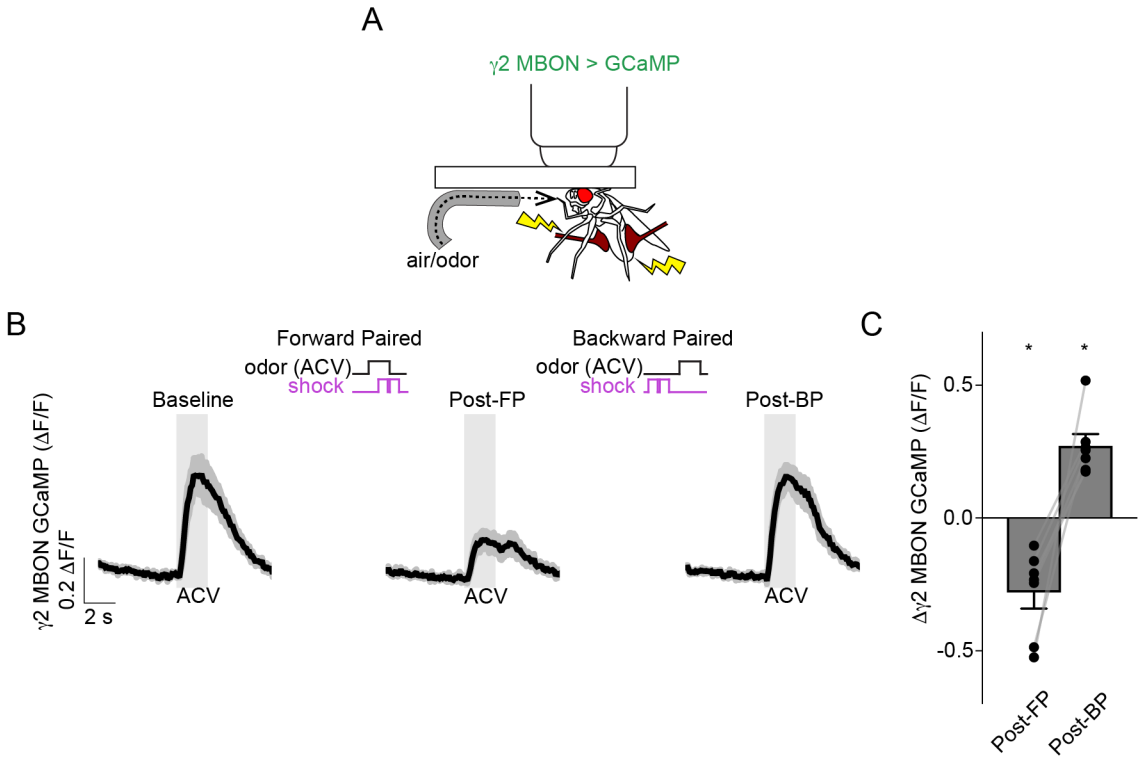
A
γ2 MBON > GCaMP
air/odor
B
Forward Paired
odor (ACV)
shock
Backward Paired
odor (ACV)
shock
Baseline
Post-FP
Post-BP
γ2 MBON GCaMP (ΔF/F)
0.2 ΔF/F
2 s
ACV
ACV
ACV
C
Δγ2 MBON GCaMP (ΔF/F)
0.5
0.0
-0.5
*
*
Post-FP
Post-BP

3.5 Directly Relating Neural and Behavioral Plasticity

While our results reveal a striking correspondence between the timescales of bidirectional neural and behavioral modulation, directly relating these forms of plasticity in *Drosophila* has been difficult in the absence of methods to measure both concurrently. Raphael Cohn, a former graduate student in the lab previously developed a closed-loop virtual olfactory paradigm, compatible with two-photon imaging, in which a fly's angular velocity on an air-supported ball was yoked to the rotation of a tube carrying a constant airstream (Figure 3.6A). In this assay, a head-fixed animal can control its orientation within the airstream and increase its upwind velocity in response to introduction of an appetitive olfactory cue (Figure 3.6B), allowing us to image neural activity in the γ4 compartment of the mushroom body during odor tracking behavior. This system is also compatible with optogenetic activation of the rewarding PAM neurons as a reinforcement signal, allowing us to perform conditioning in head-fixed animals under the microscope.

Preliminary experiments using the closed-loop system were performed to assess tracking behavior in this virtual olfactory environment and the ability for animals to modulate their behavior after repeated trials of conditioning. These initial experiments were not performed under the two-photon microscope and simply measured changes in the upwind displacement in the odor plume after interleaved trials of forward and backward pairing in a tethered fly. From these preliminary experiments, we found that forward and backward pairing with PAM activation consistently modulated the attraction to the conditioned odor, apple cider vinegar (ACV) in individual animals (Figure 3.6C), consistent with the behavior observed in freely walking animals.

Figure 3.6, Timing-Dependent Reversals in Behavior in Virtual Olfactory Environment
(**A**) Schematic of closed-loop system. A fly walks on an air-supported ball within a constant air stream whose rotation (dashed line) is yoked to the fly's heading direction. The outer disk that carries the airstream (gray) is rotated by a gear belt (black) connected to a motor getting real-time information about the angular rotation of the ball. This system can be used under a 2-photon microscope, allowing simultaneous recording of odor-evoked responses in the MB and odor-tracking behavior. (**B**) Representative 2D trajectory showing re-orientation and upwind tracking when the fly was presented with an odor (red). Fly cartoon marks the end of the trajectory. (**C**) Pilot experiment testing the effect of forward and backward pairing in back tethered animals. PAM DANs expressing CsChrimson were activated using optogenetics prior to or during the presentation of the odor apple cider vinegar, n = 25. After being placed on food containing 0.4 mM for 24-48 hours, animals were starved between 0 and 12 hrs for pilot experiment in (C). Starved animals were placed on 0.1-0.2mM retinal water or regular water overnight.

Figure 3.6

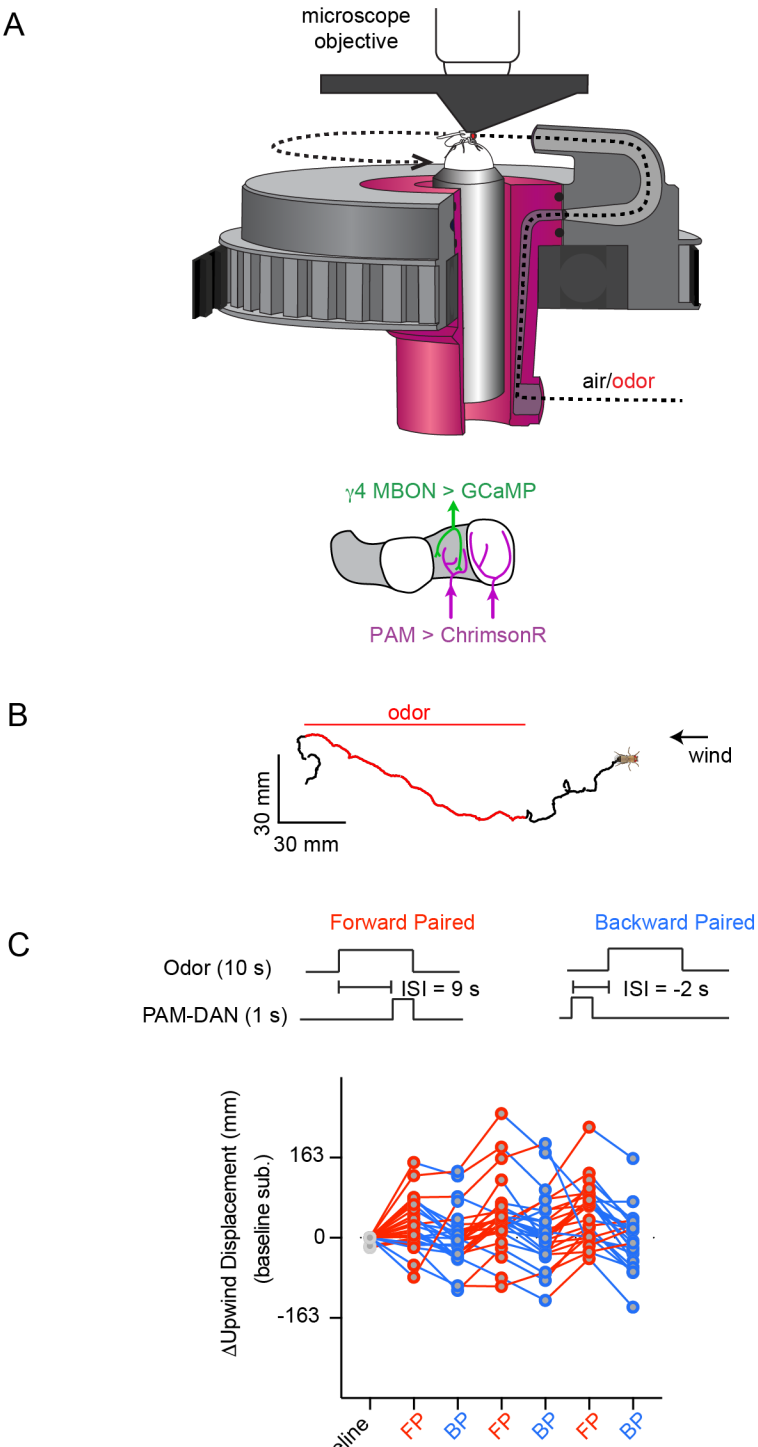
A
microscope objective
air/odor
γ4 MBON > GCaMP
PAM > ChrimsonR
B
odor
wind
30 mm
30 mm
C
Forward Paired
Backward Paired
Odor (10 s)
PAM-DAN (1 s)
ISI = 9 s
ISI = -2 s
ΔUpwind Displacement (mm)
(baseline sub.)
163
0
-163
baseline
FP
BP
FP
BP
FP
BP

To directly relate changes in animal behavior to neural plasticity, we performed synchronous functional imaging of the γ4 MBON as an animal navigates within an odor plume under the two-photon microscope. Examining the fictive two-dimensional trajectories of a single animal over multiple odor presentations revealed that forward pairing of ACV with activation of PAM neurons led to increased upwind tracking of ACV while backward pairing decreased tracking (Figure 3.7A). Notably, synchronously imaging the γ4 MBON responses during odor tracking showed a corresponding functional change: forward pairing depressed the MBON's response to ACV while backward pairing potentiated its response (Figure 3.7A). Conditioning consistently evoked bidirectional changes in both odor-evoked upwind displacement and γ4 MBON activity across animals (Figures 3.7B-G). These changes were significantly correlated, both on a trial-by-trial basis and in the averaged responses of all trials for individual animals (Figure 3.7H). Importantly, these changes in behavior were not observed as the animals navigated in clean air (measured for the 10 seconds prior to odor presentation) (Figure 3.8A-D), suggesting that modulation of odor-evoked behavior is not simply due to an overall change in the arousal state of the animal but are contingent on the presence of the reinforced odor. Thus, the ability to simultaneously record neural and behavioral plasticity as learning unfolds reveals a tight correspondence between the emergence of bidirectional changes in KC-MBON signaling within a compartment and odor attraction.

3.6 Discussion

In 1921, German zoologist and evolutionary biologist, Richard Semon, put forward the idea of the "engram" as "... the enduring, though primarily latent, modification in the irritable substance

Figure 3.7, Relating Neural and Behavioral Modulation in Closed-Loop Olfactory Arena. (**A**) Calcium responses were recorded in g4 MBON expressing GCaMP6s. PAM DANs, including g4 DANs, expressed ChrimsonR using MB042B-Gal4. Top: protocol to compare odor tracking and neural responses to ACV odor after forward pairing (post-FP) and backward pairing (post-BP). Middle: Fictive 2D trajectories of a single representative fly in baseline, post-forward pairing, and post-backward pairing trials, aligned to a common origin with average upwind displacement for all trials shown to right (red). Bottom: Corresponding odor-evoked g4 MBON responses synchronously recorded in the same animal (odor is marked by gray box). Thin gray lines represent individual odor responses; black line represents mean odor response. (**B**) Mean change in upwind displacement in post-forward pairing and post-backward pairing trials during the 10-second odor presentation. (**C**) Mean upwind displacement in 10-s ACV odor during baseline, post-forward pairing (post-FP), and post-backward pairing (post-BP) trials in animals walking in closed loop olfactory system, n = 8 flies. Each gray data point represents the mean upwind displacement across 3-4 conditioning protocols for the individual animal. (**D**) Mean upwind displacement in 10-s ACV odor during baseline, post-forward pairing, and post-backward pairing trials averaged across all training trials across all animals n = 27. (**E**) Left: average g4 MBON calcium traces for all animals during baseline, post-forward pairing, and post-backward pairing trials (odor is marked with gray box). Right: Change in odor-evoked calcium response in g4 MBON post-forward pairing and post-backward pairing. (**F-G**) Average peak odor-evoked g4 MBON responses in baseline, post-forward pairing, and post-backward pairing trials for the same 8 animals (F) and all training trials across all animals n = 27 (G). (**H**) Change in upwind displacement in odor plotted as a function of change in odor-evoked g4 MBON responses for all individual training trials (gray dots; n = 27 individual training trials across n = 8 animals) and animal averages (black dots; n = 8 animals, 3-4 training trials per animal); post-forward pairing trial (open circle) and post-backward pairing trial (closed circle). Data represented as mean ± SEM. Significance is indicated as follows for (B and E): *** $p \leq 0.001$, ** ≤ 0.01, * < 0.05; one-sample t-test from zero with Bonferroni correction. For (C-D) and (F-G) *** ≤ 0.001, ** ≤ 0.01, * < 0.05; Wilcoxon matched-pairs signed rank test with Bonferroni correction.

Figure 3.7

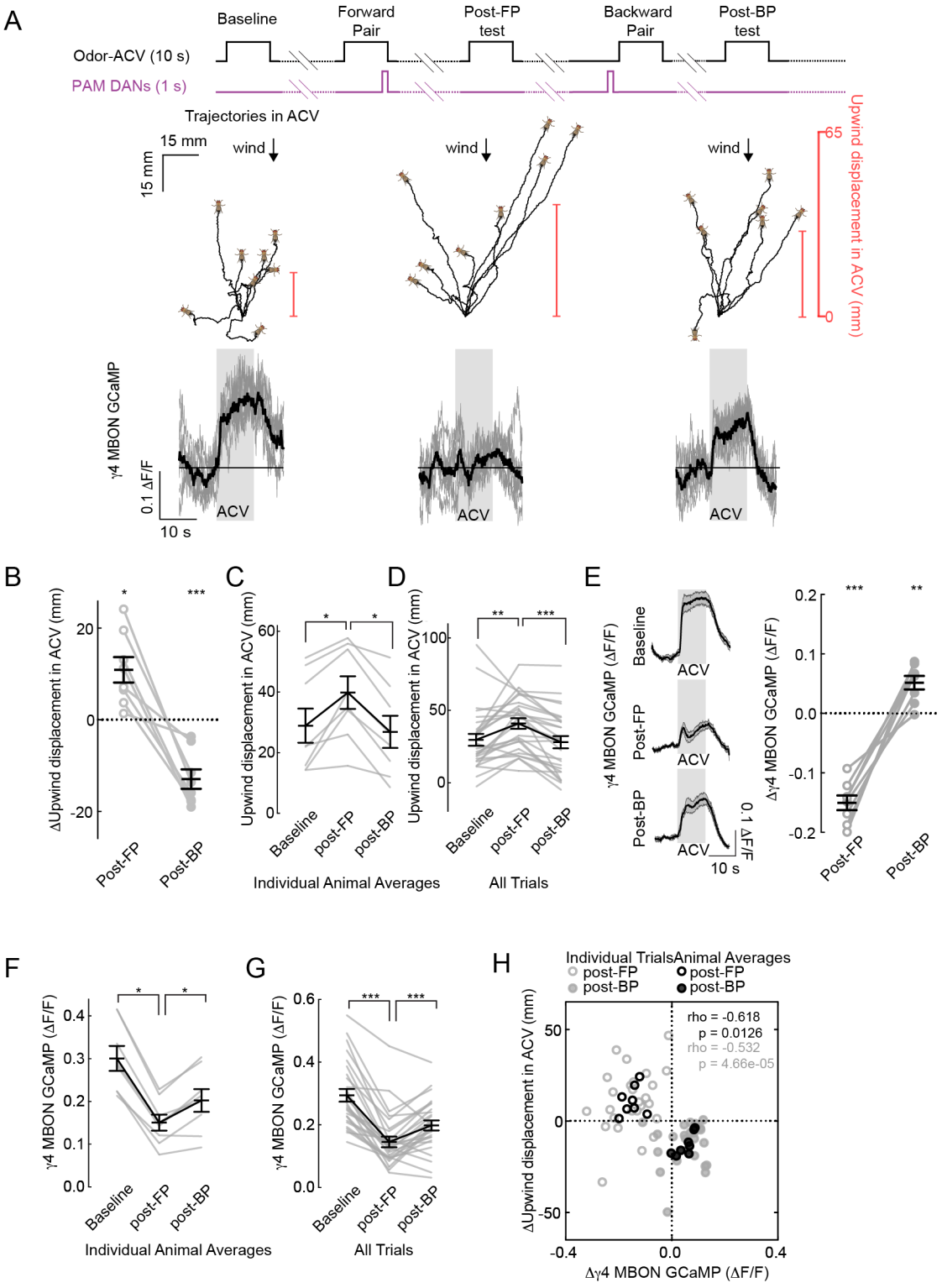
A
Baseline
Forward Pair
Post-FP test
Backward Pair
Post-BP test
Odor-ACV (10 s)
PAM DANs (1 s)
Trajectories in ACV
15 mm
15 mm
wind
wind
wind
65
0
Upwind displacement in ACV (mm)
γ4 MBON GCaMP
0.1 ΔF/F
10 s
ACV
ACV
ACV
B
ΔUpwind displacement in ACV (mm)
Post-FP
Post-BP
C
Upwind displacement in ACV (mm)
Baseline
post-FP
post-BP
Individual Animal Averages
D
Upwind displacement in ACV (mm)
Baseline
post-FP
post-BP
All Trials
E
γ4 MBON GCaMP (ΔF/F)
Baseline
Post-FP
Post-BP
ACV
0.1 ΔF/F
10 s
Δγ4 MBON GCaMP (ΔF/F)
Post-FP
Post-BP
F
γ4 MBON GCaMP (ΔF/F)
Baseline
post-FP
post-BP
Individual Animal Averages
G
γ4 MBON GCaMP (ΔF/F)
Baseline
post-FP
post-BP
All Trials
H
Individual Trials
post-FP
post-BP
Animal Averages
post-FP
post-BP
rho = -0.618
p = 0.0126
rho = -0.532
p = 4.66e-05
ΔUpwind displacement in ACV (mm)
Δγ4 MBON GCaMP (ΔF/F)

Figure 3.8, Modulation in Animal Behavior is Specific to Odor Stimulus.
(**A**) Fictive 2D trajectories for representative individual fly (same as shown in Figure 3.7A) but for the 10-s clean air prior to odor presentation. (**B**) Mean change in upwind displacement in post-forward pairing and post-backward pairing trials during the 10 seconds prior to odor when animals were in clean air n=8 animals, 3-4 trials per animal. (**C**) Mean upwind displacement in 10-s clean air prior to odor onset during baseline, post-forward pairing (post-FP), and post-backward pairing (post-BP) trials in animals walking in closed loop olfactory system, n = 8 flies. Each gray data point represents the mean upwind displacement across 3-4 conditioning protocols for the individual animal. (**D**) Mean upwind displacement in 10-s clean air prior to odor onset during baseline, post-forward pairing, and post-backward pairing trials across all training trials and all animals, n = 27 training trials across the same 8 animals. Data represented as mean ± SEM. Significance is indicated as follows for (B): NS ≥ 0.05; one-sample t-test from zero with Bonferroni correction. For (C-D) NS ≥ 0.05; Wilcoxon matched-pairs signed rank test with Bonferroni correction.

Figure 3.8

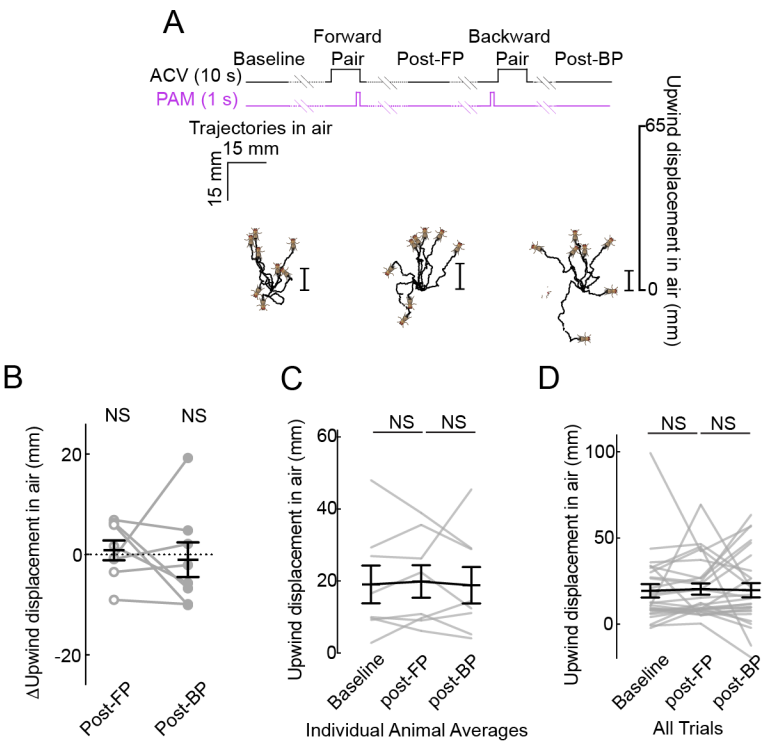
A
Forward
Backward
Baseline
Pair
Post-FP
Pair
Post-BP
ACV (10 s)
PAM (1 s)
Trajectories in air
15 mm
15 mm
65
0
Upwind displacement in air (mm)
B
NS
NS
20
0
-20
ΔUpwind displacement in air (mm)
Post-FP
Post-BP
C
NS
NS
60
40
20
0
Upwind displacement in air (mm)
Baseline
post-FP
post-BP
Individual Animal Averages
D
NS
NS
100
50
0
Upwind displacement in air (mm)
Baseline
post-FP
post-BP
All Trials

produced by a stimulus..." (Semon, 1921). The engram can be thought of as a memory trace, etched into the nervous system as a result of experience and persisting over the time course of memory. Beyond adding scientific terminologies to the lexicon of learning and memory research, Semon put forward prescient theories for how memories were stored and retrieved. For example, he proposed that "cuing" of the original memory or engram would lead to the formation of a new distinct engram and influence the strength of the original memory trace. While purely theoretical, Semon was the first to propose that an engram was not a static etch, but something that changed with use or experience (Josselyn et al., 2017).

In the 1950s, brain centers containing memory engrams were implicated through the seminal research of Brenda Milner and Wilder Graves Penfield into the memory loss observed in patients with lesions within the hippocampus (Penfield and Milner, 1958). More recently, the use of cell-type specific labeling, loss- and gain-of-function experiments, and functional imaging experiments have drawn a more definitive link between learning-dependent changes in neural activity and behavior. For example, recent mouse studies used learning-dependent cell labeling to demonstrate optogenetic re-activation of these engram cells results in memory retrieval (Ramirez et al., 2013; Ryan et al., 2015). Directly relating the emergence of neural plasticity with the evolution of adaptive, learned behaviors has been a difficult task and a central goal for many in the field of learning and memory research.

In linking the temporal requirements for behavioral and neural modulation, we found a small window within which the pairing of an odor with either the aversive activation of PPL or rewarding activation of PAM dopamine neurons drove bidirectional attraction to the conditioned

odor. Shifting the timing of DAN activation relative to odor presentation by a few hundred milliseconds was sufficient to induce a behavioral state change from odor attraction to odor avoidance. Furthermore, we found that animals continuously attend to the temporal relationships in their environment, rapidly changing their attraction to an odor as a result of a change in the temporal contiguity between the odor and reinforcement signal. These results highlight the exquisite temporal sensitivity of the mushroom body for distinguishing the temporal order of events and suggest that animals use nearly coincident input of odor and reinforcement pathways to rapidly write and update associations to reflect the changing relationships in a dynamic environment.

It is worth noting that the biphasic curves between the PPL and PAM animals differ; PPL animals form negative associations over greater ISI for forward pairing than PAM animals do in their formation of positive associations. These differences in the temporal requirements for memory across DAN populations is inline with observations that distinct DANs write and update associations with different rules (Aso and Rubin, 2016). Indeed, to minimize danger, it may be advantageous for animals to form associations between cues that predict peril even if the delay between the cue and reinforcement is extended in time. The experiments described in this chapter only begin to examine the state-space for the temporal dependence of associative learning. Indeed, broader biphasic curves have been observed in *Drosophila* through the use of longer odor presentations and stronger negative reinforcement (Aso and Rubin, 2016; König et al., 2018; Tanimoto et al., 2004). These wider curves that emerge with longer and stronger stimulations raise the question for the role of trace conditioning in the MB circuitry and the

molecular basis for how the KC-MBON synapses are modulated over these extended conditioning paradigms.

Bidirectional neural plasticity has been proposed to confer learning circuits with behavioral flexibility to rapidly write and update associations as the environment changes (Coesmans et al., 2004; Jörntell and Hansel, 2006; Lev-Ram et al., 2002). Indeed, we see that the narrow temporal window of behavioral modulation following PAM activation closely aligns with bidirectional plasticity in odor- and KC-evoked responses in the γ4 MBON. Over the past several years, research into the effects of associative conditioning on KC-MBON synapses has revealed that forward pairing drives odor-specific depression in the activity of the downstream MBON (Cohn et al., 2015; Hige et al., 2015; Owald et al., 2015; Séjourné et al., 2011). Positive reinforcement leads to depression of MBONs that elicit avoidance behavior, while negative reinforcement depresses the activity of MBONS that bias animals towards approach behavior (Aso et al., 2014b). Furthermore, strong dopamine release in the absence of odor leads to synaptic potentiation (Cohn et al., 2015; Berry et al. 2018), suggesting the presence of a strong reinforcement event drives the re-evaluation of prior associations.

The striking correspondence between the time course for neural plasticity in the γ4 MBON and behavioral modulation observed with PAM reinforcement, presented in this chapter, suggests that the MB is exquisitely sensitive to timing, resulting in graded levels of neural and behavioral plasticity that depend on the timing of events during conditioning. Similar bidirectional plasticity was observed across multiple compartments within the γ lobe innervated both by PAM and PPL DANs, suggesting a conserved mechanism for order and coincidence detection across the axons

of γ lobe KCs. In the future, it will be interesting to examine how the temporal window for bidirectional plasticity differs across the different compartments innervated by PAM and PPL pathways.

Across a variety of neural circuits involved in classical conditioning both synaptic depression and facilitation have been observed following forward pairing, suggesting that the sign of plasticity depends on the molecular machinery engaged during conditioning in the post-synaptic neuron (Bauer et al., 2002; Ito and Kano, 1982). Interestingly, the neural mechanism underlying conditioned eye blink responses in rodents is thought to require synaptic facilitation of mossy fibers synapses and also require depression of parallel-fiber synapses onto Purkinje cells in the cerebellum (Freeman and Steinmetz, 2011; Ito and Kano, 1982; Linden and Connor, 1991; Linden et al., 1991; Pugh and Raman, 2008). It is not surprising, therefore, that forward pairing drives depression across a number of compartments of the γ lobe, considering the KCs of the γ lobe are thought to be homogenous across the length of the output lobe. Furthermore, KC-MBON signaling in the α2 compartment (a compartment made up by the α/β KCs) also exhibits depression following forward conditioning (Hige et al., 2015), suggesting that the different KC population within the MB circuitry undergo similar plasticity changes depending on the timing of conditioning and therefore likely rely on similar molecular machinery.

Using a novel closed-loop olfactory environment, we were able to show for the first time that the emergence of neural plasticity within the MB circuitry correlates with learned changes in odor attraction. While we focus on correlating the activity of the γ4 MBON with behavior, it is important to note that the bidirectional behavior likely emerges as a result of synaptic plasticity

across the multiple compartments innervated by the PAM neurons. Indeed, we show that both the γ4 MBON and the γ5 MBON undergo similar neural plasticity following forward and backward pairing. This redundancy makes it difficult to show the necessity and sufficiency of plasticity in any one individual MBON for learned behaviors; however, in future experiments this could be achieved by using multiple drivers to silence various MBONs innervated by either the PAM or PPL cluster.

By examining neural and behavioral modulation over the same timescales and even concurrently within the same individuals, we reveal that bidirectional changes in KC-MBON signaling directly correlate with reversible changes in learned odor attraction from forward and backward conditioning. This suggests that modulatory pathways in the mushroom body have the capacity to transform the same dopaminergic signal into two opposing forms of neural and behavioral plasticity depending solely upon the relative timing of that signal to an odor presentation.

Chapter 4

Temporal Sensitivity Allows Animals to Contend with Complex Environments

4.1 Introduction

Olfaction is commonly used as part of a navigational strategy in the natural world to avoid harm and discover food. However, only in the laboratory, are olfactory environments finely tuned and tightly controlled. By contrast, in the wild, animals are forced to contend with turbulent odor plumes generated from dynamic wind patterns and a complexity of odor cues and blends. The complex chemical landscapes in nature suggest the high likelihood that animals encounter a variety of odors with different temporal relationships to a single reinforcement; however, the limited complexity of olfactory environments studied in the laboratory setting obscures insight into the mechanisms for the processing of high-order stimulus features that ensure animals form and maintain appropriate association in more naturalistic sensory environments.

A number of experiments in insects have begun to address how olfactory systems contend with complex and dynamic odor environments by simulating more naturalistic timescales of olfactory inputs and odor landscapes. For example, elegant electrophysiological and behavioral experiments in the moth, *Manduca sexta*, showed the capacity to navigate towards and target a

nectar resource in a simulated naturalistic, complex odor environment depends heavily on the plume frequency and volatiles present in the background, which directly influence neural representations of the target odor within the antennal lobe of the moth (Riffell et al., 2014).

In addition, behavioral experiments in *Drosophila* have explored this question by focusing on odor object segregation—a highly adaptive skill allowing animals to avoid a spoiled patch of food and instead approach a nutritive patch of food. These experiments demonstrate that *Drosophila* are remarkably sensitive to the arrival of odor stimuli, permitting them to discriminate between odor sources due to as little as a difference in a few milliseconds between cue onsets (Sehdev et al., 2018). The ability for flies to discriminate odor plumes on the millisecond timescale requires remarkable precision in the encoding of odor onset. Indeed electrophysiological recordings in olfactory sensory neurons reveal that odor-evoked spikes can be recorded with a latency of roughly ~3 ms from odor onset (Egea-Weiss et al., 2018) and furthermore, projection neurons ipsilateral to the source of odor spike a few ms prior to contralateral projection neurons (Gaudry et al., 2012), suggesting the exquisite capacity for rapid odor detection and localization in *Drosophila.* Temporal sensitivity of this kind may permit animals to form distinct associations in a complex odor environment where more than one odor may occur close in time to a reward.

In the previous chapter, I showed that the same dopaminergic signal in the mushroom body has the capacity to instruct bidirectional neural and behavioral plasticity depending on whether a single odor precedes or follows a reinforcement signal in time—a difference in time of only a few hundred milliseconds. This temporal sensitivity for bidirectional modulation may allow

animals to form distinct memories in a more complex odor environment where there is both an odor that precedes the onset of reward and an odor that follows reward offset. In the following sections, I explore the capacity for *Drosophila* to form distinct associations between multiple odors in an environment simulating a complex odor landscape and relate these distinct associations with odor coding in the MB circuitry. Experiments of this kind help expand our understanding for how animals experience their sensory world outside of the controlled environment of the laboratory and reveal hidden complexities in the coding properties of neural circuits involved in sensory-dependent learning and memory.

4.2 A Single Reinforcement Instructs Multiple Associations

Given our previous observation that odors preceding a reinforcement are endowed with distinct meaning in comparison to odors following the reinforcement in time (Figure 3.1), we asked whether a single dopaminergic reinforcement may differentially modulate future behavioral responses to two distinct monomolecular odors that bookend the reinforcement in time. The capacity to distinguish between two odors that occur close in time but with distinct temporal relationships to a reinforcement could serve as an adaptive strategy to contend with the complexity of the sensory environment of the real world.

To examine this possibility, we trained flies using two monomolecular odorants with a brief 1 second period of PAM neuron activation interposed between them, such that one odor was forward paired while the other was backward paired in time relative to the reinforcement (Figure 4.1A). We found that a single conditioning trial using this paradigm enhanced upwind tracking

to the forward-paired odor while synchronously decreasing tracking of the backward-paired odor. Inverting the order of the two odors in the subsequent conditioning trial had the opposite effect, suppressing attraction to the first odor while enhancing attraction to the second odor (Figures 4.1B-D). This odor-specific bidirectional modulation in behavior could be seen across 50 conditioning trials, in which the order of the two odors were repeatedly alternated in each conditioning trial. Importantly, animals showed this dual behavioral modulation when training flies with different odor pairs, suggesting that the capacity for a single dopamine signal to instruct multiple olfactory associations is independent of odor identity (Figure 4.2D). This sensitivity to timing for odor-specific modulation was not observed in parental control animals, further highlighting the important role of the PAM dopamine neurons in instructing these opposing associations and rapid reversals in odor-specific behaviors (Figures 4.2A-C and E). Thus, animals can extract multiple, opposing odor associations from the same DAN reinforcement.

4.3 Bidirectional Neural Plasticity From a Single Reinforcement

To verify that this odor-specific modulation was also apparent at the neural level, we replicated this conditioning paradigm in a tethered animal while monitoring olfactory responses of the γ4 MBON using functional calcium imaging (Figure 4.3A). As observed behaviorally, a single conditioning trial drove opposing forms of plasticity, depressing the response of the γ4 MBON to forward-paired odor while potentiating the response to the backward-paired odor. Moreover,

Figure 4.1, A Single Dopamine Reinforcement Instructs Two Opposing Memories
(**A**) Behavioral paradigm to examine how dopaminergic reinforcement instructs opposing memories for two odors based on their relative timing. For each conditioning trial, Odor1 (isobutyl acetate) and Odor2 (4-methylcyclohexanol) were either forward paired (FP) or backward paired (BP) with optogenetic activation of PAM DANs expressing CsChrimson. Note that the order of the two odors alternated with each conditioning trial. For each experiment, animals were conditioned 50 times such that each odor was forward paired 25 and backward paired 25 times. (**B**) Raster plot shows average upwind velocity of flies for Odor1 (pink) and Odor2 (green). Right: upwind displacement in odor plume of Odor1 (pink) and Odor2 (green) for the corresponding rows in the raster plot, mean ± SEM. (**C**) Representative upwind velocity of flies during Odor1 and Odor2 presentation (trials 7, 8, and 9 in (B)). Bold pink and green lines represent mean, light gray lines represent individual experiments; odor on is indicted by gray box. (**D**) Change in upwind displacement in Odor1 (pink) and Odor2 (green) after Odor1 was forward paired and Odor2 backward paired (left points) and after Odor1 was backward paired and Odor2 forward paired (right points), mean ± SEM. n = 8 experiments with 6 flies per experiment. Significant difference in modulation of behavior to Odor1 and Odor2 after pairing is indicated as follows: *** $p \leq 0.001$; paired t-test with Bonferroni correction.

Figure 4.1

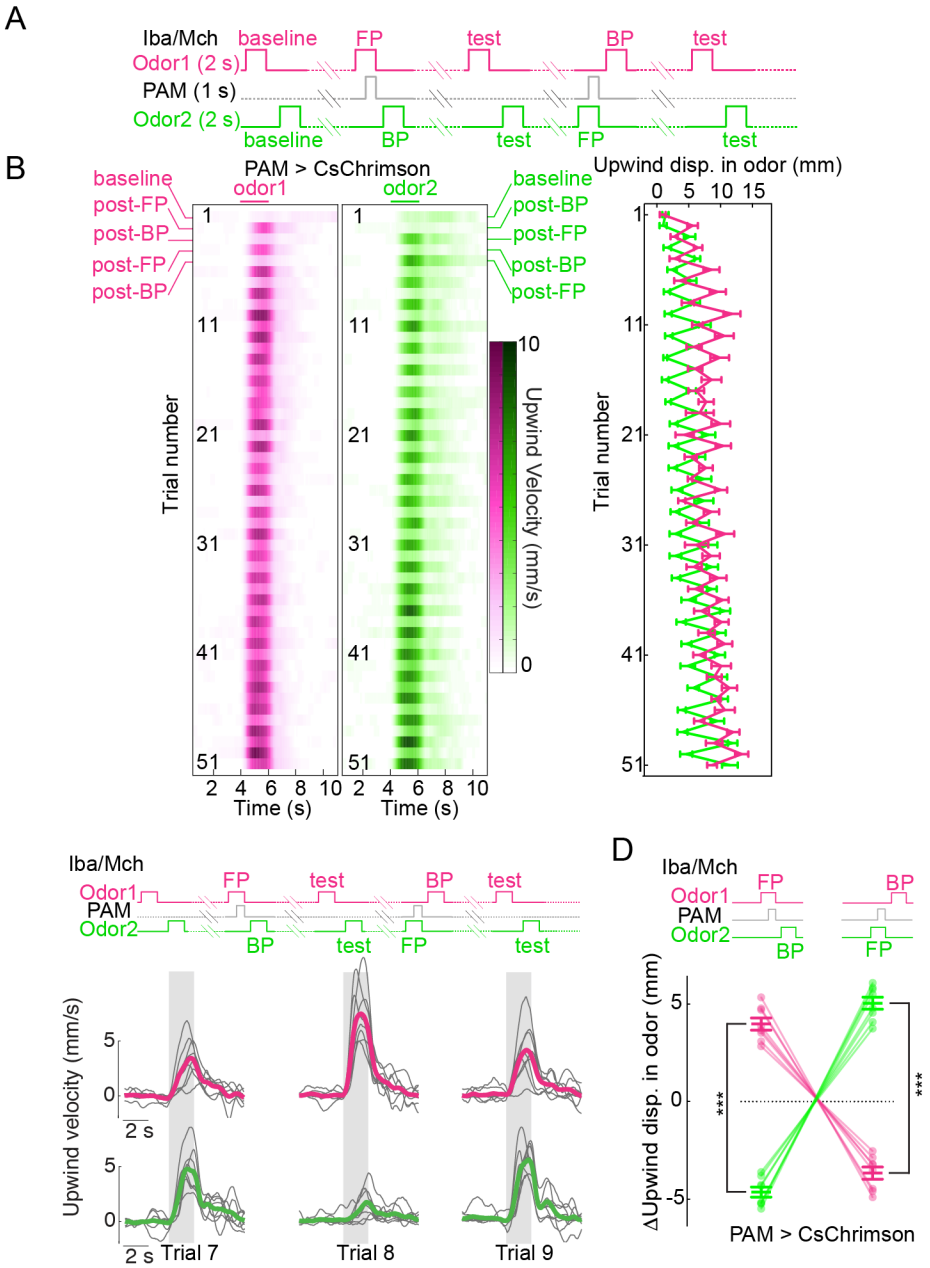
A
Iba/Mch
Odor1 (2 s)
PAM (1 s)
Odor2 (2 s)
baseline
FP
test
BP
test
baseline
BP
test
FP
test
B
PAM > CsChrimson
odor1
odor2
baseline
post-FP
post-BP
post-FP
post-BP
baseline
post-BP
post-FP
post-BP
post-FP
Trial number
Time (s)
Upwind Velocity (mm/s)
Upwind disp. in odor (mm)
C
Iba/Mch
Odor1
PAM
Odor2
Upwind velocity (mm/s)
2 s
Trial 7
Trial 8
Trial 9
D
ΔUpwind disp. in odor (mm)
PAM > CsChrimson

Figure 4.2, Modulation Depends on PAM Activation and is Independent of Odor Pairs
(**A**) Behavioral protocol, same as in Figure 4.2A (Odor1 is isobutyl acetate; Odor2 is 4-methylcyclohexanol). (**B,C**) Same analysis as in Figures 4.2B and D except using UAS-CsChrimson animals lacking the Gal4 driver, n = 7 experiments with 6 flies per experiment. Differences in modulation of behavior to Odor1 and Odor2 after pairing is indicated as follows: NS $p \geq 0.05$; paired t-test with Bonferroni correction. (**D-E**) Same behavioral protocol as in Figure 4.2A and analysis as in 4.2D except the two odors used were benzaldehyde (Odor1) and 1-hexanol (Odor2). (D) PAM > CsChrimson animals, mean ± SEM, n = 11 with 5 animals per experiment. (E) Control UAS-CsChrimson animals, mean ± SEM, n = 9 with 5 animals per experiment. Differences in modulation of behavior to Odor1 and Odor2 after pairing is indicated as follows: ** $p \leq 0.01$, NS $p \geq 0.05$; Wilcoxon match-paired sign rank test with Bonferroni correction.

Figure 4.2

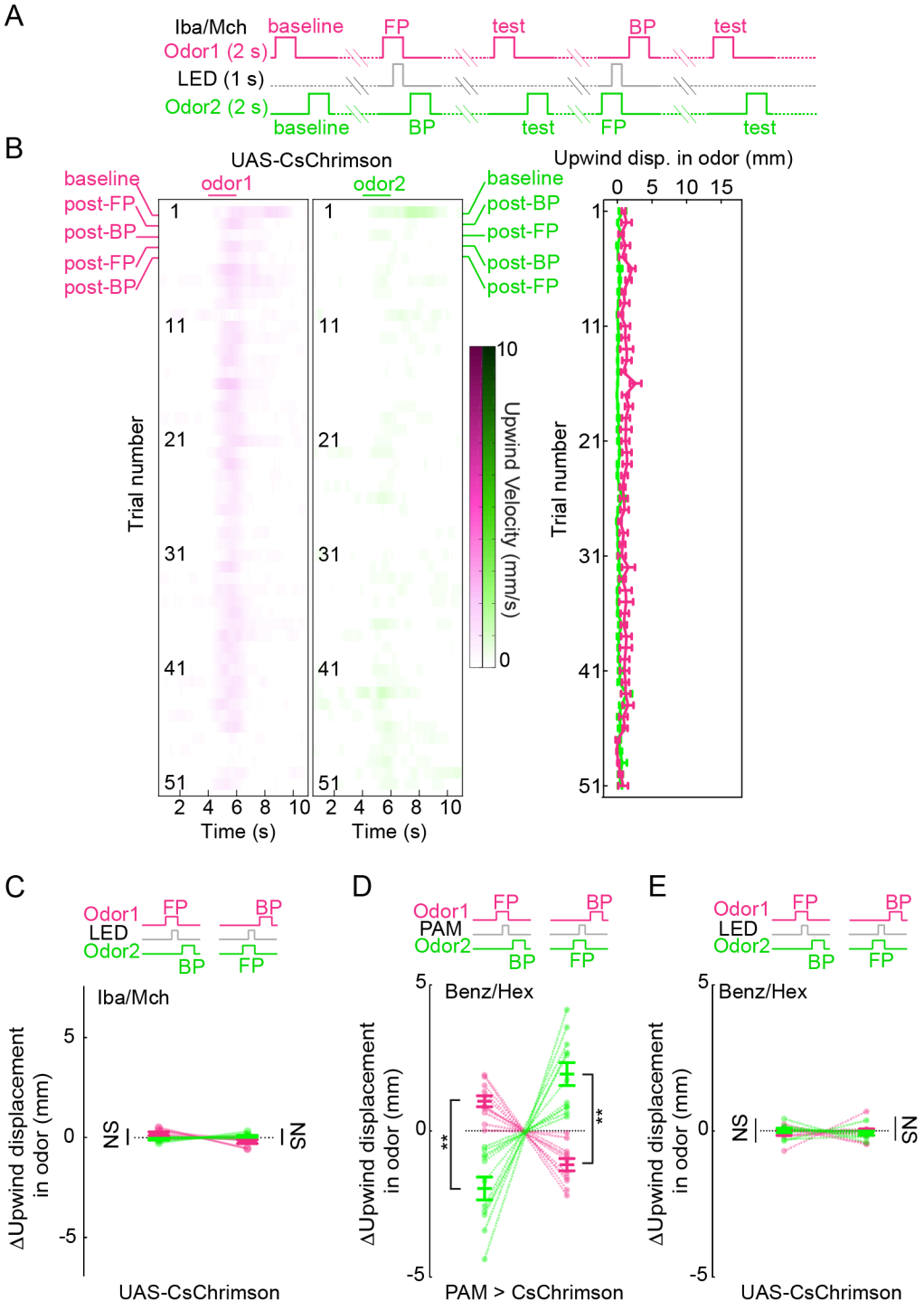
A
Iba/Mch
Odor1 (2 s)
LED (1 s)
Odor2 (2 s)
baseline
FP
test
BP
test
baseline
BP
test
FP
test
B
UAS-CsChrimson
odor1
odor2
baseline
post-FP
post-BP
post-FP
post-BP
baseline
post-BP
post-FP
post-BP
post-FP
Trial number
Time (s)
Upwind Velocity (mm/s)
Upwind disp. in odor (mm)
C
Odor1
LED
Odor2
FP
BP
BP
FP
Iba/Mch
ΔUpwind displacement in odor (mm)
NS
SN
UAS-CsChrimson
D
Odor1
PAM
Odor2
FP
BP
BP
FP
Benz/Hex
**
**
PAM > CsChrimson
E
Odor1
LED
Odor2
FP
BP
BP
FP
Benz/Hex
UAS-CsChrimson

inverting the temporal order of the two odors during a subsequent conditioning trial reversed both forms of modulation (Figures 4.3B-D). Again we were able to observe odor-specific plasticity across two different odor pairs, indicating a conserved sensitivity to timing of inputs regardless of odor identities. Together, these experiments highlight how the same dopaminergic reinforcement can synchronously drive the formation of multiple olfactory associations, allowing animals to take advantage of the different predictive temporal relationships that exist at any moment in a complex sensory environment.

4.4 Discussion

In the natural world, the sensory milieu surrounding a rewarding food source may be complex and dynamic due to turbulent wind flow and the presence of multiple odors. The volatile odors carried by turbulent plumes create a number of challenges for animals: 1) turbulent plumes create inconsistencies in odor concentration where periods of clean air are interspersed with bouts of high odor concentration and 2) the background chemical landscape can often dilute the salient odorant and minimize behavioral responses. To contend with such intermittent plumes, animals increase their speeds and reorient upwind upon the detection of an odor, and then perform a series of casts to hone in on the odor source (van Breugel and Dickinson, 2014). More recent, high-throughput analysis has parsed the elementary behaviors walking *Drosophila* use to track and search for odor sources (Álvarez-Salvado et al., 2018). Nonetheless, it is still unclear how animals contend with a dynamic odor environment to ensure they make the appropriate, causative association between an odor and a food reward amongst a backdrop of a complex odor-scape.

Figure 4.3, A Single Dopamine Reinforcement Drives Odor-Specific Plasticity in γ4 MBON (**A**) Schematic of *in vivo* preparation to examine modulation of γ4 MBON odor responses. Odor-evoked responses were recorded in γ4 MBON expressing GCaMP prior to and after pairing Odor1 and Odor2 with chemogenetic activation of γ4 DANs expressing $P2X_2$ using the 58E02-LexA driver. (**B**) Top: Conditioning paradigm with two odors. For the two conditioning trials, Odor1 and Odor2 are either forward paired or backward paired with a single activation of the PAM DANs. Note that the order of the two odors alternates across conditioning trials. The two odors used were isobutyl acetate and 4-methylcyclohexanol. Bottom: γ4 MBON responses after conditioning with two odors. n = 5 animals, mean ± SEM. (**C**) Same as in (B) except the two odors used were benzaldehyde and 1-hexanol. n = 4 animals, mean ± SEM. (**D**) Change in γ4 MBON response to Odor1 (pink) and Odor2 (green) after Odor1 was forward paired and Odor2 backward paired (left points) and after Odor1 was backward paired and Odor2 forward paired (right points). Open circles: data using isobutyl acetate and 4-methylcyclohexanol odor pairs (5 animals). Closed circles: data using benzaldehyde and 1-hexanol odor pairs (4 animals). Differences in neural response to Odor1 and Odor2 after pairing is indicated as follows: ** $p \leq 0.01$; Wilcoxon match-paired sign rank test with Bonferroni correction.

Figure 4.3

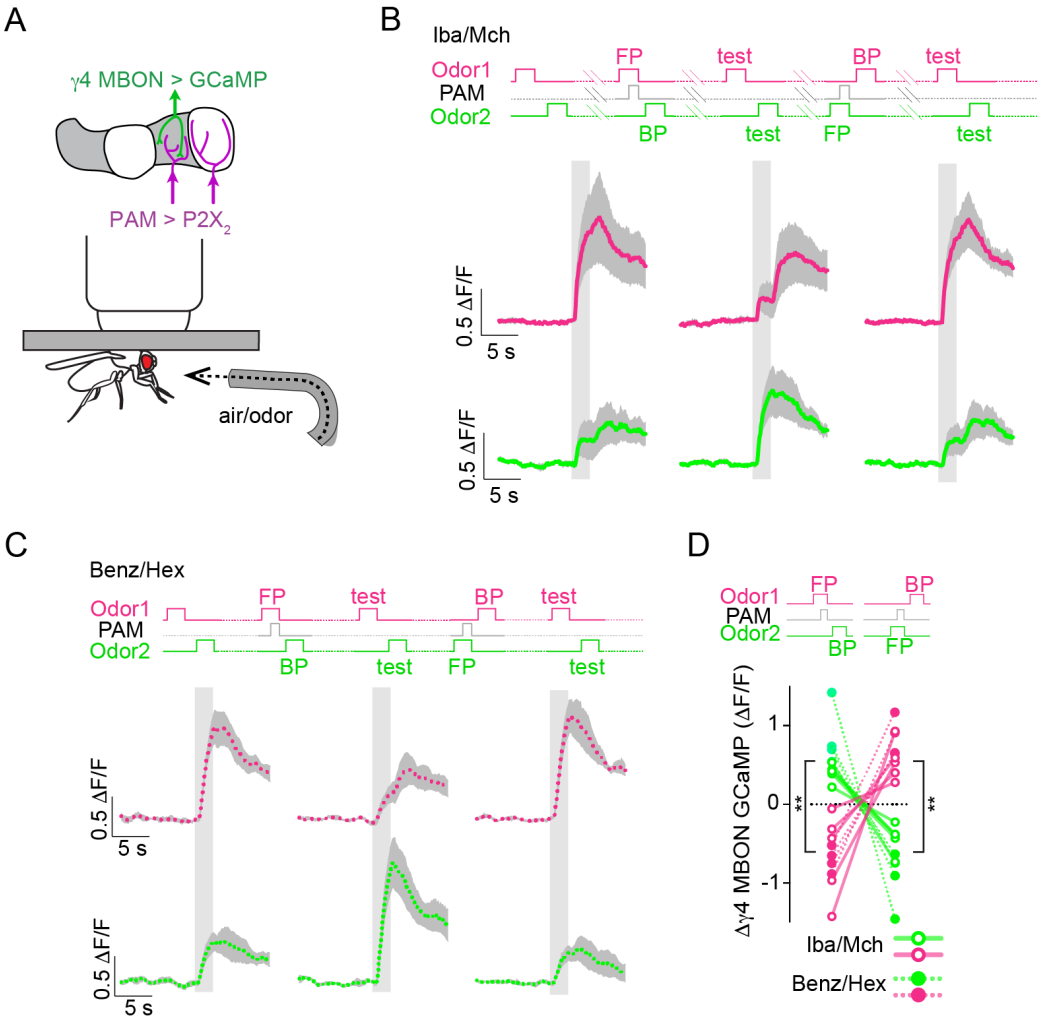
A
γ4 MBON > GCaMP
PAM > P2X2
air/odor
B
Iba/Mch
Odor1
PAM
Odor2
FP
test
BP
test
BP
test
FP
test
0.5 ΔF/F
5 s
0.5 ΔF/F
5 s
C
Benz/Hex
Odor1
PAM
Odor2
FP
test
BP
test
BP
test
FP
test
0.5 ΔF/F
5 s
0.5 ΔF/F
5 s
D
Odor1
PAM
Odor2
FP
BP
BP
FP
Δγ4 MBON GCaMP (ΔF/F)
1
0
-1
**
**
Iba/Mch
Benz/Hex

To form the appropriate associations, animals must be able to selectively attend to odors predictive of a good food patch while avoiding odors associated with a spoiled or depleted food patch. One successful strategy for staying on a healthy and nutritive food patch would be for an animal to continuously approach odor cues that promote a rise in food reinforcement and avoid odors that lead to a decrease in food reinforcement. This simple bidirectional sensitivity to cues that precede or lag a food reward in time ensures the prolonged luxury of nutritious food.

Here, we show that a single reinforcement of the PAM neurons is sufficient to drive increased attraction to odors that precede PAM activation and a synchronous decrease in attraction to odors the follow PAM activation in time. This sensitivity to timing observed at the behavioral level likely emerges from the bidirectional and odor-specific plasticity observed between the KC-MBON synapses using a similar conditioning paradigm. From these experiments, we reveal the remarkable capacity of the mushroom body to use a single DAN reinforcement to instruct two opposing olfactory associations in parallel.

Behavioral experiments in *Drosophila* have recently suggested that the compartments involved in short-term memory, the gamma compartments of the mushroom body, have the capacity to only form a single olfactory association at a time (Aso and Rubin, 2016). When an animal learns a new association, the memory of the prior association is completely eroded or unable to be retrieved (Aso and Rubin, 2016). Instead, we show that the temporal sensitivity of the mushroom body permits animals to use a single dopamine reinforcement to instruct two, opposing olfactory associations in parallel. These associations depend on the relative timing between the odor presentation and the DAN reinforcement during conditioning. While this environment is still

certainly simplistic compared to the natural environment in the wild, it has revealed useful insight into more sophisticated coding properties of the mushroom body circuitry.

This capacity for a single reinforcement to instruct bidirectional neural and behavioral plasticity in parallel may serve two important roles in odor navigation in *Drosophila*. As discussed above, this bidirectional plasticity may allow animals to differentiate between odors to approach and odors to avoid in order to obtain nutritive resources. Alternatively, this synchronous and opposing plasticity may serve to enhance the signal-to-noise of neural responses for odors truly predictive of reward over neural responses to background or non-predictive odors that happen to be encountered in close temporal proximity. These two possibilities need not be mutually exclusive and in fact animals may use enhanced signal to noise of forward paired odors relative backward paired odors as a mechanism to increase the contrast between odors that should be approached versus those to be ignored or avoided.

Chapter 5

Dopamine Pathways in Coincidence and Order Detection

5.1 Introduction

To infer the causal relationship between events requires both the detection of the order and coincidence of inputs. In the previous chapter, I showed that neural and behavioral responses are modulated depending on the temporal structure of conditioning where both the convergence of inputs and order of inputs are necessary for mediating the bidirectional responses. These results leave us with two important questions: Where is the temporal order of olfactory and dopaminergic input detected within the mushroom body circuitry? And how do these detection mechanisms influence the neural and behavioral plasticity? The bidirectional neural and behavioral modulation presented in the previous chapter occurs over a narrow temporal window. As the inter-stimulus interval between odor and DAN increases, the neural and behavioral modulation steeply drops off. In addition, the sign of plasticity depends on whether the odor precedes or follows DAN activation in time. These observations suggest that the bidirectional modulation relies on two distinct features of associative conditioning: 1) the time delay between the two inputs and 2) the sequence or ordering of the two inputs. The following chapter addresses how the MB is sensitive to both the coincidence and the order of events during conditioning to mediate the bidirectional changes in neural and behavioral responses.

Coincidence detection is defined by the convergent arrival of two distinct inputs and therefore has both a spatial and temporal component. A variety of coincidence detectors exist in the brain in mediating the integration and processing of information. For example, in the superior olivary nucleus, a delay line circuit architecture allows neurons to serve as coincidence detectors, firing maximally when receiving synchronous inputs originating from both ears (Oliver et al., 2003; Smith et al., 1993). This mechanism for coincidence detection in the brainstem is central to our ability for sound localization. By contrast, some coincidence detectors are molecules whose unique biochemical properties permit them to integrate synchronous activity from local inputs (Buhusi et al., 2016). It is thought that these molecular coincidence detectors serve a central role in driving the formation of associative memories, and indeed a number of receptors have been identified as coincidence detectors in associative learning circuits. For example, to activate the NMDA channel—a channel central to STDP and LTP—requires not just the binding of glutamate but also necessitates depolarization to remove a magnesium block (Miyashita et al., 2012; Tabone and Ramaswami, 2012). Similarly, IP_3-dependent LTD in Purkinje fibers of the cerebellum relies on both the production of IP_3 through phosopholipase C dependent cleavage of PIP2 and influx of calcium through voltage-gated calcium channels (Freeman, 2015; Sarkisov and Wang, 2008).

Unlike coincidence detectors that rely on two events happening close in time, order detectors encode the specific sequence of events. For example, a molecular coincidence detector may be activated as long as A and B occur within a small time window regardless of whether stimulus A precedes or follows B. By contrast, an order detector may require A to precede B within some time window in order for activation.

In 1949, Donald Hebb proposed that synaptic strengthening between neurons could occur as a result of repeated coincident activation of pre- and post-synaptic neurons:

> Let us assume that the persistence or repetition of a reverberatory activity (or "trace") tends to induce lasting cellular changes that add to its stability.... When an axon of cell A is near enough to excite a cell B and repeatedly or persistently takes part in firing it, some growth process or metabolic change takes place in one or both cells such that A's efficiency, as one of the cells firing B, is increased. (Hebb, 1949)

His theory was later supported by the discovery of LTP (Bliss and Lømo, 1973), in which the long-lasting depolarization of the pre-synaptic neuron permits removal of the magnesium block on post-synaptic neurons and the upregulation of another glutamatergic receptor channel called NMDA receptors, resulting in increased calcium influx and depolarization of the post-synaptic neuron (Mayer et al., 1984; Muller et al., 1988; Nowak et al., 1984). Later work in memory mutants in *Drosophila* expanded our understanding of molecular coincidence detectors through the discovery that the calcium-activated adenylate cyclase, rutabaga, plays a central role in detecting the coincident arrival of a sensory stimulus and a neuromodulator-dependent reinforcement signal to drive the formation of associative memories following forward pairing (Figure 5.1A) (Bourne and Nicoll, 1993; Levin et al., 1992; Livingstone et al., 1984). Since this discovery, a number of experiments have characterized the role of rutabaga in associative learning circuits (Gervasi et al., 2010; Tomchik and Davis, 2013; Tully and Quinn, 1985; Zars et al., 2000).

Figure 5.1, Classic Learning Mutant *Rutabaga* has Minor Effect on Plasticity.
(**A**) Schematic of signaling cascade diagraming how coincidence of sensory stimulus (odor) and reinforcement (reward or punishment) act to synergistically activate calcium-activated adenylate cyclase *Rutabaga*, a long known learning mutant in *Drosophila*. (**B-C**) Fold change in KC-evoked response in the γ4 MBON after forward and backward pairing shows a minimal deficit in *Rutabaga* (Rut^1) mutant (purple) following forward pairing and no effect in the synaptic plasticity following backward pairing. Fold change in MBON response was calculated by normalizing the peak response in calcium in γ4 MBON after pairing by the peak calcium level prior to pairing. Significant difference between control and rutabaga animals is tested with unpaired t-test: * < 0.05, ns ≥ 0.05.

Figure 5.1

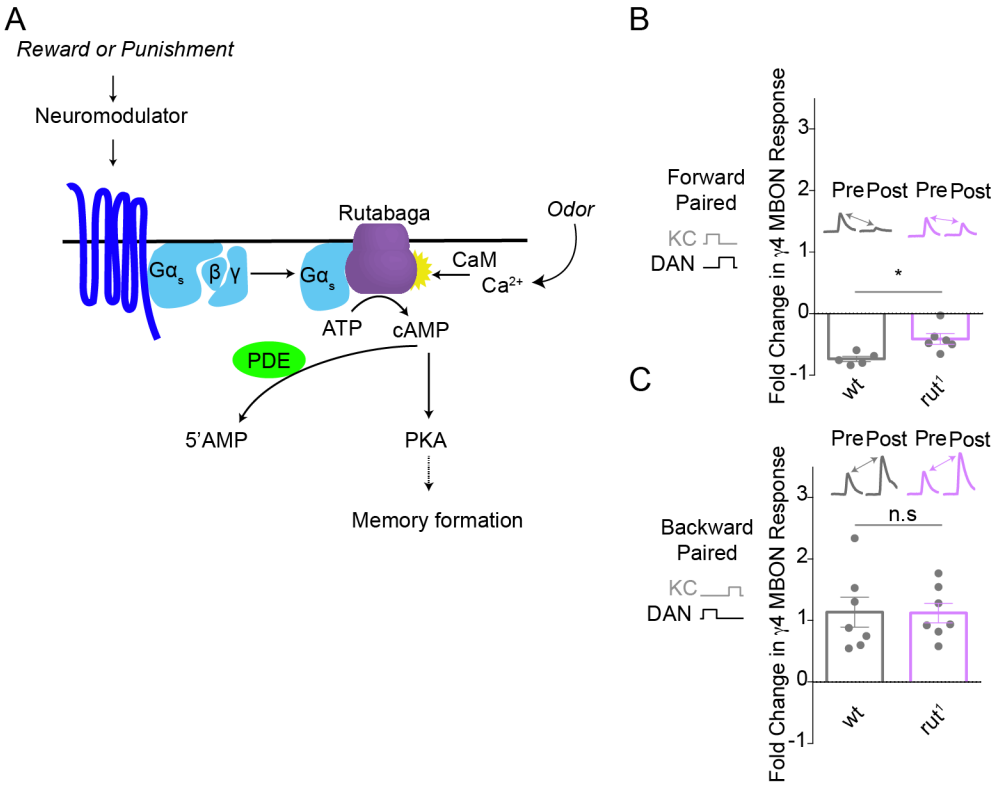
A
Reward or Punishment
Neuromodulator
Rutabaga
Odor
Gαs
β γ
Gαs
CaM
Ca2+
ATP
cAMP
PDE
5'AMP
PKA
Memory formation
B
Forward Paired
KC
DAN
Fold Change in γ4 MBON Response
Pre Post Pre Post
*
wt
rut1
C
Backward Paired
KC
DAN
Fold Change in γ4 MBON Response
Pre Post Pre Post
n.s
wt
rut1

However, preliminary experiments examining the role of the *Drosophila* rutabaga gene in the bidirectional plasticity of the mushroom body, suggest additional forms of coincidence detection and order-detection mechanisms are involved in sculpting the temporal sensitivity of associative learning and neural plasticity. In the rutabaga-learning mutant described above, we observed that synaptic depression was selectively impaired by roughly 50% following forward pairing (Figure 5.1B) but remarkably potentiation following backward pairing was unaffected (Figure 5.1C). This result confirms that rutabaga serves as a coincidence detector in partially contributing to the depression following forward pairing, but suggests it does not play a role in backward pairing. These results reveal an incomplete understanding for how temporal sensitivity is achieved in the mushroom body and suggests additional proteins are essential for the bidirectional neural plasticity.

One intriguing model for how bidirectional plasticity emerges in the mushroom body is that forward and backward pairing may selectively engage two distinct dopamine receptors, DopR1 (also termed *dumb* or dDA1) and DopR2 (also termed *damb*) that are co-expressed in the same KCs (Croset et al., 2018) and have been proposed to play distinct roles in the formation and erosion of memories (Figure 5.2A) (Berry et al., 2012; Himmelreich et al., 2017; Kim et al., 2007; Qin et al., 2012). Sequence analysis suggests the DopR1 shares homology with the D1-like mammalian receptors; by contrast, DopR2 shares greatest sequence homology with the beta-adrenergic receptor, highlighting the distinct signaling properties of these two receptors (Figure 5.2B). This suggestion is in line with *in vitro* characterization of these dopamine receptors revealing that they preferentially couple to distinct G-protein partners, with DopR1 coupling to Gαs to stimulate cAMP production and DopR2 preferentially coupling to Gαq to drive increased

Figure 5.2, *Drosophila* Dopamine Receptors Couple to Distinct Intracellular Pathways
(**A**) The role of DopR1 and DopR2 in opposing regulation of memory described at the behavioral level (Berry et al., 2012; Himmelreich et al., 2017; Kim et al., 2007; Qin et al., 2012). (**B**) Sequence homology tree of neurmodulatory receptors highlighting distinct lineage of DopR2. (**C**) Top: Schematic of bioluminescence resonance energy transfer (BRET)-based biosensors used to assess GPCR coupling properties of DopR1 and DopR2. Bottom: DopR1 preferentially couples to Gαs while DopR2 strongly couples to Gαq. (**D**) Luminescent and fluorescent signals measuring cAMP and cystolic calcium in heterologous expression system to examine second messenger production downstream of DopR1 and DopR2. In this reduced system the binding of dopamine to DopR1 and DopR2 lead to elevated cAMP levels likely through distinct mechanisms (left). By contrast, the binding of dopamine to DopR2 produces elevated calcium levels while DopR1 does not (right). This calcium rise is blocked by the addition of the Gαq inhibitor, YM-254890, suggesting the source of calcium is from endoplasmic reticulum stores. Figures C-D kindly generated and provided by Andrew Siliciano.

Figure 5.2

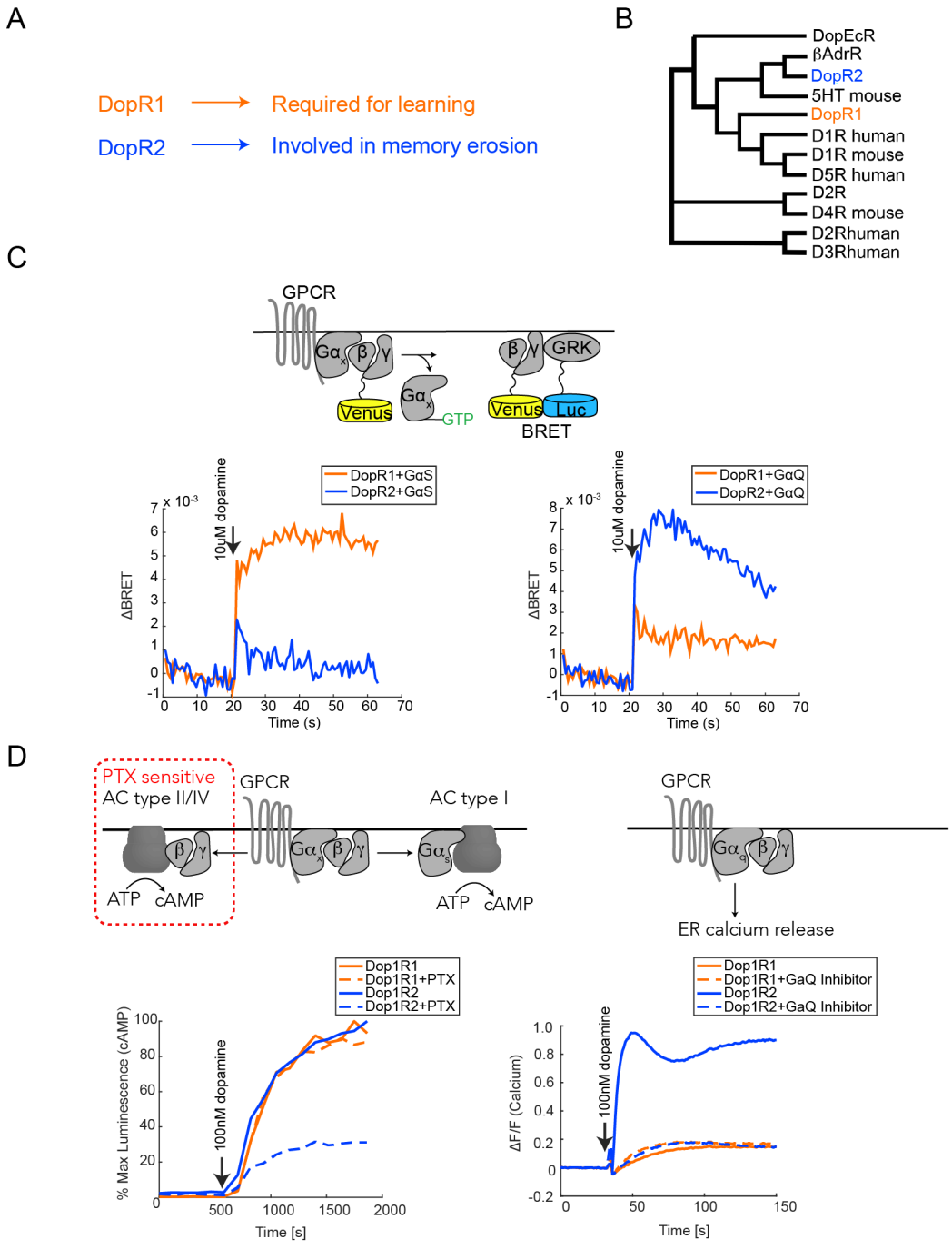
A
DopR1
Required for learning
DopR2
Involved in memory erosion
B
DopEcR
βAdrR
DopR2
5HT mouse
DopR1
D1R human
D1R mouse
D5R human
D2R
D4R mouse
D2Rhuman
D3Rhuman
C
GPCR
Gαx
β
γ
GRK
Venus
Luc
GTP
BRET
DopR1+GαS
DopR2+GαS
DopR1+GαQ
DopR2+GαQ
10uM dopamine
x 10-3
ΔBRET
Time (s)
D
PTX sensitive
AC type II/IV
AC type I
ATP
cAMP
Gαq
ER calcium release
Dop1R1
Dop1R1+PTX
Dop1R2
Dop1R2+PTX
Dop1R1+GaQ Inhibitor
Dop1R2+GaQ Inhibitor
100nM dopamine
% Max Luminescence (cAMP)
ΔF/F (Calcium)
Time [s]

cytosolic calcium (Figures 5.2C-D) (Feng et al., 1996; Gotzes et al., 1994; Han et al., 1996; Himmelreich et al., 2017; Sugamori et al., 1995). However, it is important to note DopR2 is also capable of producing pertussis toxin sensitive cAMP, suggesting additional promiscuous coupling properties of DopR2 *in vitro* (Figure 5.2D).

The observation that these two dopamine receptors selectively engage distinct signaling pathways suggests a mechanism for their opposing role in memory regulation at the behavioral level and hints at the potential for selective engagement in the bidirectional modulation of KC-MBON synapses. While, it has been proposed that DopR1 and DopR2 are selectively engaged under different levels of dopamine release due to differences in affinity levels — a mechanism similarly invoked in mammalian systems — there is little evidence for this outside of *in vitro* assays, which fail to recapitulate the critical microenvironment of *Drosophila* neurons (Berry et al., 2012; Himmelreich et al., 2017).

We address this hypothesis directly using functional imaging experiments and demonstrate that differences in affinity are insufficient to explain the interesting temporal sensitivity of these two distinct signaling pathways. In focusing on how the dopamine signals are perceived by post-synaptic neurons in the mushroom body and influence downstream signaling cascades, I hope to provide insight into how the memory relevant synapses within a learning center are sensitive to the temporal order of sensory and dopaminergic reinforcement.

5.2 Coincidence Detection Occurs in Post-Synaptic Sites

In vitro, DopR1 and DopR2 exhibit different sensitivities for dopamine, raising the possibility that these receptors could be differentially recruited if forward and backward conditioning drove different levels of DAN activity and dopamine release (Berry et al., 2012; Himmelreich et al., 2017). If the level of DAN activity and dopamine release were to differ between forward and backward pairing, it would suggest some form of coincidence or order detection occurs at the level of DANs in this circuitry.

We therefore compared DAN activity and dopamine release during forward and backward pairing in the same brain explant preparation used to measure bidirectional KC-MBON plasticity. Imaging calcium influx in DAN axon terminals revealed that forward and backward pairing evoked equivalent responses that were indistinguishable from direct stimulation of DANs alone (Figure 5.3A). Moreover, we measured the levels of dopamine released in the different conditioning paradigms using either a pHlourin fused to the monoamine transport protein, VMAT, to visualize pre-synaptic vesicle fusion and reuptake in DANs (Wu et al., 2013) (Figure 5.3B) or the $GRAB_{DA1m}$ dopamine sensor expressed in post-synaptic sites along the KC axons (Sun et al., 2018) (Figure 5.3C). Both methods revealed equivalent levels of dopamine release in forward and backward pairing, indicating that differences in dopaminergic activity cannot account for the opposing forms of neural and behavioral modulation, and suggesting that mechanisms regulating neural plasticity may lie downstream of dopamine receptors in post-synaptic neurons.

Figure 5.3, Dopamine Neurons are Insensitive to Timing of Events Suggesting Post-Synaptic Sensitivity in Kenyon Cell Axons

(**A**) GCaMP6s responses from γ4/γ5 DANs during forward pairing, backward pairing, and dopamine stimulation alone and comparison of peak response in DANs during different conditions. n = 5, mean ± SEM. (**B**) Same as in (A) except VMAT-pHluorin signals used to measure synaptic vesicle release from γ4/γ5 DANs). n = 5, mean ± SEM. (**C**) Same as in (A-B) except using a dopamine sensor ($GRAB_{DA1m}$) expressed in KC axons traversing the γ4/γ5 compartments, n = 7, mean ± SEM. Significance is indicated as follows: NS $p \geq 0.05$, ordinary one-way ANOVA. (**D**) Left: acetylcholine release from KC axons in γ4/γ5 in baseline, post-backward pairing, and post-forward pairing shows bidirectional regulation of release depending on the timing of events. Right: The change in acetylcholine release post-BP and post-FP suggests that KC axons are sensitive to the timing of events and play a role in bidirectional plasticity. n = 6, mean ± SEM.

Figure 5.3

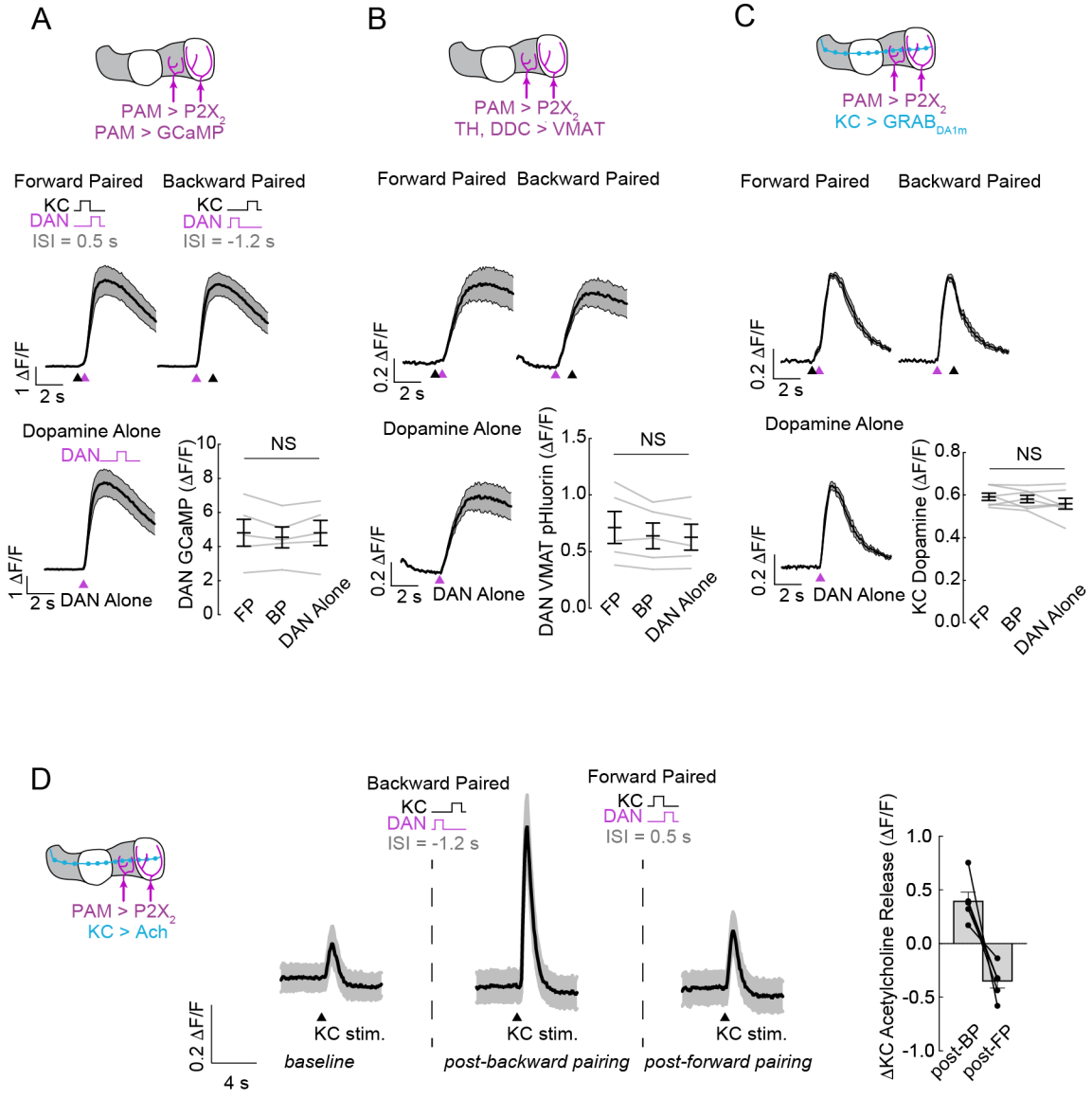
A
PAM > P2X2
PAM > GCaMP
Forward Paired
Backward Paired
KC
DAN
ISI = 0.5 s
ISI = -1.2 s
1 ΔF/F
2 s
Dopamine Alone
DAN
2 s DAN Alone
DAN GCaMP (ΔF/F)
NS
FP
BP
DAN Alone
B
PAM > P2X2
TH, DDC > VMAT
0.2 ΔF/F
DAN VMAT pHluorin (ΔF/F)
C
PAM > P2X2
KC > GRABDA1m
KC Dopamine (ΔF/F)
D
PAM > P2X2
KC > Ach
0.2 ΔF/F
4 s
KC stim.
baseline
post-backward pairing
post-forward pairing
ΔKC Acetylcholine Release (ΔF/F)
post-BP
post-FP

The KCs have long been suggested to be the critical site of coincidence detection and neural plasticity related to associative learning. Experiments measuring cAMP production in KCs has found supra-linear cAMP levels in KC axons during associative conditioning (Boto et al., 2014; Tomchik and Davis, 2009). Additionally, restoration of DopR1 exclusively in the gamma KCs have been shown to rescue learning deficits (Qin et al., 2012). In fact, activation of subsets of DANs within the MB have been shown sufficient to locally modulate second messengers in KC axons in a spatially discrete, compartmentalized manner (Cohn et al., 2015; Tomchik and Davis, 2009). Lastly, sophisticated electrophysiological experiments reveal that spiking in the post-synaptic MBONs is not required for learning-dependent plasticity in the mushroom body, further highlighting the essential role of KCs as the driving force for odor-specific plasticity in the MB (Hige et al., 2015). Collectively, these observations suggest that the temporal sensitivity of associative learning is achieved through specialized coincidence and order detectors present in the molecular machinery of KC axons.

In the previous chapter, we measured the change in neural responses in MBONs as a result of associative conditioning; however, if the coincidence and order detection mechanisms exist in KC axons, it is likely that these alterations in MBON responses arise from modulation of pre-synaptic KCs. The KCs of the MB are thought to be cholinergic, releasing acetylcholine onto post-synaptic partners, which include MBONs, DANs, and other KCs through axo-axonic connections (Takemura et al., 2017). To assess whether conditioning alters acetylcholine release in KC axons, we expressed an acetylcholine sensor in KC axons to determine whether the activity of KCs was modulated as a result of forward and backward pairing (Jing et al., 2018). While expressing this acetylcholine sensor in the post-synaptic MBONs would offer a more

direct readout of alterations in neurotransmission, this strategy was technically challenging due to weak expression of the fluorescent sensor in the MBONs. Nevertheless, we reasoned that expressing the acetylcholine sensor within KC axons would still provide an accurate readout for the release of acetylcholine from KCs.

Indeed, activating KCs directly by stimulating their dendrites in the calyx evoked measurable acetylcholine responses in the KC axons. Backward pairing of KC activation with the activation of the PAM DANs innervating the γ4 and γ5 compartments potentiated the release of acetylcholine in the KCs, and this potentiation could be depressed by instead forward pairing KC activation with PAM stimulation (Figure 5.3D). While, a more definitive statement on this matter would require silencing of KCs to block transmission to ensure the change in signal emerges directly from KC synapse, these results suggest that acetylcholine release from KC axons is bidirectionally modulated depending on forward and backward pairing and emphasizes that the neural modulation measured in the post-synaptic MBONs likely arises from changes in neurotransmitter release in the pre-synaptic KCs. . In addition, protein expression and mRNA profiling of DopR1 and DopR2 across the different neural populations of the MB indicate enrichment of DopR1 and DopR2 in KCs. Furthermore, behavioral and functional experiments have highlighted the critical role of DopR1 and DopR2 expressed in KCs in supporting aversive learning and contributing to the compartmentalized patterns of pre-synaptic modulation along KC axons, respectively (Cohn et al., 2015; Qin et al., 2012). Together, these observations provide compelling evidence that the mechanisms for the temporal sensitivity observed at the neural and behavioral level lie in the molecular machinery of the KC axons.

5.3 Dopamine Receptor Pathways are Sensitive to Temporal Order

Based on the likelihood of dopamine acting at the site of pre-synaptic KC axons, we were interested in examining the recruitment of DopR1 and DopR2 under the different conditioning paradigms of associative learning within the KCs of the γ lobe. To do this, we used optical reporters of the second-messengers downstream of Gαs (cAMP) and Gαq (endoplasmic reticulum calcium release) to examine these dopamine receptor-signaling pathways in KC axons during conditioning. While a FRET-based cAMP reporter existed in the fly and had been previously used to examine the effects of forward pairing (Boto et al., 2014; Tomchik and Davis, 2009), an optical reporter of endoplasmic reticulum (ER) calcium did not. Fortunately, a low-affinity genetically encoded calcium indicator targeted and retained in the ER lumen had recently been generated and characterized in a mammalian system (de Juan-Sanz et al., 2017). The ER calcium sensor contains an N-terminal calreticulin signaling peptide and a KDEL sequence that permits the proper trafficking and retention of the sensor in the ER lumen (Figure 5.4A) (de Juan-Sanz et al., 2017; Kendall et al., 1994). Indeed, co-expression of this ER calcium sensor with DopR2 in a heterologous expression system lead to dopamine-dependent calcium release from ER stores, which could be blocked by the application of a Gαq inhibit (YM-254890) (Figure 5.4B). This low-affinity calcium sensor (ER-GCaMP, K_d = 210μM) was inserted into a 10XUAS vector and injected into *Drosophila.* Expression of ER-GCaMP using a KC specific driver (OK107) could be visualized using a two-photon microscope (Figure 5.4C-D). With fluorescent reporters for both cAMP and ER calcium release at hand, we could now test the temporal sensitivity of these two second messenger pathways known to be downstream of DopR1 and DopR2.

Figure 5.4, Low-Affinity Endoplasmic Reticulum (ER) Calcium Sensor Permits Real-Time Analysis of ER Calcium Regulation in Kenyon Cell Axons

(**A**) Design of low-affinity GCaMP sensory targeted and retained in the ER lumen using N-terminal calreticulin peptide signal and C-terminal KDEL sequence. Adapted from (de Juan-Sanz et al., 2017). (**B**) Black: ER-calcium release resulting from dopamine binding to DopR2 in exogenously expressed HEK293T cells. Red: Blockade of ER-calcium release in the presence of the Gaq inhibitor YM-254890. Traces generated and kindly provided by Andrew Siliciano. (**C**) The ER-GCaMP-210 sensor was inserted PCR amplified using KOD Hot Start DNA polymerase and inserted into the UAS plasmid, pJFRC81 (Addgene Plasmid #36432). Baseline expression of the sensor can be observed by driving ER-GCaMP-210 in KCs using the OK107-Gal4 driver. (**D**) Schematic for fluorescent signals generated by sensor depending on whether the ER is taking up or releasing calcium.

Figure 5.4

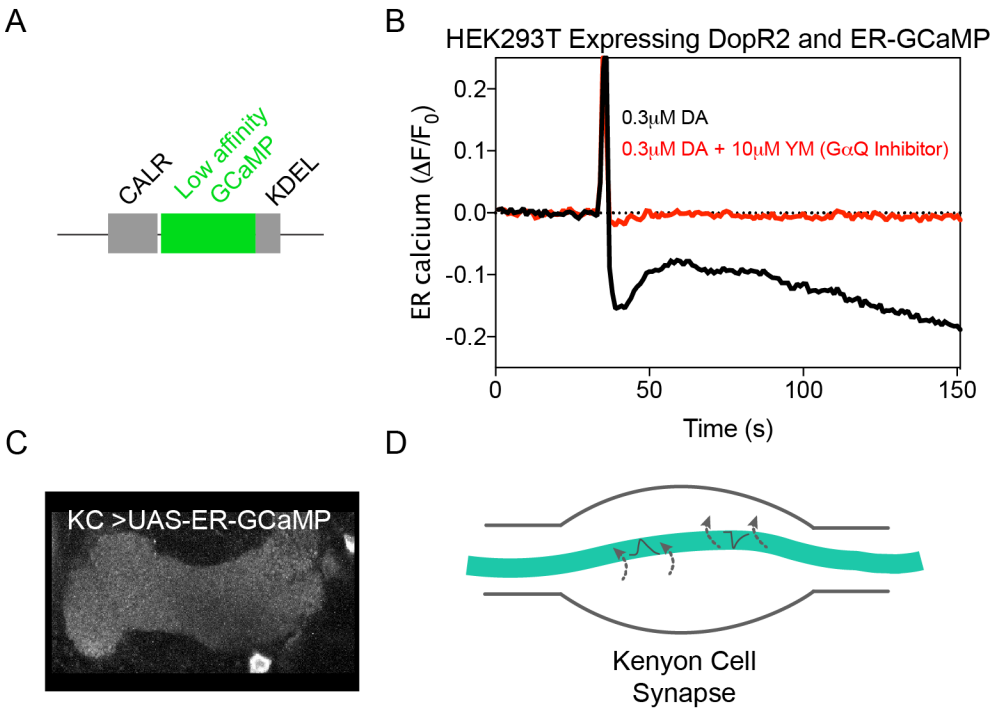
A
CALR
Low affinity GCaMP
KDEL
B
HEK293T Expressing DopR2 and ER-GCaMP
0.3μM DA
0.3μM DA + 10μM YM (GαQ Inhibitor)
ER calcium (ΔF/F0)
0.2
0.1
0.0
-0.1
-0.2
0
50
100
150
Time (s)
C
KC >UAS-ER-GCaMP
D
Kenyon Cell
Synapse

cAMP has been extensively studied as an effector of Gαs signaling that regulates synaptic plasticity (Boto et al., 2014; Brunelli et al., 1976; Kandel et al., 1976; 1983; Tomchik and Davis, 2009). Indeed, results in the *Drosophila* MB have suggested that cAMP production is maximally produced following forward pairing, suggesting this second messenger serves as the critical signaling molecule in associative conditioning. However, these experiments use a crude, and temporally imprecise way of activating KC and DANs to look at the dependence of timing on cAMP production (Tomchik and Davis, 2009), making it difficult to draw definitive conclusions over the time course of cAMP in KC axons.

We again used the simplified brain explant experiment relying on direct KC activation with iontophoresis of acetylcholine and direct activation of DANs expressing the $P2X_2$ channel, allowing for temporally precise activation of neural populations on the sub-second timescale. We monitored cAMP production in KC axons using a FRET based cAMP reporter (Shafer et al., 2008) while varying the relative timing of PAM dopaminergic reinforcement and KC stimulation, using the same inter-stimulus intervals that drove bidirectional plasticity within the γ4 compartment (Figures 3.2B-C). We found that cAMP was produced by direct DAN stimulation alone and under all conditioning parameters (Figures 5.5A and C). cAMP production was maximal when KC and DAN stimulation were temporally coincident, matching the timing that gave rise to the strongest depression of KC-MBON signaling (Figures 3.2B-C and 5.5C). These observations support biochemical and behavioral evidence that calcium sensitive adenylate cyclases, like the classic learning mutant *rutabaga*, may serve as molecular coincidence detectors to amplify cAMP production during associative conditioning (Levin et al., 1992; Livingstone et al., 1984; Mons et al., 1999; Tomchik and Davis, 2009). However, while forward and backward

pairing give rise to opposing forms of neural and behavioral plasticity, these conditioning protocols evoked comparable cAMP levels, implying that this second messenger cannot alone encode the temporal order of odor and dopaminergic reinforcement. We therefore asked whether DopR2 signaling pathways might account for the temporal sensitivity of MB plasticity. Upon activation of Gαq, inositol triphosphate (IP_3) is produced, resulting in IP_3-receptor dependent calcium release from the endoplasmic reticulum (ER) (Berridge, 1993).

To examine signaling through Gαq, we targeted a low-affinity GCaMP to the ER lumen in KC axons (de Juan-Sanz et al., 2017) and monitored calcium efflux from the ER during conditioning trials. We found that ER calcium in KC axons was selectively released during backward pairing, with no efflux apparent during forward pairing (Figures 5.5B-C). Notably, just as the inter-stimulus interval that evoked maximal cAMP production matched the timing of the strongest KC-MBON depression, the inter-stimulus interval that evoked the greatest ER calcium efflux matched the timing of the strongest potentiation (Figures 3.2B-C and 5.3C).

Therefore, while Gαs signaling is sensitive to the temporal coincidence of inputs to the mushroom body during associative conditioning, Gαq signaling depends on their temporal ordering, suggesting that these two pathways may work in concert to generate bidirectional plasticity. Indeed, a simple linear summation of the cAMP and ER signals elicited by each pairing protocol replicated the biphasic curve of KC-MBON plasticity (Figure 5.5D), indicating that the selective recruitment of these second-messenger pathways is sufficient to account for the temporal dependence of neural and behavioral modulation.

Figure 5.5, Dopamine Receptor Pathways in Kenyon Cell Axons are Sensitive to the Timing of Events

(**A-B**) Measuring second messengers, cAMP (A) and ER calcium (B), in KC axons in the γ4/γ5 compartments during conditioning with different inter-stimulus intervals (ISIs) of DAN and KC activation. (A) KCs express EPAC sensor used to measure cAMP production as change in FRET ratio (ΔR/R, where R = CFP/YFP). (B) KCs express ER-GCaMP. Measurements for (A-B) were made using an explant preparation with γ4/γ5 DANs expressing $P2X_2$ activated by iontophoresis of ATP. Black arrowheads mark time of KC stimulation. Magenta arrowheads mark time of DAN stimulation. (**C**) Average response for cAMP (gray) and ER calcium (black) in γ4/γ5 KC axons across the six ISIs tested in (A-B). n = 6, mean ± SEM for EPAC; n = 7, mean ± SEM for ER-GCaMP. Significance is indicated as follows: *** ≤ 0.001, ** ≤ 0.01, * < 0.05, NS ≥ 0.05; one-sample t-test against zero with Bonferroni correction. (**D**) Left axis (purple): Linear sum of normalized cAMP and ER calcium responses from data shown in (C) were inverted, matching the timescale of γ4 MBON plasticity. Standard error of the mean was propagated from cAMP and ER calcium responses. Right axis (black): change in KC-MBON responses after conditioning with the same six ISIs (data re-plotted from Figure 3.2C).

Figure 5.5

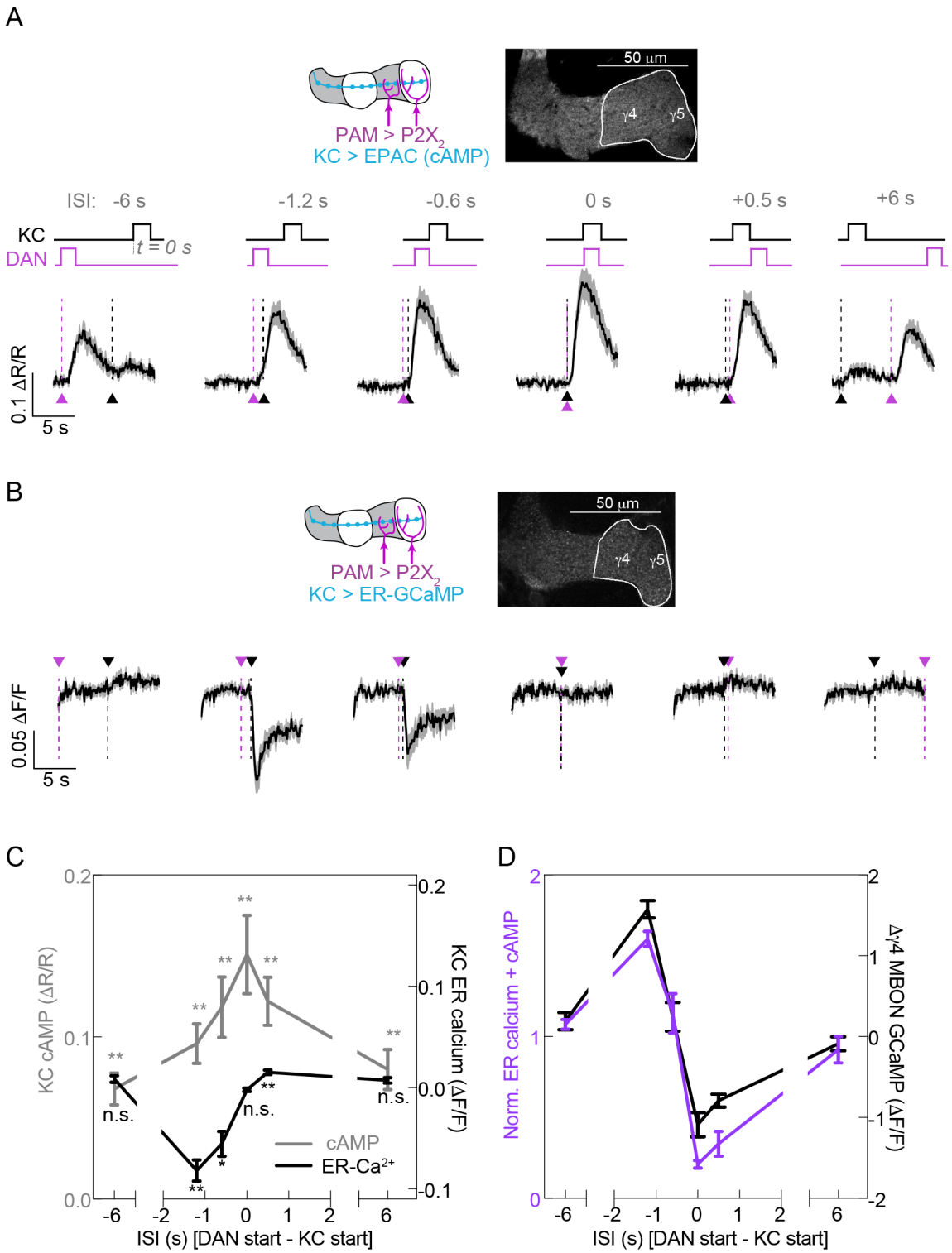
A
PAM > P2X2
KC > EPAC (cAMP)
50 µm
γ4
γ5
ISI: -6 s
-1.2 s
-0.6 s
0 s
+0.5 s
+6 s
KC
DAN
t = 0 s
0.1 ΔR/R
5 s
B
PAM > P2X2
KC > ER-GCaMP
50 µm
γ4
γ5
0.05 ΔF/F
5 s
C
KC cAMP (ΔR/R)
KC ER calcium (ΔF/F)
cAMP
ER-Ca2+
n.s.
ISI (s) [DAN start - KC start]
D
Norm. ER calcium + cAMP
Δγ4 MBON GCaMP (ΔF/F)
ISI (s) [DAN start - KC start]

The γ KCs traverse the entire length of the gamma lobe. Along this traversal, axon terminals from shock-responsive DANs innervate the proximal γ2 and γ3 compartments, while the rewarding PAM DANs innervate the medial γ4 and γ5 compartments. This compartmentalized organization of DAN innervation overlaps with the discrete innervation pattern of the MBONs tiling across all 15 compartments of the mushroom body (Aso et al., 2014a). This compartmentalized architecture permits different segments of the same KC axons to receive distinct neuromodulatory input, allowing for differential plasticity between KC synapses and each of its post-synaptic MBON targets across the lobes of the MB (Boto et al., 2014; Cohn et al., 2015). While we expect that activation of PAM DANs should selectively modulate the KC-MBON synapses within the γ4 and γ5 compartments, this compartmentalized plasticity requires the recruitment of second messenger pathways within the gamma KC axons obey the spatial innervation pattern of the compartmentalized DANs. Indeed, the regulation of independent synaptic sites along the length of a neuronal axon has been observed in mammalian and invertebrate systems and invoked as a mechanism to allow for local processing of information, adding additional flexibility and computational powers in static neural circuits (Cohn et al., 2015; Pelkey and McBain, 2007).

To address this question, we measured and compared cAMP and ER calcium release levels in the proximal γ2/γ3 compartments versus the medial γ4/γ5 compartments innervated by the activated PAM DANs during forward and backward conditioning. Indeed, both cAMP and ER calcium release show significantly lower levels in the proximal compartments (Figures 5.6A-B). The low levels of cAMP and ER calcium release observed in the γ2/γ3 compartments is not surprising considering that the 58E02-LexA driver used to activate the PAM DANs weakly innervates both

of these compartments but may also reflect that subcellular second messengers do not adhere to compartmentalized architecture with perfect fidelity. This spatial recruitment of second messengers matches the release of dopamine across the gamma lobe, as measured by expressing the dopamine sensor ($GRAB_{DA1m}$) in KCs. (Figures 5.6C). These observations align with the connectome analysis that has suggested that the low number of KC-MBON synapses receiving direct DAN innervation (6%) is ideal for ensuring minimal 'spill-over' of dopamine release into neighboring compartments (Takemura et al., 2017).

The selective release of ER calcium during backward pairing, suggests an order-dependent mechanism for the activation of this pathway. Interestingly, if the traces for ER calcium release under 7 different inter-stimulus intervals, in which the relative timing of KC activation and DAN stimulation was varied, we found ER calcium release was time-locked to the moment of KC activation (Figure 5.6E). This is in contrast to cAMP, which was produced predominantly in response to DAN activation, regardless of the activity state of KCs (Figure 5.6D). In addition, application of the Gαq inhibitor YM-254890 blocked this temporally sensitive ER calcium release (Figure 5.6F), confirming that it arises from the Gαq pathway. Together, these results reveal an order-detection mechanism regulating Gαq-dependent ER calcium release. This mechanism requires that dopamine engage DopR2 to activate the Gαq protein, resulting in the priming of a downstream molecule to an increased activity state of the KCs. It is possible that this order-detection arises from the complex regulation of IP_3R by calcium, a topic I further expanded on in the discussion of this chapter.

Figure 5.6, Characterization of Second Messenger Production in Gamma Kenyon Cells
(**A-B**) Comparison of cAMP (A) and ER-calcium release (B) in γ2/γ3 KC axons versus γ4/γ5 KC axons. Mean ± SEM, n = 12 for cAMP and 13 for ER-calcium. (**C**) Comparison of dopamine sensor ($GRAB_{DA1m}$) expressed in KC axons traversing the γ2/γ3 and γ4/γ5 compartments. Mean ± SEM n = 7. For significant difference between γ2/γ3 and γ4/γ5 compartments in (**A-C**) paired t-test was used: ** ≤ 0.01, *** ≤ 0.001, **** ≤ 0.0001. (**D**) CFP/YFP ratio of KC axons in the γ4/γ5 compartments expressing EPAC sensor during pairing of KC and DAN activation across seven different ISIs used for conditioning. All traces were collected from the same preparation and aligned to the time of KC stimulation. cAMP production occurs over multiple seconds following DAN stimulation. (**E**) ER calcium fluorescent signal in KC axons expressing ER-GCaMP traversing the γ4/γ5 compartments during pairing of KC and DAN activation across seven different ISIs used for conditioning. All traces were collected from the same preparation and aligned to the time of KC stimulation. Alignment shows time-locked ER calcium flux to KC stimulation. (**F**) Left: ER-GCaMP responses in KC axons traversing γ4/γ5 compartments during forward pairing (FP) and backward pairing (BP) in brain explant preparations bathed in 10μM of the Gaq inhibitor, YM-254890 (red traces), or in DMSO control (black traces). Right: Average ER-GCaMP responses in KC axons in the presence (red) and absence (black) of 10μM YM-254890 during forward and backward pairing. Mean ± SEM, n = 5. Significance for difference in YM-254890 treated preparations indicated as follows: * $p < 0.05$, NS ≥ 0.05, unpaired t-test. For (A-E) Black arrowhead marks KC stimulation, colored arrowheads mark DAN stimulations for indicated ISIs. For all experiments, PAM DANs expressed the $P2X_2$ channel using the 58E02-LexA driver and were activated by local iontophoresis of ATP. KCs were stimulated by iontophoresis of acetylcholine in mushroom body calyx.

Figure 5.6

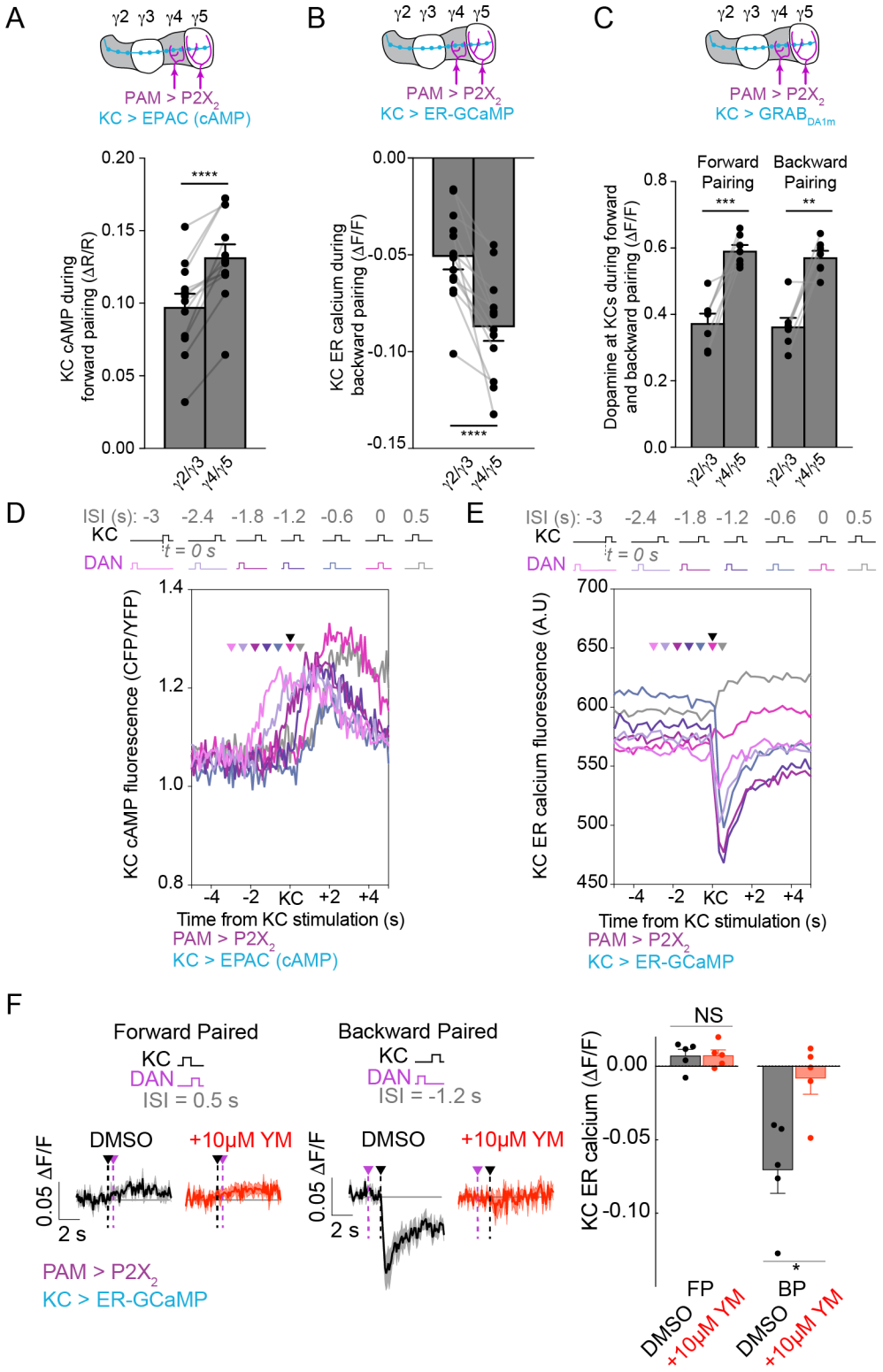
A
γ2 γ3 γ4 γ5
PAM > P2X2
KC > EPAC (cAMP)
KC cAMP during forward pairing (ΔR/R)
0.20
0.15
0.10
0.05
0.00
****
γ2/γ3
γ4/γ5
B
γ2 γ3 γ4 γ5
PAM > P2X2
KC > ER-GCaMP
KC ER calcium during backward pairing (ΔF/F)
0.00
-0.05
-0.10
-0.15
****
γ2/γ3
γ4/γ5
C
γ2 γ3 γ4 γ5
PAM > P2X2
KC > GRABDA1m
Forward Pairing
Backward Pairing
Dopamine at KCs during forward and backward pairing (ΔF/F)
0.8
0.6
0.4
0.2
0.0
***
**
γ2/γ3
γ4/γ5
D
ISI (s): -3 -2.4 -1.8 -1.2 -0.6 0 0.5
KC
DAN
t = 0 s
KC cAMP fluorescence (CFP/YFP)
1.4
1.2
1.0
0.8
-4 -2 KC +2 +4
Time from KC stimulation (s)
PAM > P2X2
KC > EPAC (cAMP)
E
ISI (s): -3 -2.4 -1.8 -1.2 -0.6 0 0.5
KC
DAN
t = 0 s
KC ER calcium fluorescence (A.U)
700
650
600
550
500
450
-4 -2 KC +2 +4
Time from KC stimulation (s)
PAM > P2X2
KC > ER-GCaMP
F
Forward Paired
KC
DAN
ISI = 0.5 s
DMSO
+10μM YM
0.05 ΔF/F
2 s
Backward Paired
KC
DAN
ISI = -1.2 s
DMSO
+10μM YM
0.05 ΔF/F
2 s
PAM > P2X2
KC > ER-GCaMP
NS
KC ER calcium (ΔF/F)
0.00
-0.05
-0.10
*
FP
BP
DMSO
+10μM YM
DMSO
+10μM YM

To confirm that second messenger signaling in KC axons depends on activation of DopR1 and DopR2, we examined cAMP and ER calcium in animals mutant for these dopamine receptors (Figure 5.7B). Despite the historic use of DopR1 mutants in assessing animal behavior, a receptor mutant compatible with functional, two-photon imaging did not exist (Keleman et al., 2012; Kim et al., 2007).

Ianessa Morantte, a research scientist in the lab used Cas9-mediated genome engineering to generate a novel DopR1 null allele (Figures 5.7A-B) to allow for functional studies of the role of this receptor in synaptic modulation. This novel DopR1 mutant resulted in a complete loss of the protein coding sequence, verified by qPCR, and loss of protein expression, verified by immunohistochemistry (5.7B). In accord with the preferential G-protein signaling of these receptors described *in vitro* (Feng et al., 1996; Gotzes et al., 1994; Han et al., 1996; Himmelreich et al., 2017; Sugamori et al., 1995), production of cAMP was strongly diminished in both forward and backward pairing in $DopR1^{-/-}$ but not $DopR2^{-/-}$ animals (Figures 5.7C-E). This suggests the majority of cAMP generated during associative conditioning in the γ KC axons is through a DopR1-dependent mechanism. In addition, the significant reduction in cAMP in the DopR1 mutant animals is more dramatic than the loss of cAMP observed in the rutabaga mutant (data not shown), suggesting that the minor deficit in synaptic depression in the rutabaga mutant is due to an incomplete loss of DopR1-dependent cAMP production.

Furthermore, the equivalent levels of cAMP in wild type compared to DopR2 mutant animals, suggests that *in vivo* DopR2 contributes only minimally, if at all, to dopamine-dependent cAMP production. Conversely, the ER calcium release elicited in backward pairing was lost completely

Figure 5.7, Select Role of DopR1 in cAMP Production in Kenyon Cell Axons

(**A**) Schematic of two sgRNAs targeting the DopR1 locus. Orange boxes represent exons. sgRNA 1 on reverse strand targets the 5' UTR and sgRNA 2 targets the 3'UTR. (**B**) Left: Immunohistochemistry with anti-DopR antibody showing absence of DopR1 protein in $DopR1^{-/-}$ adult brain. RT-PCR confirming loss of *DopR1* mRNA in $DopR1^{-/-}$ animals compared to wild type animals (n = 8 WT and 8 $DopR1^{-/-}$ brains). Right: Immunohistochemistry with anti-DopR2 antibody in the adult brain of WT and $DopR2^{-/-}$ shows absence of DopR2 protein in $DopR2^{-/-}$. Z stack projection, max intensity. Immunohistochemistry and qPCR analysis of mutant animals performed by Ianessa Morantte. (**C-D**) cAMP responses in KC axons traversing γ4/γ5 compartments in wild type (WT), $DopR1^{-/-}$, and $DopR2^{-/-}$ animals during forward (C) and backward pairing (D). KCs express EPAC sensor of cAMP. (**E**) Mean cAMP produced in forward (FP) and backward pairing (BP), n = 6 flies for all genotypes, mean ± SEM. Significance for difference between receptor mutants and wild type in cAMP production is indicated as follows: *** $p \leq 0.001$, NS ≥ 0.05; unpaired t-test with Bonferroni correction.

Figure 5.7

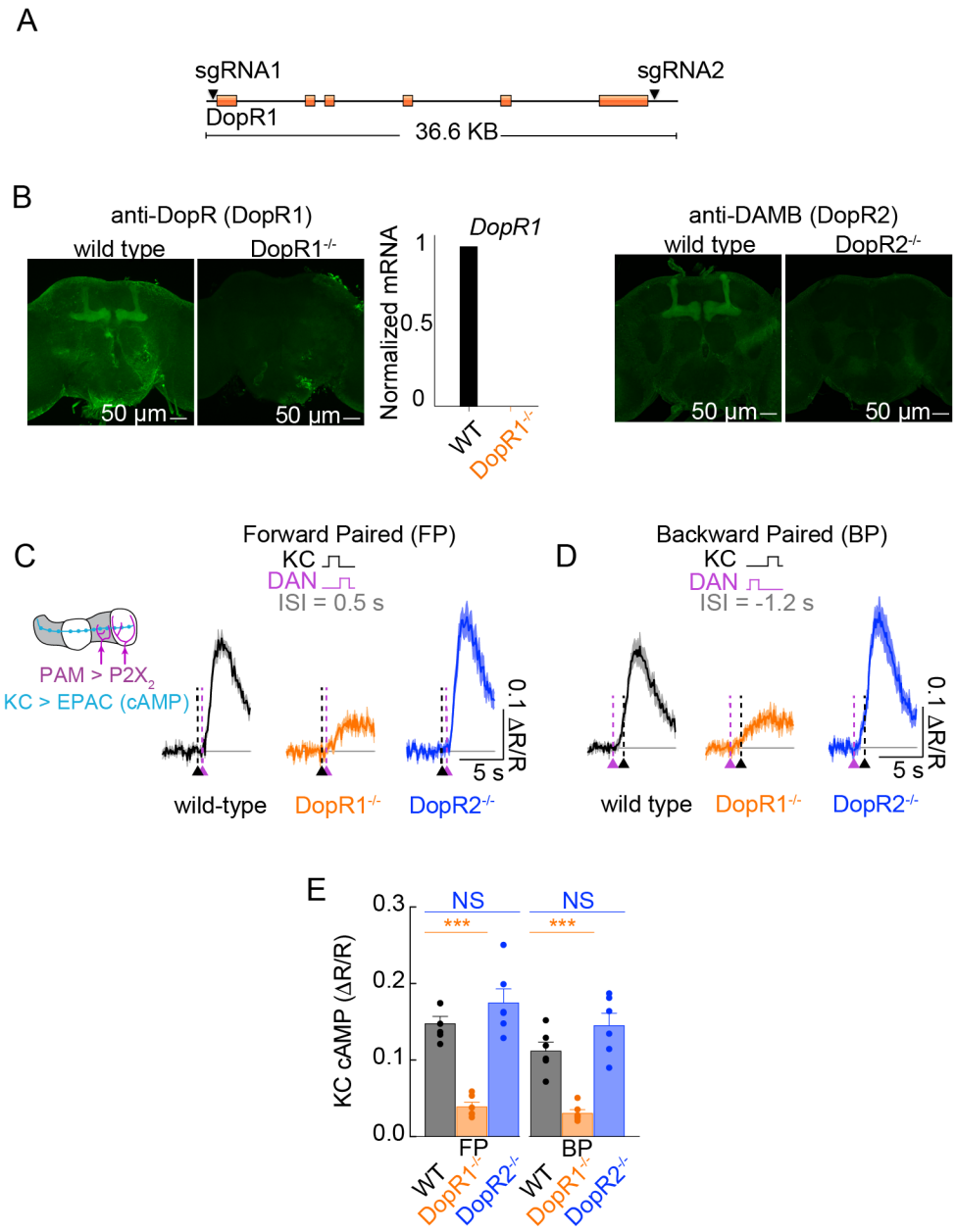
A
sgRNA1
sgRNA2
DopR1
36.6 KB
B
anti-DopR (DopR1)
wild type
DopR1-/-
50 µm
50 µm
DopR1
Normalized mRNA
1
0.5
0
WT
DopR1-/-
anti-DAMB (DopR2)
wild type
DopR2-/-
50 µm
50 µm
C
Forward Paired (FP)
KC
DAN
ISI = 0.5 s
PAM > P2X2
KC > EPAC (cAMP)
0.1 ΔR/R
5 s
wild-type
DopR1-/-
DopR2-/-
D
Backward Paired (BP)
KC
DAN
ISI = -1.2 s
0.1 ΔR/R
5 s
wild type
DopR1-/-
DopR2-/-
E
KC cAMP (ΔR/R)
0.3
0.2
0.1
0.0
NS
NS
***
***
FP
BP
WT
DopR1-/-
DopR2-/-
WT
DopR1-/-
DopR2-/-

in DopR2$^{-/-}$ but not DopR1$^{-/-}$ animals (Figures 5.8A-B), highlighting the unique role of DopR2 in driving ER calcium release during backward pairing. DopR1 and DopR2 therefore selectively signal through different biochemical pathways in the mushroom body to generate distinct patterns of second messengers during conditioning (Figure 5.8C). This suggests that the capacity for temporally-dependent bidirectional plasticity emerges from the distinct signaling properties of these two dopamine receptors.

5.4 Discussion

Neuromodulators have a profound and varied effect on animal behavior. They can act over short or long timescales, with effects that span narrow or broad spatial domains. Neuromodulatory effects are frequently determined by the geometry of the neuropil including the axonal projections of the modulatory neurons, as well as the complement of post-synaptic proteins that sense neuromodulators and initiate downstream cascades. These downstream signaling pathways often contain molecules that allow for the temporal summation of events through coincidence detection, or can instead be gated by the order of inputs.

In complex brain circuits where multiple neurmodulatory receptors are expressed among a heterogeneous population or intermingled neurons, understanding how select receptor engagement is achieved is a daunting question. Indeed, both mammalian and invertebrate studies have suggested that distinct dopamine receptors are selectively engaged due to differences in affinity for dopamine across D1- and D2-like receptors. Such a model allows for tonic dopamine release to engage the high-affinity D2 receptors where as the low-affinity D1 receptor would be

Figure 5.8, DopR2 Drives ER Calcium Release in Kenyon Cells Selectively in Backward Pairing

(**A**) ER-GCaMP responses in KC axons traversing γ4/γ5 compartments in wild type (WT), DopR1$^{-/-}$, and DopR2$^{-/-}$ during forward pairing (left) and backward pairing (right). (**B**) Mean ER calcium release during forward pairing and backward pairing across all genotypes, n = 5-6 animals for all genotypes, mean ± SEM. Significance for difference between receptor mutants and wild type in ER calcium release is indicated as follows: ** ≤ 0.01, NS ≥ 0.05; Mann-Whitney test with Bonferroni correction. (**C**) Schematic showing second messenger production during forward and backward pairing and the resulting plasticity in KC-MBON signaling.

Figure 5.8

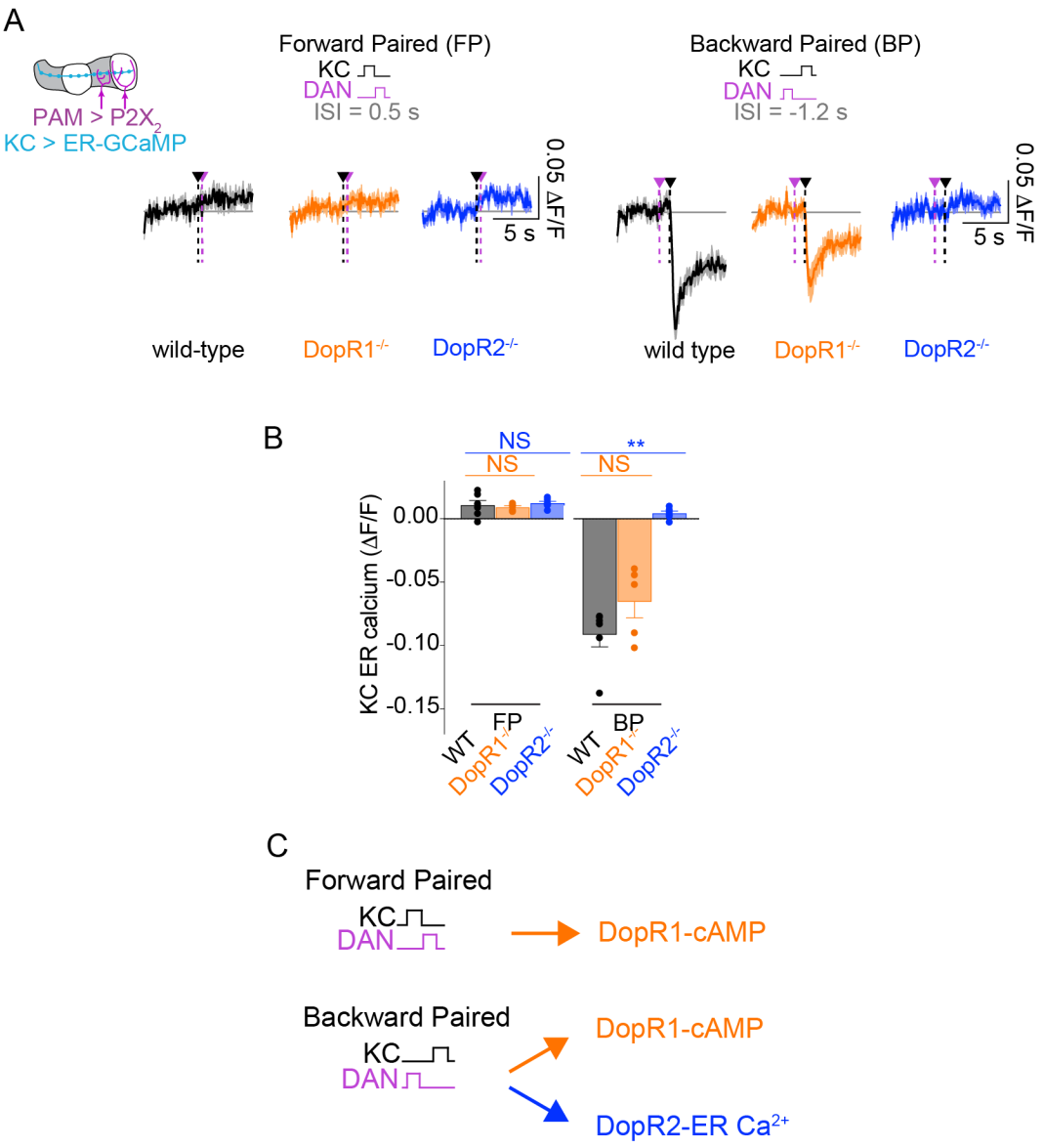
A
PAM > P2X2
KC > ER-GCaMP
Forward Paired (FP)
KC
DAN
ISI = 0.5 s
Backward Paired (BP)
KC
DAN
ISI = -1.2 s
0.05 ΔF/F
5 s
wild-type
DopR1-/-
DopR2-/-
wild type
DopR1-/-
DopR2-/-
B
NS
NS
**
NS
KC ER calcium (ΔF/F)
0.00
-0.05
-0.10
-0.15
FP
BP
WT
DopR1-/-
DopR2-/-
C
Forward Paired
KC
DAN
DopR1-cAMP
Backward Paired
KC
DAN
DopR1-cAMP
DopR2-ER Ca2+

selectively engaged during phasic release (Berry et al., 2012; Grace et al., 2007; Marcott et al., 2014; Surmeier et al., 2011); however, these experiments often rely on simplified *in vitro* assays in which the innate, microenvironments are stripped away or altered in non-physiological ways. More recent work *in vivo* has suggested this model is likely overly simplistic. Rather, it seems heterogeneous D2-expressing neural populations in the striatum and nucleus accumbens can function in both a high- or low-affinity state, encoding both phasic and tonic dopamine activity (Marcott et al., 2014; 2018). This complexity in receptor engagement across a heterogeneous population of receptor-expressing neurons emphasizes the importance of using *in vivo* dynamical sensors of the neuromodulatory state of a circuit to achieve unprecedented insight into how a circuit is altered, from the initial stages of neuromodulator release to the engagement of downstream effectors.

In Chapter 3, I showed that the order of inputs during conditioning result in bidirectional tuning of the KC-MBON synapses within the MB to drive changes in odor tracking behavior. It was reasonable to suspect that if dopamine release in forward and backward pairing were different, distinct downstream modulatory pathways could be selectively engaged if differences in affinity for dopamine truly existed across the *Drosophila* dopamine receptors; however, we found that dopamine release was equivalent across all conditioning paradigms, suggesting that dopamine neurons are likely not the site of coincidence detection and that such a site likely exists in the post-synaptic neurons. We, therefore, needed insight into the effects of dopamine on post-synaptic neurons to identify the cellular site likely involved in order and coincidence detection. Through the development and use of fluorescent reporters for dopamine-receptor second

messengers, we were able to characterize how the timing of associative conditioning influences downstream signaling pathways in the KC axons of the MB.

We show that DopR1-dependent cAMP is recruited under both forward and backward pairing with maximum production occurring with the synchronous activation of both KC and DANs. The drop off in cAMP production as the ISI increases suggests that the production of cAMP depends on the detection of coincidence, occurring likely through a calcium-activated adenylate cyclase. However, the symmetric production of cAMP in forward and backward pairing suggests this pathway is insufficient to explain the bidirectional modulation that relies on the order of events. This observation challenges the firmly held belief that synergistic levels of cAMP during associative conditioning are sufficient to explain the temporal dependence of associative learning (Abrams et al., 1991; Boto et al., 2014; Kheirbek et al., 2008; Tomchik and Davis, 2009). Prior results suggested that supralinear cAMP was produced selectively during forward pairing and was not observed during backward pairing (Tomchik and Davis, 2009); however, the limited conditioning paradigms tested and lack of temporal resolution in neuron activation likely occluded the production of cAMP in backward pairing. Indeed, if equivalent levels of cAMP were observed in forward and backward pairing, a more complex mechanism for why forward and backward pairing do not lead to equivalent neural and behavioral responses would need to be invoked. Through the use of chemogenetic tools, allowing for temporally precise activation of DANs relative to KCs, our work suggests multiple signaling pathways must be involved to shape the neural and behavioral responses to associative conditioning.

The use of a the low-affinity ER-calcium sensor revealed for the first time a central role in Gαq dependent calcium release during associative conditioning in *Drosophila*. We observed three interesting features of the DopR2-dependent ER calcium signal: 1) calcium release only occurs in backward pairing paradigms, 2) as the delay between DAN and KC activation increases, the calcium release decreases, and 3) release of calcium from the ER is time locked to the moment of KC activation during backward pairing. Together, these observations highlight the immense regulation in recruitment of this downstream pathway. Experiments in the mouse cerebellar circuitry has suggested a role of order-dependent coincidence detection in driving long-term depression in parallel fiber-Purkinje cell synapses (Sarkisov and Wang, 2008). The pairing of IP_3 production in Purkinje cells (PCs) with activation of the climbing fiber 400 ms later, resulted in a supralinear calcium response in the dendrites of the PCs. A reversal in the order of events showed minimal effects, suggesting that the supralinear responses depend both on the order and delay time between events (Sarkisov and Wang, 2008). These requirements are similar to what we observe in ER calcium release in KC axons. While the analogous circuit organization of the mushroom body and cerebellum has been well described (Farris, 2011), our observations suggest they may share conserved molecular mechanisms for temporally precise synaptic modulation.

Chapter 6

Dopamine Receptors in Bidirectional Plasticity

6.1 Introduction

Across nervous systems, dopamine pathways and receptors have been proposed to oppose one another at a macroscopic level in regulating animal behavior, and at a microscope level in the recruitment of distinct second messengers that tune synaptic activity through the regulation of individual proteins. At the macroscopic level, it is clear that dopamine plays a central role in sculpting and regulating animal behavior. A wealth of evidence suggests that dopamine signaling in the mammalian basal ganglia circuitry is critically involved in motor control (Cisek and Kalaska, 2010; Markowitz et al., 2018; Mink, 1996; 2003; Redgrave et al., 1999; Wichmann and DeLong, 2003), and loss of dopamine within this circuitry can have opposing behavioral effects—leading to hypokinesia, a hallmark of Parkinson's disease, or hyperkinesia, evident by the involuntary movements seen in patients suffering from chorea.

The dichotomous effect on movement regulation by dopamine is believed to emerge from the distinct pathways and signaling mechanisms of dopamine in the basal ganglia circuit. For example, dopamine release within the striatum acts on distinct GABAergic, medium spiny neurons (MSNs) that differ both in their expression of dopamine receptors and their projection pattern within the basal ganglia circuitry. The GABAergic neurons expressing the D1-like

receptor make up the majority of the striatonigral projections, while the striatopallidal projecting GABAergic neurons instead preferentially express the D2-like receptor (Gerfen et al., 1990). The distinct neuroanatomical circuits for the direct (striatonigral) and indirect (striatopallidal) pathway tune activity levels within cortical regions to bidirectionally modulate behaviors, with the direct pathway promoting body movements and the indirect pathway suppressing competing locomotor behaviors (Freeze et al., 2013; Kravitz and Kreitzer, 2012). Additional experiments since the discovery of these pathways have further clarified and expanded this simple model of the role of direct and indirect pathway in motor control, suggesting that both the direct and indirect pathway are engaged during locomotion to select appropriate motor programs while inhibiting unwanted behaviors (da Silva et al., 2018; Markowitz et al., 2018; Mink, 2003).

These differences in the regulation of animal behavior are thought to arise from distinct signaling properties of these two dopamine receptors at the microscopic level. The binding of dopamine to D1-like receptors stimulates adenylate cyclases through the Gαs, leading to activation of downstream protein kinase A (PKA). The excitatory effects of D1-like activation are mediated through PKA-dependent phosphorylation and regulation of downstream receptors including glutamatergic NMDA and AMPA receptors, and voltage-regulated sodium, potassium, and calcium channels (Greengard et al., 1999; Svenningsson et al., 2004). By contrast, binding of dopamine to D2-like receptors inhibits adenylate cyclases and PKA activation through the engagement of Gαi/o, leading to inhibition of the indirect pathway (Greengard et al., 1999; Svenningsson et al., 2004).

However, the intermingled dendrites of D1 and D2 expressing MSN raises the interesting question of how the direct and indirect pathways are selectively engaged for proper action selection in animals. Functional experiments in heterologous expression systems have suggested that D2 receptors have a 10- to 100-fold higher affinity when compared to D1 receptors using radiolabeled antagonists (Beaulieu and Gainetdinov, 2011; Tritsch and Sabatini, 2012); this difference in affinity levels would suggest that low-level, tonic release of dopamine would selectively engage the D2 receptor and inhibit the indirect pathway while the direct pathway would only be engaged during phasic release of dopamine. However, these experiments fail to represent that native microdomains of these receptors in the MSNs limiting the current model into how these receptors are differentially engaged in the basal ganglia circuitry. Furthermore, recent experiments parsing the dopamine pathways in mammalian circuits have highlighted the complexity of dopamine pathways in encoding multi-varied signals, including motor, reward, and punishment (Cohen et al., 2012; Lammel et al., 2014; Lerner et al., 2015).

Understanding how the brain decodes these multivariate signals both at the circuit level and at the molecular level through engagement of distinct dopamine receptors remains a complex task to achieve in mammalian circuits. Similar complexity in dopamine signaling exists in the simple nervous system of *Drosophila* (Berry et al., 2012; Cohn et al., 2015); however, the wealth of genetic tools and well-characterized neural architectures aide in the unraveling of dopamine-dependent mechanisms regulating neural and behavioral plasticity.

While there exists a clear distinction between positive and negative valence within the dopamine neurons innervating the mushroom body through the PPL and PAM DANs, these same neurons

also provide an ongoing record of the locomotor behavior of the animal. Additionally, single-cell sequencing of KCs show that these cells co-express a variety of dopamine receptors with distinct signaling. Despite this complexity, two specific dopamine receptors highly expressed in KC axons, DopR1 and DopR2, have been shown to play opposing roles in regulating olfactory memories at the behavioral level; however, it is unknown how these two receptors work to shape plasticity in post-synaptic neurons and how these two receptors are selectively engaged to mediate learning and memory.

In the previous chapter, I showed that while DopR1-dependent cAMP is produced under all conditions of DAN activation, DopR2-dependent ER calcium is produced only under specific timing conditions. Furthermore, a simple summation of these two pathways recapitulates the biphasic curve of neural plasticity in the γ4 compartment of the mushroom body, hinting at a role of these pathways in sculpting the neural plasticity. In this chapter, I will link the distinct temporal sensitivity of these dopamine receptor pathways to bidirectional neural and behavioral plasticity, providing a relatively simple model for how distinct dopamine receptors within a neural circuit can achieve opposing neural and behavioral effects through select engagement under different contexts.

6.2 DopR1 and DopR2 Underlie Opposing Forms of Neural Plasticity

The distinct temporal sensitivity of DopR1 and DopR2 signaling pathways described in the previous chapter suggests these receptors play a central role in mediating opposing forms of synaptic plasticity within the mushroom body. To test this idea, we examined the capacity for

bidirectional plasticity in the mushroom body circuitry in the background of dopamine receptor mutants. In these experiments, we used a brain explant experiment, where KCs were directly stimulated by iontophoresis of acetylcholine onto their dendrites while the PAM DANs were activated by targeted iontophoresis of ATP onto the $P2X_2$-expressing PAM dendrites. This approach was designed to directly hone in on modulation of KC-MBON synapses within a compartment by directly activating KCs and DANs, bypassing any perturbations in upstream signaling in the receptor mutants.

Indeed, the robust depression of KC-MBON signaling induced by forward pairing in wild type animals (Figure 6.1A) was absent in DopR1 mutants, instead leading to weak potentiation (Figure 6.1B). However, the potentiation following backward pairing remained intact (Figure 6.1B), suggesting a selective loss in the capacity to depress the MBON in the absence of DopR1. This neural deficit is inline with behavioral and neural literature emphasizing firstly, the importance of DopR1 in memory formation at the behavioral level following forward pairing and secondly, the role of depression in odor-drive onto MBON following forward conditioning in the KC-MBON synapses.

In contrast, both forward and backward pairing induced comparable levels of depression in KC-MBON signaling in $DopR2^{-/-}$ animals (Figure 6.1C). This result demonstrates the critical role of DopR2 in driving potentiation of KC-MBON synapses in backward pairing, and additionally, suggests that in the absence of DopR2, DopR1-dependent cAMP drives depression in KC-MBON synapses, independent of the timing of conditioning. These results highlight a novel role

Figure 6.1, DopR1 and DopR2 Differentially Regulate Bidirectional Plasticity

(**A**) KC-γ4 MBON plasticity in wild type (WT) animals in response after either forward pairing (FP) or backward pairing (BP). Left: γ4 MBON calcium responses to direct KC stimulation (black arrowhead) by iontophoresis of acetylcholine in the calyx prior to (pre) and after (post) forward or backward pairing. Right: Peak GCaMP response of γ4 MBON to KC stimulation pre and post forward or backward pairing. (**B-C**) Same as (A) except in $DopR1^{-/-}$ (B), and $DopR2^{-/-}$ (C) animals. n = 5 for all genotypes, mean ± SEM. Paired t-test, *** $p \leq 0.001$, ** ≤ 0.01, * < 0.05. For all experiments, PAM DANs expressed the $P2X_2$ channel using the 58E02-LexA driver and were activated by local iontophoresis of ATP. KCs were stimulated by iontophoresis of acetylcholine in mushroom body calyx.

Figure 6.1

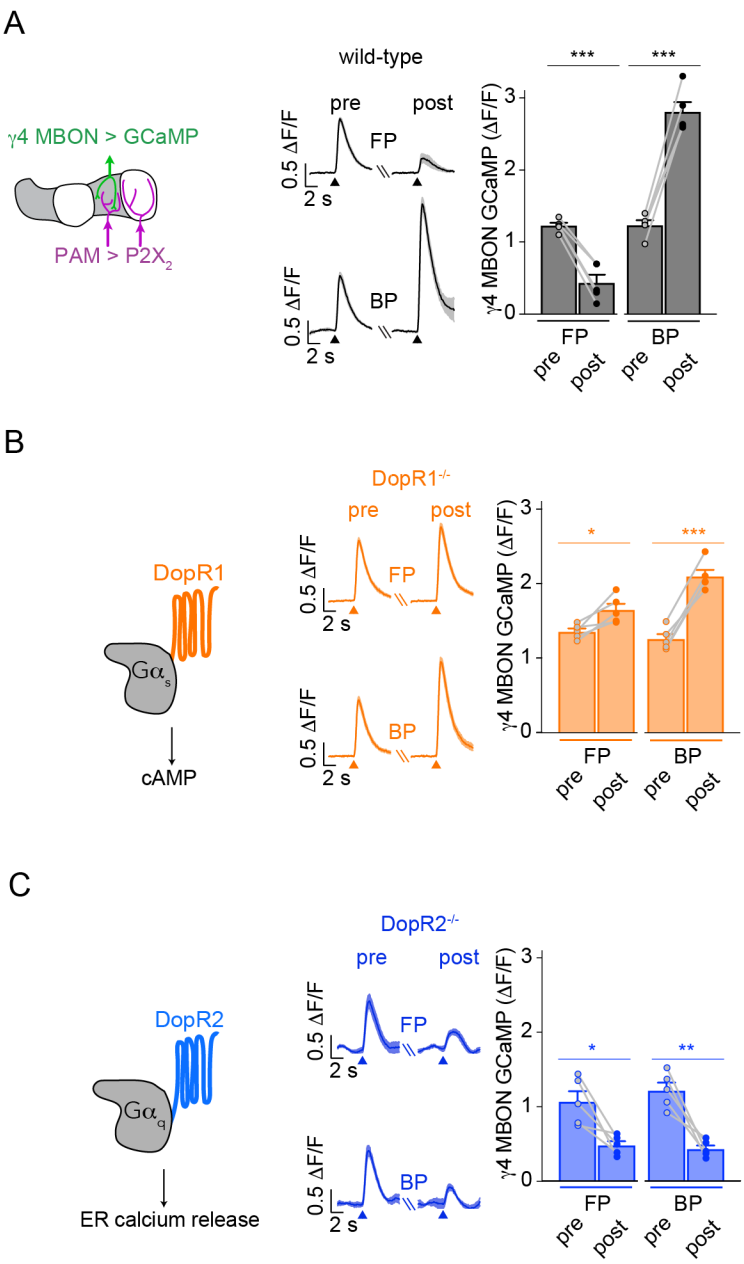
A
γ4 MBON > GCaMP
PAM > P2X2
wild-type
pre
post
FP
BP
0.5 ΔF/F
2 s
γ4 MBON GCaMP (ΔF/F)
***
***
FP
BP
pre
post
B
DopR1
Gαs
cAMP
DopR1-/-
*
***
C
DopR2
Gαq
ER calcium release
DopR2-/-
*
**

for DopR2 in associative conditioning, distinct from behavioral experiments suggesting a role of DopR2 only in memory erosion through forgetting mechanisms. Furthermore, inhibition of Gαq using YM-254890 prevented potentiation of KC-MBON signaling after backward pairing (Figure 6.2A), demonstrating that loss of either DopR2 or inhibition of its G-protein partner results in a similar deficit in synaptic plasticity. Interestingly, backward pairing led to depression in the MBON in four out of the six preparations exposed to YM-254890, highlighting the essential role of DopR2-dependent Gαq signaling in opposing the depressive effects of the DopR1 pathway. Together, these experiments suggest that DopR1 and DopR2 play opposing roles in shaping synaptic modulation within the mushroom body such that all conditioning paradigms drive potentiation in DopR1 mutants and depression in DopR2 mutants, underscoring how the coordinated signaling through these two receptors generates bidirectional plasticity.

It is important to recognize that these mutant animals lack the receptor in all neural and non-neural tissues; however, prior behavioral studies have demonstrated that DopR1 expression in γ KCs alone is sufficient to support short-term learning following forward conditioning (Qin et al., 2012), highlighting that dopamine signaling in this neural population alone can drive associative plasticity. Likewise, we demonstrate that forward and backward conditioning engages DopR1 and DopR2 second messenger-signaling cascades in KC axons, the direct post-synaptic partners of the mushroom body DANs we are activating, further suggesting the site of dopamine signaling is localized to the pre-synaptic KCs.

Figure 6.2, Potentiation from Backward Pairing Relies on Gαq Signaling and DopR2 Expression in Kenyon Cells

(**A**) Left: γ4 MBON GCaMP response to KC stimulation pre and post backward pairing in brain preparations bathed in 10μM YM-254890 (red) or in DMSO control (black). Black and red arrowheads mark KC stimulation. Right: Peak γ4 MBON response to KC stimulation pre and post backward pairing in YM-254890 (red) or control (black), * $p < 0.05$, NS ≥ 0.05, Wilcoxon matched-pairs signed rank test. (**B**) Left: KC-evoked GCaMP responses in the g4/g5 KCs pre- and post-backward pairing. Black traces are control animals; blue traces are animals expressing DopR2-RNAi in KCs (OK107-Gal4 > UAS-GCaMP6s). Right: Peak γ4 MBON response to KC stimulation pre and post backward pairing. Statistical difference between pre- and post-backward pairing responses assessed using paired t-test: **** $p \leq 0.0001$, NS ≥ 0.05.

Figure 6.2

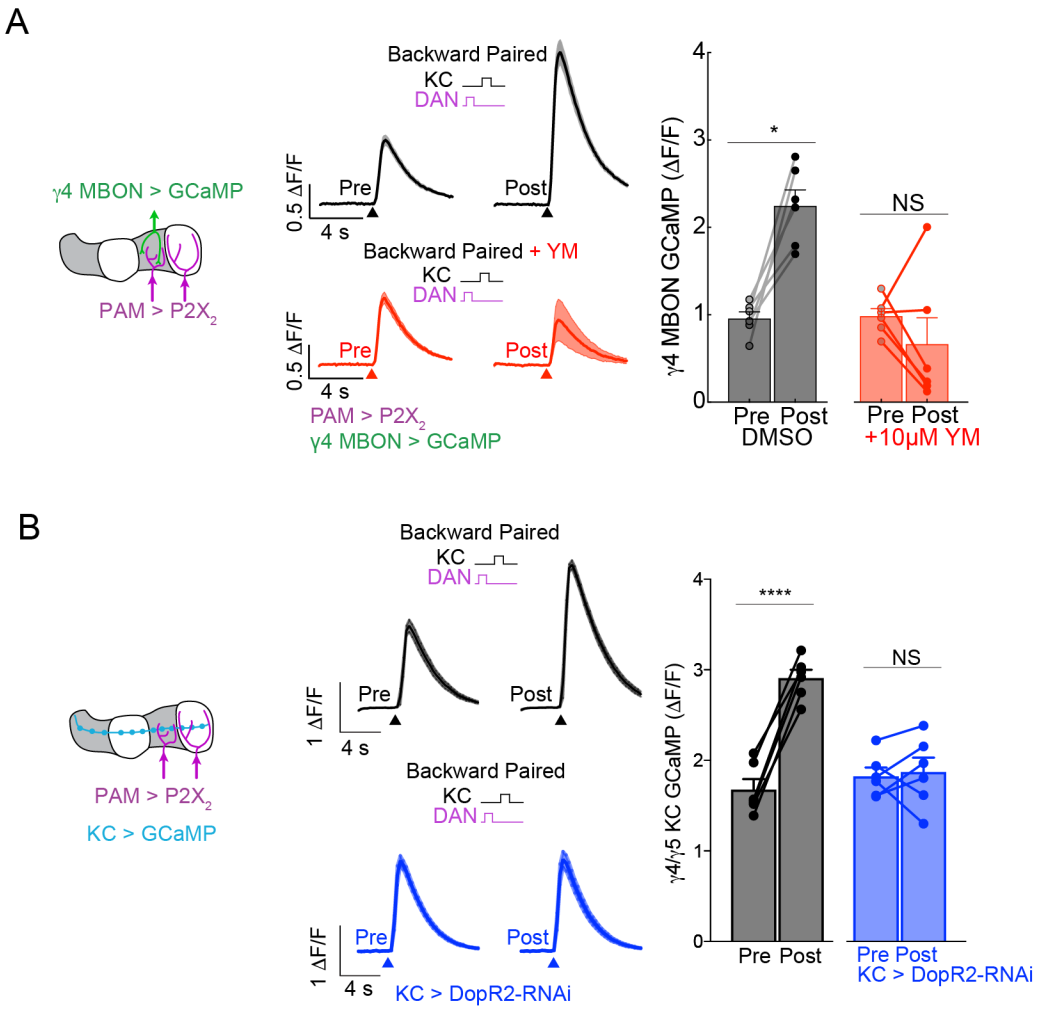
A
γ4 MBON > GCaMP
PAM > P2X2
Backward Paired
KC
DAN
Pre
Post
0.5 ΔF/F
4 s
Backward Paired + YM
PAM > P2X2
γ4 MBON > GCaMP
γ4 MBON GCaMP (ΔF/F)
*
NS
Pre Post
DMSO
Pre Post
+10μM YM
B
PAM > P2X2
KC > GCaMP
1 ΔF/F
KC > DopR2-RNAi
γ4/γ5 KC GCaMP (ΔF/F)
****
Pre Post
KC > DopR2-RNAi

Further support for a pre-synaptic role for dopamine receptor signaling comes from examining how conditioning alters calcium signaling in KC axons. We found that backward pairing resulted in potentiation of calcium entry in KC axons expressing soluble GCaMP to direct KC stimulation (Figure 6.2B). This potentiation was lost by selectively expressing DopR2-RNAi exclusively in the KCs, underscoring that KC axons are the critical site of dopamine signaling underlying bidirectional plasticity depending on the timing of events during conditioning.

6.3 DopR1 and DopR2 Underlie Opposing Forms of Behavioral Plasticity

We next examined whether the selective loss of potentiation or depression in DopR1 and DopR2 mutants could alter an animal's capacity to reversibly update behavioral preferences. As shown in Chapter 2, interleaving forward and backward pairing of ACV with PAM activation in wild type flies revealed a saw-tooth pattern of odor attraction as animals alternately increased and decreased their upwind odor tracking with each conditioning trial (Figure 6.3A). In contrast, DopR1 mutants were unable to bidirectionally modulate their behavioral responses to ACV after forward and backward pairing (Figure 6.3A-B). In fact, DopR1 mutant animals maintained a relatively low level of attraction to the conditioned odor, failing to vigorously track ACV after forward conditioning (Figure 6.3C-D). These observations are in line with behavioral evidence that DopR1 is required for writing memories within the mushroom body (Kim et al., 2007; Qin et al., 2012).

In contrast, DopR2 mutant animals strongly tracked ACV following forward and backward pairing (Figure 6.4A-B). This unwavering attraction suggests that DopR2 mutants are able to

Figure 6.3, DopR1 is Required for Memory Formation and Rapid Reversals in Behavior
(**A**) Left: Raster plot of average upwind velocity trained by alternating forward pairing (FP) and backward pairing (BP) of PAM (MB042B) > CsChrimson activation with apple cider vinegar (ACV) odor in wild type (WT) animals (magenta) or DopR1$^{-/-}$ animals (orange). Right: Upwind displacement in the 2-second ACV odor presentation corresponding to trials shown in raster. Behavioral paradigm same as in Figure 2.3A (50 conditioning trials, alternating between forward and backward pairing). The first row of the raster and upwind displacement graphs represents tracking at baseline. Subsequent rows and data points correspond to behavioral trials after forward pairing or backward pairing occurring in alternating succession (post-FP, post-BP). (**B**) Left: Change in upwind displacement in odor post-forward and post-backward pairing in WT (magenta) and DopR1$^{-/-}$ (orange) animals. The change in upwind displacement was measured relative to the preceding odor trial. Each data point represents the mean change in displacement after the 25 forward pairing (post-FP) or 25 backward pairing (post-BP) trials for each experiment. Right: Data points are re-plotted from graph on the left to compare changes in upwind displacement post-forward pairing and post-backward pairing in WT and DopR1$^{-/-}$ mutants. Unpaired t-test was used to test for differences in the change in odor behavior post-forward pairing and post-backward pairing across genotypes, **** $p \leq 0.0001$. (**C**) Upwind velocity of flies during representative trials 7, 8, 9, and 10 (corresponding to trial number shown in A) in wild type (WT, magenta) and DopR1$^{-/-}$ (orange) animals. (**D**) Mean upwind displacement in ACV odor post-forward pairing and post-backward pairing for WT and DopR1$^{-/-}$ animals. Unpaired t-test was used to test for differences in upwind odor displacement post-FP and post-BP across genotypes: ** $p \leq 0.01$, NS ≥ 0.05. n = 7 experiments with 5-6 animals per experiment for all genotypes, mean ± SEM.

Figure 6.3

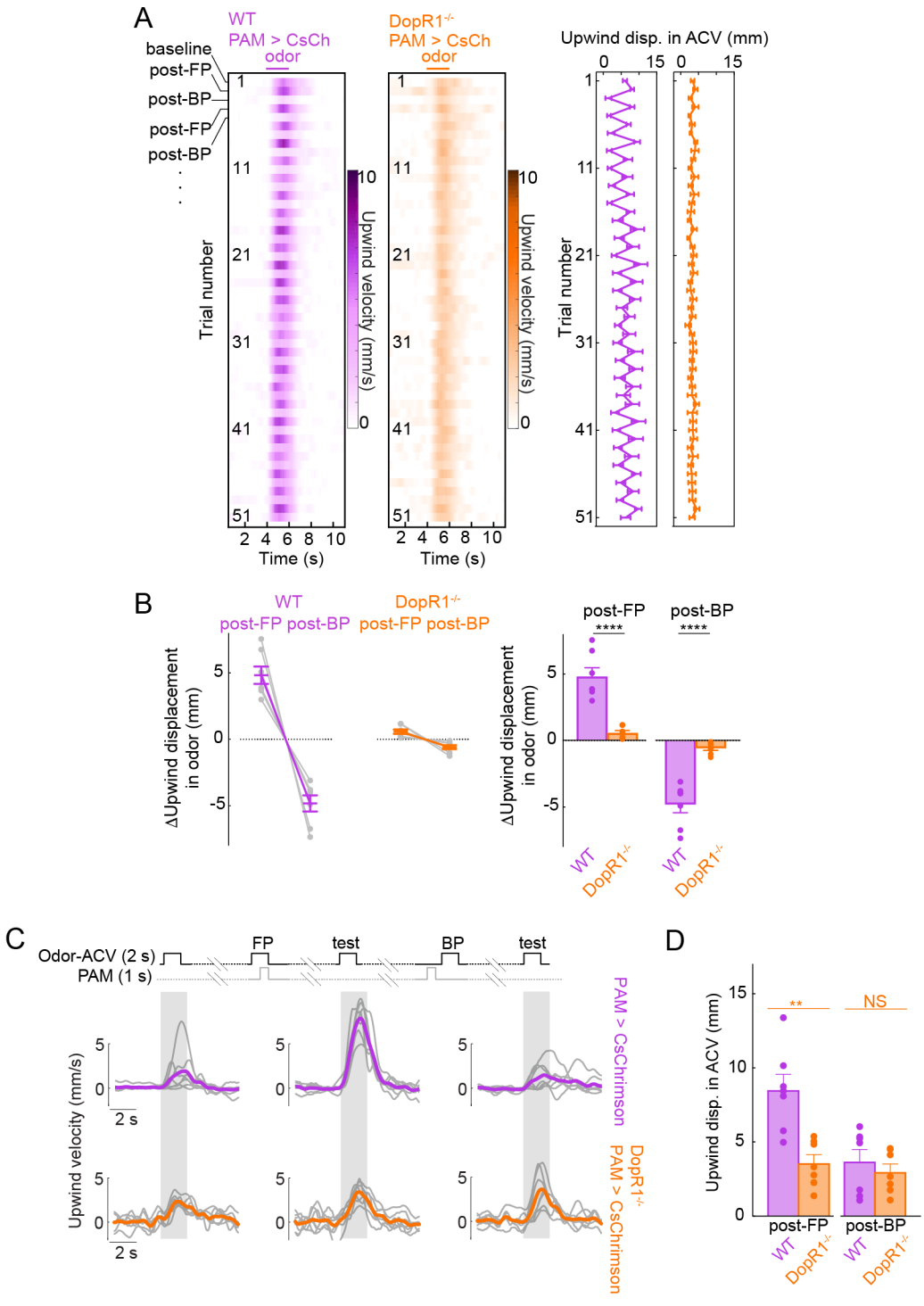
A
WT
PAM > CsCh
odor
DopR1-/-
PAM > CsCh
odor
Upwind disp. in ACV (mm)
baseline
post-FP
post-BP
post-FP
post-BP
Trial number
Upwind velocity (mm/s)
Time (s)
B
WT
post-FP post-BP
DopR1-/-
post-FP post-BP
ΔUpwind displacement in odor (mm)
post-FP
post-BP
****
WT
DopR1-/-
C
Odor-ACV (2 s)
PAM (1 s)
FP
test
BP
test
Upwind velocity (mm/s)
2 s
PAM > CsChrimson
DopR1-/-
PAM > CsChrimson
D
Upwind disp. in ACV (mm)
**
NS
post-FP
post-BP
WT
DopR1-/-

Figure 6.4, DopR2 is Required for Rapid Reversals in Behavior after Backward Pairing
(**A**) Left: Raster plot of average upwind velocity trained by alternating forward pairing (FP) and backward pairing (BP) of PAM (MB042B) > CsChrimson activation with apple cider vinegar (ACV) odor in wild type (WT) animals (magenta) or DopR2$^{-/-}$ animals (blue). Right: Upwind displacement in the 2-second ACV odor presentation corresponding to trials shown in raster. Behavioral paradigm same as in Figure 2.3A (50 conditioning trials, alternating between forward and backward pairing). The first row of the raster and upwind displacement graphs represents tracking at baseline. Subsequent rows and data points correspond to behavioral trials after forward pairing or backward pairing occurring in alternating succession (post-FP, post-BP). (**B**) Left: Change in upwind displacement in odor post-forward and post-backward pairing in WT (magenta) and DopR2$^{-/-}$ (blue) animals. The change in upwind displacement was measured relative to the preceding odor trial. Each data point represents the mean change in displacement after the 25 forward pairing (post-FP) or 25 backward pairing (post-BP) trials for each experiment. Right: Data points are re-plotted from graph on the left to compare changes in upwind displacement post-forward pairing and post-backward pairing in WT and DopR2$^{-/-}$ mutants. Unpaired t-test was used to test for differences in the change in odor behavior post-forward pairing and post-backward pairing across genotypes, **** $p \leq 0.0001$. (**C**) Upwind velocity of flies during representative trials 7, 8, 9, and 10 (corresponding to trial number shown in A) in wild type (WT, magenta) and DopR2$^{-/-}$ (blue) animals. (**D**) Mean upwind displacement in ACV odor post-forward pairing and post-backward pairing for WT and DopR2$^{-/-}$ animals. Unpaired t-test was used to test for differences in upwind odor displacement post-FP and post-BP across genotypes: * $p < 0.05$, NS ≥ 0.05. n = 7 experiments with 5-6 animals per experiment for all genotypes, mean ± SEM.

Figure 6.4

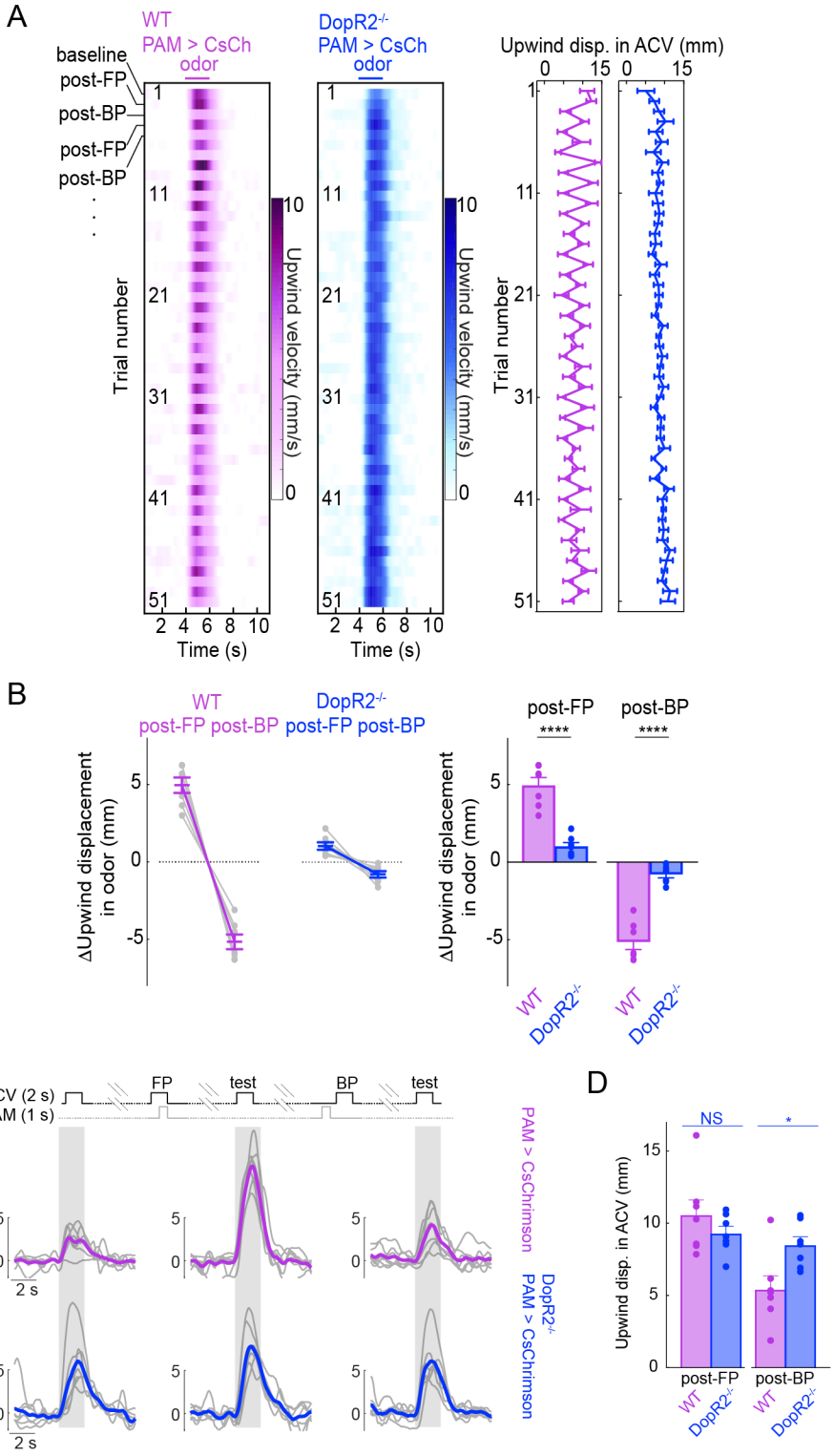
A
WT
PAM > CsCh
odor
DopR2-/-
PAM > CsCh
odor
Upwind disp. in ACV (mm)
baseline
post-FP
post-BP
post-FP
post-BP
Trial number
Upwind velocity (mm/s)
Time (s)
B
WT
post-FP post-BP
DopR2-/-
post-FP post-BP
ΔUpwind displacement in odor (mm)
post-FP
post-BP
****
****
WT
DopR2-/-
C
Odor-ACV (2 s)
PAM (1 s)
FP
test
BP
test
Upwind velocity (mm/s)
2 s
PAM > CsChrimson
DopR2-/-
PAM > CsChrimson
D
NS
*
Upwind disp. in ACV (mm)
post-FP
post-BP
WT
DopR2-/-

form a positive association but are unable to overwrite that memory in response to subsequent experience (Berry et al., 2012) (Figure 6.4C-D). The behavioral inflexibility of DopR1 and DopR2 mutants highlights how the balance of signaling through these two receptors allows animals to reversibly modify their behavioral attraction to an odor, based on the predictive temporal relationships between odor presentation and dopaminergic reinforcement.

Importantly, despite the deficit of DopR1 and DopR2 mutant animals in their ability to flexibly modulate their attraction to an odor, these animals are capable of tracking ACV at levels equivalent to wild type animals with a matched genetic background (Figure 6.5A-O). These control experiments show that the speed of DopR1, DopR2, and wild type animals are equivalent both within the clean-air stream as well as within the odor plume (Figure 6.5B-G). Additionally, the fraction of flies stationary or moving upwind in response to the odor presentation are equivalent across all three genotypes, further emphasizing the critical role of DopR1 and DopR2 in mediating odor-specific changes in animal behavior directly as a result of associative conditioning. Together, these experiments emphasize the critical role of two dopamine receptor pathways and their different temporal sensitivities for mediating the bidirectional neural and behavioral plasticity.

Figure 6.5, Dopamine Receptor Mutants Track Odor Equivalent to Wild Type Controls
(**A-O**) Behavioral analysis of locomotor metrics comparing PAM >CsCh DopR1$^{-/-}$, PAM > CsCh DopR2$^{-/-}$, and PAM > CsCh wild type animals. (**A**) Directional information of X and Y axis relative to air/odor flow. (**B-C**) Speed in the Y and X direction. (**D-E**) Average speed in Y direction in odor (D) or in the four seconds of air prior to odor presentation (E). (**F-G**) Average speed in X direction in odor (F) or in the four seconds of air prior to odor presentation (G). (**H-I**) Upwind velocity (H) and crosswind velocity (I). (**J-K**) Average upwind and crosswind velocity in the odor. (**L-M**) The fraction of stationary animals (L) and of flies walking upwind (M). (**N-O**) The average fraction of stationary animals (N) and of flies walking upwind (O) during odor presentation. Mean ± SEM, n = 4 experiments with 5 animals per experiment for all genotypes. Significance for differences in behavior metrics across genotypes tested using ordinary one-way ANOVA: NS $p \geq 0.05$. See methods for how behavior was analyzed along axes.

Figure 6.5

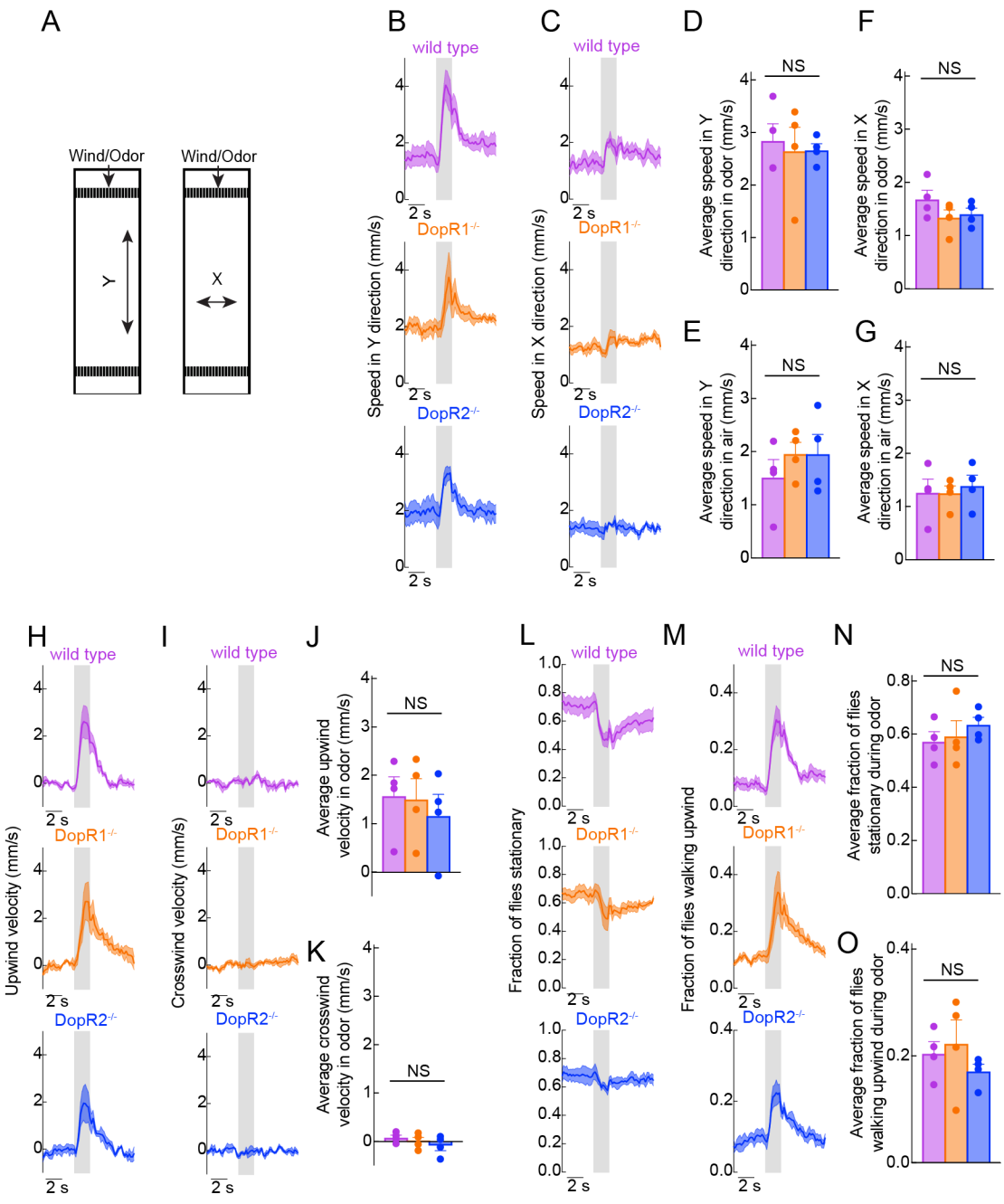
A
Wind/Odor
Wind/Odor
Y
X
B
wild type
DopR1-/-
DopR2-/-
Speed in Y direction (mm/s)
2 s
C
wild type
DopR1-/-
DopR2-/-
Speed in X direction (mm/s)
2 s
D
NS
Average speed in Y direction in odor (mm/s)
E
NS
Average speed in Y direction in air (mm/s)
F
NS
Average speed in X direction in odor (mm/s)
G
NS
Average speed in X direction in air (mm/s)
H
wild type
DopR1-/-
DopR2-/-
Upwind velocity (mm/s)
2 s
I
wild type
DopR1-/-
DopR2-/-
Crosswind velocity (mm/s)
2 s
J
NS
Average upwind velocity in odor (mm/s)
K
NS
Average crosswind velocity in odor (mm/s)
L
wild type
DopR1-/-
DopR2-/-
Fraction of flies stationary
2 s
M
wild type
DopR1-/-
DopR2-/-
Fraction of flies walking upwind
2 s
N
NS
Average fraction of flies stationary during odor
O
NS
Average fraction of flies walking upwind during odor

6.4 Discussion

In Chapter 3, I showed that the order of associative conditioning results in bidirectional plasticity between the individual KC-MBON synapses within a single compartment of the MB. These opposing forms of plasticity dependent on the timing of events suggest distinct involvement of dopamine-sensitive receptors in neurons post-synaptic to dopamine terminals. In this chapter, I showed that DopR1 and DopR2, despite both being highly expressed in KC axons, are selectively involved in the depression of synapses following forward pairing and the potentiation of synapses resulting from backward pairing, respectively.

In a final attempt to link this neural plasticity to reversals in odor attraction depending on conditioning, we found that loss of either DopR1 or DopR2 impairs the ability of animals to rapidly update their odor associations following reversals in contingency between the odor and rewarding reinforcement. Together, these experiments highlight the critical balance of these two dopamine receptors and their distinct intracellular signaling pathways in permitting animals the flexibility to form appropriate relationships that reflect the temporal relationship between events in their environment.

The observation that DopR2-RNAi expressed selectively in KC axons impairs the potentiation of KC-evoked calcium levels in KCs suggests DopR2 acts pre-synaptically to alter transmission between KC-MBON synapses. In these experiments, the time delay between conditioning and testing for neuromodulation is ~20-30 seconds, potentially enough time for phosphorylation or insertion of channels. Given the multitude of channels controlled via phosphorylation by dopamine-dependent signals, such as the GABA(A) and GluR1 AMPA receptor in striatal

circuits (Flores-Hernandez et al., 2000; Greengard, 2001; Snyder et al., 2000), the basis for this modulated calcium responses remains unknown but suggests that the release probability is altered within KC boutons following DopR2-dependent ER calcium release. However, we cannot exclude a role of post-synaptic modulation in the plasticity in odor-drive to the MBONs following forward or backward pairing. Furthermore, while electrophysiological recordings in the pre-synaptic neurons could potentially reveal the ionic currents altered during conditioning, such experiments are difficult given the MB architecture. Specifically, the soma of KCs are electrically isolated from the axons intrinsic to the output lobes; additionally, we believe the modulation is occurring locally along the KC axons, emphasizing the requirement of sharp axon recordings, a non-trivial experimental approach.

The downstream targets of cAMP and ER calcium are numerous and depend highly on the cellular machinery present in sites of activity (Thum and Gerber, 2019). It is likely that these two pathways work downstream through differential activation of PKA and protein kinase C (PKC) to shape synapse function (Leenders and Sheng, 2005; Thum and Gerber, 2019). The use of additional fluorescent sensors for PKA and PKC may help elucidate how forward and backward pairing differential recruit these two kinases to shape neural plasticity. However, it still remains unclear what the potential targets are of the DopR1 and DopR2 pathway. The observation that both forward and backward pairing drive depression in the DopR2 mutant animal suggests that DopR2 may act to antagonize the depressive-effects of cAMP-dependent DopR1, either by acting in opposition on a common downstream target or through a parallel, antagonistic, pathway. One known target for DopR2 is the scribble scaffolding protein that interacts with a Rac1 GTPase that has been suggested to mediate forgetting through active restructuring of the

actin cytoskeleton (Cervantes-Sandoval et al., 2016; Davis and Zhong, 2017; Dong et al., 2016; Shuai et al., 2010; 2015; Zhang et al., 2018). However, it is unclear whether the rapid reversals in neural plasticity and behavior we observe on the second to minute timescale could emerge from DopR2-dependent cytoskeletal reorganization. Instead, it is likely that PKA and/or PKC shape the bidirectional plasticity through direct phosphorylation of channels involved in synaptic transmission. Indeed, distinct kinases are known to have opposing roles in regulating channel function; for example, Ca^{2+}/calmodulin-dependent kinase II (CAMKII) and PKC bidirectionally regulate the open probability of the large conductance potassium channel (BK) in the medial vestibular nucleus (van Welie and Lac, 2011). A candidate screen of RNAis expressed in KC axons may allow us to further examine which channels are required for this bidirectional plasticity. Ultimately, understanding how these two dopamine pathways interact on downstream targets would provide an elegant model for how distinct neuromodulatory pathways integrate signals to sculpt synaptic transmission.

Chapter 7

Discussion and Future Experiments

7.1 Introduction

While memories are often thought of as windows into the past, their adaptive value lies in the ability to predict the future. Memory systems enable animals to use their prior experience to anticipate and prepare for future events. In the context of a dynamic and uncertain environment, however, memories must be continually retouched and rewritten to maintain their relevance and predictive value. Learning circuits must therefore accommodate two opposing demands: first, to rapidly generate associations that inform optimal behavior and second, to flexibly overwrite these associations as environmental conditions change (Dudai, 2009). Behavioral experiments across a diversity of animals have suggested that animals form distinct and opposing associations depending on whether a conditioned stimulus precedes or follows a reinforcement, allowing animals to form meaningful associations about the causal relationship between events. While this temporally sensitive learning has been well-described at the behavioral level (Aso and Rubin, 2016; Gerber et al., 2019; König et al., 2018; Tanimoto et al., 2004), understanding how such temporal specificity is achieved in associative learning circuits was a previously unexplored question.

During my thesis, I took advantage of the concise circuitry of the *Drosophila* mushroom body and the temporal resolution of optogenetics to investigate how the timing of dopaminergic

reinforcement instructs the formation of distinct and opposing olfactory memories depending on the order of events during conditioning. Our work suggests a model in which bidirectional neural and behavioral plasticity arises from the temporal sensitivity of two dopamine receptor-signaling pathways that work in opposition to regulate the strength of KC-MBON signaling within a compartment (Figure 7.1), allowing animals to maintain an accurate model of a changing world. Specifically, during forward pairing we see the selective engagement of DopR1-dependent cAMP that is likely required for driving the KC-MBON depression, leading to increased attraction to the positively conditioned odor. By contrast, in backward pairing, we see the unique engagement of DopR2-dependent ER calcium release. Loss of this ER calcium signal, either in the DopR2 mutant animals or in the presence of the Gαq inhibitor, leads to a loss in synaptic facilitation and impairs behavioral flexibility. Together, these experiments combining molecular, functional and behavioral analysis allow us to link mechanisms of learning and memory across multiple levels: from molecular pathways that regulate synaptic strength to the emergence of learned behavior.

7.2 Using Temporal Relationships to Form and Overwrite Associations

Memory retention is regulated through multiple mechanisms that span different timescales (Bouton, 2002; Davis and Zhong, 2017; Richards and Frankland, 2017). If not reinforced, memories may passively fade over time, reflecting the slow natural turnover of molecular and neural hardware. Alternatively, memory erosion may be actively triggered by changing circumstances and contingencies, as observed with fear extinction or reversal learning studied

Figure 7.1, Model for Dopamine-Dependent Bidirectional Neural and Behavioral Plasticity
Model of the selective engagement of the two dopamine receptors and their downstream signaling pathways following forward and backward pairing leading to opposing synaptic plasticity and odor tracking behavior.

Figure 7.1

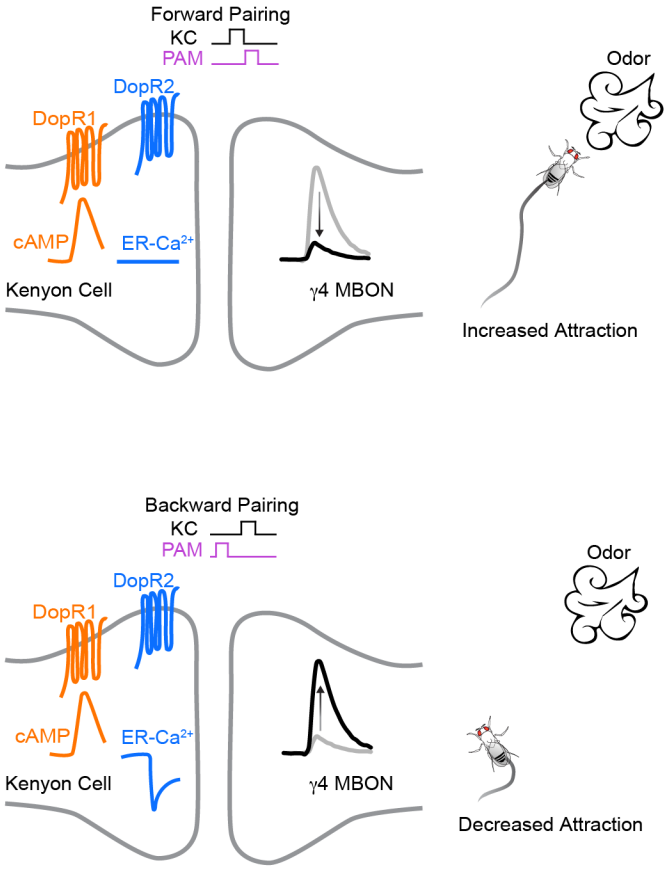
Forward Pairing
KC
PAM
DopR2
DopR1
cAMP
ER-Ca2+
Kenyon Cell
γ4 MBON
Odor
Increased Attraction
Backward Pairing
KC
PAM
DopR2
DopR1
cAMP
ER-Ca2+
Kenyon Cell
γ4 MBON
Odor
Decreased Attraction

in mammalian and invertebrate species (Izquierdo et al., 2017; Quinn et al., 1974; Shuai et al., 2010; Xue et al., 2013). Indeed, the ability to update prior associations is advantageous for animals contending with dynamic environments and is often used as a measure of cognitive flexibility.

Previous work in *Drosophila* has suggested that olfactory memories can be eroded by re-exposure to the learned odor in the absence of the anticipated dopaminergic reinforcement, violating the expected contingency between these two events (Aso and Rubin, 2016; Felsenberg et al., 2017; 2018; Schwaerzel et al., 2002). In fact, it is believed that memory erosion resulting from odor re-exposure results in the creation of a parallel, competing association with the specific odor. This type of re-evaluation relies on a circuit-based mechanism, in which distinct compartments in the mushroom body process and encode competing odor associations (Felsenberg et al., 2017; 2018).

Dopaminergic reinforcement in the absence of odor can similarly erode memories (Aso and Rubin, 2016; Berry et al., 2012). Indeed, strong or prolonged dopamine release within a compartment is sufficient to potentiate the response of KC-MBON signaling to all subsequent odor stimuli (Cohn et al., 2015) and overwrite past learned associations (Aso and Rubin, 2016; Berry et al., 2012; 2015; 2018). Furthermore, ongoing locomotor activity of *Drosophila* engages the same DANs that are involved in reinforcement learning (Berry et al., 2012; Cohn et al., 2015). This constant engagement during motor activity has been shown to result in memory erosion over time, likely due to the engagement of the same dopamine receptor pathways in KCs that are involved in associative learning. However, these forms of memory erosion occur over a

timescale of hours (Berry et al., 2012; 2015; Felsenberg et al., 2017). Such slow re-evaluation of a learned association limits the capacity for animals to rapidly update associations in an environment as dynamic and complex as the sensory world we live in.

In contrast to these forms of memory erosion, here we describe a rapid form of memory updating that is specifically sensitive to the temporal relationship between a converging sensory cue and reinforcement. We find that the brief periods of odor and dopaminergic reinforcement (1-2 seconds) are insufficient to overwrite an olfactory association when presented independently but can immediately reverse a prior association when paired together in time. The convergence of olfactory and DAN input to the mushroom body thus conveys information about the causal relationship between these events, allowing animals to immediately update their memories to reflect the changing temporal structure of their environment.

Since the 1950s, scientists have debated the relevance of backward pairing in animal behavior due to conflicting outcomes in behavioral conditioning (Spetch et al., 1981). Early reports suggested that backward conditioning had little effect on instructing associations, and in fact, backward pairing was often used as a negative control for examining the behavioral effects of forward pairing, further obscuring any insight into the behavioral effects of negative contingency conditioning (Kalish, 1954; Spence and Runquist, 1958). Around the same time, a conflicting report instead showed that animals learned to associate a tone that follows a shock as a safety signal (conditioned inhibition) (Moscovitch and LoLordo, 1968), creating a rift in the field regarding what temporal relationships animals use for causality judgments. Recently, well-controlled behavioral experiments across a wide-diversity of animals have emphasized the

importance of backward pairing in learning and memory (Andreatta et al., 2012; 2013; 2015; Aso and Rubin, 2016; König et al., 2018; Tanimoto et al., 2004). In our work, we observe that flies are capable of learning appetitive associations between cues that anticipate rewards or follow punishments and aversive associations between sensory signals that predict punishments or follow rewards. This work adds to the growing literature that negative contingency reinforcement, such as that in backward pairing, is equally as important as the learning occurring with positive contingency reinforcement (Aso and Rubin, 2016; König et al., 2018; Tanimoto et al., 2004). Interestingly, in the rodent brain, the basolateral amygdala and nucleus accumbens appear to be selectively involved in either punishment learning following forward pairing and relief learning following backward pairing, respectively, and appear to encode shock onset and offset in temporally distinct ways (Andreatta et al., 2012; Gerber et al., 2014). By contrast, we found that the same DAN populations can instruct bidirectional behaviors and plasticity in an individual compartment depending on the timing of events; however, it is possible circuit dynamics in the MB architecture contribute to the behavioral effects of conditioning.

Indeed, we found a single reinforcement can simultaneously instruct multiple olfactory associations in parallel depending on whether an odor preceded or lagged the reinforcement in time, highlighting how *Drosophila* take advantage of all the temporally correlated features of their environment that may inform causal relationships. Prior to this work, research in the MB field suggested that short-term memory compartments were only capable of storing a single association at a time (Aso and Rubin, 2016)—the learning of a new association eroded the prior association. Instead, we show that the capacity of short-term memory processing is multiplexed, allowing animals to learn which associations precede and lag a reinforcement simultaneously.

Together, these results suggest that memory erosion by backward pairing may reflect the formation of a new memory in which the odor, once predictive of a reinforcement, is now associated with its termination, analogous to the changes in contingency that occur during reversal learning (Quinn et al., 1974; Shuai et al., 2010). Our observations thus extend upon the memory updating mechanisms previously described in the mushroom body, revealing how the temporal sensitivity of this associative circuit to dopaminergic and olfactory input allows animals to quickly rewrite outdated associations.

Additionally, the implementation of a novel assay using freely behaving animals clarified how animals change their odor preferences following associative conditioning. In the classic T-maze assay, populations of flies are given a choice between the conditioned and an unconditioned odor (Quinn et al., 1974). However, these end-point assays often obscure the specific behavioral strategies animals use to contend with sensory cues that are predictive of negative or positive experiences. Here we show that negative reinforcement of either forward pairing with the aversive PPL DANs or backward pairing with the rewarding PAM DANs biases animals to both remain stationary during the odor presentation and for those that do walk, decrease their speed in the odor plume. By contrast, positive reinforcement had the opposite effect, decreasing the number of stationary animals and increasing the walking speed of animals in the odor plume. Together, these results suggest that negative and positive reinforcement by forward and backward pairing work in opposition to regulate the same facets of behavior underlying odor-tracking. This antagonism at the behavioral level is further supported by our observations that forward and backward pairing act to bidirectionally modulate the same individual KC-MBON synapses within an individual mushroom body compartment. Optogenetic activation of a variety

of MBONs in the absence of odor demonstrate that individual MBONs act to bias animal behavior towards attraction or avoidance in a manner highly correlated with the neurotransmitter of the MBONs, with cholinergic neurons mediating attraction and glutamatergic neurons biasing towards avoidance (Aso et al., 2014b). Indeed, these experiments showed that optogenetic activation did not elicit stereotyped locomotor patterns, instead suggesting that the concerted activity state of MBONs bias an animal in goal-directed behaviors (Aso et al., 2014b). Interestingly, we see that forward and backward pairing with PPL or PAM DANs bidirectionally modulate multiple aspects of animal behavior—most notably altering the probability of whether an animal will move in response to the odor stimulus and the speed with which the animal will track the odor. These results reveal how changing the activity state of MBONs alters the navigational strategies animals employ in the presence of an appetitive or aversive odor stimulus. Given the multiple compartments innervated by PAM and PPL DANs, as well as the recurrent feedback circuitry, the question remains regarding how many MBONs are influenced by positive or negative conditioning and how the concerted modulation across the MB architecture works to shape animal behavior.

7.3 Mechanisms of Temporal Order Detection

Bidirectional plasticity at the synaptic level in associative learning circuits has been invoked as a key mechanism for driving bidirectional modifications at the behavioral level (Boyden et al., 2004; Coesmans et al., 2004; Jörntell and Hansel, 2006; Lev-Ram et al., 2002). The capacity for bidirectional synaptic modulation could thus allow animals to form distinct associations

depending on the timing of events of forward and backward pairing and additionally allow for the erosion of outdated associations to permit storage of more relevant information.

For example, spike-timing dependent plasticity (STDP) can bidirectionally tune the strength of synaptic connections between neurons depending on the relative timing of spikes in pre- and post-synaptic neurons (Bell et al., 1997; Bi and Rubin, 2005; Cassenaer and Laurent, 2012; Dan and Poo, 2004). STDP therefore mirrors the sensitivity to temporal order we observe behaviorally in associative learning. However, STDP requires nearly coincident firing patterns on a millisecond timescale, far more rapid than the temporal relationships between stimuli typically required for associative learning (Drew and Abbott, 2006). More recent work has identified plasticity mechanisms in learning circuits that aligned with the delays of circuit processing and accommodate the behaviors the circuit promotes (Suvrathan et al., 2018). Specifically, timing delays in the perforant pathway of the hippocampus (Basu et al., 2013; Leroy et al., 2017), pyramidal neurons in the amygdala (Cho et al., 2011), place cells in the CA1 area (Bittner et al., 2017), and Purkinje Cell circuits in the cerebellum (Suvrathan et al., 2018) have all found expanded windows for the integration of temporal coincidence that drive learned changes in behavior. Thus, a big push has been made in recent years to determine the plasticity mechanisms relevant to support learned changes in animal behavior.

Here, by examining neural and behavioral modulation over the same timescales we reveal that bidirectional changes in KC-MBON signaling directly correlate with reversible changes in learned odor attraction from forward and backward conditioning. Importantly, the closed-loop behavioral experiments described in Chapter 3 reveal that the neural and behavioral plasticity

emerge concurrently following the same dopaminergic reinforcement signal. The aligned emergence of plasticity at the behavioral and neural level further emphasizes the link between dopamine-dependent modulation in the KC-MBON synapses and learned changes in odor tracking behavior. These results are inline with previous, indirect measures comparing changes in neural activity with behavior across independent experimental preparations (Hige et al., 2015; Owald and Waddell, 2015; Owald et al., 2015; Séjourné et al., 2011).

Within the mushroom body, each compartment serves as a site of convergence between odor-specific KC signaling and dopaminergic reinforcement, allowing dopamine receptor signaling pathways within KC axons to detect the temporal order of these inputs. Different odors are thought to activate unique ensembles of KCs (Campbell et al., 2013; Caron et al., 2013; Gruntman and Turner, 2013) whose axons traverse through the tiled compartments of a mushroom body lobe. We found that patterns of dopamine release and dopamine receptor second messenger signaling cascades both adhere to the compartmentalized architecture of the lobes (Boto et al., 2014; Cohn et al., 2015), permitting the different synapses along the same KC axon to be independently regulated. Within a compartment, multiple neuromodulatory mechanisms can be engaged to further tune neurotransmission, depending on the structure of conditioning. Indeed, we demonstrate that a single dopaminergic reinforcement can drive odor-specific bidirectional plasticity of KC-MBON synapses activated by odors that precede or follow the reinforcement are differentially regulated. Thus dopamine acts with both exquisite spatial and temporal precision to fine tune synaptic transmission in the mushroom body. While it has been known that KC axons express a diversity of dopamine receptors (Crittenden et al., 1998; Crocker et al., 2016; Han et al., 1996; Kim et al., 2007), prior to this work it has remained unclear how

the different modulatory pathways are engaged in KC axons depending on the context of learning.

In both vertebrates and invertebrates, dopamine can shape circuit function in diverse ways by engaging distinct classes of receptors that couple to different signaling cascades (Tritsch and Sabatini, 2012). In *Drosophila*, DopR1 and DopR2 have been previously proposed to play opposing roles in olfactory memory regulation at the behavioral level, with DopR1 essential to memory formation and DopR2 necessary for the long, steady decay of memory (Berry et al., 2012; Kim et al., 2007). Our work reveals that the opposing behavioral roles of DopR1 and DopR2 are mirrored by their antagonistic regulation of KC-MBON signaling, with DopR1 required for the depression ensuing from forward pairing, while DopR2 is essential for the potentiation that follows backward pairing. Thus the same dopaminergic signal can simultaneously write multiple odor associations by directing opposing forms of plasticity at different KC-MBON synapses, effectively expanding the coding capacity of a single compartment.

The discrete innervation patterns of DANs permit the local modulation of KC-MBON synapses in individual compartments. Indeed, we show that bidirectional plasticity is a conserved feature across multiple compartments, suggesting a conserved sensitivity to the timing of events exists across the KC-MBON synapses of the γ lobe. However, it remains to be addressed whether the synaptic plasticity across different compartments depends on DopR1 and DopR2 in a similar manner. It is likely naïve to consider the examination of the dopamine receptor-dependent plasticity rules of a single compartment represents the whole picture of dopamine-dependent

modulation across all 15 compartments of the mushroom body. Indeed, complex feedback interactions exist across many compartments of the mushroom body, raising the intriguing possibility that plasticity in one compartment can tune the output of an entirely distinct compartment. Evidence for this cross compartmental influence has been invoked in mediating the opposing behavioral effects of aversive and appetitive conditioning (Felsenberg et al., 2018; Owald et al., 2015). Additionally, sugar-feeding and shock drive coordinated patterns of dopamine release across compartments; specifically, shock activates the γ2/γ3 DANs and synchronously decreases activity in the γ4/γ5 DANs (Cohn et al., 2015). This patterning of DAN activity with natural reinforcers raises the question for whether PAM and PPL compartments are opposingly modulated by aversive or rewarding conditioning.

Nonetheless, our results indicate that the coupling of DopR1 and DopR2 is highly selective in γ lobe KCs *in vivo*, as mutation of DopR1 results in a deficit in cAMP production while mutation of DopR2 leads to a loss of ER calcium release. We found that DopR1-mediated cAMP production is enhanced by coincident KC and DAN activation, consistent with calcium-activated adenylyl cyclases acting as molecular coincidence detectors due to their dual regulation by Gαs and calcium (Levin et al., 1992; Livingstone et al., 1984; Mons et al., 1999; Tomchik and Davis, 2009). However, DopR1 drives equivalent production of cAMP during both forward and backward pairing, demonstrating that this pathway cannot autonomously encode the temporal order of events to drive bidirectional neural and behavioral modulation. In contrast, DopR2 signaling strictly depends on the temporal order of KC and DAN activation, as efflux from ER calcium stores is exclusively evoked during backward pairing, indicating that it serves as a temporal order detector.

Which component of the DopR2 signaling cascade is sensitive to the temporal sequence of KC and DAN input? IP_3 receptors that gate calcium release from the ER lumen represent an interesting order-detection candidate as their complex regulation by both IP_3 and cytosolic calcium renders them inherently sensitive to the sequence of agonist binding: IP_3 binding unmasks a calcium regulatory site required for channel opening, while high calcium in the absence of IP_3 inhibits channel activity (Adkins and Taylor, 1999; Paknejad and Hite, 2018; Srikanth et al., 2004). Indeed, we observe that ER calcium release during backward pairing is time-locked to KC stimulation, suggesting that this second-messenger is 'gated' in a temporally precise way by KC activity. Additionally, we see that loss of Gαq or IP_3 receptors impairs the ability of DopR2-dependent calcium release in HEK293T cells (Figure 7.2A-B). In the cerebellum, bidirectional plasticity at parallel fiber-Purkinje neuron synapses relies on calcium release from the ER lumen via IP_3 receptors (Finch and Augustine, 1998; Sarkisov and Wang, 2008; Wang et al., 2000). The analogous circuit organization of the mushroom body and cerebellum (Farris, 2011) makes it tempting to speculate on the potentially conserved molecular mechanisms for temporally precise synaptic modulation across these circuits. Further experimentation on the role of calcium-dependent IP_3 activation in backward pairing would clarify the order-detection mechanism of this pathway in mediating synaptic potentiation of KC-MBON synapses.

Another important question remaining is how this time course of bidirectional plasticity is established? Unlike the time course for STDP that unfolds over a time course of tens of milliseconds, here we show bidirectional plasticity that occurs over time frame of seconds. This

discrepancy in time course between STDP and the plasticity we observe is undoubtedly due to differences in the molecular pathways involved—specifically, STDP relies on the very rapid molecular events of NMDA receptor activation and coincidence of magnesium release. Instead, the time course we observe is defined by the engagement of second messengers downstream of GPCRs. These slower molecular pathways permit the alignment of neural plasticity with the emergence of learned behavior.

Indeed, the temporal sensitivity of DopR1 and DopR2 signaling within KC axons is sufficient to account for the time course of bidirectional neural and behavioral plasticity, highlighting how the balance of these two pathways tunes the strength of KC-MBON synapses to generate flexible behavioral responses to odor. cAMP and cytosolic calcium regulate a myriad of different cellular pathways, offering a wide array of potential targets to control synaptic function, as described above in the previous chapter. Additionally, presynaptic levels of ER calcium have been shown to finely tune activity-driven calcium entry and regulate release probability (de Juan-Sanz et al., 2017; Mattson et al., 2000), both of which may play an important role in the potentiation of KC-MBON synapses following backward pairing. However, the link between DopR1 and DopR2 and its downstream effectors have yet to be elucidated. Expanding the repertoire of biochemical reporters may offer a link between the dynamic engagement of receptor signaling on behaviorally relevant timescales and synaptic regulation; specifically, using fluorescent reporters of PKA, PKC and IP_3 may help our understanding of when particular molecules and kinases are engaged during associative conditioning (Komatsu et al., 2011; Oura et al., 2016). In addition, kinase activity could be assessed using biochemical approaches to examine phosphorylation

Figure 7.2, DopR2-Dependent Calcium Release Depends on Gαq and IP3R Expression
(**A**) Cytosolic calcium response in DopR2-expressing HEK293T cells in the background of wild type cells (black trace), Gαq knock out cells (light gray trace), or Gαq knock out cells with rescued expression of the Gαq protein (dark gray trace). Application of dopamine (30 nM) marked with black arrow. (**B**) Same as above except light gray trace is in background of IP_3R knock out HEK293T cell line. Data traces kindly provided by Andrew Siliciano.

Figure 7.2

A

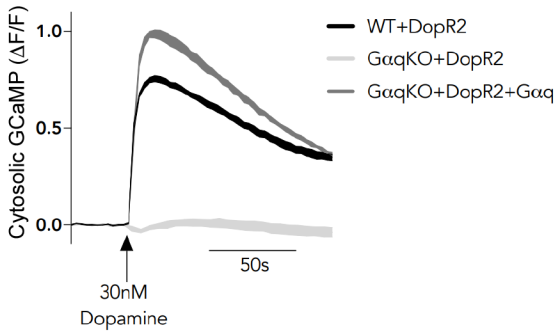
Cytosolic GCaMP (ΔF/F)
1.0
0.5
0.0
WT+DopR2
GαqKO+DopR2
GαqKO+DopR2+Gαq
50s
30nM
Dopamine

B

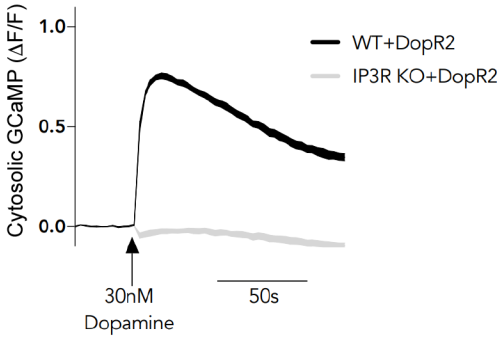
Cytosolic GCaMP (ΔF/F)
1.0
0.5
0.0
WT+DopR2
IP3R KO+DopR2
50s
30nM
Dopamine

changes and RNAi knockdown of candidate genes coupled with functional experiments may link the dopamine receptors to their downstream effectors.

7.4 The Timescales of Neural Plasticity and Memory

Together, our work supports the idea that dopamine receptor signaling pathways in KC axons serve as a key site of temporal coincidence and order detection during associative learning. While we initially focused on the γ4 compartment, whose MBON contributes to odor avoidance behavior, we found similar reversible plasticity could be instructed by the γ2 and γ5 DANs within their cognate compartments with a similar temporal sensitivity to the plasticity driven by the γ4 DANs, indicating that bidirectional modulation of KC-MBON signaling is a general feature shared by compartments of the γ lobe, including those innervated by either PAM or PPL dopaminergic pathways. Such plasticity across the γ lobe of the mushroom body may allow animals to avoid odors that predict punishment through the depression of approach MBONs, like γ2, or become attracted to odors that predict reward through the weakening of MBONs that drive avoidance, like γ4 or γ5, or learn opposite associations with odors that follow these reinforcements in time by potentiating the activity of the same, individual MBONs. However, we have yet to explore whether additional compartments share a similar dependence on DopR1 and DopR2 signaling in KC-MBON modulation.

Additionally, the ability to form and overwrite associations on a trial-by-trial basis allows for adaptive behavior in a noisy and changing environment where the temporal relationships between events may quickly change. However, animals also have the capacity to store relevant memories persistently, even for a lifetime. Therefore, the reversible plasticity we describe must co-exist with additional mechanisms to allow for the formation and retention of longer-term associations. Recent work has described intrinsic differences between mushroom body compartments in their susceptibility to memory erosion (Aso and Rubin, 2016). Furthermore, while KCs innervating the γ lobe are essential for short-term associations (Blum et al., 2009), other populations, specifically the α/β KCs, support long-term memory formation and retention, leading to the proposal that transient and enduring memories are written in parallel at different synaptic sites within the mushroom body circuitry. An intriguing possibility is that the differential expression or coupling of dopamine receptor signaling pathways in distinct KC classes may tune synaptic plasticity rules to regulate the persistence of information storage.

We were, therefore, interested in examining how the capacity for bidirectional plasticity differs across compartments involved in short- and long-term memory. The α1 compartment is located in the ventral region of the mushroom body and has been shown to be essential for the formation and retrieval of an appetitive long-term memory (Ichinose et al., 2015). Additional characterization has shown that memories processed in this compartment are resilient to erosion by odor re-exposure or strong activation of the innervating DANs (Aso and Rubin, 2016), suggesting inflexibility to dopamine-dependent modulation that is distinct from the rapid and reversible modulation observed in the compartments of the γ lobe. Indeed, preliminary experiments revealed that while the α1 MBON undergoes depression following forward pairing,

there was no effect on neural activity following from backward pairing (Figure 7.3A). This reveals that distinct neural plasticity rules exist across the different lobes of the mushroom body and suggests such differences may underlie the distinct kinetics of short- and long-term memory encoding and maintenance.

To further explore this idea, we performed fluorescence activated cell sorting (FACS) of soma from genetically labeled γ and α/β KCs and transcriptionally profiled these populations in search of differentially expressed candidate genes that may determine the rules governing neural plasticity in learning (Figure 7.3B-C). We generated 4 RNA-seq libraries for γ and α/β KC types (in duplicate). These libraries were generated from high-quality RNA isolated from 100,000 FAC-sorted GFP-tagged γ or α/β KCs that were sequenced at a depth of 25-40 million reads per sample—a depth shown to identify 75% of truly differentially expressed genes (Liu et al., 2013). Our sequencing results matched single-cell profiling of γ and α/β KC types (Crocker et al., 2016), confirming expression of dopamine receptors, the vesicular acetylcholine transporter, and the octopamine receptor—all known to be highly expressed in KC axons.

From our sequencing results, we identified an interesting candidate gene, PKA-C3, enriched in γ over α/β KC, which encodes the major catalytic domain of the cAMP dependent protein kinase (7.3D). Interestingly, mutation of this gene in *Drosophila* (DCO), leads to a reduction in age-related memory loss (Yamazaki et al., 2007), suggesting the high levels of cAMP and PKA activity work in opposition to long-term memory storage. In line with this, α/β KCs are enriched in genes encoding phosphodiesterase enzymes (PDE6 and PDE8) that catalyze the breakdown of cAMP (7.3D). Together, these results suggest that memory kinetics may be finely tuned by

Figure 7.3, Different KC Populations Exhibit Distinct Rules for Synaptic Plasticity and Show Differential Expression of Transcript and Proteins Involved in Plasticity.

(**A**) Comparing fold change in in Kenyon Cell-evoked response in γ4 MBON and α1 MBON following forward and backward pairing. The γ4 and α1 DANs are both activated by activating DAN dendrites using exogenously expressed ATP-gated $P2X_2$ channel using the 58E02-LexA driver that labels both DAN populations. Electrode containing ATP was targeted specifically to either γ4 or α1 DANs, which are located in distinct regions of the brain. The α1 MBON shows depression following forward pairing but no potentiation following backward pairing. (**B**) GFP+ KC sub-populations labeled using split-gal4 drivers. These GFP+ populations were sorted from brains of adult flies. The α/β core and shell KCs were sorted and sequenced independently but then sequencing results were pooled since populations were similar in transcript profiling. (**C**) Differential gene enrichment in of γ and α/β KCs. Negative $\log_2$ (fold change) corresponds to genes enriched in γ over α/β and positive to genes enriched in α/β over γ. Red indicates enriched genes with false discovery rate adjusted p-values<0.05. (**D**) Categorization of enriched genes in γ and α/β KCs. Size of circle represents enrichment for type of proteins within KC population. (**E**) Pattern of Gaq GPCR protein shows differential level of expression across γ and α/β KCs. Immunofluorescence images in (E) kindly provided by Ianessa Morantte.

Figure 7.3

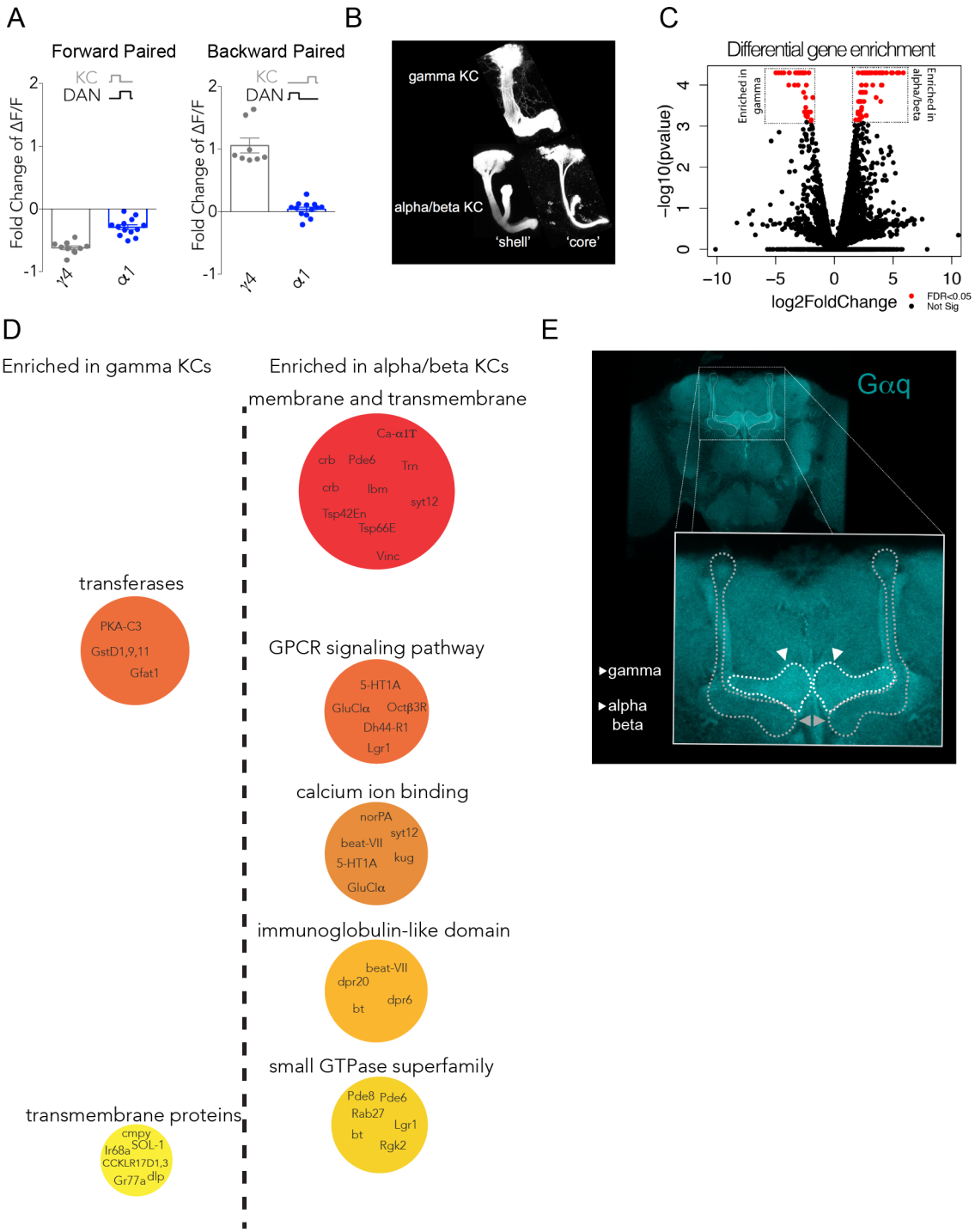
A
Forward Paired
Backward Paired
KC
DAN
Fold Change of ΔF/F
γ4
α1
B
gamma KC
alpha/beta KC
'shell'
'core'
C
Differential gene enrichment
Enriched in gamma
Enriched in alpha/beta
−log10(pvalue)
log2FoldChange
FDR<0.05
Not Sig
D
Enriched in gamma KCs
Enriched in alpha/beta KCs
membrane and transmembrane
Ca-α1T
crb
Pde6
Trn
lbm
syt12
Tsp42En
Tsp66E
Vinc
transferases
PKA-C3
GstD1,9,11
Gfat1
GPCR signaling pathway
5-HT1A
GluClα
Octβ3R
Dh44-R1
Lgr1
calcium ion binding
norPA
beat-VII
syt12
5-HT1A
kug
GluClα
immunoglobulin-like domain
beat-VII
dpr20
dpr6
bt
small GTPase superfamily
Pde8
Pde6
Rab27
Lgr1
bt
Rgk2
transmembrane proteins
cmpy
Ir68a
SOL-1
CCKLR17D1,3
Gr77a
dlp
E
Gαq
gamma
alpha
beta

differing levels of cAMP across the two KC populations—with the labile γ KCs enriched in PKA and the more rigid α/β KCs reinforced with PDEs. Additionally, levels of the Gαq protein appear differential expressed with higher levels in the γ KCs in comparison to the α/β KCs (Figure 7.3E). Together, these experiments suggest that high signaling of cAMP and PKA in addition to Gαq may allow for greater flexibility and plasticity in the γ KCs while lower levels of these signaling pathways in the long-term memory associated α/β KCs may result in more rigid and stable modulation. Functional dissection of these signaling cascades across the different lobes of the mushroom body may provide insight into the distinct timescales of memory formation and erosion.

In summary, the data presented in this thesis reveal how the balance of two neuromodulatory pathways allow animals to form distinct associations between sensory cues associated with reinforcement onset in comparison to cues associated with the offset of reinforcement. This capacity for differential associations depending on the timing and order of events is essential for animals to form and maintain meaningful associations in a complex sensory environment. Additionally, we reveal that these associations can be updated on a trial-by-trial basis, permitting animals to change their associations depending on the most up-to-date contingency between the cue and reinforcement. These rapid reversals may be an ideal mechanism for short-term memory processing; however, in addition to the dynamics of short-term memory animals must also be able to form stable, long lasting associations. In the future, it will be interesting to link the differences in the molecular machinery between KC populations to the rules for neural plasticity and ultimately to the different kinetics in short- versus long-term memory.

Methods and Materials

Generation of ER-GCaMP transgenic flies

The coding sequence for the low-affinity ER calcium sensor (ER-GCaMP6-210) (de Juan-Sanz et al., 2017) containing an N-terminal calreticulin signaling peptide and KDEL ER retention sequence was PCR amplified using KOD Hot Start DNA polymerase. Restriction sites were added to the 5' and 3' end of the coding sequence (*Xho1* and *Xba1*, respectively). The amplified product and pJFRC81 (Addgene Plasmid #36432) were digested with *Xho1* and *Xba1* and ligated together. The resulting plasmid was used to generate transgenic flies by PhiC31 mediated integration into VK00005 and attp5 (Bestgene Inc.)

Primer sets to clone sensor and add restriction sites:

5' – GCG GCTCGA GGG TAC CAA CTT AAA AAA AAA AAT CAA ACA AAA TGG GAC TGC TGT CTG TGC CTC – 3'

5' – TTC ATT CTA GAT CAC AGC TCA TCC TTG CCT CCG – 3'

Crispr-Cas9 mediated deletion of DopR1

Existing DopR1 mutants were generated either imprecisely using a larger chromosomal inversion (*dumb*^{1}*,* (Kim et al., 2007)*),* through disruption by a transposable PiggyBac element and therefore incompatible with 2-photon imaging (*dumb*^{2}, (Kim et al., 2007)*)*, or were actually hypomorphs (Keleman et al., 2012) based on immunohistochemistry. We therefore generated a novel DopR1 mutant compatible with functional imaging. Two gRNAs were designed to direct Cas9-mediated cleavage to the 5' and 3' UTRs of the *Dop1R* gene locus. gRNA off-target

potential was determined using Crispr optimal target finder (http://tools.flycrispr.molbio.wisc.edu/targetFinder/index.php) gRNA sequences were PCR amplified with Q5 High-Fidelity master mix (NEB) and cloned into pCFD4 by Gibson assembly (NEB). The resulting vector was sequence verified and injected into nos-Cas (Bloomington stock 54591) embryos (Rainbow Transgenic Flies). G0 flies were individually crossed to a balancer strain prior to being screened for the deletion by PCR-based genotyping. Each G0 founder positive for the deletion was further verified by Sanger sequencing. F1 progeny from a deletion positive G0 parent were individually crossed to a balancer strain then screened for transmission of the deletion. Multiple unique deletion lines were obtained and a single line was then used for further experimentation. Loss of DopR1 protein expression in the mutant was verified by immunohistochemistry with anti-DopR1 antibody (a gift from Tim Lebetsky) and qRT-PCR in adult fly brains.

Fly strains and husbandry

Flies used for *ex vivo* brain explant preparations and functional imaging in Figure 3F and S3E-F, flies were maintained on conventional cornmeal-agar-molasses at 25°C and 60-70% relative humidity, under a 12 hr light:12 hr dark cycle. Flies used for optogenetic behavioral experiments were maintained at 25°C and 60-70% relative humidity in constant darkness. For optogenetic experiments, 1-3 day old females were transferred to cornmeal-agar-molasses food containing 0.4 mM all trans-Retinal (Sigma #R2500) and reared in the dark for 48 hours before behavioral experiments. Flies were not food-deprived prior to any functional or behavioral experiments.

Strains and sources:

20X-UAS-IVS-CsChrimson.mVenus-attP18, 20X-UAS-IVS-CsChrimson.mVenus-attP40, 20X-UAS-ChrimsonR.mCherry-attP2 (gifts from Vivek Jayaraman, Janelia Research Campus); VT026001-Gal4 (Vienna Drosophila Resource Center (VDRC)); MB042B, MB504B, R53C03-LexA, R58E02-LexA, UAS-GCaMP6s, LexAOP-GCaMP6s (Bloomington Drosophila Stock Center); OK107-Gal4 (Connolly et al., 1996); *TH-Gal4* (Friggi-Grelin et al., 2003); *DDC-Gal4* (Li et al., 2000); LexAOP-P2X$_2$ (gift from Orie T. Shafer, University of Michigan); UAS-EPAC (Shafer et al., 2008); DopR2$^{-/-}$ (Keleman et al., 2012); *UAS-GRAB$_{DA1m}$* (Sun et al., 2018); UAS-VMAT-pHluorin (Wu et al., 2013)

Detailed fly genotypes used by figure (with neuronal expression description):

Figures 2.2, 2.3, 2.4, 2.5, 2.6, 3.1, 3.6, 4.1, 4.2:

w^{1118} UAS-IVS-CsChrimson.mVenus; R58E02-p65ADZp (PAM DAN split); R22E04-ZpGdbd (PAM DAN split)

w^{1118} UAS-IVS-CsChrimson.mVenus; 52H03-p65ADZp (PPL DAN split); TH-ZpGDBD (PPL DAN split)

w^{1118} UAS-IVS-CsChrimson.mVenus

Figures 3.2, 3.3, 4.3, 6.1A, 6.2A:

R58E02-LexA (γ4-5 DANs), LexAOP-P2X$_2$; VT026001-gal4 (γ4 MBON), UAS-GCaMP6s

Figure 3.4A:

R58E02-LexA (γ4-5 DANs), LexAOP-P2X$_2$/ UAS-GCaMP6s; 66C08-gal4 (γ5 MBON)

Figure 3.4B:

73F07-LexA (γ2 DANs), LexAOP-P2X$_2$; 25D01-gal4 (γ2 MBON), UAS-GCaMP6s

Figure 3.5:

25D01-LexA (γ2 MBON), LexAOP-GCaMP6s

Figure 5.1B-C:

Rut^{1}; R58E02-LexA (γ4-5 DANs), LexAOP-$P2X_2$; VT026001-gal4 (γ4 MBON), UAS-GCaMP6s

R58E02-LexA (γ4-5 DANs), LexAOP-$P2X_2$; VT026001-gal4 (γ4 MBON), UAS-GCaMP6s

Figures 3.7, 3.8:

w^{1118}; R58E02-p65ADZp (PAM DAN split)/53C03-LexA (γ4 MBON), LexAOP-GCaMP6s; R22E04-ZpGdbd (PAM DAN split)/UAS-ChrimsonR.mCherry

Figure 5.3A:

R58E02-LexA (γ4-5 DANs), LexAOP-$P2X_2$; LexAOP-GCaMP6s

Figure 5.3B:

R58E02-LexA (γ4-5 DANs), LexAOP-$P2X_2$; TH-Gal4 (DAN subset), DDC-Gal4 (DAN subset)/UAS-VMAT-pHluorin

Figure 5.3C:

R58E02-LexA (γ4-5 DANs), LexAOP-$P2X_2$; UAS-$GRAB_{DA1m}$; OK107-Gal4 (KCs)

Figure 5.3D:

R58E02-LexA (γ4-5 DANs), LexAOP-$P2X_2$/UAS-$Ach_{4.3}$; ; OK107-Gal4 (KCs)

Figures 5.5A,C, 5.6A,D, 5.7C-E:

R58E02-LexA (γ4-5 DANs), LexAOP-$P2X_2$; UAS-EPAC (cAMP); OK107-Gal4 (KCs)

Figures 5.5B-C, 5.6B,E-F, 5.8A-B:

R58E02-LexA (γ4-5 DANs), LexAOP-$P2X_2$; UAS-ER-GCaMP; OK107-Gal4 (KCs)

Figures 5.6C-E:

R58E02-LexA (γ4-5 DANs), LexAOP-P2X$_2$/UAS-EPAC (cAMP); DopR1$^{-/-}$/DopR1$^{-/-}$; OK107-Gal4 (KCs)

R58E02-LexA (γ4-5 DANs), LexAOP-P2X$_2$/UAS-EPAC (cAMP); DopR2$^{-/-}$ DopR2$^{-/-}$; OK107-Gal4 (KCs)

Figures 5.7A-B:

R58E02-LexA (γ4-5 DANs), LexAOP-P2X$_2$/UAS-ER-GCaMP; DopR1$^{-/-}$/DopR1$^{-/-}$; OK107-Gal4 (KCs)

R58E02-LexA (γ4-5 DANs), LexAOP-P2X$_2$/UAS-ER-GCaMP; DopR2$^{-/-}$/DopR2$^{-/-}$; OK107-Gal4 (KCs)

Figures 6.1B-C:

R58E02-LexA (γ4-5 DANs), LexAOP-P2X$_2$/UAS-GCaMP6s; VT026001-gal4 (γ4 MBON), DopR1$^{-/-}$/ VT026001-gal4 (γ4 MBON), DopR1$^{-/-}$

R58E02-LexA (γ4-5 DANs), LexAOP-P2X$_2$/UAS-GCaMP6s; VT026001-gal4 (γ4 MBON), DopR2$^{-/-}$/ VT026001-gal4 (γ4 MBON), DopR2$^{-/-}$

Figure 6.2B:

R58E02-LexA (γ4-5 DANs), LexAOP-P2X$_2$/UAS-GCaMP6s; UAS-DopR2-RNAi; OK107-Gal4 (KCs)

Figures 6.3, 6.4, 6.5:

w^{1118}; R58E02-p65ADZp (PAM DAN split)/ UAS-IVS-CsChrimson.mVenus; R22E04-ZpGdbd (PAM DAN split)

w^{1118}; R58E02-p65ADZp (PAM DAN split)/ UAS-IVS-CsChrimson.mVenus; R22E04-ZpGdbd (PAM DAN subset), DopR1$^{-/-}$/ R22E04-ZpGdbd (PAM DAN split), DopR1$^{-/-}$

w^{1118}; R58E02-p65ADZp (PAM DAN split)/ UAS-IVS-CsChrimson.mVenus; R22E04-ZpGdbd (PAM DAN split), DopR2$^{-/-}$ R22E04-ZpGdbd (PAM DAN subset), DopR2$^{-/-}$

Figure 7.2A:

R58E02-LexA (γ4-5 DANs), LexAOP-P2X$_2$; VT026001-gal4 (γ4 MBON), UAS-GCaMP6s/R52G04-gal4 (a1 MBON)

Figure 7.2B:

R13F03, UAS-CD8GFP (γ KC split); R89B01 (γ KC split)

R52H09, UAS-CD8GFP (α/β shell KC split); R18F09 (α/β shell KC split)

13F02, UAS-CD8GFP (α/β core KC split); 58F02 (α/β core KC split)

Functional Imaging

All functional imaging experiments were performed on an Ultima two-photon laser scanning microscope (Bruker Nanosystems) equipped with a Chameleon Ultra II Ti:Sapphire laser. The excitation wavelength was 920 nm for all experiments except for FRET imaging of the EPAC sensor, which was excited at 850 nm. Emitted fluorescence was detected with either photomultiplier-tube or GaAsP photodiode (Hamamatsu) detectors. Images were acquired with an Olympus objective, either 40X, 0.8 NA or 60X, 1.0 NA at 512 × 512 pixel resolution**.** Quantification of neural activity was performed by normalizing fluorescence intensity changes (ΔF/F) or CFP/YFP fluorescence ratio changes (ΔR/R) to control for variations in reporter expression and imaging parameters across neurons and experiments. ROIs were manually drawn using anatomic landmarks. The inter-stimulus interval between KC stimulation or odor presentation and DAN activation was calculated by subtracting the onset of KC stimulation/odor presentation (time zero) from the onset of DAN activation.

In *ex vivo* experiments, brains from 1-4 day old male or female flies were dissected in saline (108 mM NaCl, 5 mM KCl, 2 mM $CaCl_2$, 8.2 mM $MgCl_2$, 4 mM $NaHCO_3$, 1 mM NaH_2PO_4, 5 mM trehalose, 10 mM sucrose, 5 mM HEPES, pH 7.5 with osmolarity adjusted to 265 mOsm), briefly (30 s) treated with collagenase (Sigma #C0130) at 2 mg/mL in saline, washed with fresh saline, and then pinned with fine tungsten wires to a thin Sylgard sheet (World Precision Instruments) in a 35 mm petri dish (Falcon) filled with saline. For *in vivo* imaging experiments in which we examined odor-specific modulation of γ4 MBON responses (Figure 3F and S3E-F), 1-4 day old female flies were prepared as described previously (Cohn et al., 2015; Murthy and Turner, 2013; Ruta et al., 2010). For *in vivo* imaging experiments in which we examined odor-specific modulation of odor and behavioral responses in the closed-loop assay (Figures 4 and S4), flies were prepared as described previously (Green et al., 2017) with minor modifications. Briefly, 3-5 day old female flies were temporarily anesthetized using CO_2 (for < 30 s) and then tethered to a milled plastic holder (Green et al., 2017) using UV-curable glue (Loctite) applied to each eye and thorax. The proboscis was glued in an extended position to minimize brain motion during imaging. The dish was then filled with saline and the cuticle covering the dorsal portion of the head was removed. Muscle 16 and obstructing trachea were removed. Care was taken to keep the antennae and antennal nerves intact. On rare occasions, flies showed no movement or odor responses and were discarded.

Imaging in *ex vivo* brain explants

(Figures 3.2, 3.3A-B, 3.4, 5.1B-C, 5.3, 5.5, 5.6, 5.7, 5.8, 6.1, 6.2)

Stimulation of Kenyon Cells

Stimulation of Kenyon Cell dendrites was performed as described previously (Cohn et al., 2015). Briefly, glass-stimulating electrodes were pulled to a resistance of 4–5 MΩ and filled with 10 mM acetylcholine (Sigma) in saline. Stimulating electrodes were positioned into the mushroom body calyx viewed under IR-DIC optics. Square voltage pulses (500 ms, 0.1-15V for all imaging experiments) were used to iontophorese acetylcholine into the calyx and excite Kenyon Cells. Pulse trains were generated by a stimulator (Grass Technologies) triggered by Prairie View software. The inter-trial interval for calycal stimulations was at least 20 seconds to assure activity levels returned to baseline. On the rare occasion that MBON responses could not be evoked or were unusually variable in the absence of conditioning, the mushroom body in other hemisphere of the brain was tested or the prep was discarded.

Activation of DANs expressing $P2X_2$

To chemogenetically stimulate DANS (Figure 2D-E, S2A-D, 5A-E, S5A-H, 6A-G, S6C-D), R58E02-LexA or 73F07-LexA was used to drive expression of the $P2X_2$ channel in either the PAM DANs or γ2 DAN, respectively. Glass stimulating electrodes pulled to a resistance of 4-5 MΩ were filled with 2 mM ATP in saline and positioned dorsal to the mushroom body's medial lobes, in the superior medial protocerebrum (Cohn et al., 2015) at the site of rich DAN dendritic innervation. To validate that placement of the electrode in the superior medial protocerebrum drove activation of DANs, in a subset of experiments, responses of DANs expressing GCaMP were directly measured. DANs were stimulated using a train of five 100-ms pulses at 2.5-5V

with an inter-pulse interval of 20 ms. Trains were generated by a stimulator (Grass Technologies) that was triggered by Prairie View software.

MBON modulation to KC activation

KC-evoked responses in the γ2, γ4, and γ5 MBON were measured as the peak fluorescence evoked in the 2 seconds following KC stimulation, normalized to baseline fluorescence (2-3 seconds prior to KC stimulation). To compare KC-evoked calcium responses in the γ2, γ4, and γ5 MBON, prior to and after conditioning the mean traces and peak responses for the two KC stimulations prior to pairing were used as baseline measurements ('pre'), and the mean fluorescent traces and peak responses for the first two responses to KC stimulation after pairing were used for the post-pairing measurements ('post'). This was done to control for any inter-trial variability, which was minimal in explant preparations. On the rare occasion that MBON responses could not be evoked or were highly variable in the absence of conditioning, the other side of the brain was tested or the prep was discarded.

To calculate the change in evoked response in the MBONs due to conditioning in Figure 3.3A-B and 3.4A-B, the mean peak fluorescence response prior to pairing was subtracted from the response post pairing as schematized in Figure 2D. To calculate the fold change in the *Rutabaga* mutants, the change in evoked response was normalized by the baseline-evoked response (Figure 5.1B-C). For the γ4 and γ5 MBON experiments in the inter-stimulus interval (ISI, DAN onset minus KC onset) used for forward pairing was 0.5 seconds and the ISI for backward pairing was -1.2 seconds. For γ2 MBON experiments, the ISI used for forward pairing was 0 seconds with KC activation onset coincident with DAN stimulation and the ISI for backward pairing was -1.2

seconds. These ISI were chosen as they induced the most robust bidirectional plasticity across preparations. In some explant preparations in Figures 3.4A-B, each mushroom body was treated as an independent sample. Each data point in Figures 3.3A-B, 3.4A-B, 5.1B-C, 6.1, 6.2A represents plasticity evoked by a single conditioning trial within an independent sample. To examine the time course of plasticity decay and to confirm the reversible nature of plasticity in the brain explant preparation we also performed sequential forward and backward pairing within the same preparation (Figure 3.2). Prior to and after forward and backward pairing in Figure 3.2, γ4 MBON responses to each individual KC stimulation were plotted to assess decay over time. To examine deficits in γ4 MBON plasticity in dopamine receptor mutants (Figure 6.1) wild type and receptor mutant preparations were interleaved. The GCaMP responses of the γ4 MBON in DopR2 mutants exhibited higher fluctuations than typically observed in wild type animals but these were averaged out across experiments and did not obscure baseline KC-evoked responses. The time between a conditioning trial and the first post-conditioning trial was at least 20 seconds.

KC modulation From Backward Pairing

Analysis of KC-evoked calcium or acetylcholine responses in the KC axons traversing the γ4/γ5 compartments following conditioning (Figures 5.3D and 6.2B) same as described above for MBON analysis.

Imaging of fluorescent reporters in KC and DAN axons (Figure 5.3, 5.5, 5.6, 5.7, 5.8)

To quantify ER calcium release in KC axons (OK107-Gal4 > UAS-ER-GCaMP) during conditioning, we averaged the response for 1 second post KC activation to account for the rapid kinetics of this signal, the fact that ER calcium release was time-locked to KC stimulation, and

its relatively low signal to noise (Figure 5.6E). ER-GCaMP fluorescence was normalized by the mean intensity for 2-4 seconds prior to KC stimulation.

The $GRAB_{DA1m}$ sensor was expressed in KC axons using the cell-type specific OK107-Gal4. TH,DDC-Gal4 driver was used to express VMAT-pHluorin in DANs and the 58E02-LexA driver was used to express GCaMP6s in the γ4/γ5 DANs . VMAT-pHluorin, $GRAB_{DA1m}$, and TH,DDC traces exhibited a higher signal enabling us to use the peak response evoked in the γ4/γ5 compartments during conditioning. VMAT-pHluorin, $GRAB_{DA1m}$, and GCaMP6s responses were normalized by the mean intensity for 2-4 seconds prior to stimulation.

Ratiometric imaging of the FRET-based cAMP sensor, EPAC, was performed, in the γ4/γ5 KC axon segments (OK107-Gal4 > UAS-EPAC) during conditioning). A Semrock filter set (#FF506-Di03-25x36, #FF01-483/32-25, #FF01-534/30-25) was used to spectrally separate and monitor CFP and YFP emission and responses were imaged at 850 nm. The CFP/YFP ratio was measured for each frame with an increase in this ratio corresponding to increased cAMP levels. To measure cAMP evoked during conditioning, we averaged the CFP/YFP ratio for the 4 seconds post DAN activation normalized to the CFP/YFP ratio in the 2-4 seconds prior to stimulation to account for the slow kinetics of this signal and the fact that cAMP was produced under all conditions and in response to direct DAN activation (Figure 5.6D).

In Figures 5.6A-C, evoked levels of dopamine release ($GRAB_{DA1m}$), cAMP (EPAC), and ER calcium release (ER-GCaMP) in the KC axons (OK107) in the proximal γ2/γ3 compartments and the PAM innervated γ4/γ5 compartments during conditioning were measured as described above

and compared to assess local production of second messengers along KC axons. For this comparison aggregated cAMP and ER calcium data from wild type animals in Figures 5.5A-B, 5.7C, and 5.8A, and the data of dopamine levels in KCs from Figure 5.3C were re-analyzed to compare fluorescent responses across the distal (γ2/γ3) and proximal (γ4/γ5) compartments of gamma lobe structure. Compartmental bounds were determined anatomically. All pairing conditions were tested in each brain preparation, and the order of pairing conditions tested was varied across experimental preparations.

YM-254890 (Gαq inhibitor) with ER-calcium in KC axons and γ4-MBON

The Gαq inhibitor, YM-254890 (Wako Chemicals #257-00631), was applied (10μM in DMSO) to the saline bathing an explant preparations. Control experiments using saline with equivalent amounts of DMSO were interleaved with drug treatments to test the effect of YM-254890.

Behavioral analysis in laminar flow chambers

Chamber construction

Fly chamber component pieces were cut from acrylic sheets using a laser cutter. The lid and base of each chamber were cut from transparent acrylic (Clear Cast Acrylic Sheet, 12" x 24" x 1/16", McMaster Carr). Two holes on opposite sides of the lid were tapped for 10-32 threaded Luer lock connectors. A single hole was cut in the base to allow flies to be loaded and unloaded. A spacer was cut from a 3-mm black scratch-resistant acrylic sheet (McMaster-Carr) with a central empty chamber (20 mm x 50 mm) flanked by two manifolds. Narrow channels were etched between the manifolds and central chamber using a low-power setting of the laser cutter. This permitted airflow between the chamber and the manifolds while confining flies within the

chamber. The dimensions of the inside chamber were 20 mm x 50 mm x 3 mm. The base, spacer, and lid were glued together using acrylic solvent and the edges of the chamber were further sealed with epoxy (Devcon 5 Minute® Epoxy) to make them airtight. 10-32 Luer connectors were screwed into the top of the chamber and sealed around the edges with epoxy.

Behavioral set-up

Flies in chambers were assayed in a custom-built training and testing rig. Chambers were placed on a 3-mm thick white acrylic sheet suspended on aluminum posts above a 3 x 4 array of 627 nm LEDs (Luxeon Rebel). LEDs were attached to metal heat sinks (Mouser #532-374624B32G), which were secured at 5 cm intervals to a 30 x 30 cm aluminum wire cloth sheet (McMaster-Carr #9227T53). LEDs were driven by Recom Power RCD-24-0.70/W/X2 drivers, which were powered by a variable DC power supply. Infrared LED strips (940 nm, LED Lights World) attached to the wire cloth between the heat sinks provided back-illumination of the platform. A Firefly camera (Point Grey) was mounted in a central hole within an acrylic lid suspended 30 cm above the platform on aluminum posts. Flies were recorded at 30 frames/second. Odor presentation and airflow were controlled using 3-way micro solenoid valves. A vacuum line was used to draw air into each chamber at a rate of 0.75-1.25 L/min/chamber. Two valves were used to control the direction of airflow, and additional valves were used to switch between clean air and different odors. Valves were powered by a 12 V DC power supply and switched on and off using VO14642AT solid state relays. Chamber design and valve system shown in Figure 2.1A. Valve relays and LED drivers were controlled by the output pins of an Arduino running custom software. Custom software written in C was used for data acquisition and instrument control

during individual trials of odor/light presentation. Python scripts were used to execute sequences of trials.

Odor presentation

Odorants were placed in glass bottles with lids containing two luer connectors. One connector was attached to an odor inlet valve and the other was left open to allow room air to enter the bottle. By default, air entered the apparatus through a bottle containing distilled water. To deliver odor pulses, the solenoid valve to the water bottle was closed while simultaneously opening the valve to an odor bottle. The valves were then switched back to their resting position after the specified odor presentation interval (Figure 2.1A).

For each baseline, post-forward pairing, and post-backward pairing trial, animals experienced two odor presentations for each odor tested—one presentation originating from the top of the chamber and the second presentation originating from the bottom. The air-flow direction across the chamber was switched 19 seconds prior to odor onset and 20.6 seconds after odor offset. The mean upwind displacement for the group of flies for the two odor presentations originating from the top and bottom of the chamber was used to assess odor-tracking behavior for each trial. This was done to control for any variability in air/odor flow between the two chamber sides. All training trials lasted 11.6 seconds except for training trials in Figure 3.1, which lasted 20 seconds to accommodate the longer inter-stimulus intervals between LED and odor presentation. Testing trials began 60 seconds after a training trial.

Apple cider vinegar (Heinz) was used for testing and training for experiments in Figures 2.1B,

2.2, 2.3, 2.4, 2.5, 2.6, 3.1, 6.3, 6.4, 6.5. The two odorants used in Figures 4.1 and 4.2A-C to test for odor-specific behavioral modulation were isobutyl acetate (Odor1) and 4-methylcyclohexanol, cis+trans (Odor2); the two odors used in Figure 4.2D-E were benzaldehyde (Odor1) and 1-hexanol (Odor2). All monomolecular odors were diluted to a final concentration of 1:1000 in heavy mineral oil. All odor presentations were 2 seconds in duration.

Optogenetic activation of DANs

PPL and PAM DANs expressing the light sensitive ion channel, CsChrimson, were activated using 1-second illumination with 627 nm LEDs. Split-Gal4s were used to drive CsChrimson in either the PAM cluster (MB042B) or PPL cluster (MB504B) DANs. The intensity of light within each chamber during LED illumination was roughly 18-40 $\mu W/mm^2$.

Associative conditioning

4-7 flies were loaded into each chamber through the bottom port using a mouth pipette, and the bottom port was sealed with a piece of transparent Scotch tape (exact number of flies used per experiment referenced in table below). Chambers were aligned in an acrylic frame on the imaging platform and connected in parallel to air inlets using Tygon tubing.

To examine the effect of a single forward pairing (FP) conditioning trial on ACV tracking behavior (Figure 2.2D), PPL > Chrimson animals experienced multiple baseline trials followed by a single forward pairing trial in which apple cider vinegar (ACV) was presented for 2 s, and LED illumination was provided during the final second of odor presentation. Animals then experienced 15 odor test trials to assess the time course of memory decay. To assess the ability

of backward pairing (BP) to reverse a negative association following forward pairing (Figure 2.2E), PPL > Chrimson animals were conditioned as described above, however, after a single odor test trial, animals were conditioned by backward pairing in which a 1-s pulse of LED illumination preceded ACV presentation by 2 seconds. Animals then experienced 14 odor trials post-BP to examine the decay in the memory formed by BP. To examine the effect of a single BP trial to alter ACV tracking in nominally naïve PAM > CsChrimson, the upwind displacement in a single baseline odor trial was compared to the displacement in the first test odor trial immediately following a single BP conditioning in which a 1-second pulse of LED illumination was provided to activate PAM DANs two seconds prior to ACV presentation (Figure 2.4D).

For experiments comparing the effect of interleaving FP and BP on ACV tracking behavior (Figures 2.2B-C, 2.3, 2.4B-C, 2.5B-J, 2.6C, 6.3, and 6.4), 25 training trials of FP and 25 trials of BP were interleaved with test trials in between each training trial. The timing of FP and BP are described above. To assess whether odor re-exposure or DAN re-activation alone (Figures 2.6A-C) could erode forward pairing associations to the same extent as backward pairing, 25 forward pairing trials were interleaved with 25 trials with the same timing as backward pairing but with either the odor or DAN stimulation omitted.

To examine the relationship between ISI and behavioral modulation in ACV tracking behavior (Figures 3.1A-B), five different ISIs were tested. In each experiment, 10 trainings of each of the five ISIs were tested in a random order over the course of an experiment, again with test trials in between each training trial. The randomization of ISI tested was used to account for any dependence on the trial structure.

To examine how a single reinforcement can instruct multiple odor-specific associations (Figures Figures 4.1A-D and 4.2A-E), we trained flies with two monomolecular odorants which were sequentially presented in each baseline, post-FP, and post-BP trial. During the conditioning trials, each odorant was presented for 2 s with a 1 s inter-stimulus interval of clean air. PAM > Chrimson activation began 1 s after the start of the first odor presentation and 2 s prior to the presentation of the second odor. Experiments consisted of 25 training trials in which odor 1 was forward paired and odor 2 was backward paired and 25 training trials in which odor 2 was forward paired and odor 1 was backward paired.

To compare baseline locomotor parameters and odor tracking behavior in nominally naïve wild type and dopamine receptor mutant PAM > Chrimson animals (Figure 6.5B-O), responses to ACV were measured over 9 odor trials, with each odor trial consisting of one odor presentation originating from the top of the chamber and one originating from the bottom as described above. Various behavioral metrics of wild type, DopR1$^{-/-}$, and DopR2$^{-/-}$ animals prior to and during the odor were compared across genotypes. Analysis of behavioral metrics described below.

All experiments were performed in the dark. Chambers were cleaned at the beginning or end of each experimental day by using a syringe to flush them thoroughly with water followed by 70% ethanol. Chambers were air-dried by connecting them to a vacuum line. Chambers were not cleaned between experiments within the same day; no difference in behavior was observed across subsequent experiments within the same day testing the same conditioning paradigm. In addition, time of day had no observable effect on conditioning. Genotype assignments to

different chambers were varied across experiments to avoid bias due to variability in chamber construction or position within the apparatus. Different genotypes were tested in parallel in all experiments. Behavioral responses to ACV were often variable in the first 1-2 baseline trials and were discarded from analysis to assure a stable readout of nominally naïve attraction.

Tracking of fly trajectories and behavioral analysis (Figure 2.2B, 2.5B-J, 6.5B-O)

The trajectories of individual flies were tracked across trials to examine how behavioral metrics were altered as a result conditioning (Figure 2.5B-J), or to compare locomotor characteristics of wild type, DopR1$^{-/-}$, and DopR2$^{-/-}$ animals (Figure 6.5B-O) by capturing movies of flies throughout the trial. A background image was generated by taking the maximum value of each pixel over the entire movie. To account for fluctuations in illumination intensity, this background image was rescaled frame-by-frame by the average pixel intensity. After subtracting the rescaled background, the image was bandpass-filtered, and flies were detected with a local maximum-finding algorithm (derived from the function pkfnd.m, which can be found at http://site.physics.georgetown.edu/matlab/code.html). Centroid positions of flies were then calculated from the original background-subtracted image using the function cntrd.m (http://site.physics.georgetown.edu/matlab/code.html). Fly localizations from individual frames were combined into multi-frame tracks using the function track.m (http://site.physics.georgetown.edu/matlab/code.html). The Y-axis and X-axis were defined as the axes parallel or perpendicular to the air/odor stream, respectively. For Figures 2.5B-J and 6.5B-O, X and Y speeds were defined as the absolute values of the velocity components in the X and Y directions. To examine Y-speed exclusively in moving animals a threshold of < 1 pixel/s (0.3 mm/s) was used. The fraction of stationary flies was defined as the proportion of animals

moving < 0.3 mm/s; the fraction of animals walking sideways was defined as the proportion of flies moving > 0.3 mm/s and within +/- 45 degrees of the X-axis; and the fractions of animals walking upwind or downwind were defined as the proportions of animals moving > 0.3 mm/s and within +/- 45 degrees of the positive or negative Y-axis, respectively.

Center of mass tracking (Figures 2.2C-E, 2.3A-D, 2.4B-D, 2.6A-C, 3.1A-B, 4.1A-D, 4.2A-E, 6.3A-D, 6.4A-D)

To measure the aggregate behavior of groups of flies, background subtraction was performed as above, and background noise was further suppressed by setting to zero all pixels below an empirically-determined threshold. The same threshold was applied to all chambers in each experiment, and the output of the analysis was not sensitive to the exact choice of threshold. The centroid position of all flies was then calculated for each background-subtracted frame. Upwind center-of-mass velocities were smoothed using a 15-frame moving average across each testing trial. The upwind velocity raster plots for each trial show animal behavior over an 11-second time window with odor on between 4-6 seconds. Upwind displacement during odor presentation was defined as the difference in center-of-mass position along the airflow direction between time of odor onset and time of odor offset. Change in upwind displacement after conditioning was calculated by subtracting the upwind displacement in the trial immediately preceding the conditioning trial from the upwind displacement in the trial immediately following the conditioning trial. Positive changes in upwind displacement therefore indicate increased upwind odor tracking and negative changes indicate decreased upwind odor tracking. This was done for all conditioning trials across each experiment. The mean change in upwind displacement across all training trials of the same training paradigm in an experiment was used to compare behavioral

modulation across different conditioning paradigms and experiments. To compare upwind displacement after a single FP or BP conditioning trial (Figures 2.2D-E and 2.4D) the raw upwind displacement values in the center of mass of flies in odor trials immediately proceeding and following conditioning were compared to assess the effects of conditioning. In Figure 2.2D the upwind displacement in the first two odor trials following FP were compared to assess initial memory decay. For the receptor mutants (Figure 6.3D and 6.4D), the raw upwind displacement values in the center of mass of flies post-FP and post-BP were compared between wild type and receptor mutant animals.

Figure	**Genotype**	**Chambers (N)**	**Total flies**
2.4B-C	PAM (MB042B) > CsCh	8	48
2.2B-C and 2.3A-C	PPL (MB504B) > CsCh	8	48
2.2D	PPL (MB504B) > CsCh	11	66
2.2E	PPL (MB504B) > CsCh	11	66
2.3C-D	CsCh	8	48
2.4D	PAM (MB042B) > CsCh	8	44
2.6C	PAM (MB042B) > CsCh (FP-BP experiment)	7	43
2.6C	PPL (MB504B) > CsCh (FP-BP experiment)	7	42
2.6A and C	PAM (MB042B) > CsCh (FP-Odor Alone)	7	42
2.6A and C	PPL (MB504B) > CsCh (FP-Odor Alone)	8	48
2.6B-C	PAM (MB042B) > CsCh (FP-DAN Alone)	8	48
2.6B-C	PPL (MB504B) > CsCh (FP-DAN Alone)	8	48
3.1A-B	PAM (MB042B) > CsCh	6	34
3.1A-B	PPL (MB504B) > CsCh	6	34
3.1A	CsCh	7	38
4.1B-D	PAM (MB042B) > CsCh	8	48
4.2B-C	CsCh	7	42
4.2D	PAM (MB042B) > CsCh	11	55
4.2E	CsCh	9	45
6.3A-D	PAM (MB042B) > CsCh (controls for DopR1$^{-/-}$)	7	42
6.3A-D	PAM (MB042B) > CsCh, DopR1$^{-/-}$	7	42

6.4A-D	PAM (MB042B) > CsCh (controls for DopR2$^{-/-}$)	7	37
6.4A-D	PAM (MB042B) > CsCh, DopR2$^{-/-}$	7	42
6.5B-O	PAM (MB042B) > CsCh	4	20
6.5B-O	PAM (MB042B) > CsCh, DopR1$^{-/-}$	4	20
6.5B-O	PAM (MB042B) > CsCh, DopR2$^{-/-}$	4	20

Conditioning of odor responses in tethered flies (Figure 4.3 and 3.3C)

Tethered flies were stimulated with odor by directing a continuous stream (400 mL/min) of clean air through a 2 mm diameter teflon tube directed at the fly's antenna (carrier stream). 5% of the total airstream was diverted through the headspace of either an empty or odor filled 10 mL glass vial (odor stream). At a trigger, a custom-built solenoid valve controller system redirected the odor stream from the empty vial to the vial containing various odorants diluted 1:10 in heavy mineral oil (Sigma). The odorants used in Figure 4.3B were isobutylacetate (odor 1) and cis+trans 4-methylcyclohexanol (odor 2). The odorants used in Figure 4.3C were 1-hexanol and benzaldehyde. For half of the experiments in Figure 4.3C, 1-hexanol was odor 1 and benzaldehyde was odor 2; for the other half of experiments the odor identities were reversed. Each odor presentation was 2 s in duration. Each odor was presented 2-4 times during baseline and post-pairing trials and the responses in γ4 MBON for each odor were averaged. Odor-evoked responses in the γ4 MBON were normalized by the mean fluorescence for 10 s prior to odor presentation. In Figures 3F and S3E-F, 58E02 DANs expressing the $P2X_2$ channel were activated as described above. During conditioning trials, the two odors were each presented for 2 s. DANs were stimulated using four 100-ms pulses at 5V with an inter-pulse interval of 20 ms. The DAN stimulation started 1.5 s after the start of the first odor presentation and 1.7 s prior to the presentation of the second odor. To compare the odor-specific modulation in the γ4 MBON

across the odor pairs (Figure 4.3D), the average response for each odor prior to a conditioning paradigm was subtracted from the mean peak response for each odor immediately post pairing; the change in evoked responses for odor 1 and odor 2 following conditioning were compared. Odor-evoked responses were determined by taking the peak fluorescence during the 2-s odor presentation. The same type of experiment was done in Figure 3.3C except one odor remained unpaired throughout the duration of the experiment to look at non-specific changes in odor responses in the γ4 MBON.

Odor and shock stimulation in tethered flies (Figure 3.5)

Animals were tethered to a holder as above (Green et al., 2017) but modified to include a polypropylene luer with a 2 mm opening directed at the antenna of the fly for odor delivery. Odor stimulation was performed as described above, however, in these experiments 40% of the total airstream was diverted through the headspace of an empty or pure ACV filled 10 mL glass vial to ensure consistent responses in the γ2 MBON. ACV was presented twice to each fly in baseline, post-FP, and post-BP trials and averaged as described above. If the γ2 MBONs in both hemispheres were visible in the same imaging plane, odor-evoked responses from both output neurons were averaged together. After positioning the fly under the microscope, two copper washers were precisely placed under visual control to make contact with either side of the fly's abdomen. Electrical leads from the two washers were connected to a stimulator (Grass Technologies), which was used to apply two 1 s shocks of 70 V that were separated in time by a 200 ms delay. In forward pairing trials, odor onset preceded shock onset by 500 ms. In backward pairing trials, the onset of shock preceded odor onset by 3 s.

Behavioral and functional imaging in closed-loop system (Figures 3.6, 3.7, and 3.8)

Closed-loop arena

An air-supported foam ball (~6.5 mm diameter, Matsubara Sangyo Co.), modified based on (Green et al., 2017; Seelig and Jayaraman, 2015) and positioned within the fly's grasp to allow the fly to 'walk' on the ball during imaging. On the rare occasion an animal could not maintain control of the ball because of placement on the ball, the trial was discarded and the fly repositioned for further analysis. The ball was recorded at 60-61 fps using a Point Grey Firefly Camera with Infinity Lens (94 mm focal length) focused on the ball, which was illuminated by infrared LED lights. Ball rotation was calculated in real time using FicTrac software running on Ubuntu 12.04 on computers with processors with speeds of at least 3GHz. The heading of the fly, as calculated by FicTrac, was transmitted to an Arduino Mega via serial port. Custom Arduino code was used to translate heading into tube position controlled by motors described below.

The closed loop air-delivery system was custom designed using OnShape (www.onshape.com) and 3D printed using Visijet Crystal material at XHD resolution in a 3DSystems Projet 3510 HD Plus. O-ring OD and ID Gland surfaces were designed with excess material for printing then manually modified on a lathe for improved RMS [surface] finishing. Tube rotation over 360 degrees was driven by a bipolar stepper motor (Pololu item #1206) controlled through a A4988 Stepper Motor Driver Carrier (Pololu #2980) coupled by a Dust-Free Timing Belt XL Series, 1/4" Width (McMaster-Carr, 1679K121, Trade No. 130xL025) to the rotating tube system,

which rotated mounted on an Ultra-Corrosion-Resistant Stainless Steel Ball Bearing (3/4" Shaft Diameter, 1-5/8" OD, Mcmaster-Carr 5908K19). Air channel was kept airtight using oil resistant o-rings (1/16 Fractional Width, Dash Number 020, Mcmaster-Carr 2418T126). Motor rotation was measured by a rotary encoder (CUI Inc., AMT10 Series) that was used in order to correct for skipped steps. Preliminary experiments in Figure 3.6C where carried out not under the 2-photon microscope. Animals were repeatedly trained with interleaving trials of forward and backward pairing to test for bidirectional modulation in tracking. Ideal training conditions were determined off this data set and used in Figures 3.7 and 3.8.

Odor stimulation in walking flies in the closed loop system (Figures 3.7-3.8)

Odor stimulation was achieved by directing a continuous stream (400 mL/min) of clean air through a 2 mm diameter tube made of Visijet Crystal material directed at the fly's antenna. 20% of the total airstream was diverted through the headspace of a 500 mL glass bottle containing water. At a trigger, a custom-built solenoid valve controller system redirected the odor stream from the water bottle to a bottle containing pure ACV. A 10 s odor presentation was used to allow the fly time to respond to and track the odor. Shorter odor presentations led to less consistent tracking in naïve animals, potentially due to the need to compensate for the inertia of the ball. In baseline, post-forward pairing and post-backward pairing test trials, animals were presented with two 10 s ACV odor presentations separated by 30 s of clean air. The peak odor-evoked fluorescence in the γ4 MBON and the total upwind displacement in ACV for the two 10 s odor presentations were averaged together for baseline and test trial measurements. Odor responses in the γ4 MBON were normalized by the mean intensity for 10 s prior to the first odor presentation in each baseline and test trial. The odor-evoked responses in the γ4 MBON in both

hemispheres were averaged for analysis except in one preparation where the γ4 MBON was visible in only one hemisphere. Due to a small latency in image capture rate, a systematic delay was introduced in image sequences between baseline, post-forward pairing, and post-backward pairing test trials to properly align odor delivery with neural responses.

Conditioning of flies in the closed loop paradigm (Figures 3.7-3.8)

The split-Gal4 driver was used to drive expression of UAS-ChrimsonR.mCherry in the PAM cluster (MB042B). ChrimsonR.mCherry activation was performed by 1-second constant illumination of 565 nm (CoolLED, PE-100) light of roughly 150 $\mu W/mm^2$ intensity directed at the brain of the fly through the microscope objective. The LED was triggered from the two-photon Prairie View software.

Tethered animals expressing UAS-ChrimsonR.mCherry in PAM neurons and LexAOP-GCaMP6s in the γ4 MBON were placed on an air-supported foam ball under the two-photon microscope and allowed time to acclimate until consistent walking was initiated. Each fly then experienced 3-4 full training paradigms consisting of a baseline trial, a forward-paired conditioning trial (ACV was presented for 10 s with LED illumination during the last second), post-FP test trial, a backward-paired conditioning trial (DANs were activated for 1 s using LED illumination and then 1 s later a 10 s ACV presentation), and post-BP test trial. The delay between the end of a conditioning trial and start of a testing trial was 40 s.

The difference in upwind position from ACV onset and ACV offset was used to calculate the

upwind displacement of the fly in the 10-s ACV odor presentation. The upwind displacement in clean air was also measured for the ten seconds prior to each odor presentation to control for odor-independent modulation in behavior (Figure 3.8). If behavior-tracking was dropped by FicTrac at odor onset or offset, the behavioral analysis of upwind displacement for that odor presentation was excluded from the analysis. The change in upwind displacement after forward and backward pairing was measured by subtracting the mean upwind displacement in the odor trials preceding FP or BP from the odor trials immediately following FP or BP. Likewise, the change in the γ4 MBON response after forward and backward pairing was measured by subtracting GCaMP response of odor trials preceding FP or BP from the odor trials immediately following FP or BP. A 500 ms delay was used for determining upwind displacement and peak neural response to the odor to account for lag in odor delivery to the antennae of the animal based on neural responses. The behavioral and neural modulation was plotted for each of the 3-4 training paradigms per animal to examine trial-to-trial variability (Figures 3.7D, G, H-gray dots and 3.8D); in addition, the mean of the 3-4 training session per animal were analyzed to look at animal-to-animal variability (Figures 3.7B-C, E, F, H-black dots and 3.8C).

Immunohistochemistry

Day 1 adult brains were dissected in Schneider's media (Sigma) then immediately transferred to cold 1% PFA (Electron Microscopy Sciences) and fixed overnight at 4°C. Following overnight incubation samples were washed in PAT3 Buffer (0.5% BSA/0.5% Triton/1X PBS pH 7.4) 3 times. Brains were blocked in 3% Normal Goat Serum for 90 minutes at RT. Primary antibodies 1:2000 rabbit anti-DAMB (Figure 5.7B) (a gift from Ron Davis) (Feng et al., 1996), 1:20 guinea pig anti-DopR (Figure 5.7B) (Lebestky et al., 2009), 1:1000 chicken anti-GFP (Abcam ab13970)

(Figures 2.2A and 2.4A) and 1:50 mouse anti-brp (Developmental Studies Hybridoma Bank nc82) (Figures 2.2A and 2.4A) were incubated 3 hours at RT then 2-3 days at 4°C. Brains were washed extensively in PAT3 Buffer. Secondary Alexa Fluor antibodies (Life Technologies) were incubated 3 hours at RT then 2-3 days at 4°C. Brains were washed 3 times in PAT3 Buffer then once in 1X PBS. Samples were mounted in Vectashield (Vector Laboratories). Images were captured on a Zeiss LSM 880 using a Plan-Apochromat 20X (0.8 NA) objective.

RNA Isolation and qRT-PCR (Figure 5.7B)

Total RNA was isolated from the dissected brains of eight 1-day-old adult wild type and DopR1$^{-/-}$ females. RNA was extracted using Qiazol reagent (QIAGEN) then column purified by RNeasy micro kit (QIAGEN). cDNA was generated using Quantitect Reverse Transcriptase kit (QIAGEN). Taqman real-time qPCR experiments were performed on a QuantStudio 12K Flex Real-Time PCR System (Thermo Fisher Scientific) following the manufacturer's instructions. Data were analyzed using the comparative $2\Delta\Delta Ct$ method using alphaTub84B as an endogenous control. The average fold-change relative to wild type was calculated. The following Taqman assays from Life Technologies were used: *alphaTub84B* (Dm02361072_s1) and *DopR1* (Dm02134814_m1).

Statistical analysis

Statistical analysis was performed using Prism and MATLAB with Bonferroni correction to p values when multiple comparisons were performed. The Shapiro-Wilk normality test was used to assess normality across all individual experiments. If the null hypothesis was rejected, Wilcoxon match-pairs signed rank or Mann-Whitney tests were used to compare for differences between

two groups; otherwise, paired or unpaired t-tests were used. All tests were two-tailed. Ordinary one-way ANOVA was used to test for differences across the three genotypes of wild type, DopR1$^{-/-}$, and DopR2$^{-/-}$ in locomotor parameters and odor tracking behavior. An RM one-way ANOVA was used to test for differences in DAN activation, VMAT release, and extracellular dopamine levels between FP, BP, and DAN activation alone. One-sample t-tests or Wilcoxon signed rank tests against zero were used to assess the significance of changes in KC- or odor-evoked responses in the γ2, γ4, and γ5 MBONs, behavioral modulation after conditioning trials, and changes in cAMP and ER-calcium levels in KC axons during conditioning. Spearman's rank correlation was used to measure the correlation between changes in upwind displacement in odor and the change in odor-evoked calcium responses in the γ4 MBON across individual trials or averages for each animal. Exact statistical test used referenced in each figure legend.

References

Abrams, T.W., Karl, K.A., and Kandel, E.R. (1991). Biochemical studies of stimulus convergence during classical conditioning in Aplysia: dual regulation of adenylate cyclase by Ca2+/calmodulin and transmitter. Journal of Neuroscience *11*, 2655–2665.

Adkins, C.E., and Taylor, C.W. (1999). Lateral inhibition of inositol 1,4,5-trisphosphate receptors by cytosolic Ca(2+). Current Biology *9*, 1115–1118.

Álvarez-Salvado, E., Licata, A.M., Connor, E.G., McHugh, M.K., King, B.M., Stavropoulos, N., Victor, J.D., Crimaldi, J.P., and Nagel, K.I. (2018). Elementary sensory-motor transformations underlying olfactory navigation in walking fruit-flies. eLife *7*, e04577.

Andreatta, M., Fendt, M., Mühlberger, A., Wieser, M.J., Imobersteg, S., Yarali, A., Gerber, B., and Pauli, P. (2012). Onset and offset of aversive events establish distinct memories requiring fear and reward networks. Learn. Mem. *19*, 518–526.

Andreatta, M., Mühlberger, A., and Pauli, P. (2015). When does pleasure start after the end of pain? The time course of relief. J. Comp. Neurol. *524*, 1653–1667.

Andreatta, M., Mühlberger, A., Glotzbach-Schoon, E., and Pauli, P. (2013). Pain predictability reverses valence ratings of a relief-associated stimulus. Front Syst Neurosci *7*, 53.

Arbuthnott, G.W., and Wickens, J. (2007). Space, time and dopamine. Trends Neurosci. *30*, 62–69.

Aso, Y., and Rubin, G.M. (2016). Dopaminergic neurons write and update memories with cell-type-specific rules. eLife *5*, 156.

Aso, Y., Hattori, D., Yu, Y., Johnston, R.M., Iyer, N.A., Ngo, T.-T.B., Dionne, H., Abbott, L.F., Axel, R., Tanimoto, H., et al. (2014a). The neuronal architecture of the mushroom body provides a logic for associative learning. eLife *3*, e04577.

Aso, Y., Herb, A., Ogueta, M., Siwanowicz, I., Templier, T., Friedrich, A.B., Ito, K., Scholz, H., and Tanimoto, H. (2012). Three dopamine pathways induce aversive odor memories with different stability. PLoS Genet. *8*, e1002768.

Aso, Y., Sitaraman, D., Ichinose, T., Kaun, K.R., Vogt, K., Belliart-Guérin, G., Plaçais, P.-Y., Robie, A.A., Yamagata, N., Schnaitmann, C., et al. (2014b). Mushroom body output neurons encode valence and guide memory-based action selection in Drosophila. eLife *3*, e04580.

Aso, Y., Siwanowicz, I., Bräcker, L., Ito, K., Kitamoto, T., and Tanimoto, H. (2010). Specific dopaminergic neurons for the formation of labile aversive memory. Curr. Biol. *20*, 1445–1451.

Auchter, A., Cormack, L.K., Niv, Y., Gonzalez-Lima, F., and Monfils, M.H. (2017). Reconsolidation-Extinction Interactions in Fear Memory Attenuation: The Role of Inter-Trial

Interval Variability. Front Behav Neurosci *11*, 2.

Azevedo, F.A.C., Carvalho, L.R.B., Grinberg, L.T., Farfel, J.M., Ferretti, R.E.L., Leite, R.E.P., Jacob Filho, W., Lent, R., and Herculano-Houzel, S. (2009). Equal numbers of neuronal and nonneuronal cells make the human brain an isometrically scaled-up primate brain. J. Comp. Neurol. *513*, 532–541.

Bargmann, C.I. (2012). Beyond the connectome: How neuromodulators shape neural circuits. Bioessays *34*, 458–465.

Basu, J., Srinivas, K.V., Cheung, S.K., Taniguchi, H., Huang, Z.J., and Siegelbaum, S.A. (2013). A cortico-hippocampal learning rule shapes inhibitory microcircuit activity to enhance hippocampal information flow. Neuron *79*, 1208–1221.

Bauer, E.P., Schafe, G.E., and LeDoux, J.E. (2002). NMDA receptors and L-type voltage-gated calcium channels contribute to long-term potentiation and different components of fear memory formation in the lateral amygdala. J. Neurosci. *22*, 5239–5249.

Baxter, D.A., and Byrne, J.H. (2006). Feeding behavior of Aplysia: a model system for comparing cellular mechanisms of classical and operant conditioning. Learn. Mem. *13*, 669–680.

Bayer, H.M., and Glimcher, P.W. (2005). Midbrain Dopamine Neurons Encode a Quantitative Reward Prediction Error Signal. Neuron *47*, 129–141.

Beaulieu, J.-M., and Gainetdinov, R.R. (2011). The physiology, signaling, and pharmacology of dopamine receptors. Pharmacol. Rev. *63*, 182–217.

Bell, C.C., Han, V.Z., Sugawara, Y., and Grant, K. (1997). Synaptic plasticity in a cerebellum-like structure depends on temporal order. Nature *387*, 278–281.

Bergado Acosta, J.R., Kahl, E., Kogias, G., Uzuneser, T.C., and Fendt, M. (2017). Relief learning requires a coincident activation of dopamine D1 and NMDA receptors within the nucleus accumbens. Neuropharmacology *114*, 58–66.

Berman, D.E., and Dudai, Y. (2001). Memory extinction, learning anew, and learning the new: dissociations in the molecular machinery of learning in cortex. Science *291*, 2417–2419.

Berridge, M.J. (1993). Inositol trisphosphate and calcium signalling. Nature *361*, 315–325.

Berry, J.A., Cervantes-Sandoval, I., Chakraborty, M., and Davis, R.L. (2015). Sleep Facilitates Memory by Blocking Dopamine Neuron-Mediated Forgetting. Cell *161*, 1656–1667.

Berry, J.A., Cervantes-Sandoval, I., Nicholas, E.P., and Davis, R.L. (2012). Dopamine is required for learning and forgetting in Drosophila. Neuron *74*, 530–542.

Berry, J.A., Phan, A., and Davis, R.L. (2018). Dopamine Neurons Mediate Learning and Forgetting through Bidirectional Modulation of a Memory Trace. CellReports *25*, 651–662.e655.

Bi, G.-Q., and Rubin, J. (2005). Timing in synaptic plasticity: from detection to integration. Trends Neurosci. *28*, 222–228.

Bittner, K.C., Milstein, A.D., Grienberger, C., Romani, S., and Magee, J.C. (2017). Behavioral time scale synaptic plasticity underlies CA1 place fields. Science *357*, 1033–1036.

Björklund, A., and Dunnett, S.B. (2007). Dopamine neuron systems in the brain: an update. Trends Neurosci. *30*, 194–202.

Bliss, T.V.P., and Lømo, T. (1973). Long-lasting potentiation of synaptic transmission in the dentate area of the anaesthetized rabbit following stimulation of the perforant path. The Journal of Physiology *232*, 331–356.

Blum, A.L., Li, W., Cressy, M., and Dubnau, J. (2009). Short- and long-term memory in Drosophila require cAMP signaling in distinct neuron types. Curr. Biol. *19*, 1341–1350.

Boisseau, R.P., Vogel, D., and Dussutour, A. (2016). Habituation in non-neural organisms: evidence from slime moulds. Proc. Biol. Sci. *283*, 20160446.

Bolshakov, V.Y., and Siegelbaum, S.A. (1994). Postsynaptic induction and presynaptic expression of hippocampal long-term depression. Science *264*, 1148–1152.

Boto, T., Louis, T., Jindachomthong, K., Jalink, K., and Tomchik, S.M. (2014). Dopaminergic Modulation of cAMP Drives Nonlinear Plasticity across the Drosophila Mushroom Body Lobes. Current Biology *24*, 822–831.

Bourne, H.R., and Nicoll, R. (1993). Molecular machines integrate coincident synaptic signals. Cell *72 Suppl*, 65–75.

Bouton, M.E. (2002). Context, ambiguity, and unlearning: sources of relapse after behavioral extinction. Biol. Psychiatry *52*, 976–986.

Bouton, M.E. (2004). Context and behavioral processes in extinction. Learn. Mem. *11*, 485–494.

Boyden, E.S., Katoh, A., and Raymond, J.L. (2004). Cerebellum-dependent learning: the role of multiple plasticity mechanisms. Annu. Rev. Neurosci. *27*, 581–609.

Bromberg-Martin, E.S., Matsumoto, M., and Hikosaka, O. (2010). Dopamine in motivational control: rewarding, aversive, and alerting. Neuron *68*, 815–834.

Brunelli, M., Castellucci, V., and Kandel, E.R. (1976). Synaptic facilitation and behavioral sensitization in Aplysia: possible role of serotonin and cyclic AMP. Science *194*, 1178–1181.

Buhusi, C.V., Oprisan, S.A., and Buhusi, M. (2016). Clocks within Clocks: Timing by Coincidence Detection. Cobeha *8*, 207–213.

Burke, C.J., Huetteroth, W., Owald, D., Perisse, E., Krashes, M.J., Das, G., Gohl, D., Silies, M., Certel, S., and Waddell, S. (2012). Layered reward signalling through octopamine and dopamine

in Drosophila. Nature *492*, 433–437.

Cajal, S.R.Y. (1894). The Croonian Lecture: La Fine Structure des Centres Nerveux. Proceedings of the Royal Society of London *55*, 444–468.

Campbell, R.A.A., Honegger, K.S., Qin, H., Li, W., Demir, E., and Turner, G.C. (2013). Imaging a population code for odor identity in the Drosophila mushroom body. J. Neurosci. *33*, 10568–10581.

Cardé, R.T., and Willis, M.A. (2008). Navigational strategies used by insects to find distant, wind-borne sources of odor. J. Chem. Ecol. *34*, 854–866.

Carey, M., and Lisberger, S. (2002). Embarrassed, but not depressed: eye opening lessons for cerebellar learning. Neuron *35*, 223–226.

Caron, S.J.C., Ruta, V., Abbott, L.F., and Axel, R. (2013). Random convergence of olfactory inputs in the Drosophila mushroom body. Nature *497*, 113–117.

Cassenaer, S., and Laurent, G. (2012). Conditional modulation of spike-timing-dependent plasticity for olfactory learning. Nature *482*, 47–52.

Cervantes-Sandoval, I., Chakraborty, M., MacMullen, C., and Davis, R.L. (2016). Scribble Scaffolds a Signalosome for Active Forgetting. Neuron *90*, 1230–1242.

Cervantes-Sandoval, I., Martin-Peña, A., Berry, J.A., and Davis, R.L. (2013). System-like consolidation of olfactory memories in Drosophila. J. Neurosci. *33*, 9846–9854.

Cho, J.-H., Bayazitov, I.T., Meloni, E.G., Myers, K.M., Carlezon, W.A., Zakharenko, S.S., and Bolshakov, V.Y. (2011). Coactivation of thalamic and cortical pathways induces input timing-dependent plasticity in amygdala. Nat Neurosci *15*, 113–122.

Cisek, P., and Kalaska, J.F. (2010). Neural Mechanisms for Interacting with a World Full of Action Choices. Annu. Rev. Neurosci. *33*, 269–298.

Claridge-Chang, A., Roorda, R.D., Vrontou, E., Sjulson, L., Li, H., Hirsh, J., and Miesenböck, G. (2009). Writing memories with light-addressable reinforcement circuitry. Cell *139*, 405–415.

Coddington, L.T., and Dudman, J.T. (2018). The timing of action determines reward prediction signals in identified midbrain dopamine neurons. Nat Neurosci 1–15.

Coesmans, M., Weber, J.T., De Zeeuw, C.I., and Hansel, C. (2004). Bidirectional parallel fiber plasticity in the cerebellum under climbing fiber control. Neuron *44*, 691–700.

Cohen, J.Y., Haesler, S., Vong, L., Lowell, B.B., and Uchida, N. (2012). Neuron-type-specific signals for reward and punishment in the ventral tegmental area. Nature *482*, 85–88.

Cohn, R., Morantte, I., and Ruta, V. (2015). Coordinated and Compartmentalized Neuromodulation Shapes Sensory Processing in Drosophila. Cell *163*, 1742–1755.

Connolly, J.B., Roberts, I.J., Armstrong, J.D., Kaiser, K., Forte, M., Tully, T., and O'Kane, C.J. (1996). Associative learning disrupted by impaired Gs signaling in Drosophila mushroom bodies. Science *274*, 2104–2107.

Corbett, D., and Wise, R.A. (1980). Intracranial self-stimulation in relation to the ascending dopaminergic systems of the midbrain: a moveable electrode mapping study. Brain Res. *185*, 1–15.

Crittenden, J.R., Skoulakis, E.M., Han, K.A., Kalderon, D., and Davis, R.L. (1998). Tripartite mushroom body architecture revealed by antigenic markers. Learn. Mem. *5*, 38–51.

Crocker, A., Guan, X.-J., Murphy, C.T., and Murthy, M. (2016). Cell-Type-Specific Transcriptome Analysis in the Drosophila Mushroom Body Reveals Memory-Related Changes in Gene Expression. CellReports *15*, 1580–1596.

Croset, V., Treiber, C.D., and Waddell, S. (2018). Cellular diversity in the Drosophila midbrain revealed by single-cell transcriptomics. eLife *7*, 312.

D'Ardenne, K., McClure, S.M., Nystrom, L.E., and Cohen, J.D. (2008). BOLD responses reflecting dopaminergic signals in the human ventral tegmental area. Science *319*, 1264–1267.

da Silva, J.A., Tecuapetla, F., Paixão, V., and Costa, R.M. (2018). Dopamine neuron activity before action initiation gates and invigorates future movements. Nature *554*, 244–248.

Dan, Y., and Poo, M.-M. (2004). Spike timing-dependent plasticity of neural circuits. Neuron *44*, 23–30.

Davis, M., Antoniadis, E.A., Amaral, D.G., and Winslow, J.T. (2008). Acoustic startle reflex in rhesus monkeys: a review. Reviews in the Neurosciences *19*, 171–185.

Davis, R.L. (2011). Traces of Drosophila memory. Neuron *70*, 8–19.

Davis, R.L., and Zhong, Y. (2017). The Biology of Forgetting-A Perspective. Neuron *95*, 490–503.

de Belle, J.S., and Heisenberg, M. (1994). Associative odor learning in Drosophila abolished by chemical ablation of mushroom bodies. Science *263*, 692–695.

de Juan-Sanz, J., Holt, G.T., Schreiter, E.R., de Juan, F., Kim, D.S., and Ryan, T.A. (2017). Axonal Endoplasmic Reticulum Ca(2+) Content Controls Release Probability in CNS Nerve Terminals. Neuron *93*, 867–881.e6.

Dolan, M.-J., Belliart-Guérin, G., Bates, A.S., Frechter, S., Lampin-Saint-Amaux, A., Aso, Y., Roberts, R.J.V., Schlegel, P., Wong, A., Hammad, A., et al. (2018). Communication from Learned to Innate Olfactory Processing Centers Is Required for Memory Retrieval in Drosophila. Neuron *100*, 651–668.e658.

Dong, T., He, J., Wang, S., Wang, L., Cheng, Y., and Zhong, Y. (2016). Inability to activate

Rac1-dependent forgetting contributes to behavioral inflexibility in mutants of multiple autism-risk genes. Proc. Natl. Acad. Sci. U.S.a. *113*, 7644–7649.

Drew, P.J., and Abbott, L.F. (2006). Extending the effects of spike-timing-dependent plasticity to behavioral timescales. Proc. Natl. Acad. Sci. U.S.a. *103*, 8876–8881.

Dubnau, J., and Tully, T. (2001). Functional anatomy: from molecule to memory. Current Biology *11*, R240–R243.

Dudai, Y., Jan, Y.N., Byers, D., Quinn, W.G., and Benzer, S. (1976). dunce, a mutant of Drosophila deficient in learning. Proc. Natl. Acad. Sci. U.S.a. *73*, 1684–1688.

Dudai, Y. (2009). Predicting not to predict too much: how the cellular machinery of memory anticipates the uncertain future. Philos. Trans. R. Soc. Lond., B, Biol. Sci. *364*, 1255–1262.

Dujardin, F. (1850). Mémoire sur le système nerveux des insectes. Ann Sci Nat Zool 195–206.

Egea-Weiss, A., Renner, A., Kleineidam, C.J., and Szyszka, P. (2018). High Precision of Spike Timing across Olfactory Receptor Neurons Allows Rapid Odor Coding in Drosophila. iScience *4*, 76–83.

Engelhard, B., Finkelstein, J., Cox, J., Fleming, W., Jang, H.J., Ornelas, S., Koay, S.A., Thiberge, S., Daw, N., Tank, D., et al. (2018). Specialized and spatially organized coding of sensory, motor, and cognitive variables in midbrain dopamine neurons. bioRxiv 456194.

Eshel, N., Bukwich, M., Rao, V., Hemmelder, V., Tian, J., and Uchida, N. (2015). Arithmetic and local circuitry underlying dopamine prediction errors. Nature *525*, 243–246.

Farris, S.M. (2011). Are mushroom bodies cerebellum-like structures? Arthropod Struct Dev *40*, 368–379.

Felsenberg, J., Barnstedt, O., Cognigni, P., Lin, S., and Waddell, S. (2017). Re-evaluation of learned information in Drosophila. Nature *544*, 240–244.

Felsenberg, J., Jacob, P.F., Walker, T., Barnstedt, O., Edmondson-Stait, A.J., Pleijzier, M.W., Otto, N., Schlegel, P., Sharifi, N., Perisse, E., et al. (2018). Integration of Parallel Opposing Memories Underlies Memory Extinction. Cell *175*, 709–722.e715.

Felsenberg, J., Plath, J.A., Lorang, S., Morgenstern, L., and Eisenhardt, D. (2013). Short- and long-term memories formed upon backward conditioning in honeybees (Apis mellifera). Learn. Mem. *21*, 37–45.

Feng, G., Hannan, F., Reale, V., Hon, Y.Y., Kousky, C.T., Evans, P.D., and Hall, L.M. (1996). Cloning and functional characterization of a novel dopamine receptor from Drosophila melanogaster. Journal of Neuroscience *16*, 3925–3933.

Finch, E.A., and Augustine, G.J. (1998). Local calcium signalling by inositol-1,4,5-trisphosphate in Purkinje cell dendrites. Nature *396*, 753–756.

Flagel, S.B., Clark, J.J., Robinson, T.E., Mayo, L., Czuj, A., Willuhn, I., Akers, C.A., Clinton, S.M., Phillips, P.E.M., and Akil, H. (2011). A selective role for dopamine in stimulus-reward learning. Nature *469*, 53–57.

Flores-Hernandez, J., Hernandez, S., Snyder, G.L., Yan, Z., Fienberg, A.A., Moss, S.J., Greengard, P., and Surmeier, D.J. (2000). D(1) dopamine receptor activation reduces GABA(A) receptor currents in neostriatal neurons through a PKA/DARPP-32/PP1 signaling cascade. Journal of Neurophysiology *83*, 2996–3004.

Flores-Hernández, J., Cepeda, C., Hernández-Echeagaray, E., Calvert, C.R., Jokel, E.S., Fienberg, A.A., Greengard, P., and Levine, M.S. (2002). Dopamine enhancement of NMDA currents in dissociated medium-sized striatal neurons: role of D1 receptors and DARPP-32. Journal of Neurophysiology *88*, 3010–3020.

Floresco, S.B., West, A.R., Ash, B., Moore, H., and Grace, A.A. (2003). Afferent modulation of dopamine neuron firing differentially regulates tonic and phasic dopamine transmission. Nat Neurosci *6*, 968–973.

Freeman, J.H. (2015). Cerebellar learning mechanisms. Brain Res. *1621*, 260–269.

Freeman, J.H., and Steinmetz, A.B. (2011). Neural circuitry and plasticity mechanisms underlying delay eyeblink conditioning. Learn. Mem. *18*, 666–677.

Freeze, B.S., Kravitz, A.V., Hammack, N., Berke, J.D., and Kreitzer, A.C. (2013). Control of basal ganglia output by direct and indirect pathway projection neurons. J. Neurosci. *33*, 18531–18539.

Friggi-Grelin, F., Coulom, H., Meller, M., Gomez, D., Hirsh, J., and Birman, S. (2003). Targeted gene expression in Drosophila dopaminergic cells using regulatory sequences from tyrosine hydroxylase. J. Neurobiol. *54*, 618–627.

Gaudry, Q., Hong, E.J., Kain, J., de Bivort, B.L., and Wilson, R.I. (2012). Asymmetric neurotransmitter release enables rapid odour lateralization in Drosophila. Nature *493*, 424–428.

Gerber, B., Scherer, S., Neuser, K., Michels, B., Hendel, T., Stocker, R.F., and Heisenberg, M. (2004). Visual learning in individually assayed Drosophila larvae. J. Exp. Biol. *207*, 179–188.

Gerber, B., König, C., Fendt, M., Andreatta, M., Romanos, M., Pauli, P., and Yarali, A. (2019). Timing-dependent valence reversal: a principle of reinforcement processing and its possible implications. Current Opinion in Behavioral Sciences *26*, 114–120.

Gerber, B., Yarali, A., Diegelmann, S., Wotjak, C.T., Pauli, P., and Fendt, M. (2014). Pain-relief learning in flies, rats, and man: basic research and applied perspectives. Learn. Mem. *21*, 232–252.

Gerfen, C.R. (1992). The neostriatal mosaic: multiple levels of compartmental organization. J. Neural Transm. Suppl. *36*, 43–59.

Gerfen, C.R., Engber, T.M., Mahan, L.C., Susel, Z., Chase, T.N., Monsma, F.J., and Sibley, D.R. (1990). D1 and D2 dopamine receptor-regulated gene expression of striatonigral and striatopallidal neurons. Science *250*, 1429–1432.

Gerfen, C.R., and Surmeier, D.J. (2011). Modulation of striatal projection systems by dopamine. Annu. Rev. Neurosci. *34*, 441–466.

Gervasi, N., TchEnio, P., and Preat, T. (2010). PKA Dynamics in a Drosophila Learning Center: Coincidence Detection by Rutabaga Adenylyl Cyclase and Spatial Regulation by Dunce Phosphodiesterase. Neuron *65*, 516–529.

Gonon, F. (1997). Prolonged and extrasynaptic excitatory action of dopamine mediated by D1 receptors in the rat striatum in vivo. Journal of Neuroscience *17*, 5972–5978.

Goodwin, S.F., Del Vecchio, M., Velinzon, K., Hogel, C., Russell, S.R., Tully, T., and Kaiser, K. (1997). Defective learning in mutants of the Drosophila gene for a regulatory subunit of cAMP-dependent protein kinase. Journal of Neuroscience *17*, 8817–8827.

Gotzes, F., Balfanz, S., and Baumann, A. (1994). Primary structure and functional characterization of a Drosophila dopamine receptor with high homology to human D1/5 receptors. Recept. Channels *2*, 131–141.

Grace, A.A., Floresco, S.B., Goto, Y., and Lodge, D.J. (2007). Regulation of firing of dopaminergic neurons and control of goal-directed behaviors. Trends Neurosci. *30*, 220–227.

Green, J., Adachi, A., Shah, K.K., Hirokawa, J.D., Magani, P.S., and Maimon, G. (2017). A neural circuit architecture for angular integration in Drosophila. Nature *546*, 101–106.

Greengard, P. (2001). The neurobiology of slow synaptic transmission. Science *294*, 1024–1030.

Greengard, P., Allen, P.B., and Nairn, A.C. (1999). Beyond the dopamine receptor: the DARPP-32/protein phosphatase-1 cascade. Neuron *23*, 435–447.

Groschner, L.N., Chan Wah Hak, L., Bogacz, R., DasGupta, S., and Miesenböck, G. (2018). Dendritic Integration of Sensory Evidence in Perceptual Decision-Making. Cell *173*, 894–905.e13.

Gruntman, E., and Turner, G.C. (2013). Integration of the olfactory code across dendritic claws of single mushroom body neurons. Nat Neurosci *16*, 1821–1829.

Han, K.A., Millar, N.S., Grotewiel, M.S., and Davis, R.L. (1996). DAMB, a novel dopamine receptor expressed specifically in Drosophila mushroom bodies. Neuron *16*, 1127–1135.

Hebb, D.O. (1949). The Organization of Behavior (New York: Wiley & Sons).

Heisenberg, M., Borst, A., Wagner, S., and Byers, D. (1985). Drosophila mushroom body mutants are deficient in olfactory learning. J. Neurogenet. *2*, 1–30.

Heisenberg, M. (2003). Mushroom body memoir: from maps to models. Nat. Rev. Neurosci. *4*, 266–275.

Herculano-Houzel, S. (2009). The human brain in numbers: a linearly scaled-up primate brain. Front Hum Neurosci *3*, 31.

Heth, C.D., and Rescorla, R.A. (1973). Simultaneous and backward fear conditioning in the rat. J Comp Physiol Psychol *82*, 434–443.

Hige, T., Aso, Y., Modi, M.N., Rubin, G.M., and Turner, G.C. (2015). Heterosynaptic Plasticity Underlies Aversive Olfactory Learning in Drosophila. Neuron *88*, 985–998.

Higley, M.J., and Sabatini, B.L. (2010). Competitive regulation of synaptic Ca2+ influx by D2 dopamine and A2A adenosine receptors. Nat Neurosci *13*, 958–966.

Himmelreich, S., Masuho, I., Berry, J.A., MacMullen, C., Skamangas, N.K., Martemyanov, K.A., and Davis, R.L. (2017). Dopamine Receptor DAMB Signals via Gq to Mediate Forgetting in Drosophila. CellReports *21*, 2074–2081.

Hollerman, J.R., Tremblay, L., and Schultz, W. (1998). Influence of reward expectation on behavior-related neuronal activity in primate striatum. Journal of Neurophysiology *80*, 947–963.

Ichinose, T., Aso, Y., Yamagata, N., Abe, A., Rubin, G.M., and Tanimoto, H. (2015). Reward signal in a recurrent circuit drives appetitive long-term memory formation. eLife *4*, e10719.

Ito, M., and Kano, M. (1982). Long-lasting depression of parallel fiber-Purkinje cell transmission induced by conjunctive stimulation of parallel fibers and climbing fibers in the cerebellar cortex. Neuroscience Letters *33*, 253–258.

Ito, M., Sakurai, M., and Tongroach, P. (1982). Climbing fibre induced depression of both mossy fibre responsiveness and glutamate sensitivity of cerebellar Purkinje cells. The Journal of Physiology *324*, 113–134.

Izquierdo, A., Brigman, J.L., Radke, A.K., Rudebeck, P.H., and Holmes, A. (2017). The neural basis of reversal learning: An updated perspective. Neuroscience *345*, 12–26.

Jing, M., Zhang, P., Wang, G., Feng, J., Mesik, L., Zeng, J., Jiang, H., Wang, S., Looby, J.C., Guagliardo, N.A., et al. (2018). A genetically encoded fluorescent acetylcholine indicator for in vitro and in vivo studies. Nat. Biotechnol. *36*, 726–737.

Josselyn, S.A., Köhler, S., and Frankland, P.W. (2017). Heroes of the Engram. J. Neurosci. *37*, 4647–4657.

Jörntell, H., and Hansel, C. (2006). Synaptic Memories Upside Down: Bidirectional Plasticity at Cerebellar Parallel Fiber-Purkinje Cell Synapses. Neuron *52*, 227–238.

Kalish, H.I. (1954). Strength of fear as a function of the number of acquisition and extinction trials. J Exp Psychol *47*, 1–9.

Kandel, E.R., Abrams, T., Bernier, L., Carew, T.J., Hawkins, R.D., and Schwartz, J.H. (1983). Classical conditioning and sensitization share aspects of the same molecular cascade in Aplysia. Cold Spring Harb. Symp. Quant. Biol. *48 Pt 2*, 821–830.

Kandel, E.R., Brunelli, M., Byrne, J., and Castellucci, V. (1976). A common presynaptic locus for the synaptic changes underlying short-term habituation and sensitization of the gill-withdrawal reflex in Aplysia. Cold Spring Harb. Symp. Quant. Biol. *40*, 465–482.

Kandel, E.R., Schwartz, J.H., and Jessell, T.M. (2000). Principles of Neural Science (McGraw Hill).

Keene, A.C., and Waddell, S. (2007). Drosophila olfactory memory: single genes to complex neural circuits. Nat. Rev. Neurosci. *8*, 341–354.

Keleman, K., Vrontou, E., Krüttner, S., Yu, J.Y., Kurtovic-Kozaric, A., and Dickson, B.J. (2012). Dopamine neurons modulate pheromone responses in Drosophila courtship learning. Nature *489*, 145–149.

Kendall, J.M., Badminton, M.N., Dormer, R.L., and Campbell, A.K. (1994). Changes in free calcium in the endoplasmic reticulum of living cells detected using targeted aequorin. Anal. Biochem. *221*, 173–181.

Kheirbek, M.A., Beeler, J.A., Ishikawa, Y., and Zhuang, X. (2008). A cAMP pathway underlying reward prediction in associative learning. J. Neurosci. *28*, 11401–11408.

Kim, Y.-C., Lee, H.-G., and Han, K.-A. (2007). D1 dopamine receptor dDA1 is required in the mushroom body neurons for aversive and appetitive learning in Drosophila. J. Neurosci. *27*, 7640–7647.

Komatsu, N., Aoki, K., Yamada, M., Yukinaga, H., Fujita, Y., Kamioka, Y., and Matsuda, M. (2011). Development of an optimized backbone of FRET biosensors for kinases and GTPases. Mol. Biol. Cell *22*, 4647–4656.

König, C., Khalili, A., Ganesan, M., Nishu, A.P., Garza, A.P., Niewalda, T., Gerber, B., Aso, Y., and Yarali, A. (2018). Reinforcement signaling of punishment versus relief in fruit flies. Learn. Mem. *25*, 247–257.

Krashes, M.J., Keene, A.C., Leung, B., Armstrong, J.D., and Waddell, S. (2007). Sequential use of mushroom body neuron subsets during drosophila odor memory processing. Neuron *53*, 103–115.

Kravitz, A.V., and Kreitzer, A.C. (2012). Striatal mechanisms underlying movement, reinforcement, and punishment. Physiology (Bethesda) *27*, 167–177.

Lammel, S., Lim, B.K., and Malenka, R.C. (2014). Reward and aversion in a heterogeneous midbrain dopamine system. Neuropharmacology *76 Pt B*, 351–359.

Lebestky, T., Chang, J.-S.C., Dankert, H., Zelnik, L., Kim, Y.-C., Han, K.-A., Wolf, F.W.,

Perona, P., and Anderson, D.J. (2009). Two different forms of arousal in Drosophila are oppositely regulated by the dopamine D1 receptor ortholog DopR via distinct neural circuits. Neuron *64*, 522–536.

Lechner, H.A., and Byrne, J.H. (1998). New perspectives on classical conditioning: a synthesis of Hebbian and non-Hebbian mechanisms. Neuron *20*, 355–358.

LeDoux, J.E. (1996). The Emotional Brain: The Mysterious Underpinnings of Emotional Life (Simon & Schuster).

Lee, S.W., O'Doherty, J.P., and Shimojo, S. (2015). Neural computations mediating one-shot learning in the human brain. PLoS Biol. *13*, e1002137.

Leenders, A.G.M., and Sheng, Z.-H. (2005). Modulation of neurotransmitter release by the second messenger-activated protein kinases: implications for presynaptic plasticity. Pharmacol. Ther. *105*, 69–84.

Lerner, T.N., Shilyansky, C., Davidson, T.J., Evans, K.E., Beier, K.T., Zalocusky, K.A., Crow, A.K., Malenka, R.C., Luo, L., Tomer, R., et al. (2015). Intact-Brain Analyses Reveal Distinct Information Carried by SNc Dopamine Subcircuits. Cell *162*, 635–647.

Leroy, F., Brann, D.H., Meira, T., and Siegelbaum, S.A. (2017). Input-Timing-Dependent Plasticity in the Hippocampal CA2 Region and Its Potential Role in Social Memory. Neuron *95*, 1089–1102.e5.

Lev-Ram, V., Wong, S.T., Storm, D.R., and Tsien, R.Y. (2002). A new form of cerebellar long-term potentiation is postsynaptic and depends on nitric oxide but not cAMP. Proc. Natl. Acad. Sci. U.S.a. *99*, 8389–8393.

Levin, L.R., Han, P.L., Hwang, P.M., Feinstein, P.G., Davis, R.L., and Reed, R.R. (1992). The Drosophila learning and memory gene rutabaga encodes a Ca2+/Calmodulin-responsive adenylyl cyclase. Cell *68*, 479–489.

Levy, W.B., and Steward, O. (1983). Temporal contiguity requirements for long-term associative potentiation/depression in the hippocampus. Neuroscience *8*, 791–797.

Li, H., Chaney, S., Roberts, I.J., Forte, M., and Hirsh, J. (2000). Ectopic G-protein expression in dopamine and serotonin neurons blocks cocaine sensitization in Drosophila melanogaster. Current Biology *10*, 211–214.

Linden, D.J., and Connor, J.A. (1991). Participation of postsynaptic PKC in cerebellar long-term depression in culture. Science *254*, 1656–1659.

Linden, D.J., Dickinson, M.H., Smeyne, M., and Connor, J.A. (1991). A long-term depression of AMPA currents in cultured cerebellar Purkinje neurons. Neuron *7*, 81–89.

Liu, C., Plaçais, P.-Y., Yamagata, N., Pfeiffer, B.D., Aso, Y., Friedrich, A.B., Siwanowicz, I., Rubin, G.M., Preat, T., and Tanimoto, H. (2012). A subset of dopamine neurons signals reward

for odour memory in Drosophila. Nature *488*, 512–516.

Liu, Y., Ferguson, J.F., Xue, C., Silverman, I.M., Gregory, B., Reilly, M.P., and Li, M. (2013). Evaluating the impact of sequencing depth on transcriptome profiling in human adipose. PLoS ONE *8*, e66883.

Livingstone, M.S., Sziber, P.P., and Quinn, W.G. (1984). Loss of calcium/calmodulin responsiveness in adenylate cyclase of rutabaga, a Drosophila learning mutant. Cell *37*, 205–215.

Logsdon, S., Johnstone, A.F.M., Viele, K., and Cooper, R.L. (2006). Regulation of synaptic vesicles pools within motor nerve terminals during short-term facilitation and neuromodulation. J. Appl. Physiol. *100*, 662–671.

Mao, Z., and Davis, R.L. (2009). Eight different types of dopaminergic neurons innervate the Drosophila mushroom body neuropil: anatomical and physiological heterogeneity. Front. Neural Circuits *3*, 5.

Marcott, P.F., Gong, S., Donthamsetti, P., Grinnell, S.G., Nelson, M.N., Newman, A.H., Birnbaumer, L., Martemyanov, K.A., Javitch, J.A., and Ford, C.P. (2018). Regional Heterogeneity of D2-Receptor Signaling in the Dorsal Striatum and Nucleus Accumbens. Neuron *98*, 575–587.e4.

Marcott, P.F., Mamaligas, A.A., and Ford, C.P. (2014). Phasic dopamine release drives rapid activation of striatal D2-receptors. Neuron *84*, 164–176.

Markowitz, J.E., Gillis, W.F., Beron, C.C., Neufeld, S.Q., Robertson, K., Bhagat, N.D., Peterson, R.E., Peterson, E., Hyun, M., Linderman, S.W., et al. (2018). The Striatum Organizes 3D Behavior via Moment-to-Moment Action Selection. Cell *174*, 44–58.e17.

Masse, N.Y., Turner, G.C., and Jefferis, G.S.X.E. (2009). Olfactory information processing in Drosophila. Curr. Biol. *19*, R700–R713.

Matsuda, W., Furuta, T., Nakamura, K.C., Hioki, H., Fujiyama, F., Arai, R., and Kaneko, T. (2009). Single nigrostriatal dopaminergic neurons form widely spread and highly dense axonal arborizations in the neostriatum. J. Neurosci. *29*, 444–453.

Matsumoto, H., Tian, J., Uchida, N., and Watabe-Uchida, M. (2016). Midbrain dopamine neurons signal aversion in a reward-context-dependent manner. eLife *5*, 7025.

Mattson, M.P., LaFerla, F.M., Chan, S.L., Leissring, M.A., Shepel, P.N., and Geiger, J.D. (2000). Calcium signaling in the ER: its role in neuronal plasticity and neurodegenerative disorders. Trends Neurosci. *23*, 222–229.

Mauk, M.D., and Donegan, N.H. (1997). A model of Pavlovian eyelid conditioning based on the synaptic organization of the cerebellum. Learn. Mem. *4*, 130–158.

Mayer, D., Kahl, E., Uzuneser, T.C., and Fendt, M. (2018). Role of the mesolimbic dopamine system in relief learning. Neuropsychopharmacology *43*, 1651–1659.

Mayer, M.L., Westbrook, G.L., and Guthrie, P.B. (1984). Voltage-dependent block by Mg2+ of NMDA responses in spinal cord neurones. Nature *309*, 261–263.

McKay, B.E., Placzek, A.N., and Dani, J.A. (2007). Regulation of synaptic transmission and plasticity by neuronal nicotinic acetylcholine receptors. Biochem. Pharmacol. *74*, 1120–1133.

Meeks, J.P., and Holy, T.E. (2008). Pavlov's moth: olfactory learning and spike timing-dependent plasticity. Nat Neurosci *11*, 1126–1127.

Milner, B., and Penfield, W. (1955). The effect of hippocampal lesions on recent memory. Trans Am Neurol Assoc 42–48.

Mink, J.W. (1996). The Basal Ganglia: Focused Selection and Inhibition of Competing Motor Programs. Progress in Neurobiology *50*, 381–425.

Mink, J.W. (2003). The Basal Ganglia and involuntary movements: impaired inhibition of competing motor patterns. Arch. Neurol. *60*, 1365–1368.

Mistlberger, R.E. (1994). Circadian food-anticipatory activity: formal models and physiological mechanisms. Neurosci Biobehav Rev *18*, 171–195.

Miyashita, T., Oda, Y., Horiuchi, J., Yin, J.C.P., Morimoto, T., and Saitoe, M. (2012). Mg2+ Block of Drosophila NMDA Receptors Is Required for Long-Term Memory Formation and CREB-Dependent Gene Expression. Neuron *74*, 887–898.

Mons, N., Guillou, J.L., and Jaffard, R. (1999). The role of Ca2+/calmodulin-stimulable adenylyl cyclases as molecular coincidence detectors in memory formation. Cell. Mol. Life Sci. *55*, 525–533.

Montague, P.R., Dayan, P., and Sejnowski, T.J. (1996). A framework for mesencephalic dopamine systems based on predictive Hebbian learning. Journal of Neuroscience *16*, 1936–1947.

Moscarello, J.M., and LeDoux, J.E. (2013). Active avoidance learning requires prefrontal suppression of amygdala-mediated defensive reactions. J. Neurosci. *33*, 3815–3823.

Moscovitch, A., and LoLordo, V.M. (1968). Role of safety in the Pavlovian backward fear conditioning procedure. J Comp Physiol Psychol *66*, 673–678.

Moyer, J.R., Deyo, R.A., and Disterhoft, J.F. (1990). Hippocampectomy disrupts trace eye-blink conditioning in rabbits. Behav. Neurosci. *104*, 243–252.

Muller, D., Joly, M., and Lynch, G. (1988). Contributions of quisqualate and NMDA receptors to the induction and expression of LTP. Science *242*, 1694–1697.

Murthy, M., and Turner, G. (2013). Whole-cell in vivo patch-clamp recordings in the Drosophila brain. Cold Spring Harb Protoc *2013*, 140–148.

Murthy, M., Fiete, I., and Laurent, G. (2008). Testing odor response stereotypy in the Drosophila mushroom body. Neuron *59*, 1009–1023.

Nadim, F., and Bucher, D. (2014). Neuromodulation of neurons and synapses. Current Opinion in Neurobiology *29*, 48–56.

Neve, K.A., Seamans, J.K., and Trantham-Davidson, H. (2004). Dopamine receptor signaling. J. Recept. Signal Transduct. Res. *24*, 165–205.

Nowak, L., Bregestovski, P., Ascher, P., Herbet, A., and Prochiantz, A. (1984). Magnesium gates glutamate-activated channels in mouse central neurones. Nature *307*, 462–465.

Olds, J., and Milner, P. (1954). Positive reinforcement produced by electrical stimulation of septal area and other regions of rat brain. J Comp Physiol Psychol *47*, 419–427.

Oliver, D.L., Beckius, G.E., Bishop, D.C., Loftus, W.C., and Batra, R. (2003). Topography of interaural temporal disparity coding in projections of medial superior olive to inferior colliculus. J. Neurosci. *23*, 7438–7449.

Oura, T., Murata, K., Morita, T., Nezu, A., Arisawa, M., Shuto, S., and Tanimura, A. (2016). Highly Sensitive Measurement of Inositol 1,4,5-Trisphosphate by Using a New Fluorescent Ligand and Ligand Binding Domain Combination. Chembiochem *17*, 1509–1512.

Owald, D., and Waddell, S. (2015). Olfactory learning skews mushroom body output pathways to steer behavioral choice in Drosophila. Current Opinion in Neurobiology *35*, 178–184.

Owald, D., Felsenberg, J., Talbot, C.B., Das, G., Perisse, E., Huetteroth, W., and Waddell, S. (2015). Activity of defined mushroom body output neurons underlies learned olfactory behavior in Drosophila. Neuron *86*, 417–427.

Paknejad, N., and Hite, R.K. (2018). Structural basis for the regulation of inositol trisphosphate receptors by Ca2+ and IP3. Nat. Struct. Mol. Biol. *25*, 660–668.

Pascual, A., and Préat, T. (2001). Localization of long-term memory within the Drosophila mushroom body. Science *294*, 1115–1117.

Pavlov, P.I. (1927). Conditioned reflexes: An investigation of the physiological activity of the cerebral cortex. Ann Neurosci *17*, 136–141.

Pelkey, K.A., and McBain, C.J. (2007). Differential regulation at functionally divergent release sites along a common axon. Current Opinion in Neurobiology *17*, 366–373.

Penfield, W., and Milner, B. (1958). Memory deficit produced by bilateral lesions in the hippocampal zone. AMA Arch Neurol Psychiatry *79*, 475–497.

Phelps, E.A., and LeDoux, J.E. (2005). Contributions of the amygdala to emotion processing: from animal models to human behavior. Neuron *48*, 175–187.

Pugh, J.R., and Raman, I.M. (2008). Mechanisms of potentiation of mossy fiber EPSCs in the cerebellar nuclei by coincident synaptic excitation and inhibition. J. Neurosci. *28*, 10549–10560.

Qin, H., Cressy, M., Li, W., Coravos, J.S., Izzi, S.A., and Dubnau, J. (2012). Gamma neurons mediate dopaminergic input during aversive olfactory memory formation in Drosophila. Curr. Biol. *22*, 608–614.

Quinn, W.G., Harris, W.A., and Benzer, S. (1974). Conditioned behavior in Drosophila melanogaster. Proc. Natl. Acad. Sci. U.S.a. *71*, 708–712.

Quirk, G.J., and Mueller, D. (2008). Neural mechanisms of extinction learning and retrieval. Neuropsychopharmacology *33*, 56–72.

Ramirez, S., Liu, X., Lin, P.-A., Suh, J., Pignatelli, M., Redondo, R.L., Ryan, T.J., and Tonegawa, S. (2013). Creating a false memory in the hippocampus. Science *341*, 387–391.

Redgrave, P., Prescott, T.J., and Gurney, K. (1999). The basal ganglia: a vertebrate solution to the selection problem? Neuroscience *89*, 1009–1023.

Regehr, W.G., Carey, M.R., and Best, A.R. (2009). Activity-dependent regulation of synapses by retrograde messengers. Neuron *63*, 154–170.

Rescorla, R.A. (1967). Pavlovian conditioning and its proper control procedures. Psychol Rev *74*, 71–80.

Rescorla, R.A. (1988). Behavioral studies of Pavlovian conditioning. Annu. Rev. Neurosci. *11*, 329–352.

Rescorla, R.A. (1971). Variation in the effectiveness of reinforcement and nonreinforcement following prior inhibitory conditioning. Learning and Motivation *2*, 113–123.

Reynolds, J.N., Hyland, B.I., and Wickens, J.R. (2001). A cellular mechanism of reward-related learning. Nature *413*, 67–70.

Reynolds, J.N.J., and Wickens, J.R. (2002). Dopamine-dependent plasticity of corticostriatal synapses. Neural Netw *15*, 507–521.

Richards, B.A., and Frankland, P.W. (2017). The Persistence and Transience of Memory. Neuron *94*, 1071–1084.

Riffell, J.A., Shlizerman, E., Sanders, E., Abrell, L., Medina, B., Hinterwirth, A.J., and Kutz, J.N. (2014). Sensory biology. Flower discrimination by pollinators in a dynamic chemical environment. Science *344*, 1515–1518.

Roberts, W.H. (1930). The Effect of Delayed Feeding on White Rats in a Problem Cage. The Pedagogical Seminary and Journal of Genetic Psychology *37*, 35–58.

Roesch, M.R., Calu, D.J., and Schoenbaum, G. (2007). Dopamine neurons encode the better

option in rats deciding between differently delayed or sized rewards. Nat Neurosci *10*, 1615–1624.

Roseberry, T.K., Lee, A.M., Lalive, A.L., Wilbrecht, L., Bonci, A., and Kreitzer, A.C. (2016). Cell-Type-Specific Control of Brainstem Locomotor Circuits by Basal Ganglia. Cell *164*, 526–537.

Ruta, V., Datta, S.R., Vasconcelos, M.L., Freeland, J., Looger, L.L., and Axel, R. (2010). A dimorphic pheromone circuit in Drosophila from sensory input to descending output. Nature *468*, 686–690.

Ryan, T.J., Roy, D.S., Pignatelli, M., Arons, A., and Tonegawa, S. (2015). Memory. Engram cells retain memory under retrograde amnesia. Science *348*, 1007–1013.

Ryou, J.W., Cho, S.Y., and Kim, H.T. (1998). Lesion of the cerebellar interpositus nucleus or the red nucleus affects classically conditioned neuronal activity in the hippocampus. Prog. Neuropsychopharmacol. Biol. Psychiatry *22*, 169–185.

Sarkisov, D.V., and Wang, S.S.-H. (2008). Order-dependent coincidence detection in cerebellar Purkinje neurons at the inositol trisphosphate receptor. J. Neurosci. *28*, 133–142.

Schultz, W., Dayan, P., and Montague, P.R. (1997). A neural substrate of prediction and reward. Science *275*, 1593–1599.

Schultz, W. (2002). Getting formal with dopamine and reward. Neuron *36*, 241–263.

Schwaerzel, M., Heisenberg, M., and Zars, T. (2002). Extinction antagonizes olfactory memory at the subcellular level. Neuron *35*, 951–960.

Seelig, J.D., and Jayaraman, V. (2015). Neural dynamics for landmark orientation and angular path integration. Nature *521*, 186–191.

Sehdev, A., Mohammed, Y.G., Triphan, T., and Szyszka, P. (2018). Olfactory object recognition based on fine-scale stimulus timing in Drosophila. bioRxiv 418632.

Semon, R. (1921). The nmeme. (London: George Allen & Unwin).

Séjourné, J., Plaçais, P.-Y., Aso, Y., Siwanowicz, I., Trannoy, S., Thoma, V., Tedjakumala, S.R., Rubin, G.M., TchEnio, P., Ito, K., et al. (2011). Mushroom body efferent neurons responsible for aversive olfactory memory retrieval in Drosophila. Nat Neurosci *14*, 903–910.

Shafer, O.T., Kim, D.J., Dunbar-Yaffe, R., Nikolaev, V.O., Lohse, M.J., and Taghert, P.H. (2008). Widespread receptivity to neuropeptide PDF throughout the neuronal circadian clock network of Drosophila revealed by real-time cyclic AMP imaging. Neuron *58*, 223–237.

Sheffield, M.E., and Dombeck, D.A. (2019). Dendritic mechanisms of hippocampal place field formation. Current Opinion in Neurobiology *54*, 1–11.

Shen, W., Flajolet, M., Greengard, P., and Surmeier, D.J. (2008). Dichotomous dopaminergic control of striatal synaptic plasticity. Science *321*, 848–851.

Shuai, Y., Hirokawa, A., Ai, Y., Zhang, M., Li, W., and Zhong, Y. (2015). Dissecting neural pathways for forgetting in Drosophila olfactory aversive memory. Proc. Natl. Acad. Sci. U.S.a. *112*, E6663–E6672.

Shuai, Y., Lu, B., Hu, Y., Wang, L., Sun, K., and Zhong, Y. (2010). Forgetting is regulated through Rac activity in Drosophila. Cell *140*, 579–589.

Siegel, S., and Domjan, M. (1971). Backward conditoning as an inhibitory procedure. Learning and Motivation *2*, 1–11.

Skoulakis, E.M., Kalderon, D., and Davis, R.L. (1993). Preferential expression in mushroom bodies of the catalytic subunit of protein kinase A and its role in learning and memory. Neuron *11*, 197–208.

Smith, M.P., and Buchanan, G. (1954). Acquisition of secondary reward by cues associated with shock reduction. J Exp Psychol *48*, 123–126.

Smith, P.H., Joris, P.X., and Yin, T.C. (1993). Projections of physiologically characterized spherical bushy cell axons from the cochlear nucleus of the cat: evidence for delay lines to the medial superior olive. J. Comp. Neurol. *331*, 245–260.

Snyder, G.L., Allen, P.B., Fienberg, A.A., Valle, C.G., Huganir, R.L., Nairn, A.C., and Greengard, P. (2000). Regulation of phosphorylation of the GluR1 AMPA receptor in the neostriatum by dopamine and psychostimulants in vivo. Journal of Neuroscience *20*, 4480–4488.

Spence, K.W., and Runquist, W.N. (1958). Temporal effects of conditioned fear on the eyelid reflex. J Exp Psychol *55*, 613–616.

Spetch, M.L., Wilkie, D.M., and Pinel, J.P. (1981). Backward conditioning: A reevaluation of the empirical evidence. Psychological Bulletin *89*, 163–175.

Srikanth, S., Wang, Z., Tu, H., Nair, S., Mathew, M.K., Hasan, G., and Bezprozvanny, I. (2004). Functional properties of the Drosophila melanogaster inositol 1,4,5-trisphosphate receptor mutants. Biophysical Journal *86*, 3634–3646.

Strausfeld, N.J., Hansen, L., Li, Y., Gomez, R.S., and Ito, K. (1998). Evolution, discovery, and interpretations of arthropod mushroom bodies. Learn. Mem. *5*, 11–37.

Sugamori, K.S., Demchyshyn, L.L., McConkey, F., Forte, M.A., and Niznik, H.B. (1995). A primordial dopamine D1-like adenylyl cyclase-linked receptor from Drosophila melanogaster displaying poor affinity for benzazepines. FEBS Lett. *362*, 131–138.

Sun, F., Zeng, J., Jing, M., Zhou, J., Feng, J., Owen, S.F., Luo, Y., Li, F., Wang, H., Yamaguchi, T., et al. (2018). A Genetically Encoded Fluorescent Sensor Enables Rapid and Specific Detection of Dopamine in Flies, Fish, and Mice. Cell *174*, 481–496.e19.

Sun, X., Zhao, Y., and Wolf, M.E. (2005). Dopamine receptor stimulation modulates AMPA receptor synaptic insertion in prefrontal cortex neurons. J. Neurosci. *25*, 7342–7351.

Surmeier, D.J., Carrillo-Reid, L., and Bargas, J. (2011). Dopaminergic modulation of striatal neurons, circuits, and assemblies. Neuroscience *198*, 3–18.

Suvrathan, A., Payne, H.L., and Raymond, J.L. (2018). Timing Rules for Synaptic Plasticity Matched to Behavioral Function. Neuron *97*, 248–250.

Svenningsson, P., Nishi, A., Fisone, G., Girault, J.-A., Nairn, A.C., and Greengard, P. (2004). DARPP-32: an integrator of neurotransmission. Annu. Rev. Pharmacol. Toxicol. *44*, 269–296.

Tabone, C.J., and Ramaswami, M. (2012). Is NMDA receptor-coincidence detection required for learning and memory? Neuron *74*, 767–769.

Takemura, S.-Y., Aso, Y., Hige, T., Wong, A., Lu, Z., Xu, C.S., Rivlin, P.K., Hess, H., Zhao, T., Parag, T., et al. (2017). A connectome of a learning and memory center in the adult Drosophila brain. eLife *6*, 5643.

Tanimoto, H., Heisenberg, M., and Gerber, B. (2004). Experimental psychology: Event timing turns punishment to reward. Nature *430*, 983–983.

Technau, G., and Heisenberg, M. (1982). Neural reorganization during metamorphosis of the corpora pedunculata in Drosophila melanogaster. Nature *295*, 405–407.

Thompson, R.F. (2005). In search of memory traces. Annu Rev Psychol *56*, 1–23.

Thum, A.S., and Gerber, B. (2019). Connectomics and function of a memory network: the mushroom body of larval Drosophila. Current Opinion in Neurobiology *54*, 146–154.

Tomchik, S.M., and Davis, R.L. (2009). Dynamics of learning-related cAMP signaling and stimulus integration in the Drosophila olfactory pathway. Neuron *64*, 510–521.

Tomchik, S.M., and Davis, R.L. (2013). Drosophila Memory Research through Four Eras. In Invertebrate Learning and Memory, (Elsevier), pp. 359–377.

Trannoy, S., Redt-Clouet, C., Dura, J.-M., and Preat, T. (2011). Parallel processing of appetitive short- and long-term memories in Drosophila. Curr. Biol. *21*, 1647–1653.

Tritsch, N.X., and Sabatini, B.L. (2012). Dopaminergic modulation of synaptic transmission in cortex and striatum. Neuron *76*, 33–50.

Tully, T., and Quinn, W.G. (1985). Classical conditioning and retention in normal and mutant Drosophila melanogaster. J. Comp. Physiol. A *157*, 263–277.

Tully, T., Cambiazo, V., and Kruse, L. (1994). Memory through metamorphosis in normal and mutant Drosophila. Journal of Neuroscience *14*, 68–74.

Turner, G.C., Bazhenov, M., and Laurent, G. (2008). Olfactory representations by Drosophila mushroom body neurons. Journal of Neurophysiology *99*, 734–746.

van Breugel, F., and Dickinson, M.H. (2014). Plume-tracking behavior of flying Drosophila emerges from a set of distinct sensory-motor reflexes. Curr. Biol. *24*, 274–286.

van Welie, I., and Lac, du, S. (2011). Bidirectional control of BK channel open probability by CAMKII and PKC in medial vestibular nucleus neurons. Journal of Neurophysiology *105*, 1651–1659.

Waddell, S. (2016). Neural Plasticity: Dopamine Tunes the Mushroom Body Output Network. Curr. Biol. *26*, R109–R112.

Waelti, P., Dickinson, A., and Schultz, W. (2001). Dopamine responses comply with basic assumptions of formal learning theory. Nature *412*, 43–48.

Wang, S.S., Denk, W., and Häusser, M. (2000). Coincidence detection in single dendritic spines mediated by calcium release. Nat Neurosci *3*, 1266–1273.

Watabe-Uchida, M., Eshel, N., and Uchida, N. (2017). Neural Circuitry of Reward Prediction Error. Annu. Rev. Neurosci. *40*, 373–394.

Wichmann, T., and DeLong, M.R. (2003). Pathophysiology of Parkinson's disease: the MPTP primate model of the human disorder. Annals of the New York Academy of Sciences *991*, 199–213.

Wu, T.-H., Lu, Y.-N., Chuang, C.-L., Wu, C.-L., Chiang, A.-S., Krantz, D.E., and Chang, H.-Y. (2013). Loss of vesicular dopamine release precedes tauopathy in degenerative dopaminergic neurons in a Drosophila model expressing human tau. Acta Neuropathol. *125*, 711–725.

Xia, S., Miyashita, T., Fu, T.-F., Lin, W.-Y., Wu, C.-L., Pyzocha, L., Lin, I.-R., Saitoe, M., Tully, T., and Chiang, A.-S. (2005). NMDA receptors mediate olfactory learning and memory in Drosophila. Current Biology *15*, 603–615.

Xue, G., Xue, F., Droutman, V., Lu, Z.-L., Bechara, A., and Read, S. (2013). Common neural mechanisms underlying reversal learning by reward and punishment. PLoS ONE *8*, e82169.

Yamagata, N., Ichinose, T., Aso, Y., Plaçais, P.-Y., Friedrich, A.B., Sima, R.J., Preat, T., Rubin, G.M., and Tanimoto, H. (2015). Distinct dopamine neurons mediate reward signals for short- and long-term memories. Proc. Natl. Acad. Sci. U.S.a. *112*, 578–583.

Yamazaki, D., Horiuchi, J., Nakagami, Y., Nagano, S., Tamura, T., and Saitoe, M. (2007). The Drosophila DCO mutation suppresses age-related memory impairment without affecting lifespan. Nat Neurosci *10*, 478–484.

Yan, Z., Hsieh-Wilson, L., Feng, J., Tomizawa, K., Allen, P.B., Fienberg, A.A., Nairn, A.C., and Greengard, P. (1999). Protein phosphatase 1 modulation of neostriatal AMPA channels: regulation by DARPP-32 and spinophilin. Nat Neurosci *2*, 13–17.

Yin, J.C., Wallach, J.S., Del Vecchio, M., Wilder, E.L., Zhou, H., Quinn, W.G., and Tully, T. (1994). Induction of a dominant negative CREB transgene specifically blocks long-term memory in Drosophila. Cell *79*, 49–58.

Zars, T., Wolf, R., Davis, R., and Heisenberg, M. (2000). Tissue-specific expression of a type I adenylyl cyclase rescues the rutabaga mutant memory defect: in search of the engram. Learn. Mem. *7*, 18–31.

Zhang, X., Li, Q., Wang, L., Liu, Z.-J., and Zhong, Y. (2018). Active Protection: Learning-Activated Raf/MAPK Activity Protects Labile Memory from Rac1-Independent Forgetting. Neuron *98*, 142–155.e144.

Zovkic, I.B., Guzman-Karlsson, M.C., and Sweatt, J.D. (2013). Epigenetic regulation of memory formation and maintenance. Learn. Mem. *20*, 61–74.

Zucker, R.S., Kennedy, D., and Selverston, A.I. (1971). Neuronal circuit mediating escape responses in crayfish. Science *173*, 645–650.

Zweifel, L.S., Fadok, J.P., Argilli, E., Garelick, M.G., Jones, G.L., Dickerson, T.M.K., Allen, J.M., Mizumori, S.J.Y., Bonci, A., and Palmiter, R.D. (2011). Activation of dopamine neurons is critical for aversive conditioning and prevention of generalized anxiety. Nat Neurosci *14*, 620–626.